Activating Oxygen and Degrading the Water Treatment Industry's Most Challenging Micropollutant with TAML Activators and Oxidants

Dissertation by

Liang Tang

In Partial Fulfillment of the Requirements for the Degree of

Doctor of Philosophy

Thesis Advisor

Terrence J. Collins

Department of Chemistry,

Carnegie Mellon University, Pittsburgh, Pennsylvania

Submitted September, 2016

To my dear husband, Dr. Renzhi Liu.

To my mother, Yiping Wen.

To my grandparents, Qinan Zhao and Yuhu Wen.

To the loving memory of my father, Shufeng Tang.

Acknowledgements

It has been a long journey toward the accomplishment of my Ph.D. degree, which I would not have been able to achieve without all the support, encouragement, help and company I have received. I would like to take this opportunity to thank everyone who has generously shared their time, thoughts, and effort with me during my graduate studies and research. I would like to thank you all and would like to present special thanks for several people.

First and foremost, I would like to thank my advisor, Prof. Terrence Collins. Thank you so much for all your support and continuous guidance throughout my graduate studies. I really enjoyed the level of freedom you have given to us to pursue our own scientific curiosity, and I truly appreciate all the important suggestions you have given to my research. Thank you for encouraging me all the time and helping me develop myself. I still remember when you encouraged me to attend the Green Chemistry Gordon Research Conference in Italy during my second year of graduate study. You said you would like to throw your students to the sea to learn to swim because you believe all your students can swim, and I did learn and develop tremendously during the conference. I am genuinely grateful for the extraordinary opportunities you have provided to your students. I would also like to thank you for opening the world of "green chemistry" to me, not only academically, but also in everyday life. Your enthusiasm and deep thoughts on green chemistry are so inspiring: all these years, I have been learning in the field of green chemistry and sustainability, which has been influential on me and also my family and friends.

I would like to thank Prof. Alexander Ryabov, who has guided me through kinetic study and the area of reverse micelles. Thank you so much for our discussions, also for teaching me how to conduct research as a new graduate student, from how to write clean and tidy lab notes to how to write a paper clearly and concisely, from how to make a buffer to how to make measurements in the simplest way. The reverse micelle study would not have been possible without your guidance and helpful discussions. I also appreciate very much your clear English when I had just come to the US and started with your class. The energetic and unambiguous pronunciations of your speech made your class so clear to understand that a non-native English speaking student like me could focus on the class content and follow your speech easily during the class.

I would like to thank my committee members: Prof. Rongchao Jin (chair), Prof. Kevin Noonan and Prof. Anindya Ghosh for taking your time to read my thesis and provide valuable feedback. Thank you for your helpful discussions and suggestions during our many meetings. Thank you for your willingness to help me.

I would like to thank Prof. Roberto Gil and Dr. Gayathri Withers. My study on metaldehyde would not have been possible without your generous discussion, help and guidance on the use of NMR. Thank you for your patient explanation every time I have a question or problem with the NMR instrument. I have learned a lot on what NMR can do from you, and I really appreciate that you generously share your knowledge on NMR with me.

I would like to thank Dr. Matthew A. DeNardo. We have worked together for a long time, and I am so obliged to have worked with you. You are so knowledgeable and thoughtful on projects. Thank you so much for always helping me and sharing with me your ideas. Also thank you so much for taking your precious time to polish my writing.

I would like to thank Dr. Jesse A. Miller. Thank you so much for all the helpful discussions on selecting projects, solving problems and tips on living in the US during my very first year in a foreign country as a new graduate student.

I would like to thank Dr. Longzhu Q. Shen. Thank you for being ready to help every time I have a problem. Thank you for the valuable discussions we have had, and thank you for your patient training on the instruments in our lab. Thank you for encouraging me and providing important suggestions during my graduate studies.

I would like to thank Drs. Soumen Kundu and Karla I. Arias. Thank you for helping me all the time when I have problems. I still remember you both taking time to help me fix an HPLC problem one evening even though you were about to head home. Both of you are so nice that whenever I have a problem, you are ready to help.

I would like to thank the members of the Kiwi group, past and present, Dr. Matthew R. Mills, Genoa R Warner, Yogesh Somasundar, Dr. Qizhi Ren, Paul Kornbluh, Bryce Fotiu-Wojtowicz, Brendan McGee, for sharing memorable time in the lab with me, for discussing research and life with me, and for all the fun we have had together. I would especially like

to thank Genoa, who has shared an office with me. Thank you for going to yoga class with me, and thank you for sharing with me your healthy lifestyle.

I would like to thank Prof. Rakesh Kanda from Brunel University for always being ready to offer suggestions and help.

I would like to thank Mr. Ron Ripper from Hauck Environmental Engineering Lab for being so patient in training me on the IC instrument and helping me solve problems with IC all the time.

I would like to thank my teaching mentors, including Profs. Subha R. Das, Susan T. Graul and Gizelle Sherwood. Thank you for being patient, and I feel so lucky that I could have the chance to work with you.

I would like to thank Dr. Rea Freeland, who is always ready to help. I still remember our discussion on how to give a talk for the ICC test. Thank you for your friendly reminders and suggestions on all the Ph.D. requirements and deadlines.

I would like to thank Valerie Bridge, Sara Wainer, Brenda Chambers, Patsey Haddock, Tim Sager, all the staff in the stock room and mail room, and the department writing consultants. Thank you for always being friendly, helpful and supportive to me.

I would like to thank my friends Dr. Mingjiang Zhong, Dr. Jing Kong, Dr. Penglin Ye, Mo Li, Shuo Zhao, and Qing Ye from the Department of Chemistry. Thank you for all the happy times we have spent together and thank you for all your help.

I would like to thank all my fellow students: Lisa, Dia, Kitty, Priya, Tonia, Hongkun, Xiang, Anthony, Sourav, Andrew, Christian, Arunava, Jake, Matteus, and Jim. I still remember the first day we met in department orientation. You are among the first people I have ever known in the US; thank you all for your company as we pursue higher degrees together, and thank you for all the time, discussion and help you have shared with me.

There will never be enough words to express my appreciations to my family. Thank you to my mom, Yiping Wen, for always being by my side on whatever I have decided. Thank you for letting me know that the most important thing in life is being happy. Thank you for being proud of your daughter all the time and always being my firm support. My

grandparents, Qinan Zhao and Yuhu Wen, thank you for loving me as if I were your youngest daughter. Thank you for teaching me the most precious thing in the world — love. Thank you to my aunt and uncle, Meijuan Shen and Jianguo Wen, for taking care of me during my growth. Thank you for supporting the whole family. Thank you to my parents-in-law, Beiqi Chen and Guoliang Liu, for all your support and love to me and Renzhi. Finally and most importantly, I would like to thank my dear husband, Renzhi. It has been a wonderful miracle that we have met and fallen in love with each other at our best age at Peking University, came to Carnegie Mellon University together for graduate study, and started our own family. Thank you for all your love, and I love you, too.

Sep 13, 2016

Table of Contents

List of Figures

List of Charts

List of Schemes

List of Tables

Abstract

The immense industrial development and large population of our time demands the development of innovative, cost-effective, and universal water treatment processes to remove anthropogenic contaminants and pathogens and provide sufficient clean potable water. TAML activators are a family of green oxidation catalysts that deliver superior catalysis for the oxidation of hazardous environmental pollutants at environmentally relevant concentrations. This is translating into advanced water treatment processes that are more effective than existing processes. In this thesis, TAML catalysis has been studied in the decomposition of the extremely persistent micropollutant, metaldehyde, under laboratory conditions to guide development of a better real world option. TAML/H_2O_2 slowly degrades metaldehyde to acetaldehyde and acetic acid via a process that was monitored by nuclear magnetic resonance spectroscopy (^{1}H NMR). Further study found that substituting NaClO for H_2O_2 in the TAML system increased the turnover number of one 0.4 μM aliquot of catalyst to 106 from 32 under laboratory conditions in pH 7 (0.01 M phosphate, D_2O) at 25 °C. This showed that oxidant substitution results in a ~3-fold higher catalyst efficiency without altering the reaction rate, identifying oxidant choice as a significant design tool for TAML processes. The observation of metaldehyde decomposition under mild conditions provides a further indication that TAML catalysis holds immense promise for advancing water treatment to add to the conclusions of Brunel University UK collaborative studies on London wastewater. A detailed kinetic study of catalyst activation is presented delivering advanced understanding of the catalyst activation process which is rate determining in most TAML applications. Finally, the potential applications of TAML catalysis are extended through a study of the reactivity of less

reactive TAML/O_2 systems in reverse micelles of Aerosol OT (AOT) in *n*-octane. *n*-Octane serves as a proximate reservoir supplying O_2 to result in partial oxidation of Fe^{III}- to Fe^{IV}-containing species, mostly the $Fe^{III}Fe^{IV}$ (major) and $Fe^{IV}Fe^{IV}$ (minor) dimers which coexist with the Fe^{III}-TAML monomeric species. The speciation depends on the pH and the degree of hydration w_0, *viz*. the amount of water in the reverse micelles. Reactive electron donors such as NADH, Pinacyanol chloride (PNC) and hydroquinone undergo the TAML-catalyzed oxidation by O_2. Kinetic evidence is presented for the existence of unusual second-order catalytic pathways in the oxidation of NADH to NAD^+ and in the bleaching of PNC. Depending on the substrate and reaction conditions, a second-order pathway in catalyst either dominates or proceeds in obvious combination with a first-order pathway in catalyst. Despite the limitation of low reactivity, the new systems highlight an encouraging step in replacing TAML peroxidase-like chemistry with more attractive dioxygen-activation chemistry.

Chapter 1 Industrial development and population growth have created an immense need for the development of efficient, cost-effective, and universal water treatment processes to provide sufficient clean domestic water. Current water treatment systems are not adequate for treating water containing emerging micropollutants (MPs) such as pharmaceuticals, personal care products (PPCPs) and pesticides, some of which are endocrine disruptors (EDs). This chapter gives a review of traditional oxidative water treatment processes which are mainly used for disinfection—the review covers the complications of disinfection byproducts. Newly developed oxidative water treatment processes including advanced oxidative processes (AOPs) and ferrate which are both of potential application in water

remediation are also discussed. TAML activators are a family of green oxidation catalysts that are superior in catalyzing the oxidation of hazardous environmental pollutants, and are presented and discussed around the promise they hold for advanced water treatment processes. A brief background of TAML activators is presented along with a succinct introduction of the work in this thesis.

Chapter 2 The extremely persistent molluscicide, metaldehyde is so widely used on farms and gardens that it is often detected in drinking water sources of various countries at concentrations of regulatory concern. Metaldehyde contamination restricts treatment options. This chapter includes a critical survey and comparison of the available remediation technologies. Then a study of TAML/H_2O_2 decomposition of metaldehyde under laboratory conditions is detailed emphasizing to guiding value it holds for development of a better real world option. TAML/H_2O_2 slowly degrades metaldehyde to acetaldehyde and acetic acid. Nuclear magnetic resonance spectroscopy (^{1}H NMR) was used to monitor the degradation. Within the pH range of 6.5–9, the reaction rate is greatest at pH 7. Under optimum conditions, one aliquot of TAML (400 nM) catalyzed 5% degradation over 10 hours with a turnover number of 40. Five sequential TAML aliquots (2 mM overall) effected a 31% removal over 60 hours. The observation of metaldehyde decomposition under mild conditions provides a further indication that TAML catalysis holds promise for advancing water treatment. These results turned our attention to developing more aggressive TAML activators, which we expect will advance the observed technical performance.

Chapter 3 The presence and extreme persistence of metaldehyde in environmental waters have stimulated interest in methods of metaldehyde removal. In Chapter 2, it was shown that the catalytic TAML/H_2O_2 system is capable of slowly oxidizing metaldehyde into a mixture of acetic acid and acetaldehyde which was monitored by nuclear magnetic resonance spectroscopy (^{1}H NMR). In this chapter, an extension is presented showing that substituting NaClO for H_2O_2 in the TAML system increased the turnover number of one 0.4 μM aliquot of catalyst from 32 to 106 under laboratory conditions in pH 7 (0.01 M phosphate) D_2O at 25 °C. TAML/NaClO and H_2O_2 systems effect 14.7 and 4.5% removal in 80 and 10 hours, respectively. Thus, this oxidant substitution results in a ~3-fold higher catalyst efficiency without altering reaction rate. In longer experiments with a total length of 47 days, 91% removal of 330 μM metaldehyde is achieved by 0.02 M NaClO catalyzed by 15 sequential 0.4 μM TAML aliquots added every 72 hours. The study illustrates that extremely long performance times are achievable with certain TAML activators. The major reaction product is benign acetic acid. Potential disinfection byproducts associated with chlorine were also analyzed in TAML/NaClO system. Preliminary results showed that chloroform is formed during cinnamic acid oxidation and bromate could form when bromide presents in water. On the other hand, chlorite can be consumed as slow-reacting oxidant under the catalysis of TAML activator.

Chapter 4 The rate constants of TAML catalyst activation by H_2O_2 has been examined under various conditions including mixed organic solvent/water, D_2O and varied temperature. The rate constant inversely decreased with increased organic solvent proportion suggesting a possible binding mechanism of the organic compound to the

catalyst that impedes catalyst activation. A kinetic isotope effect (KIE) of ~1.7 was found for two TAML activators, indicating the involvement of a proton transfer step in the rate-determining step of catalyst activation. Experiment analysis of the rates at variable temperature enabled the calculation of catalyst activation enthalpy, which is 15.3 ± 0.7 kcal mol^{-1}, implying that bond formation is accompanied by bond cleavage during the transition state.

Chapter 5 Iron TAML activators of peroxides are functional catalase-peroxidase mimics. Switching from hydrogen peroxide (H_2O_2) to dioxygen (O_2) as the primary oxidant was achieved by using a system of reverse micelles of Aerosol OT (AOT) in *n*-octane. Hydrophilic TAML activators are localized in the aqueous microreactors of reverse micelles where water is present in much lower abundance than in bulk water. *n*-Octane serves as a proximate reservoir supplying O_2 to result in partial oxidation of Fe^{III} to Fe^{IV}-containing species, mostly the $Fe^{III}Fe^{IV}$ (major) and $Fe^{IV}Fe^{IV}$ (minor) dimers which coexist with the Fe^{III} TAML monomeric species. The speciation depends on the pH and the degree of hydration w_0, *viz*. the amount of water in the reverse micelles. Reactive electron donors such as NADH, Pinacyanol chloride and hydroquinone undergo the TAML-catalyzed oxidation by O_2. The oxidation of NADH, studied in most detail, is much faster at the lowest degree of hydration w_0 (in "drier micelles") and is accelerated by light through NADH photochemistry. Kinetic evidence is presented for the existence of unusual second-order catalytic pathways in the oxidation of NADH to NAD^+ and the bleaching of blue Pinacyanol chloride (PNC) dye. Depending on the substrate and reaction conditions, a second-order pathway in catalyst either dominates or proceeds in obvious combination with

a first-order pathway in catalyst. Detailed kinetic analysis of the experimental data supports the hypothesis that the reactive intermediate is associated with the mixed-valent dimer system, $Fe^{III}Fe^{IV}$. Dyes that are more resistant to oxidation than Pinacyanol chloride (Orange II, Safranine O) are not oxidized in the reverse micellar media. Despite the limitation of low reactivity, the new systems highlight an encouraging step in replacing TAML peroxidase-like chemistry with more attractive dioxygen-activation chemistry.

Chapter 6 The preliminary results of analysis on disinfection byproduct (DBP) bromate in TAML/H_2O_2 system was presented. The potential of TAML oxidation processes to produce bromate from adventitious bromide in water must be clearly understood because bromate is a human carcinogen. No significant bromate formation was observed, as expected from present understanding to the bromate formation mechanism. The oxidations of TAML catalyst at high concentration by oxidants H_2O_2 and NaClO were examined via UV-vis spectrophotometer. Preliminary results exhibited different catalyst behaviors with these two oxidants, suggesting dissimilar inactivation pathway at high catalyst concentrations. This work is important for understanding the boundary conditions of TAML concentrations for effective catalysis under ultra-dilute conditions.

Chapter 1

Introduction and Thesis Statement

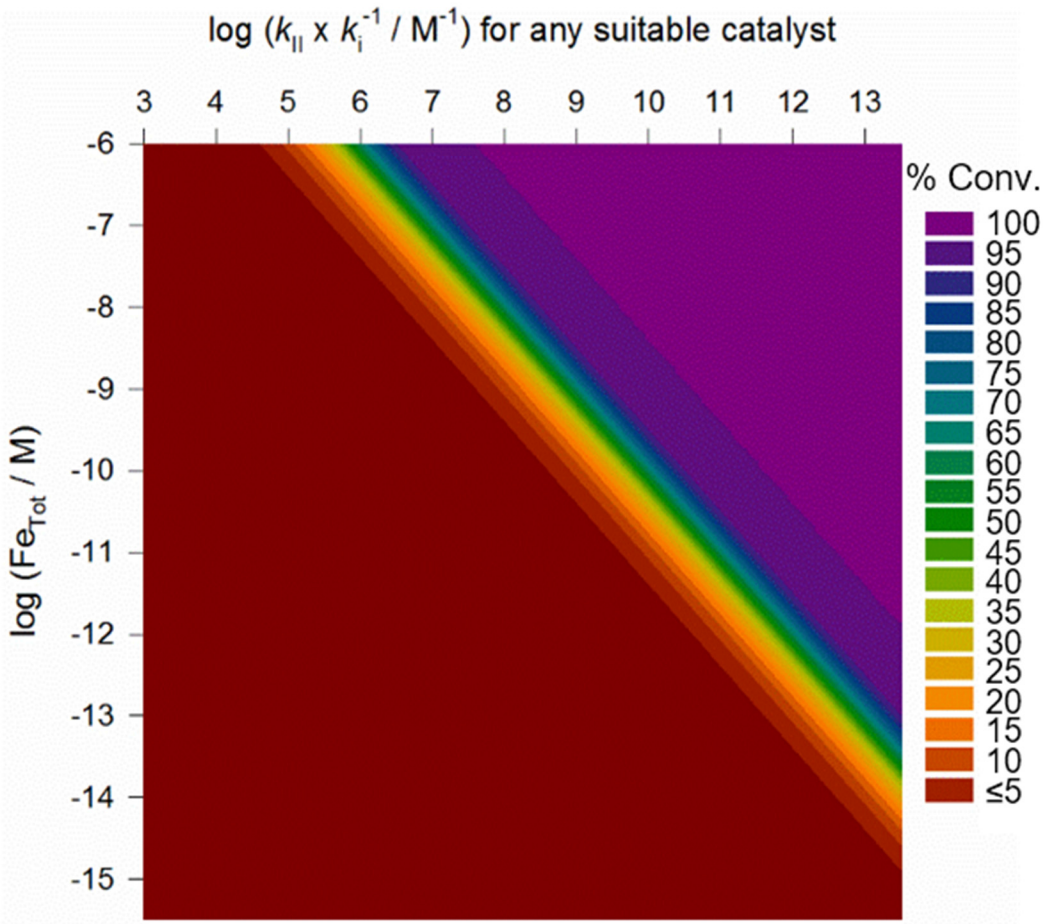

1.1 Introduction of Water Treatment Processes

Water is essential for all creatures—live jellyfish are ~95–98% water and humans are at least 50% by weight[1,2] No creature can survive without water. However, the public service advertisement "Don't let your tear be the last drop of water in the world" aiming at calling on the public to save water and reduce water waste used to confuse me as a child. Although we are consuming large quantities of water every day, it ultimately returns to nature—none vanishes from the water cycle.[3] Moreover, 71% of Earth's surface is covered with water indicating a sufficient water supply.[4] Why do we need to worry about water at all? It turns out that water crises have been occurring all over the world, not because of lack of water sources, but significantly because of insufficient water treatment or inadequate capital to purify and distribute clean freshwater for potable and domestic uses. Effective water purification is beyond the reach of most of humanity on cost basis alone. The key to solving the potable water deficiencies lies in the development of novel water treatment processes that are reliable and economical. Although humans have existed for millions of years, it is astonishing that comparatively complete water treatment plants were only realized in the past century[5] (Scheme 1.1),[6] are not deployed in large numbers of poorer jurisdictions, and are still less than ideal and under development. Emerging water issues associated with swift industrial development and a global population explosion demand the evolution of better water treatment systems that can make safer solutions more accessible and effective by balancing technical, cost, environmental and health performances. Fortunately, advances in the biological, chemical, and medical sciences and technologies promise this possibility.

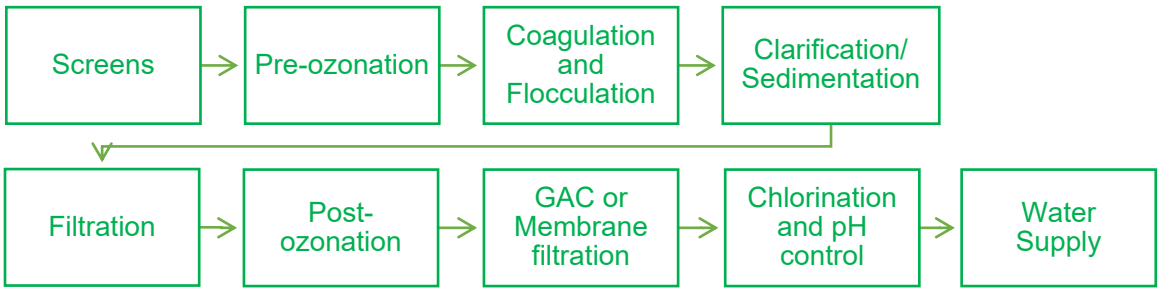

Scheme 1.1 Schematic diagram of a typical process for drinking water treatment.[6]

Water filtration plants were first introduced during the 19th century to remove pathogens from water. Since filtration does not completely eradicate pathogens, chlorination was then employed to kill pathogenic microbes—until the early 20th century chlorine was continuously added to the water supply for disinfection purposes.[5] In the United States (US), typical surface water treatment for potable use undergoes four major steps before storage which include these critical water treatment stages: coagulation/flocculation, sedimentation, filtration and disinfection.[7] The main purpose of the first three steps is the removal of undissolved solids and some charged particles (Table 1.1).[6] The only process that can reduce concentrations of undesired small, polar, organic compounds is disinfection. However, disinfection processes are intended to kill pathogens and remain effective throughout the distribution process, not to remove unwanted organic compounds.[8]

Widespread deployment of anthropogenic chemicals in distributive technologies has resulted in their contamination of water at biologically active concentrations, even when these may be only low parts-per-billion (ppb) to low parts-per-trillion (ppt). "***Endocrine disruptors*** (***EDs***) are chemicals that may interfere with the body's endocrine system and produce adverse developmental, reproductive, neurological, and immune effects in humans

and wildlife".[9] The presence of water contaminants that are EDs is of concern as adverse health effects associated with low dose exposure (low ng/L) commonly occur and some of these effects feature the multi-generational disruptions.[10,11] Pesticides, herbicides and pharmaceuticals and personal care products (PPCPs) have also been frequently detected in water supplies and wastewater effluents.[12] Some of these chemicals of concern are extremely resistant to the most commonly employed water treatment processes including biological degradation (activated sludge and biological trickling filters),[13,14] coagulation, sedimentation and filtration.[12,15] While disinfection processes typically involve treatment with strong oxidants which are capable of transforming most of these chemicals,[12] toxic disinfection byproducts (DBPs) are often formed. These may be more harmful than the initial agent, more resistant to degradation, or both.

1.1.1 Oxidative disinfection processes and associated DBPs

Since it prevents transmission of water-born infectious diseases such as typhoid and cholera, disinfection is a crucial stage of drinking water treatment.[11] The practice of killing pathogenic microbes to make water safe to drink is ancient. Boiling water for sterilization can be traced back to 4000 BCE and the addition of small quantities of silver and copper to water to rid it of active pathogens has also been applied since BCE.[5] Nevertheless, these practices are costly and hard to scale. Thus citywide disinfection was not realized until chlorination was incorporated into the treatment practices of water plants in the 1890s—it had been applied in London to eliminate sewage odors as early as ca. 1850.[5] With the exception of disinfection with low dose (~70 mJ/cm^2) ultraviolet (UV) light, which does not readily convert most compounds (Scheme 1.2),[8,16] the most prominent disinfection processes involve the addition of chemical disinfectants. Those most frequently used today

include chlorine, chloramines, chlorine dioxide and ozone. While these chemicals are added to inactivate pathogenic microorganisms, there may also be added benefits to their use. Some also inhibit biofilm formation, oxidize reduced inorganic solutes including sulfide and ferrous iron, and can prevent biofouling and improve the performance of filters when used in pre-treatments.[17]

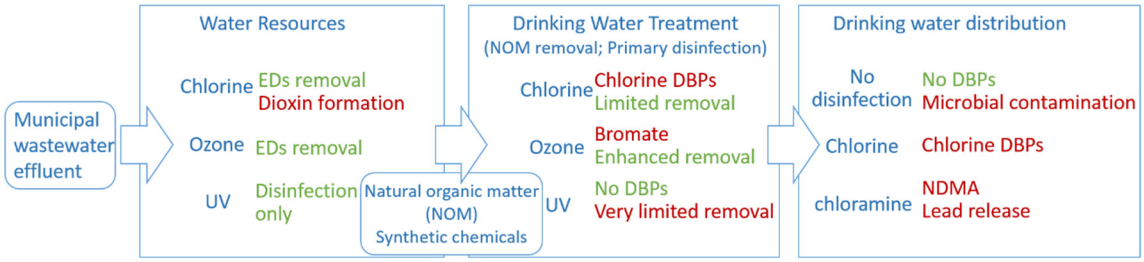

Scheme 1.2 Schematic comparison of the advantages and disadvantages of traditional oxidation/disinfection processes.[8]

1.1.1.1 Chlorine. As the first disinfectant used in large-scale water treatment, chlorine has been continuously added to the water supply since 1902.[5] Since disinfection has greatly improved water quality and saved millions of lives from water-born infectious diseases,[5,11] the chlorination of water has greatly benefitted society. As a strong oxidant, chlorine is capable of reacting with electron-rich organic compounds including many EDs to give chlorinated products which have generally been considered to be less potent and less reactive than their precursors.[8] However, as has been known since 1974, some chlorination DBPs including trihalomethanes (THMs) are hazardous.[18] THMs are probable human carcinogens and have also shown reproductive and developmental toxicity.[17] In addition to chlorinated products, brominated and iodinated DBPs may also form if bromide and iodide

anions are present at elevated concentrations. The production of brominated and iodinated DBPs is exceptionally problematic, because they are usually more carcinogenic or mutagenic than their chlorinated analogs.[17] Other major halogenated DBPs include haloacetic acids, halophenols, haloacetonitriles, and halogenated nitromethanes which are either carcinogenic, mutagenic or sources of odors.[17] The main precursor of halogenated DBPs is natural organic matter (NOM), especially aromatic compounds.[8,18,19] Chlorine also reacts with PPCPs and pesticides leading to chlorinated compounds that are of environmental concern. For example, the reaction between the widely used antimicrobial ED triclosan gives di-, tri-, and tetrachlorinated dioxins which are also EDs.[8] The concentrations of bromate, a major DBP produced during ozonation, formed in chlorination processes are usually insignificant since chlorine only reacts slowly with bromide in homogeneous solution.[20] However, the presence of CuO and NiO pipe deposits in drinking water distribution systems significantly accelerates bromide oxidation by chlorine leading to the formation of higher concentrations of bromate.[20] When practiced at drinking water treatment plants with aged distribution systems, chlorination has added benefits including disinfection during water storage and distribution by residual chlorine which reduces microbial growth and prevention of the lead release from aged water pipes by formation of sparingly soluble lead oxide (PbO_2).[8]

1.1.1.2 Chloramine. One method of avoiding chlorination DBPs is the removal of THM precursors using activated charcoal or enhanced coagulations. Alternatively, disinfection with chloramines does not result in the formation of DBPs observed in chlorination.[8] The use of chloramine to replace chlorine is a less expensive approach to avoid the chlorine-associated DBP problems.[17] In addition, chloramines are more stable than free chlorine and,

therefore, are longer-lived residual disinfectants for continued treatment during water distribution.[17] This family of disinfectants is relatively mild enabling its use in controlling biofouling of membrane systems for wastewater reclamation without causing damage to the membrane.[17] However, when nitrogen-containing compounds are present in water, chloramine treatment produces its own set of extremely potent carcinogenic DBPs including cyanogen halides (i.e., CNCl and CNBr) and *N*-nitrosamines. On ingestion, the former are rapidly metabolized to cyanide.[17] The latter are even more carcinogenic than THMs,[21] making chloramination less optimal compared to chlorination for treatment of some waters. *N*-Nitrosodimethylamine (NDMA) is the most studied *N*-nitrosamine.[21] NDMA was previously found to be a contaminant originating from the production of rocket fuel, plasticizers, batteries, polymers, and other industrial sources. NDMA also forms from the slow oxidation of inorganic and organic nitrogen-containing species by chlorine (Scheme 1.3). Chloramines are produced by adding excess ammonia to water before chlorine addition.[8] The addition of ammonia increases the rate of NDMA production by an order of magnitude over that observed in chlorination alone leading to increased NDMA concentrations. In one study, NDMA concentrations >10 ng/L were detected in 6% of drinking water systems that employed chloramination while NDMA levels >5 ng/L were not detected in any of the systems that relied on disinfection by chlorination alone.[21]

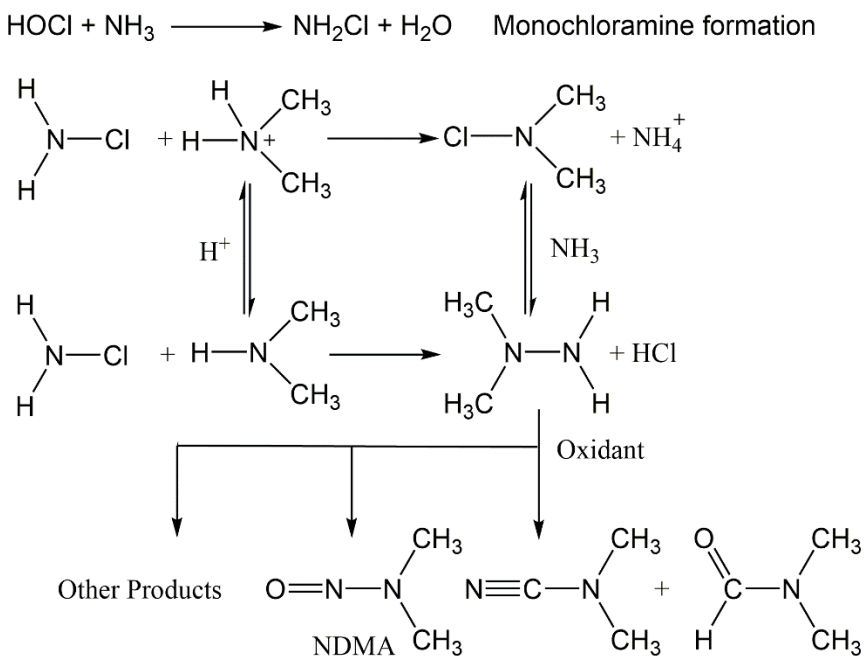

Scheme 1.3 NDMA formation pathways during chloramination of dimethylamine.[21]

The high NDMA concentrations detected in the chloramination systems are particularly problematic. Though no federal maximum contaminant level (MCL) has been established for NDMA, the US Environmental Protection Agency (EPA) has set a preliminary remediation goal of 1.3 ng/L in ground water.[11,21,22] NDMA contamination is very difficult to remediate. Since it is a small, uncharged, hydrophilic molecule with high vapor pressure, NDMA is poorly removed by conventional air stripping, reverse osmosis (RO), or activated carbon (see section 1.1.2 for terminology).[21] Moreover, even hydrophilic sorbents including silica, acrylic resins and zeolite are ineffective. UV treatment can effectively remove NDMA,[21] however, this adds to the cost and complexity of water treatment operations. Moreover, UV photolysis may not destroy NDMA precursors, leading to the possibility that NDMA will reform during distribution of drinking water if residual chlorine/chloramine is present.

1.1.1.3 Chlorine dioxide. Another alternative to chlorination, treatment with the mild oxidant chlorine dioxide (ClO_2), has been extensively deployed in Europe and Israel for primary drinking water disinfection.[17] The major DBPs associated with ClO_2 treatment are inorganic chlorite (ClO_2^-) and chlorate (ClO_3^-), both of which are bioactive. Laboratory tests indicate that sodium chlorite is a potential reproductive, neuro-developmental and endocrine toxicant.[23] The EPA maximum residual disinfectant level (MRDL) for chlorite is 0.8 mg/L.[24] The effects of disinfection processes using combinations of ClO_2 and chlorination or chloramination have been determined. While pre-oxidation with ClO_2 before chlorine treatment is effective in reducing THM formation, the ClO_2 and chloramine treatment of water containing high-concentration bromide results in greater formation of brominated THMs and cyanogen bromide (CNBr) than chloramine treatment alone.[17]

1.1.1.4 Ozone. DBP formation is a major drawback to disinfection with chlorine and chlorine derivatives. Molecular ozone, a selective electrophile that reacts with amines, phenols, and double bonds, is applied worldwide as a disinfectant and oxidant to reduce DBPs. Ozone also removes iron, manganese, micropollutants (MPs) and chemicals that have undesirable taste, odor, or appearance.[8,25,26] However, ozonation also produces DBPs. When conducted in the presence of bromide, ozonation produces the carcinogen bromate.[27] This too is a major drawback as bromide is present in all water sources. Bromide concentrations in freshwaters and seawaters vary widely with values of ~10 to >1000 μg L^{-1} and 67 mg L^{-1}, respectively.[28] Ozonation of raw water containing [Br^-] as low as 50 μg L^{-1} produces [BrO_3^-] exceeding the European Union drinking water commission[29] and US EPA[24] drinking water MCL of 10 μg L^{-1}.[30] Ozonation of high Br^-- containing water can produce BrO_3^- at concentrations one or two orders of magnitude above MCL.[17] Ozonation

can form bromate either via a molecular ozone pathway or a radical pathway (Scheme 1.4). The molecular ozone pathway is mainly composed of two steps, in the first step, bromide is efficiently converted into hypobromite and hypobromous acid, the former is further oxidized by 2 equivalents of O_3 to produce bromate, or it can react with radicals to form bromate via several steps.[27,31] Two strategies employed to reduce bromate formation are addition of ammonia to consume HOBr and decreasing pH to suppress OBr^- oxidation—unfortunately neither is very effective in reducing bromate formation when the water contains high concentrations of bromide.[17,25] Chlorination before ammonia addition can further decrease bromate formation four-fold compared to the ammonia process alone.[25] However, chlorination DBPs are produced if a high concentration of NOM is dissolved in the water. Like NDMA, bromate can be destroyed by relatively low doses of UV, x-ray, γ-ray, or energetic-particle radiation to give oxygen and hypobromite.[32] However, these additional treatments impose additional costs.

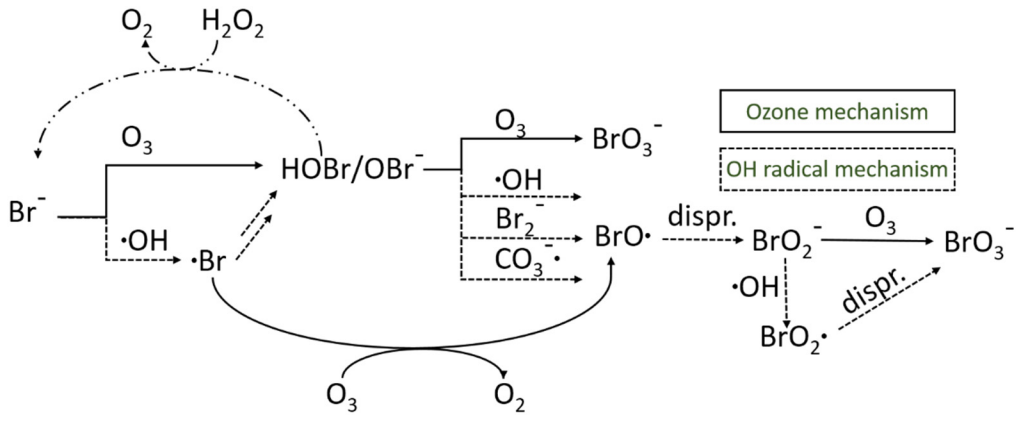

Scheme 1.4 Bromate (BrO_3^-) formation mechanism during ozonation from bromide (Br^-) via both molecular ozone pathway and the OH radical pathway.[27,31]

Ozonation of water containing high concentrations of NOM and bromide also produces brominated THMs, phenols, acetic acids, cyanogen halides, nitromethanes and acetonitriles, though mostly at concentrations far below the regulatory limits.[17] Pre-ozonation can increase the formation of certain halogenated DBPs such as the brominated nitromethanes.[17] NDMA formation has also been reported for the ozone treatment of drinking water and wastewater.[26]

Water treatment processes which combine selected disinfection processes can generate DBPs not crucial for either process. For example, the combination of chloramination and ozonation of waters high in NOM and Br^- concentrations leads to production of dihaloaldehydes while that of chlorine dioxide and either chlorination or chloramination leads to elevated concentrations of 3-chloro-4-(dichloromethyl)-5-hydroxy-2(5H)-furanone (MX) and bromated MXs (BMXs).[11]

The removal of organic pollutants from water by oxidative disinfection is an undesirable strategy due to the ecological implications of DBP formation and release. Thus technologies designed to remove emerging organic chemicals including EDs, pesticides and PPCPs are desirable for both waste and drinking water treatment, especially for those waters that are heavily polluted. Table 1.1 summarizes the available water treatment processes typically employed and the water-quality problems each can address.[6] Among these, only reverse osmosis (RO), activated charcoal (AC) and pre-ozonation are capable of eliminating most pesticides and organic chemicals (only volatile chemicals are well removed by air stripping and the application of RO is largely limited to desalination due to very high costs and problematic fouling of membranes[33,34]). Of these, packed-bed granular activated carbon (GAC) is considered the "Best Available Technology" for the removal of

various regulated organic pollutants.[12] However, as an adsorptive technology, activated charcoal only transports chemicals from one medium (water) to another (charcoal) without chemical transformations.[15] Thus periodic regeneration is necessary since saturated ACs release chemicals into treated water.[6] While powdered activated carbon (PAC) often outperforms GAC, it has the same drawbacks and introduces additional complications associated with its handling.[6] The classes of chemicals well removed by AC and ozone are limited by the mechanisms by which each operates. Moreover, some compounds (atrazine, iopromide, meprobamate, tris(2-carboxyethyl)phosphine (TCEP)) are not well removed by either process.[12] Consequently, an innovative, cost-effective, and largely universal process that removes aqueous pollutants efficiently without producing hazardous byproducts or contaminated material can greatly advance water treatment.

Table 1.1 Water-treatment processes available and water-quality problems addressed.[6]

Process	1	2	3	4	5	6	7	8	9	10	11	12	13	14
Coarse screening	■													
Fine screening	■													
Raw-water storage		■								■				
Preliminary settlement		■												
Aeration					■	■								
Air stripping									■	■				
Coagulation and flocculation			■	■		■				■		■		
Gravity clarification			■	■		■				■		■		
DAF			■	■		■				■		■		
Slow sand filtration			■	■		■				■		■		
Rapid gravity filtration			■	■		■				■		■		
Microfiltration			■	■						■		■		
Ultrafiltration				■						■				
Reverse osmosis							■	■	■		■			
Activated carbon adsorption				■	■			■						
Pre-ozonation				■	■			■	■			■		
Post-ozonation								■	■					■
Ion exchange							■							
Chemical oxidation						■								
pH control						■							■	■
Phosphate dosing													■	
Chlorination						■								■

1. debris; 2. high-sediment load; 3. turbidity; 4. color; 5. taste and odor; 6. iron and manganese; 7. nitrate; 8. pesticides; 9. volatile organic chemicals; 10. *Cryptosporidium*; 11. salinity; 12. algae; 13. plumbosolvency; 14. microbiological quality

1.1.2 Terminology Explanation

Below are the explanations for terminologies used in water treatment processes adjusted from the book <Basic Water Treatment>.[6]

Coagulation: Destabilization and initial coalescing of colloidal particles, specifically hydrophobic colloids.

Flocculation: Long term process of forming larger particles from the small particles formed by coagulation.

Sedimentation: Settlement of the majority of the solids via gravity from water.[35]

Filtration: The process of passing water at low speed through a granular bed that retains most solid matter while permitting the water to pass.

Disinfection: The killing of pathogenic organisms (viruses, bacteria and protozoa) that cause diseases.

Screening: Passage of surface water through a grate to retain debris and aquatic plants while permitting water to pass into treatment facilities.

Raw-water storage: Storage of raw water prior to works to avoid abrupt water source pollution, improve water quality upon settlement of suspended solids and reduce pathogenic organisms, and balance the water supply and demand.

Aeration: Oxygenation of raw water to release carbon dioxide and hydrogen sulfide as well as to oxidize iron and manganese forming precipitates.

Air stripping: Passage of air through water to promote the release of volatile organic chemicals (e.g. trichloroethane and tetrachloroethane) and carbon dioxide.

Reverse osmosis (RO): Removal of all particles and dissolved chemicals from water except a small proportion of dissolved undissociated molecules and dissolved gases by passage through a membrane.

Activated carbon adsorption: Dosing of powdered activated carbon (PAC) to the water or passing of the water through granular activated carbon (GAC) to remove dissolved organic chemicals.

Ozonation: Dosing of ozone in water to use both ozone and hydroxyl radicals for disinfection and oxidation of synthetic organic chemicals and natural color.

Ion exchange: Passing of water through a bed of ion-exchange resin to remove nitrate or soften water, and also for lowering total organic carbon (TOC).

Dissolved air flotation (DAF): A rapid clarification process that mixes a flow of air-supersaturated water with a flocculated suspension into the bottom of the tank to gather low-density solids as a foam on top of the tank, usually preceded by coagulation and flocculation.

Chemical oxidation: The use of an oxidant such as oxygen, chlorine, ozone, chlorine dioxide or potassium permanganate to oxidize contaminants and precipitate iron and manganese.

pH control: Dosing of a chemical to adjust water pH for treatment purposes and to meet the drinking water requirement.

Phosphate dosing: Dosing of orthophosphate to minimize lead concentrations to ~5μg/L.

1.1.3 Emergent Water Treatment Processes

Much work has been devoted to the study of advanced water treatment processes for removal of aqueous organic pollutants. The most studied processes include advanced oxidation processes (AOPs) and ferrate (VI) oxidations.

1.1.3.1 Advanced oxidation processes (AOPs). AOPs are collection of oxidation processes that apply the reactive and non-selective hydroxyl radical (•OH) which is a powerful

oxidant capable of attacking and even mineralizing pollutants.[36] The high reactivity of the •OH makes AOPs well suited to the removal of chemicals that resist traditional treatment processes. Hydrogen peroxide (H_2O_2) based processes, photocatalysis, ozone based processes, and combinations of these are the most widely studied AOPs.[37,38]

1.1.3.1.1 UV/H_2O_2. One of the most broadly studied AOPs, the UV/H_2O_2 process, effects removal of EDs, pesticides and PPCPs including taste and odor compounds, nitrosamines, volatile organic compounds and 1,4-dioxane and has been applied in pilot plants and water treatment plants.[39-42] UV/H_2O_2 produces •OH from homolytic cleavage of O–O bond in H_2O_2.[37] The UV/H_2O_2 process is not restricted by pH and proceeds more rapidly under alkaline conditons.[36,37] Since UV alone is capable of degrading photosensitive compounds such as NDMA and bromate,[21,32] the combination of UV and H_2O_2 incorporates the advantages of both direct UV and AOPs, although the UV dosage employed is typically two orders of magnitude higher than that of disinfection.[16] Such high doses are necessary because of the low extinction coefficient of H_2O_2 (ε_{254} = 18.6−19.6 M^{-1} cm^{-1}),[37,43] which leads to a very low usage efficiency of costly UV light.[44,45] The process also suffers from inefficient use of H_2O_2 with ca. only 10−50% percent consumed resulting in a residual of 50−90% unreacted H_2O_2 after treatment.[42]

1.1.3.1.2 Fenton reaction. This classic catalytic reaction was discovered by Fenton in 1894[36] making it the first AOP. It applies Fe^{2+} as catalyst and H_2O_2 as source of •OH. The catalytic cycle of Fenton reaction is illustrated in Scheme 1.5.[37] Fenton reaction is effective in destroying phenols and herbicides in water.[37] Due to the simplicity of Fenton reaction, it has been applied in removing recalcitrant chemicals such as phenols, formaldehyde, pesticides, wood preservatives, plastic additives, and rubber chemicals from wastewater in

industries.[36,38] One major restriction of Fenton reactions is that a strict pH control is required and a low pH (2.7-2.8) is necessary for catalysis.[37]

In addition, the traditional Fenton reaction produces large quantities of iron sludge waste.[36] Several modified Fenton processes have been developed. Photo-assisted Fenton processes drastically reduce iron sludge waste[36] by irradiating Fe^{3+} photolysis to generate Fe^{2+} which reacts with H_2O_2 to produce •OH. H_2O_2 also photolyzes to •OH by UV light.[46] Photo-sensitizers such as ferrioxalate can be added to further improve this process.[37] Fenton-like processes have also been developed which rely on the release of iron ions from heterogeneous catalysts.[38]

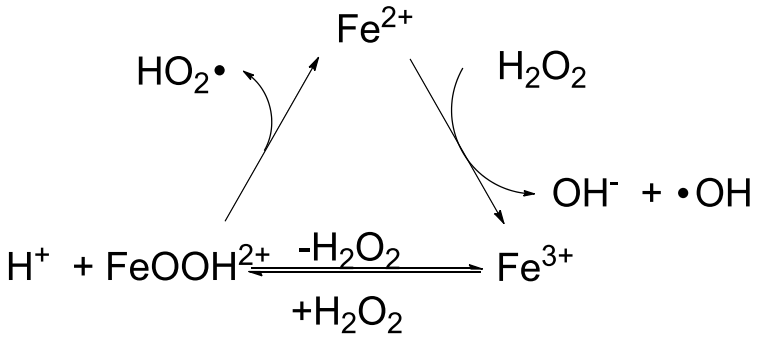

Scheme 1.5 Catalytic cycle of classic Fenton reaction.[37]

1.1.3.1.3 Photocatalysis. Photocatalytic AOPs generate •OH through the use of a semiconductor metal oxide as a heterogeneous catalyst to oxidize H_2O or HO^- to reactive •OH.[36,37] TiO_2 is the most promising among the catalysts tested due to its high stability, excellent performance and low cost.[37] UV/TiO_2 has been used in slurry or supported by glass rings to remove 4-chlorophenol and isoproturon in wastewater treatment.[15] TiO_2 has a high extinction coefficient of $\varepsilon_{254} = 2255\ M^{-1}\ cm^{-1}$.[43] Therefore, it utilizes UV light much

more efficiently than UV/H_2O_2. However, UV/TiO_2 is more easily impeded by the presence of background dissolved organic carbon (DOC) including NOM, which adsorbs to the TiO_2 surface blocking active sites.[43,47] In addition, the process becomes less efficient in the presence of carbonate due to clumping of the TiO_2 nanoparticles which also reduces the available surface area.[47] As discussed in Chapter 2, these limitations render UV/TiO_2 completely ineffective removing the persistent MP metaldehyde from surface water, though it performs as well as UV/H_2O_2 in laboratory grade water (see Chapter 2 for details).[43]

1.1.3.1.4 Ozone. As discussed in section 1.1.1.4, ozone is a potent oxidant that is capable of both MP oxidation and disinfection. Ozone is also regarded as AOP because O_3 is unstable in water and decomposes to form •OH, though the production of •OH reduces disinfection efficiency.[48] Basic conditions expedite this decomposition process and can be used to encourage •OH formation shifting ozonation towards AOP. The impact of NOM on ozone stability in natural waters is unpredictable since some components promote ozone decay while others inhibit it.[48]

1.1.3.1.5 UV/O_3. The UV/O_3 process is comprised of a photolysis step that generates singlet and triplet oxygen atoms (^1D and ^3P) from O_3. The former then reacts with H_2O to form H_2O_2 (^1D) and the latter with organic compounds (^3P).[48]

1.1.3.1.6 O_3/H_2O_2. The addition of H_2O_2 into O_3 processes accelerates •OH formation thereby reducing contact times for •OH exposure. However, this method does not significantly increase the total •OH exposure since the net result of the process is the production of one •OH radical per ozone molecule.[48,49] Due to its comparatively low cost, combined technical performance attributes of both ozonation and AOP, and the safety and

simplicity of handling H_2O_2, O_3/H_2O_2 is the most commonly applied AOP.[48] In addition, conventional (drinking-) water treatment plants already employing ozone for disinfection can be easily retrofitted for ozone-based AOPs—by extending ozonation time, increasing reaction pH, adding H_2O_2 or combining UV irradiation, a conventional ozonation process is converted to an AOP.[48] This technique is recommended for waters in which ozone is stable and the pollutant degradation is slow.[49] However, when O_3 is involved in an AOP, bromate formation is not fully addressed. While H_2O_2 is effective in controlling bromate formation by quickly reducing the critical intermediate $HBrO/BrO^-$ (Scheme 1.4) back to Br^-, this only mutes one of the two bromate forming pathways. Since the other pathway involves both molecular O_3 and •OH and does not rely on $HBrO/BrO^-$ intermediate to form bromate, this carcinogen cannot be eliminated.[31] The amount of bromate formed compared to conventional ozonation depends on the relative dosage of H_2O_2 and O_3.[50]

1.1.3.1.6 Ultrasound. Ultrasound has also been found to facilitate hydroxyl radical production with or without oxidants and has been used in wastewater treatment.[51] However, due to the high energy densities required, the costs of ultrasonic processes are one to two orders of magnitude greater than those of the other AOPs as introduced in this section.[51] Consequently, the outlook for ultrasonic AOPs is substantially less favorable.

To summarize, AOPs are considered a highly promising water treatment technology for organic pollutants that are not removed by conventional techniques.[15] Among all the AOPs developed to date, the O_3, UV/H_2O_2, O_3/H_2O_2 and $UV/O_3/H_2O_2$ processes have the greatest potential for widespread deployment in real-world water treatment practices. However, despite the advantages of the highly-reactive and non-selective •OH, AOPs share common limitations—they are less efficient in treating waters containing high concentrations of

•OH scavengers, typically DOC and carbonate/bicarbonate.[38,48] AOP requires comparatively intensive employment of both capital and energy, and should therefore only be used on the most recalcitrant compounds, i.e., pretreatment is necessary to reduce costs.[10] Additionally, if H_2O_2 is used in an AOP, it must be quenched prior to chlorine disinfection since the existence of H_2O_2 consumes extra chlorine.[42] Regulated DBP levels have also been found to increase if UV/H_2O_2 AOP is quenched by chlorine.[42]

1.1.3.2 Ferrate (VI). Due to its combined effects of oxidant, disinfectant and coagulant, there is much interest in the wider employment of ferrate (Fe(VI)) in water treatment processes.[52] Ferrate is a selective oxidant capable of oxidizing electron-rich organic moieties such as phenolic EDs and olefins, reduced sulfur and nitrogen-containing compounds, metals such as arsenic, and metal complexes like copper (I) cyanide.[52-54] Non-toxic Fe(III) is the major by-product of ferrate oxidation.[53] Micropollutant oxidation by ferrate is equivalent to or slightly less effective than ozone. Ferrate treatments have the additional benefit of phosphate removal due to the ability of the ferric hydroxide by-product to act as a coagulant.[54] Nevertheless, additional Fe(III) is required to further remove phosphate in order to achieve regulatory limits.[54] As a stoichiometric reagent when used on its own, a ferrate concentration that is equal to or higher than the chemical of concern must be applied in order to largely remove the pollutant. However, the combination of ferrate and ionizing radiation can produce the more powerful oxidant Fe(V), and the process also gives •OH which can contribute to the oxidation process.[53] When applied in real-world water where the matrix contains substantial amount of NOM that competes with target chemicals for ferrate, a much larger ferrate dosage is demanded for the prescribed removal of pollutants.[52] The concentration at which ferrate is effective as a

disinfectant is also high—50 μM ferrate is required to effectively inactivate *E. Coli*, an organism used as an indicator.[53] Though the reduction potentials of the ferrate species present at any pH remains high,[53] the instability of those formed at lower pH render ferrate unsuitable for use under acidic conditions.[12]

1.2 TAML/H_2O_2 catalysis: A promising water treatment technology

TAML activators of peroxides (Chart 1.1) are a family of green oxidation catalysts that function similarly to catalase-peroxidase enzymes.[55-57] In the resting state, an Fe^{III} atom occupies the cavity of a deprotonated tetraamido macrocyclic ligand and harnesses the power of H_2O_2 to oxidize targeted molecules in aqueous solutions.[58] TAML catalysts have been investigated for low dose adverse effects (80 nM–250 μM) using in vitro cellular and in vivo zebrafish development assays—all three catalysts used in this study and shown in Chart 1.1 were found to be non-toxic.[59,60] The superior activity of TAML activators in catalysis of the oxidation of hazardous environmental pollutants in water including, *inter alia*, polychlorophenols, natural and synthetic estrogens, pesticides, dyes and active pharmaceutical ingredients by hydrogen peroxide and organic peroxide has been demonstrated.[4,59,61-71]

Chart 1.1 Representative catalysts **1a**, **1b** and **2a** of TAML family used in this study. TAML® is a registered trademark covering tetra-organic-amido-*N* macrocyclic ligand complexes.[72]

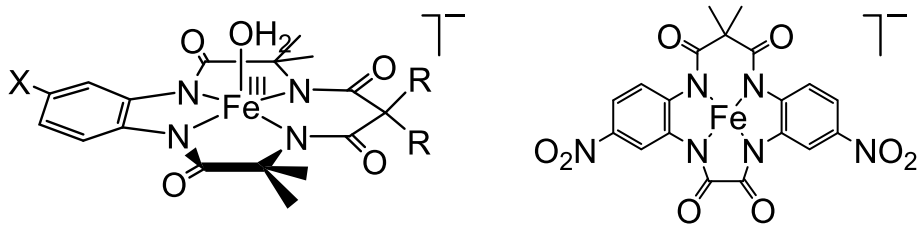

1: X/R = H/Me (**a**); NO_2/F (**b**) **2a**

Though both the Fenton and TAML systems involve iron and H_2O_2, TAML catalysis differs from all AOPs because it does not rely on •OH production—TAML reaction rates are not altered by addition of the radical scavengers cumene or mannitol.[73,74] The TAML reactive intermediates are Fe^{IV} and Fe^{V} relatives of the peroxidase Compounds II and I, respectively.[75,76] In typical aqueous TAML processes, the resting catalysts (Rc) are activated by an oxidant (Ox) such as H_2O_2 to give active catalysts (Ac) that either oxidize a substrate (S) returning Rc and products or undergo catalyst inactivation to form inactive catalysts (Ic) (Scheme 1.6). The rate of substrate oxidation can be modeled by eq. 1.1.[64]

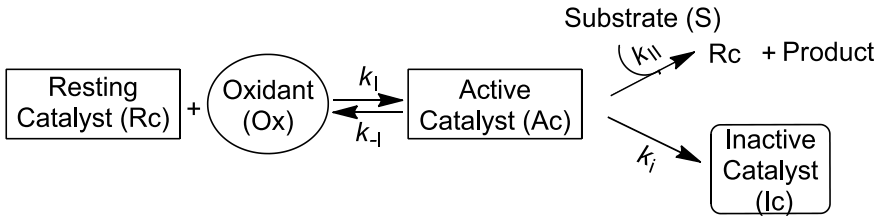

Scheme 1.6 General mechanism of TAML activator catalysis in water.

$$\frac{d[S]}{dt} = \frac{k_I k_{II}[Ox][S]}{k_{-I} + k_I[Ox] + k_{II}[S]} Fe_{Tot} \quad (1.1)$$

1.2.1 Fixed percent of substrate conversion regardless of initial substrate concentration as a feature of TAML catalysis.

Understanding of TAML catalysis has been greatly advanced by the development of eq. 1.2, a mathematical relationship for the final [S], S_∞, as the outcome of the competition between the substrate oxidation (k_{II}) and catalyst inactivation (k_i) processes for Ac (S_0 and Fe_{Tot} are the initial [S] and total [TAML], respectively).[77] Equation 1.2 only applies to oxidation processes where there is an excess of the primary oxidant, substrate consumption is incomplete (S_∞>0), and $Fe_{Tot} < 10^{-6}$ M, i.e. conditions are set such that the catalyst is the limiting species and is completely inactivated through processes that are unimolecular in catalyst before all of the substrate has been oxidized. As indicated by eqs 1.1 and 1.2, though the k_I often plays a role in determining the rate of substrate consumption, the balance between the rates of the k_{II} and k_i processes alone governs the static technical performance of TAML systems.

$$\ln \frac{S_0}{S_\infty} = \frac{k_{II}}{k_i} Fe_{Tot} \tag{1.2}$$

$$\%\ \text{Conversion} = \frac{S_0 - S_\infty}{S_0} \times 100\ \% = \frac{\Delta S}{S_0} \times 100\ \% = \left(1 - e^{-\frac{k_{II}}{k_i} Fe_{Tot}}\right) \times 100\% \tag{1.3}$$

Equation 1.3, a form derived from eq. 1.2, facilitates calculation of the percent conversion of a given substrate under any one set of conditions. As indicated by eq 1.3, the percent removal of any one substrate effected by any one [TAML] aliquot is fixed for each TAML catalyst and substrate pair regardless of S_0 because k_{II}/k_i is constant. Consequently, the performance (percent removal) of any one catalyst aliquot giving a final solution [TAML] of < 10^{-6} M in any oxidation process can be predicted once k_{II}/k_i is known. Figure 1.1, a visual representation of eq. 1.3 as it applies to TAML catalysis, is a useful tool for

determining the catalyst dosage required to achieve a desired removal as well as the removals that can be achieved through TAML catalysis. This feature of TAML catalysis is further established and explored in the TAML/NaClO oxidation of metaldehyde presented in Chapter 3.

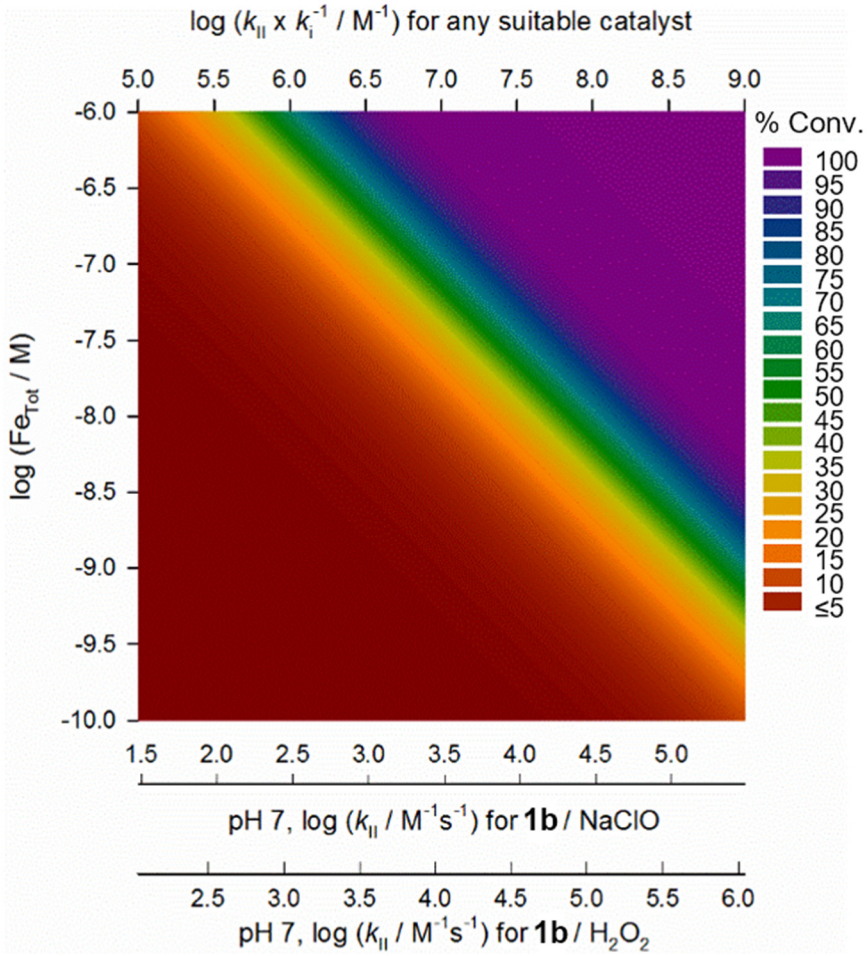

Figure 1.1 Percent of substrate transformed as a function of k_{II}/k_i and Fe_{Tot}. Values were calculated by eq 1.3 using data reported in Chapters 2 and 3.

1.2.2 Turnover number (TON) in TAML catalysis

Since percent conversion is fixed in any one process, the number of moles of S oxidized declines as S_0 declines. Consequently, the TON also declines with S_0 as indicated in eq. 1.4. This occurs because the rate of the substrate oxidation step (-d[S]/dt = k_{II}[S][Ac]) diminishes with [S] while that of Ac inactivation (d[Ic]/dt = k_i[Ac]) does not, and these compete for [Ac]. Since the absolute substrate removal declines with S_0, assessments of the relative technical performances of TAML catalysts and processes on the basis of TON and material efficiency ($\frac{\text{mass of substrate transformed}}{\text{mass of material added}}$) must be made using data collected under identical conditions. Therefore, TON, which is often used to compare the relative efficiencies of catalysts, is of limited utility for comparing aqueous TAML processes. Nevertheless, insight into the effects of substrate dilution on TAML processes can be gained through interpretation of the TON expression eq 1.4 under two limiting cases.

$$\text{TON} = \frac{\left(1-e^{-\frac{k_{II}}{k_i}\text{Fe}_{\text{Tot}}}\right)}{\text{Fe}_{\text{Tot}}}\text{S}_0 \tag{1.4}$$

$$e^{-\frac{k_{II}}{k_i}\text{Fe}_{\text{Tot}}} = \sum_{n=0}^{\infty}\frac{\left(-\frac{k_{II}}{k_i}\text{Fe}_{\text{Tot}}\right)^n}{n!} = 1 + \left(-\frac{k_{II}}{k_i}\text{Fe}_{\text{Tot}}\right) + \delta\left(-\frac{k_{II}}{k_i}\text{Fe}_{\text{Tot}}\right) \tag{1.5}$$

Here $\delta\left(-\frac{k_{II}}{k_i}\text{Fe}_{\text{Tot}}\right) = \sum_{n=2}^{\infty}\frac{\left(-\frac{k_{II}}{k_i}\text{Fe}_{\text{Tot}}\right)^n}{n!}$ which can be ignored when $\frac{k_{II}}{k_i}\text{Fe}_{\text{Tot}} < 1$

$$\text{TON} \approx \frac{\left(1-(1+\left(-\frac{k_{II}}{k_i}\text{Fe}_{\text{Tot}}\right))\right)}{\text{Fe}_{\text{Tot}}}\text{S}_0 = \frac{k_{II}}{k_i}\text{S}_0 \tag{1.6}$$

For slowly reacting substrates with a low k_{II} such as metaldehyde studied in Chapters 2 and 3 (the experimental **1b**/H_2O_2 k_{II} value is 120 $M^{-1}s^{-1}$) where $k_{II}Fe^{III}_{Tot}/k_i < 1$, eq 1.4 can be approximated by the first term of a Maclaurin series, TON ~ $k_{II}S_0/k_i$ (eqs. 1.5 and 1.6,

contributions from the higher order terms of the series are negligible). This TON relation is simply the ratio of the rates of the substrate oxidation and inactivation steps discussed above. Consequently, TON is independent of Fe_{Tot} for slowly transformed substrates. In contrast, for rapidly transformed, high k_{II} substrates, TON is inversely proportional to Fe^{III}_{Tot}. Here, $e^{-\frac{k_{II}}{k_i}Fe^{III}_{Tot}} \leq 0.1$ and the numerator of eq 1.4 approaches 1. As a result, TON $\sim S_0/Fe^{III}_{Tot}$. The TON increases with progressively decreasing catalyst aliquot size derive from the progressively smaller ΔS. Here, smaller aliquots give higher TON because the higher removals that can be performed by greater catalyst loadings cause substantial dilution of the substrate throughout the catalytic process. This result is deceptive. This does not mean that multiple small aliquots are more efficient at achieving a set percent transformation than their equivalent one large aliquot because dilution lowers the average TON of both equally (the next paragraph gives a mathematical proof).

Mathematical proof: For Fe_{Tot} = a, b% removal is obtained. Equation 1.2 becomes:

$$\ln\frac{S_0}{S_0(100-b)\%} = \frac{k_{II}}{k_i}a$$

$$\Rightarrow b = 100 \times (1 - e^{-\frac{k_{II}}{k_i}a})$$

when one aliquot $Fe_{Tot} = \frac{a}{n}$, and the substrate is treated with n aliquots of catalyst. The overall removal c% can be calculated via following equation, where c has an identical expression as b:

$$c\% = (1 - \left(\frac{S_1}{S_0}\right)^n) \times 100\% = (1 - (e^{-\frac{k_{II}a}{k_i n}})^n) \times 100\%$$

$$\Rightarrow c = 100 \times (1 - (e^{-\frac{k_{II}a}{k_i n}\times n})) = 100 \times (1 - e^{-\frac{k_{II}}{k_i}a}) = b$$

S_1 represents the substrate concentration after the first $\frac{a}{n}$ catalyst aliquot treatment. Since the percent removal is the same across the treatments, the percent of the substrate remaining is also the same for each aliquot catalyst treatment and is calculated from the first aliquot catalyst treatment. This calculation shows that the percent removal c equals b, which means that several smaller catalyst aliquots do the same amount of work as the equivalent one large aliquot provided $[Fe_{Tot}] < 10^{-6}$ M.

1.3 Introduction to this work

The background presented above provides essential knowledge for understanding why TAML catalysis is a revolutionary technology, the most important advance in water purification since the introduction of ozone for drinking water treatment in the early 20th century. This work adds significantly to demonstrating the potential of TAML catalysis for advancing water treatment and extends TAML catalysis to oxygen activation in reverse micelles. The ability of TAML catalysts to remediate very difficult to oxidize aqueous pollutants is demonstrated through a study of the slow oxidation of metaldehyde, an extremely persistent MP that is not effectively removed by conventional water treatment processes including chlorine, ozone, or activated carbon. A study of the impact of substituting NaClO for H_2O_2 in the TAML system which most effectively removes metaldehyde reveals oxidant substitution to be a method for improving the performance of TAML processes and the trajectory for developing more effective TAML systems to be maximizing the k_{II}/k_i ratio. Studies are undertaken to determine whether several DBPs that are of concern for current disinfection processes are produced in TAML systems to examine the impacts of applying TAML catalysis in water purification. A detailed kinetic

study of catalyst activation is presented that has advanced understanding of the k_I process which is rate determining in most TAML applications. Finally, the potential applications of TAML catalysis are extended through a study of the reactivity of less reactive TAML/O_2 systems in reverse micelles.

1.4 References

(1) Hsieh, Y. H. P.; Rudloe, J. *Trends Food. Sci. Tech.* **1994**, *5*, 225.

(2) Helmenstine, A. M. http://chemistry.about.com/od/waterchemistry/f/How-Much-Of-Your-Body-Is-Water.htm, 2015.

(3) In *The Water Cycle*; The USGS Water Science School: http://water.usgs.gov/edu/watercycle.html, 2016.

(4) Banerjee, D.; Markley, A. L.; Yano, T.; Ghosh, A.; Berget, P. B.; Minkley, E. G.; Khetan, S. K.; Collins, T. J. *Angew. Chem. Int. Edit.* **2006**, *45*, 3974.

(5) Sedlak, D. *Water 4.0—The past, Present, and Future of the World's Most Vital Resource*; Yale University Press: New Haven, London, 2014.

(6) Binnie, C.; Kimber, M. *Basic Water Treatment*; Fifth ed.; ICE Publishing: London, UK, 2013.

(7) *2006 Community Water System Survey*, Office of Water, US EPA, 2009.

(8) Sedlak, D. L.; von Gunten, U. *Science* **2011**, *331*, 42.

(9) In *Endocrine Disruptors*; NIEHS: http://www.niehs.nih.gov/health/topics/agents/endocrine/index.cfm, 2015.

(10) Del Moro, G.; Mancini, A.; Mascolo, G.; Di Iaconi, C. *Chem. Eng. J.* **2013**, *218*, 133.

(11) Richardson, S. D. *Trac-Trend Anal. Chem.* **2003**, *22*, 666.

(12) Westerhoff, P.; Yoon, Y.; Snyder, S.; Wert, E. *Environ. Sci. Technol.* **2005**, *39*, 6649.

(13) Bolong, N.; Ismail, A. F.; Salim, M. R.; Matsuura, T. *Desalination* **2009**, *239*, 229.

(14) Johnson, A. C.; Sumpter, J. P. *Environ. Sci. Technol.* **2001**, *35*, 4697.

(15) Oller, I.; Malato, S.; Sanchez-Perez, J. A. *Sci. Total Environ.* **2011**, *409*, 4141.

(16) G. F. IJpelaar; D. J. H. Harmsen; Heringa, M. *UV disinfection and UV/H_2O_2 oxidation: by-product formation and control*, Kiwa WR, 2007.

(17) Agus, E.; Voutchkov, N.; Sedlak, D. L. *Desalination* **2009**, *237*, 214.

(18) Gallard, H.; von Gunten, U. *Water Res.* **2002**, *36*, 65.

(19) Westerhoff, P.; Chao, P.; Mash, H. *Water Res.* **2004**, *38*, 1502.

(20) Liu, C.; von Gunten, U.; Croue, J. P. *Water Res.* **2013**, *47*, 5307.

(21) Mitch, W. A.; Sharp, J. O.; Trussell, R. R.; Valentine, R. L.; Alvarez-Cohen, L.; Sedlak, D. L. *Environ. Eng. Sci.* **2003**, *20*, 389.

(22) USEPA *Technical Fact Sheet-N-Nitroso-dimethylamine (NDMA)*, 2014.

(23) Condie, L. W. *J. Am. Water Works Ass.* **1986**, *78*, 73.

(24) USEPA *National Primary Drinking Water Regulations*, 2009.

(25) Buffle, M. O.; Galli, S.; von Gunten, U. *Environ. Sci. Technol.* **2004**, *38*, 5187.

(26) Zimmermann, S. G.; Wittenwiler, M.; Hollender, J.; Krauss, M.; Ort, C.; Siegrist, H.; von Gunten, U. *Water Res.* **2011**, *45*, 605.

(27) von Gunten, U.; Hoigne, J. *Environ. Sci. Technol.* **1994**, *28*, 1234.

(28) Heeb, M. B.; Criquet, J.; Zimmermann-Steffens, S. G.; von Gunten, U. *Water Res.* **2014**, *48*, 15.

(29) von Gunten, U.; Bruchet, A.; Costentin, E. *J. Am. Water Works Ass.* **1996**, *88*, 53.

(30) von Gunten, U. *Water Res.* **2003**, *37*, 1469.

(31) von Gunten, U.; Oliveras, Y. *Environ. Sci. Technol.* **1998**, *32*, 63.

(32) Herley, P. J. *J. Chem. Phys.* **1967**, *46*, 627.

(33) Zhang, R.; Liu, Y.; He, M.; Su, Y.; Zhao, X.; Elimelech, M.; Jiang, Z. *Chem. Soc. Rev.* **2016**, *Advanced Article*.

(34) Greenlee, L. F.; Lawler, D. F.; Freeman, B. D.; Marrot, B.; Moulin, P. *Water Res.* **2009**, *43*, 2317.

(35) EPA. https://iaspub.epa.gov/tdb/pages/treatment/treatmentOverview.do?treatmentProcessId=1934681921.

(36) Vogelpohl, A. *Water Sci. Technol.* **2007**, *55*, 207.

(37) Andreozzi, R.; Caprio, V.; Insola, A.; Marotta, R. *Catal. Today* **1999**, *53*, 51.

(38) Pera-Titus, M.; Garcia-Molina, V.; Banos, M. A.; Gimenez, J.; Esplugas, S. *Appl. Catal. B Environ.* **2004**, *47*, 219.

(39) Scheideler, J.; Bosmith, A. *Aqua Gas* **2014**, *94*, 52.

(40) TrojanUV. *TrojanUV Solutions: Removal of Metaldehyde, a Pesticide Found in UK Drinking Water Sources.* .

(41) Rosenfeldt, E. J.; Linden, K. G. *Environ. Sci. Technol.* **2004**, *38*, 5476.

(42) Cotton, C.; Dotson, A.; Joussét, S.; Linden, K.; Collins, J. In *WQTC Conference Proceedings*; American Water Works Associations: Savannah, GA, 2010.

(43) Autin, O.; Hart, J.; Jarvis, P.; MacAdam, J.; Parsons, S. A.; Jefferson, B. *Water Res.* **2012**, *46*, 5655.

(44) James, C. P.; Germain, E.; Judd, S. *Sep. Purif. Technol.* **2014**, *127*, 77.

(45) Katsoyiannis, I. A.; Canonica, S.; von Gunten, U. *Water Res.* **2011**, *45*, 3811.

(46) Pignatello, J. J.; Oliveros, E.; MacKay, A. *Crit. Rev. Env. Sci. Tec.* **2006**, *36*, 1.

(47) Autin, O.; Hart, J.; Jarvis, P.; MacAdam, J.; Parsons, S. A.; Jefferson, B. *Water Res.* **2013**, *47*, 2041.

(48) von Gunten, U. *Water Res.* **2003**, *37*, 1443.

(49) Rosenfeldt, E. J.; Linden, K. G.; Canonica, S.; von Gunten, U. *Water Res.* **2006**, *40*, 3695.

(50) von Gunten, U.; Bruchet, a.; Costentin, E. *AWWA* **1996**, *88*, 53.

(51) Mahamuni, N. N.; Adewuyi, Y. G. *Ultrason. Sonochem.* **2010**, *17*, 990.

(52) Lee, Y.; Yoon, J.; Von Gunten, U. *Environ. Sci. Technol.* **2005**, *39*, 8978.

(53) Sharma, V. K. *Adv. Environ. Res.* **2002**, *6*, 143.

(54) Lee, Y.; Zimmermann, S. G.; Kieu, A. T.; von Gunten, U. *Environ. Sci. Technol.* **2009**, *43*, 3831.

(55) Collins, T. J. *Acc. Chem. Res.* **2002**, *35*, 782.

(56) Collins, T. J.; Khetan, S. K.; Ryabov, A. D. In *Handbook of Green Chemistry*; Anastas, P. T., Crabtree, R. H., Eds.; WILEY-VCH Verlag GmbH & KgaA: Weinheim, 2009, p 39.

(57) Ryabov, A. D.; Collins, T. J. *Adv. Inorg. Chem.* **2009**, *61*, 471.

(58) Tang, L. L.; Gunderson, W. A.; Weitz, A. C.; Hendrich, M. P.; Ryabov, A. D.; Collins, T. J. *J. Am. Chem. Soc.* **2015**, *137*, 9704.

(59) Ellis, W. C.; Tran, C. T.; Roy, R.; Rusten, M.; Fischer, A.; Ryabov, A. D.; Blumberg, B.; Collins, T. J. *J. Am. Chem. Soc.* **2010**, *132*, 9774.

(60) Truong, L.; DeNardo, M. A.; Kundu, S.; Collins, T. J.; Tanguay, R. L. *Green Chem.* **2013**, *15*, 2339.

(61) Sen Gupta, S.; Stadler, M.; Noser, C. A.; Ghosh, A.; Steinhoff, B.; Lenoir, D.; Horwitz, C. P.; Schramm, K. W.; Collins, T. J. *Science* **2002**, *296*, 326.

(62) Chanda, A.; Khetan, S. K.; Banerjee, D.; Ghosh, A.; Collins, T. J. *J. Am. Chem. Soc.* **2006**, *128*, 12058.

(63) Beach, E. S.; Malecky, R. T.; Gil, R. R.; Horwitz, C. P.; Collins, T. J. *Catal. Sci. Technol.* **2011**, *1*, 437.

(64) Chahbane, N.; Popescu, D. L.; Mitchell, D. A.; Chanda, A.; Lenoir, D.; Ryabov, A. D.; Schramm, K. W.; Collins, T. J. *Green Chem.* **2007**, *9*, 49.

(65) Mondal, S.; Hangun-Balkir, Y.; Alexandrova, L.; Link, D.; Howard, B.; Zandhuis, P.; Cugini, A.; Horwitz, C. P.; Collins, T. J. *Catal. Today* **2006**, *116*, 554.

(66) Shappell, N. W.; Vrabel, M. A.; Madsen, P. J.; Harrington, G.; Billey, L. O.; Hakk, H.; Larsen, G. L.; Beach, E. S.; Horwitz, C. P.; Ro, K.; Hunt, P. G.; Collins, T. J. *Environ. Sci. Technol.* **2008**, *42*, 1296.

(67) Shen, L. Q.; Beach, E. S.; Xiang, Y.; Tshudy, D. J.; Khanina, N.; Horwitz, C. P.; Bier, M. E.; Collins, T. J. *Environ. Sci. Technol.* **2011**, *45*, 7882.

(68) Kundu, S.; Chanda, A.; Espinosa-Marvan, L.; Khetan, S. K.; Collins, T. J. *Catal. Sci. Technol.* **2012**, *2*, 1165.

(69) Mills, M. R.; Arias-Salazar, K.; Baynes, A.; Shen, L. Q.; Churchley, J.; Beresford, N.; Gayathri, C.; Gil, R. R.; Kanda, R.; Jobling, S.; Collins, T. J. *Scientific Reports* **2015**, *5*, article number: 10511.

(70) Ghosh, A.; Mitchell, D. A.; Chanda, A.; Ryabov, A. D.; Popescu, D. L.; Upham, E.; Collins, G. J.; Collins, T. J. *J. Am. Chem. Soc.* **2008**, *130*, 15116.

(71) Ellis, W. C.; Tran, C. T.; Denardo, M. A.; Fischer, A.; Ryabov, A. D.; Collins, T. J. *J. Am. Chem. Soc.* **2009**, *131*, 18052.

(72) Collins, T. J.; Gordon-Wylie, S. W. US Patent 5,847,120, 1998.

(73) Collins, T. J.; Ryabov, A. D.; EPA: 2004-2007.

(74) Ghosh, A.; de Oliveira, F. T.; Yano, T.; Nishioka, T.; Beach, E. S.; Kinoshita, I.; Munck, E.; Ryabov, A. D.; Horwitz, C. P.; Collins, T. J. *J. Am. Chem. Soc.* **2005**, *127*, 2505.

(75) Chanda, A.; Shan, X.; Chakrabarti, M.; Ellis, W.; Popescu, D.; Tiago de Oliveria, F.; Wang, D.; Que, L., Jr.; Collins, T. J.; Münck, E.; Bominaar, E. L. *Inorg. Chem.* **2008**, *47*, 3669.

(76) Dunford, H. B. *Heme Peroxidases*; Wiley-VCH: NY, Chichester, Weinheim, 1999.

(77) Emelianenko, M.; Torrejon, D.; DeNardo, M. A.; Socolofsky, A. K.; Ryabov, A. D.; Collins, T. J. *J. Math. Chem.* **2014**, *52*, 1460.

Chapter 2

Is the TAML/H_2O_2 system more advanced in terms of oxidizing "invincible" substrates?

—Degrading the Water Treatment Industry's Most Challenging Micropollutant, Metaldehyde

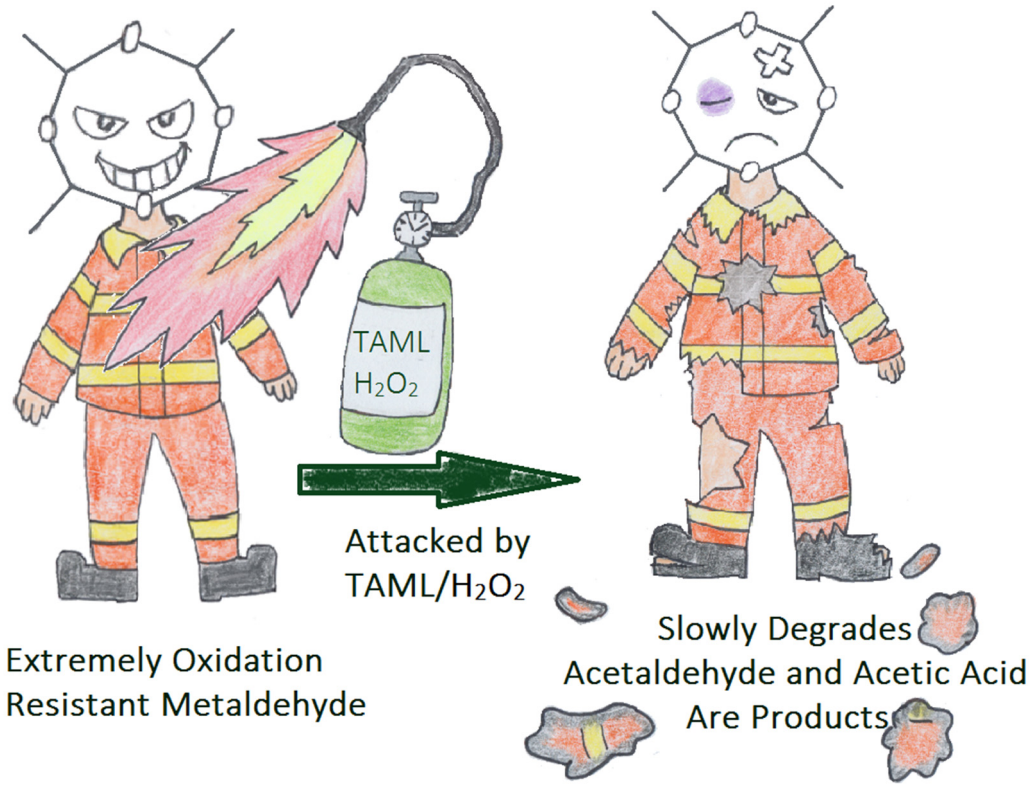

2.1 Introduction

Metaldehyde (Met), the cyclic tetramer of acetaldehyde (Chart 2.1), is deployed as a molluscicide to control populations of gastropods including slugs and snails. Met accomplishes this by blocking the rehydration of gastropod mucous cells which impedes locomotion.[1] The rat oral LD_{50} of 283-690 mg/kg (Table 2.1) implies that Met is only lethal at high concentrations.[2,3] According to the European Food Safety Authority (EFSA), the current environmental concentrations of Met do not pose a threat to human health.[4] However, studies have shown that Met contamination is harmful to the environment. Even single dose exposures to low soil [Met] of <100 ppm significantly decreases the survival and reproductive capacity of an arthropod *F. Candida*.[5] In addition, exposure to the UK prescribed concentration or value (PCV) for all pesticides including Met of 0.1 μg/L has been shown to cause higher incidences of hemocyte mortality, or decreased cell size and diminished non-specific esterase activity in pacific oysters *Crassostrea gigas*—which of these effects is observed depends on the oyster family.[1] Due to the environmental persistence and potential toxicity of metaldehyde, Met alternatives have been investigated. Since it is classified as Generally Recognized As Safe (GRAS) by the US Food and Drug Administration (FDA) and present in food, caffeine was once regarded as "an environmentally acceptable" general purpose pesticide and proposed as a Met substitute.[6] However, caffeine is more toxic than Met and less environmentally friendly since larger quantities are required for the treatment of mollusks.[7] Recently, environmental groups have emerged that encourage the use of better practices in the application of metaldehyde pellets in order to reduce the presence of Met in the environment by minimizing the quantities applied to soils.[8] Nevertheless, the recurrence of Met in source waters remains a concern.

Table 2.1 Properties of metaldehyde.

Distribution / tonnes	$t_{1/2, H_2O}$ / days	Soil Lifetime / days	log (Kow)	Solubility / mg L^{-1}	ε_{254} / M^{-1} cm^{-1}	LD_{50} / mg kg^{-1}
1400[a]	6150[b]	60[c] 45[d]	0.12[9,10]	200[e]	21.4[11]	420-690[f]

[a]UK, tonnes 2008–2012;[10] [b]Hydrolysis half-life resulting from H_2O reaction, compounds having values >14 days have been determined to be potential groundwater contaminants;[12,13] [c]50–78% oxidized to CO_2 in aerobic soil;[9] [d]To reach 10% mineralization in anaerobic soil;[9] [e]Aq. 20 °C, pH 5, 6.5, 7.2, 9;[9,10] [f] Oral rat.[2]

Chart 2.1 Structures of Met and the TAML catalysts used in this chapter.

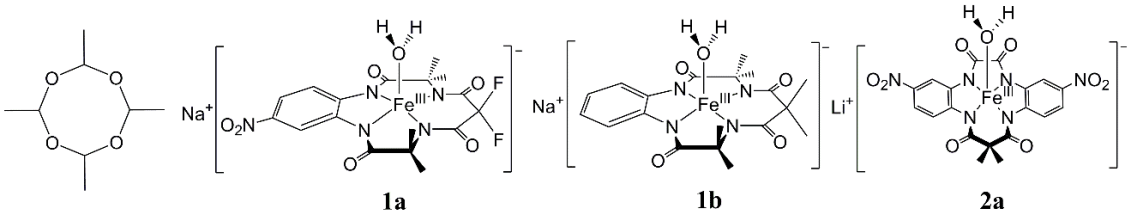

2.1.1 The Met problem in the United Kingdom (UK)

Though Met has been employed since the 1940s, it has not been detected in surface water until the past decade. The relatively recent date of Met detection is likely due to improvements in analytical techniques.[14] Met is one of the most recalcitrant anthropogenic water contaminants with a half-life in water of nearly 17 years.[12] At low concentrations in water, the broad distribution, moderate water solubility and enduring persistence conspire to make Met a contaminant of regulatory concern impacting, for example, UK, French, and Swedish drinking water sources (Table 2.1).[14-17] The UK Environment Agency has reported that between 2009 and 2011 Met was found in 81 of 647 reservoirs in England and Wales.[18] Reports from the UK Drinking Water Inspectorate (DWI, Figure 2.1)[19] indicate that in England and Wales, the majority of the failures of drinking water to meet

the PCV for pesticides are due to detections of Met at concentrations in excess of this regulatory limit (Table 2.2). These occur most frequently in the Central and Eastern as well as London and South East regions indicating that Met contamination impacts a considerable amount of the English population.

Table 2.2 Incidences of failures to meet the individual pesticide and metaldehyde 0.1 µg/L regulation in England and Wales during the years 2008−2015 according to the DWI drinking water annual report.[19]

Year	Wales		England								Total	
			Central and Eastern region		London and South East region		Northern region		Western region			
	Met[a]	Pet[b]	Met[a]	Pet[b]	Met[a]	Pet[b]	Met[a]	Pet[b]	Met[a]	Pet[b]	Met[a]	Pet[b]
2008	0	0	0	4	7	11	0	2	8	9	15	26
2009	0	2	282	296	59	63	19	24	0	2	360	387
2010	0	0	55	65	3	3	2	3	1	2	61	73
2011	0	0	37	38	3	7	6	9	0	2	46	56
2012	0	0	91	91	90	95	50	65	2	2	233	253
2013	0	3	265	269	57	72	2	3	0	2	324	349
2014	0	1	84	87	33	35	16	19	1	1	134	143
2015	0	0	36	38	19	19	10	12	0	0	65	69
Total	0	6	850	888	271	305	105	137	12	20	1238	1356

[a]Met: Number of tests not meeting the metaldehyde standard; [b]Pet: Number of tests not meeting the pesticide standard.

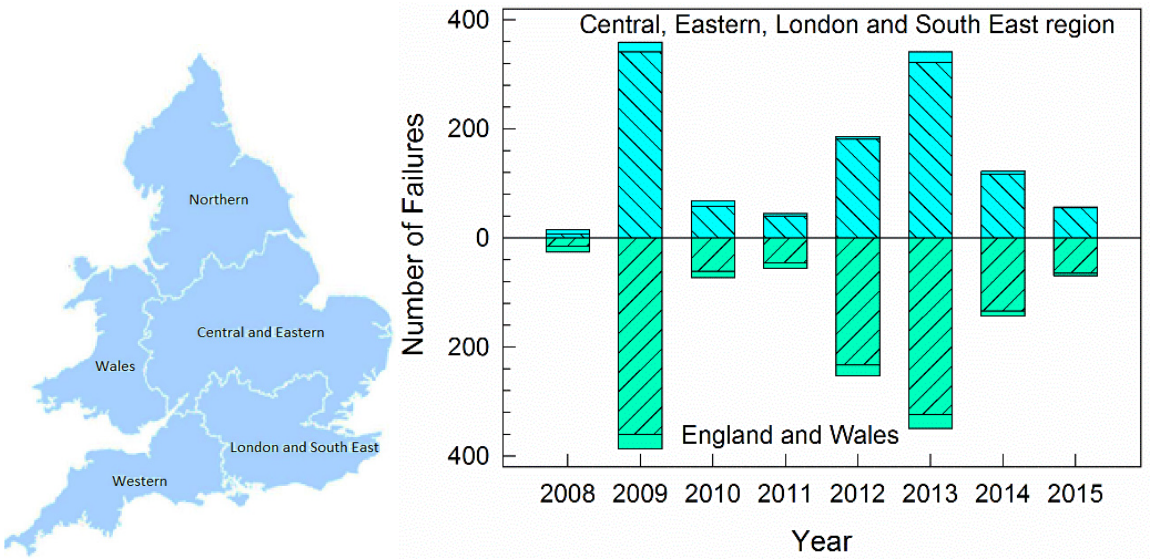

Figure 2.1 Left: Schematic map of England and Wales showing the partitions of the regions considered in Table 2.2 adopted from the DWI drinking water annual report.[19] Right: Bar chart showing number of drinking water tests not meeting the individual pesticide standard in the Central, Eastern, London and South East regions of England alone (top) and in England and Wales together (bottom) with those attributable to Met alone indicated by the shaded bars.

2.1.2 Available remediation methods for Met[20]

The detection of Met in European drinking water sources[15-17,21] has sparked interest in methods for its removal. For most micropollutants (MPs), weighing the combined merits of familiarity to the industry and technical, cost and environmental performances has led to the conclusion that adsorption on activated carbon (AC), granular (GAC) or powdered (PAC), or oxidative degradation by ozone are the most desirable treatment processes—ozone and AC processes are being developed today for final stage removal of MPs from Swiss municipal water treatment effluent.[22] However, these two processes are not very effective at removing Met. Consequently, a much more expensive UV/H_2O_2 process has been deployed in some UK and German cities.[23,24] A mini-review of currently available

Met remediation methods from the literature has been produced here to establish the extraordinary difficulty of treating Met contaminated waters. Here, the technical performances of available remediation technologies have been critically surveyed and compared. The mini-review is organized into three sections: (*i*) absorptive technologies, (*ii*) UV-dependent technologies, and (*iii*) oxidative, acid catalyzed, and biological technologies. Three tables (Tables 2.3−2.5) summarizing the corresponding studies are presented at the end of this section.

As discussed in Chapter 1, TAML catalysis suffers from diminished substrate (S) concentration conversion (Δ[S]) with decreasing [S] as a consequence of competition between the catalyst inactivation and substrate oxidation processes. A similar trend may hold for other water purification technologies. For example, a constant % adsorption is observed for three different forms of PAC studied (Figure 2.2).[25] The uncertainty of whether the removals reported for other Met removal methods will scale proportionately from the tested $[Met]_0$ to environmental concentrations complicates comparisons between these technologies. As a result, only qualitative comparisons are provided in this review.

2.1.2.1. Adsorptive Technologies. Classical adsorptive technologies employ AC derived products. These are widely used in municipal and drinking water treatment.[26] The analysis contained in this section indicates that while GAC can effect a 30−50% removal of Met, it cannot reliably achieve the PCV if the influent concentration is greater than 0.15 μg/L.[11] Typical October−December peak concentrations in, for example, the rivers of Yorkshire range from 0.4–0.6 μg/L.[9,11,27] Higher removals have been reported for higher surface area powdered activated carbon (PAC) where the difficulty of implementation[9] is associated

with the practical details of handling PAC (Table 2.3, E3 and 4)—reaching the PCV also requires disposal of a substantial amount of PAC waste.[25]

Recent work has shown that some adsorbents are more efficient than AC for Met remediation, including particularly attractive increases in adsorption efficiency at low [Met]. Phenolic resin-derived activated carbons (PC) of similar particle size to PAC have been reported to adsorb Met better than either GAC or PAC[9] in the absence of interference from NOM or inorganic salts (Table 2.3, E3, 6, and 13).[9] However, concerns have been raised about leeching of phenolic components into treated water,[10] and cost and regeneration issues remain to be clarified. The authors note that the sulfonate groups of PC could cause a chemical transformation of Met, but the method has largely been considered to be adsorptive.[9]

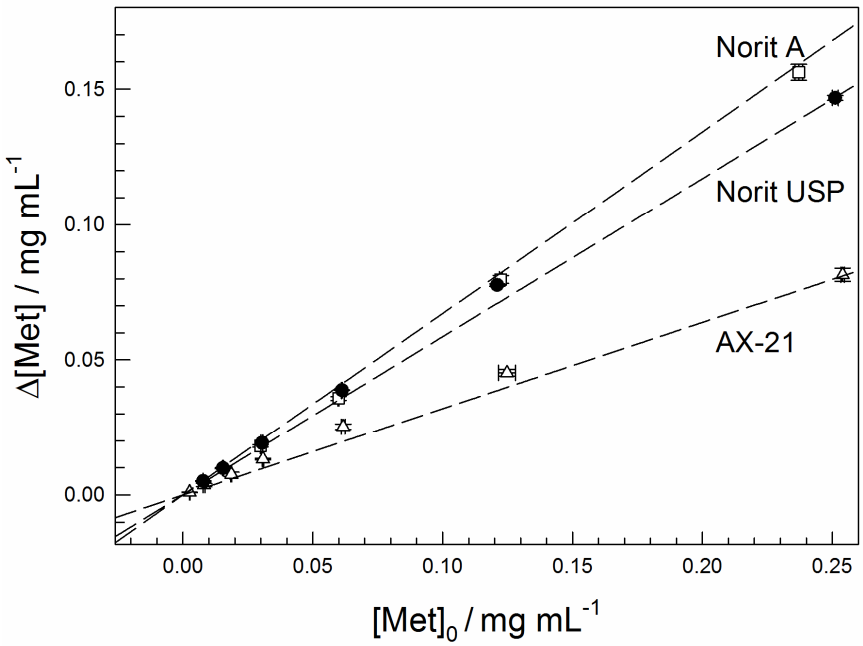

Figure 2.2 Met removal ($\Delta[Met] = [Met]_0 - [Met]_\infty$) as a function of initial Met concentration ($[Met]_0$) for treatment with three forms of activated charcoal.[25] Conditions are as described in Table 2.3.

2.1.2.2. UV_{254}-dependent technologies. A substantial body of research has been dedicated to developing UV-based methods for Met removal. Table 2.4 lists the performance of each studied process with the relevant operational parameters. The most successful approaches involve advanced oxidation processes (AOPs). These rely upon the high reactivity and low selectivity of the hydroxyl radical (•OH).[28] UV_{254}/H_2O_2, the most effective Met-removing AOP in the available literature, has been shown to be capable of 98% removal (Table 2.4, E8) and is currently deployed in Lincoln, UK.[23] The rate of Met decomposition was competitively reduced, but not quashed, by the presence of more easily oxidized natural organic matter (NOM) surrogates.[11,29] Alkalinity (bicarbonate/carbonate) does not greatly impact the technical performance (Table 2.4, E11 and 12). However, remediation of low [Met] requires a UV dosage that is significantly greater than the 750 mJ cm^{-2} or less typically delivered for less resilient contaminants by already expensive UV_{254}/H_2O_2 treatments.[24,29,30] This is noteworthy as approximately 65% of the cost of UV_{254}/H_2O_2 has been ascribed to the energy consumption with an additional 25% attributable to lamp replacement.[28,31]

With a ε_{254} value that is ca. two orders of magnitude greater than that of H_2O_2, TiO_2 generates •OH more efficiently at the mediator surface—the efficiency is reduced by rapid electron-hole recombination.[11] Under appropriate conditions, UV_{254}/TiO_2 can completely degrade Met (Table 2.4, E16). However, the approach is very sensitive to dissolved organic carbon (DOC) showing a drop in total Met degradation from 100% to 7% in the presence of 8.7 mg L^{-1} DOC, despite a doubling of the UV dosage (Table 2.4, E16 and 17). Since •OH are produced at the particle surface and not in solution as for UV_{254}/H_2O_2, NOM diminishes •OH production all the way to complete inhibition by reactively coating the

surface of the particles.[11] Carbonate, the most prevalent buffering ion in natural waters also negatively impacts the technical performance of UV_{254}/TiO_2. Clumping of the TiO_2 particles in the presence of carbonate ions decreases the reactive surface area and degradation rate.[29] Since DOC interference of Met degradation by UV_{254}/H_2O_2 can be overcome by increasing UV dosage (Table 2.4, E4 and 5) while that of UV_{254}/TiO_2 cannot (Table 2.4, E15 and 16) and UV_{254}/H_2O_2 is not significantly impacted by the presence of alkalinity while UV_{254}/TiO_2 is (Table 2.4, E18 and 20), the former has been determined to be more promising.[11,29]

2.1.2.3. Oxidative, Acid Catalyzed, and Biological Technologies. Other efforts have been made to decrease the energy demands of •OH production. While O_3 alone is ineffective at reducing Met to meet the PCV,[11,32] in a pilot trial O_3/H_2O_2 was found to reduce Met by 72% (Table 2.5, E4).[5,21] This is well below the performance of UV_{254}/H_2O_2 (95% removal; Table 2.4, E6) under the same conditions. While treatment with O_3/H_2O_2 costs more than treatment with O_3 alone, the total cost of using O_3/H_2O_2 on a large scale has been estimated to be 33% less than projected for UV_{254}/H_2O_2.[24] An energy optimized process which follows O_3/H_2O_2 with UV_{254}, (90% removal, Table 2.5, E14) requires less than half the UV flux of UV_{254}/H_2O_2 while matching the efficiency with respect to H_2O_2 and thus saves ~13% energy.[24]

In situ remediation approaches that do not rely upon •OH have also been pursued. The Arvia process is based on a continuous adsorption-electrochemical regeneration cycle that couples adsorption to Nyex™, a graphite intercalation compound, with electrochemical oxidation.[10] This method achieved 99% conversion of Met (Table 2.5, E6). Acetaldehyde is not observed as a product leading the developers to conclude that the final product is

CO_2. The Met adsorption capacity of Nyex is limited to 18 μg g^{-1} and this value decreases by 20% in the presence of 10 mg L^{-1} total organic carbon (TOC). While the adsorbent can be reused without deterioration over at least seven cycles, regenerative energy demands are high with an optimum voltage of 3.8 V at a fixed applied current of 0.5 A.[10]

Met decomposition with sulfonic acid functionalized mesoporous silica (SAFMS) represents an interesting in situ destructive approach.[33] The high local proton concentration within the SAFMS pores has been reported to drive acid catalyzed decomposition of Met to yield acetaldehyde, a probable human carcinogen[34,35] which is undesirable though no international drinking water guideline has been established. Chlorination of acetaldehyde containing water can result in the formation of chloral hydrate (trichloroacetaldehyde), which may subsequently degrade to chloroform depending on the pH, temperature, and maturity of the water.[36] The SAFMS process is coupled with adsorption of the acetaldehyde product on an amine bearing macroporous ion exchange resin. Met was reduced by greater than 95% (Table 2.5, E7). Sulfonic acid functionalized macronets (MN502) developed in the same group perform similarly (Table 2.5, E8). Since Ca^{2+}, a common drinking water ion, interferes with sulfonic acid groups, the performance of both SAFMS and MN502 would be expected to decrease in its presence—only the latter has been studied in this regard to date (Table 2.5, E9). The sulfonic and phosphoric acid groups of ion exchange resin S957 display similar performance (Table 2.5, E10).

As indicated by this extensive survey of the available treatment methods, Met contamination of source waters underscores the need for new remediation technologies that can deliver high technical, cost, environmental and health performances. A safe, simple, cost-effective treatment would make supplementary water supplies much more readily

available from sources that are contaminated by agricultural runoff of this molluscicide. In the UK, such an innovation would facilitate the delivery of cleaner water to London and other cities, as already noted for Yorkshire, in water shortage periods where the cities need to reach farther afield into agricultural regions where source waters are typically unacceptably contaminated.

The TAML process studied here effects a 31% removal over 60 h, the current catalyst limited TAML time frame is longer than others. The major TAML products are acetic acid and acetaldehyde in a 3:1 ratio. The TAML/NaClO process discussed in Chapter 3 further improves TAML performance, a longer reaction time resulting in a deeper removal was realized by switching the oxidant to NaClO. A 91% removal of metaldehyde can be achieved for a 330 μM metaldehyde solution (Table 2.5, E12). The only major product of Met treatment with TAML/NaClO is acetic acid. Even the best performing catalyst available is not quite long-lived enough under optimized conditions to provide a Met removal solution. Consequently, Met provides an ideal stress test for benchmarking future catalysts in the quest for more reactive and cost-effective TAML systems capable of removing even the most persistent MP.

Table 2.3 Adsorption based treatment methods. Note $[Met]_0$ is in mg L^{-1}.

E#	Method	$[Met]_0$ mg/L	Removal %	pH	Other Conditions	Ref
1	Activated Carbon (AC)	62	63	6.2	0.50 mg mL^{-1} carbon, 40 mL scale. Carbon reported to be 47% activated	9
2	Granular Activated Carbon (GAC)	200	30	NA	1 mg mL^{-1} carbon, 500 mL scale	15
3		62	15	6.2	0.75 mg mL^{-1} carbon 2% ethanol, 40 mL scale shaken for 30 min. at 25 °C	9
4	Powder Activated Carbon (PAC)	62.2	42	7	0.162 mg mL^{-1} AX-21, shaken for 20 min. at 24 °C[a]	25
5		2.5	39	7	0.0245 mg mL^{-1} AX-21, shaken for 20 min. at 24 °C[a]	25
6		51	37	6.2	0.50 mg mL^{-1} Picactiff EPII PAC, 40 mL scale	9
7		30	60	7	0.62 mg mL^{-1} Norit A, pH 9 charcoal	25
8		51	26	6.2	0.50 mg mL^{-1} Picapture HP120 8/15 PAC, 40 mL scale	9
9		7.7	67	7	0.22 mg mL^{-1} Norit USP, neutral charcoal pH	25
10		51	20	6.2	0.50 mg mL^{-1} Ceca cpw PAC, 40 mL scale	9
11		51	19	6.2	0.50 mg mL^{-1} Norit-CGP super PAC, 40 mL scale	9
12		NA	NA	NA	Final metaldehyde below regulatory levels. Developed by Veolia Water Solutions & Technologies and Affinity Water[b]	10
13	Microporous Phenolic Carbon	51	40	6.2	0.50 mg mL^{-1} carbon, particle size 45–125 µm, 40 mL scale	9
14		51	38	6.2	0.50 mg mL^{-1} carbon, particle size 210–250 µm, 40 mL scale	9
15	Tailored Phenolic Carbon (PC)	64	91	6.2	Nano-mesoporous carbon synthesized from porous phenolic resin, with ethylene glycol crossed-linked resin, 0.75 mg mL^{-1} resin, 2% ethanol, 40 mL scale, shaken 100 min. at 25 °C	9
16		0.001	NA	NA		
17	Hypercross-linked Macronet MN200	200	45	NA	1 mg mL^{-1} MN200, 500 mL scale	15

[a]Assuming a scale of 1 L; [b]Cited reference unavailable: Veolia Water Solutions & Technologies and Affinity Water. Removal of Metaldehyde from Drinking Water. 2013

Table 2.4 UV-based treatment methods. Note $[Met]_0$ is in μg L^{-1}.

E#	Method	UV-dose mJ cm^{-2}	$[Met]_0$ μg L^{-1}	Removal %	pH[a]	Other Conditions	Ref
1	Direct UV	1750	1000	2	nat.	NA	11
2		NA	0.17–0.27	15	NA	[b]	11
3		NA	500	18	7	Reaction time: 10 min	12
4	UV_{254}/H_2O_2	600	1000	95	nat.	8 mM H_2O_2, 250 mL scale	11
5		1200	1000	92	nat.	8 mM H_2O_2, DOC = 8.7 mg L^{-1}, 250 mL scale	11
6		2600	0.5–3	95	8	Pilot plant, 20 ppm H_2O_2 (0.6 mM), water flow = 0.3–0.6 m^3 h^{-1}	24
7		600	1000	41	nat.	100 mM H_2O_2, 250 mL scale	11
8		2003	0.2	98	5.5	Pilot Plant Reverse Osmosis Permeate, 2 mg L^{-1} H_2O_2 (0.06 mM), < 16 mg L^{-1} alkalinity, 0.2 mg L^{-1} TOC, water flow = 1–3 m^3 h^{-1}	31
9		739	2	45	7.3	Pilot Plant Microfiltration Permeate, 20 mg L^{-1} H_2O_2 (0.6 mM), 212 mg L^{-1} alkalinity, 7.7 mg L^{-1} TOC, water flow = 1–3 m^3 h^{-1}	31
10		6300	10	>90	nat.	Annular photoreactor, 8 mM H_2O_2, 3.5 mg L^{-1} DOC, 120 mg L^{-1} alkalinity, reaction time: 7.5 min.	37
11		1500	10	90	nat.	8 mM H_2O_2, 250 mL scale	29
12		1500	10	84	nat.	8 mM H_2O_2, 250 mL scale, 120 mg L^{-1} alkalinity	29
13		NA	NA	65	nat.	TrojanUV reactors, 20 million liters day^{-1}	23

14	O_3/H_2O_2 followed by UV_{254}	1200	0.5–3	90	8	Pilot Plant, 16–22 g m^{-3} H_2O_2 (0.5– 0.65 mM), 8 g m^{-3} O_3 (0.2 mM), water flow = 0.3–0.6 m^3 h^{-1}	24
15	UV_{254}/TiO_2	1500	1000	20	nat.	0.8 mg L^{-1} TiO_2, 250 mL scale	11
16		600	1000	100	nat.	24 mg L^{-1} TiO_2, 250 mL scale	11
17		1200	1000	7	nat.	24 mg L^{-1} TiO_2, 8.7 mg L^{-1} DOC, 250 mL scale	11
18		1500	10	93	nat.	100 mg L^{-1} TiO_2, 250 mL scale	29
19		16800	10	<50	nat.	Annular photoreactor, 100 mg L^{-1} TiO_2, 3.5 mg L^{-1} DOC, 120 mg L^{-1} alkalinity	37
20		1500	10	45	nat.	100 mg L^{-1} TiO_2, 120 mg L^{-1} alkalinity, 250 mL scale	29
21	UV_{254}/Nano-sized Zinc Oxide Composites (NZnC)	NA	500	33	7	Influent volume = 60 cm^3, 25 g NZnC, reaction time: 10 min.	12

[a]"Nat." represents "natural pH" which means the pH of the water was not adjusted; [b]Cited reference unavailable: Lamming, E. M., 2010. Ultra Violet (UV) and Hydrogen Peroxide Treatment of Metaldehyde, Master's thesis. Cranfield University.

Table 2.5 Oxidative, Acid Catalyzed, and Biological Technologies. Note $[Met]_0$ is in µg L^{-1}.

E#	Method	$[Met]_0$ / µg/L	Removal / %	pH[a]	Other Conditions	Ref
1	Chlorine	NA	NA	NA	No removal	32
2	Ozone	0.05–0.2	4	NA	Surface water, 4 mg L^{-1} O_3[b]	11
3		NA	NA	NA	No removal	32
4	O_3/H_2O_2 in pilot plant	0.5–3	72	8	Flow rate: 30–40 m^3 h^{-1}, 8 g m^{-3} O_3 (0.2 mM), 16–22 g m^{-3} H_2O_2 (0.5–0.65 mM)	24
5	Slow Sand Filtration with Active Biofilm	1 or 10	90	nat.	333 mg mL^{-1} sand, raw water, 300 mL scale Reaction time: For 1 µg L^{-1} Met, 48 h; For 10 µg L^{-1} Met, 48 h by acclimated active sand, 72 h by non-acclimated active sand	38

6	Coupled Adsorption and Electrochemical Destruction (Arvia Process)	11	99	6–7	67 mg mL^{-1} dry Nyex™, added as 130 mg mL^{-1} pre-cleaned Nyex™, 1.5 L scale 15 min mixing, 10 min settling, 15 min regeneration with 0.5 A current. 4 cycles	10
7	Sulfonic Acid Functionalized Mesoporous Silicas (SAFMS)	2.0×10^5	>95	NA	1 mg mL^{-1} SA-SBA-15 (sulfonic acid functionalized mesoporous silicas with 10% sulfuric acid loading), 200 mL scale Acetaldehyde formed was absorbed by either silica AF-SBA-15 (amine functionalized silicas) or ion exchange resin A830 with an acrylic matrix and complex amine functionalities	33
8	Sulfonic Acid Functionalized Macronets	2.0×10^5	>95	NA	1 mg mL^{-1} MN502 (macronets), 200 mL scale Acetaldehyde formed was absorbed by ion exchange resin A830.	39
9		2.0×10^5	80	NA	Same as above with $[Ca^{2+}]$ = 100–20000 mg L^{-1}	39
10	Ion Exchange Resin S957	2.0×10^5	90	NA	1 mg mL^{-1} adsorbent, 500 mL scale	15
11	**1a**/H_2O_2	5.8×10^4	31	7	$[\mathbf{1a}]_{total} = 2\times10^{-6}$ M, $[H_2O_2]_{total}$ = 10.6 mM, 0.01M phosphate buffer in D_2O, 600 µL scale, 60 h, conversion to 3:1 acetic acid:acetaldehyde	c
12	**1a**/NaClO	5.85×10^4	91	7	$[\mathbf{1a}]_{total} = 6\times10^{-6}$ M, $[NaClO]_{total}$ = 20 mM, 0.01M phosphate buffer in D_2O, 600 µL scale, 47 d, conversion to acetic acid	d

[a]"Nat." represents "natural pH" which means the pH of the water was not adjusted; [b]Cited reference unavailable: Hall, T., Holden, B., Haley, J., Treatment for metaldehyde and other problem pesticides. 4th Developments in Water Treatment and Supply Conference, Cheltenham, June 7–8 2011. [c]Study in this chapter. [d]Study discussed in Chapter 3.

2.1.3 Stereoisomers of metaldehyde

Hassel and Mark first reported on the structure of Met in crystals grown from ethanol, but were unable to define it.[40] Pauling and Carpenter later determined the structure to be **I** (Chart 2.2A).[41] In **I** all four carbon atoms lie in one plane, the oxygen atoms lie in another plane parallel to that of the carbon atoms, and all four of the carbon bound methyl groups adopt equatorial positions. Though **I** is the most common, there are 4 possible stereoisomers of Met. Separation of a Met mixture by liquid-gas chromatography has enabled the isolation and characterization of isomers **II** and **III**.[42] Isomers **II** and **III** (Chart 2.2B) differ from **I** by the raising of one oxygen above the plane of the carbon atoms and the orientation of one or two of the methyl groups trans to the plane of the remaining oxygen atoms. Isomer **II** has one methyl group trans to this plane, and isomer **III** has two. The positions of these methyl groups relative to the ring (axial or equatorial) are unknown. The infrared (IR) spectra of **I**, **II**, and **III** are distinct enabling each to be distinguished from the others.[42] As expected, the IR spectra of both the purchased Met sample and that purified for use in this study by recrystallization from ethanol are (Figure 2.3) mainly composed of isomer **I**.

Chart 2.2 Models of metaldehyde isomers. The black circles represent carbon atoms and the white circles represent oxygen atoms.

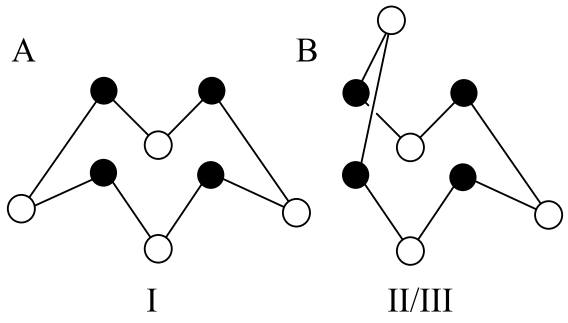

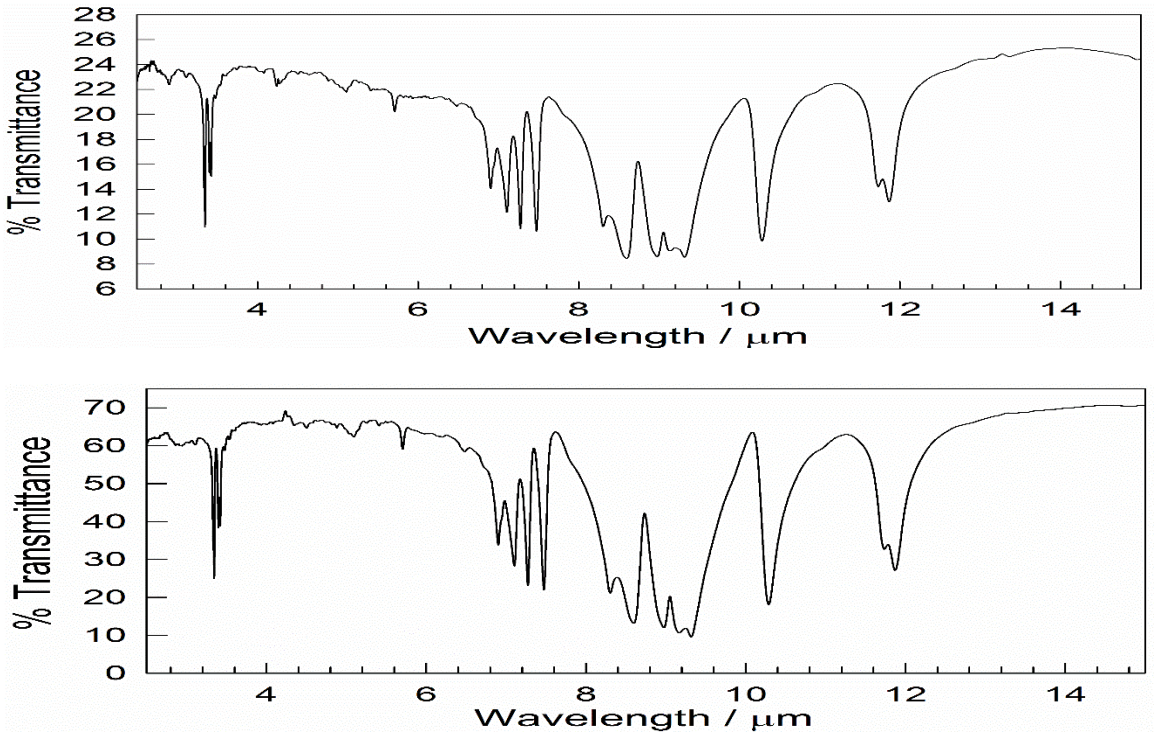

Figure 2.3 IR spectra (in KBr) of purchased Met and Met after recrystallization from ethanol. Upper: purchased Met. Lower: recrystallized Met.

2.1.4 The use of NMR spectroscopy as a monitoring tool

The oxidation of Met was monitored by ^{1}H NMR. Presaturation[43,44] was used to suppress water proton signals. Since an internal standard would have been susceptible to TAML/H_2O_2 oxidation, none was added. The quantification of metaldehyde and products was enabled by maintaining consistency of the RF power delivered to the coil in the NMR probe (90° pulse), always tuning/matching the coil before each measurement, using the same number of scans and the same receiver gain. As a result, the intensities of the observed signals are directly proportional to the absolute quantities of the specific protons responsible for each signal.[44,45]

The traditional method of detecting Met in an aqueous matrix involves solid phase extraction, dissolution in an organic solvent, and quantification by GC-MS.[46] This study employs *in situ* NMR as a monitoring method because it conveys certain advantages over the traditional method, especially because the process is slow, including (*i*) the reaction can be analyzed without quenching or pre-treatment, (*ii*) extraction of analytes into organic solvents or matrices is not required thereby reducing sources of experimental error, (*iii*) the concentrations of proton-bearing products and substrate can be analyzed at the same time without intensity calibration,[43] (*iv*) small molecules can be detected without derivatization,[47] (*v*) one sample can be analyzed at multiple time points without destruction or quenching, and (*vi*) lower volume reaction mixtures can be analyzed with ease.[48] These characteristics enable the real-time identification and quantification of multiple analytes in a small reaction volume without risk of altering their molecular structures in the analytical procedure. Thus, we show that ^{1}H NMR is a powerful analytical tool for monitoring the degradation of Met at higher concentrations (~300 μM).

2.2 Results and discussion

Herein, the oxidation of Met (0.3 mM) by H_2O_2 (5–10 mM) catalyzed by TAML activators (0.4–2 μM) is examined. Met consumption and product formation were observed and quantified in situ by 1D ^{1}H nuclear magnetic resonance (NMR) with application of the presaturation method to suppress water protons. The performance of three TAML activators spanning a range of reactivity and lifetime was assessed under ambient conditions. The rate of Met consumption and the efficiency of TAML/H_2O_2 for Met remediation have been examined. The work below proves that TAML/peroxide can slowly

degrade Met in laboratory experiments as a first step toward examining the much more complicated question of whether or not it can provide a real-world solution.

2.2.1 General observations

The oxidation of Met was monitored by ^{1}H NMR (Figure 2.4). The identities of the major products, acetic acid and acetaldehyde, were confirmed by spiking with authentic standards. More acetic acid was produced than acetaldehyde. These degradation products possess rat LD_{50} values of 3310 and 661 mg kg^{-1} (oral), respectively, significantly greater than that of Met (Table 2.1) implying that the products of TAML catalyzed Met degradation are more benign than Met itself.[2,49-51]

Reactions were initiated by the addition of one aliquot of H_2O_2 to a solution of a TAML catalyst and Met in an NMR tube. The samples were stored in dark NMR autosampler holders throughout the measurement periods to minimize Met degradation by UV/H_2O_2.[52] Little decomposition of Met was observed in the presence of H_2O_2 alone indicating that the uncatalyzed process does not contribute significantly to the observed degradation (Figure 2.6A). As shown in Figure 2.6, the rate of decomposition of metaldehyde as well as that of the production of acetaldehyde decreased over the reaction time period of 600 minutes. The production of acetic acid (Figure 2.7) follows the same trend as that of acetaldehyde (Figure 2.6B).

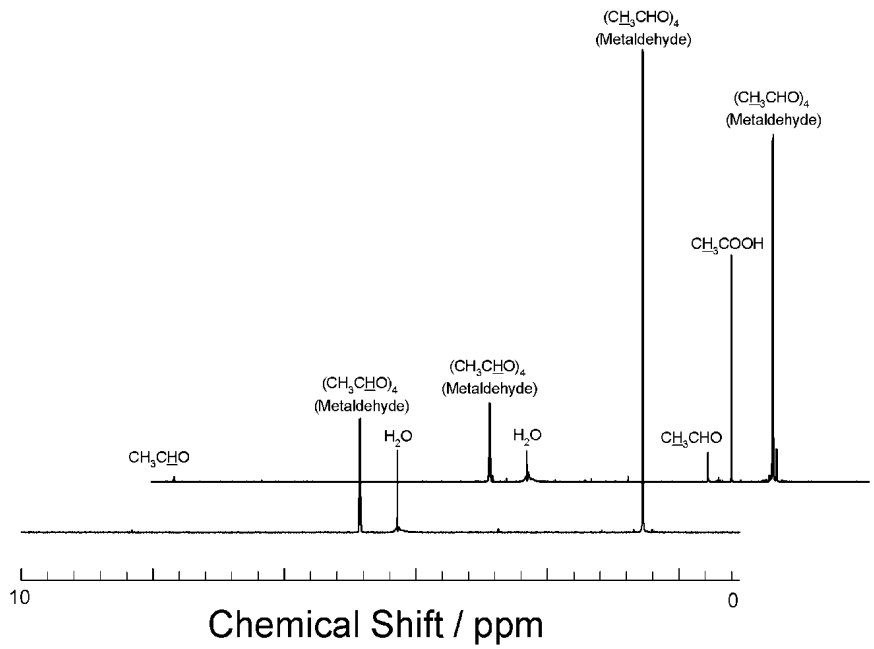

Figure 2.4 An example of the ^{1}H NMR spectra (D_2O, pH 7) from which quantitative analyses were derived. The bottom spectrum was collected at ca. 20 min and the top at 60 h. Conditions: pH 7 (0.01 M phosphate, D_2O), [Met] = 3.18×10^{-4} M, [H_2O_2] = 5.30×10^{-3} M (180 ppm = 83% of the mineralization requirement), [**1a**] = 4.00×10^{-7} M. An additional aliquot of **1a** (total = 2 μM) was added to the reaction mixture every 12 h and an additional aliquot of H_2O_2 (total = 360 ppm) was added at 36 h.

2.2.2 Comparative performance of three catalysts in pH 7 buffered solutions

The relative performances of **1b** and **2a** in the degradation of Met were assessed for comparison with that of **1a** (Table 2.6). All **1** catalysts share the same basic ligand structure (Chart 2.1). Catalyst **1a** differs from **1b** by appendage of a nitro group to the aromatic ring and substitution of fluorine atoms for the geminal dimethyl groups of the malonamide residue.[53] These substitutions increase both the rate at which the catalyst is activated by H_2O_2 to form the active catalysts (Ac) and that at which Ac oxidizes a substrate at neutral pH.[53] The overall rate of TAML catalysis is typically a function of one or both of these processes. Addition of electron-withdrawing groups to the macrocycle typically increases

the oxidative aggression of the resulting TAML catalyst. Consequently, the rate of Met oxidation catalyzed by **1a** was expected to be greater than that of **1b** as has been observed for other micropollutants.[54,55] Indeed **1a** oxidized metaldehyde with a rate, r, of 8.36×10^{-2} min^{-1} where $r = d[S]/dt \times 1/[Fe]_0$, faster than **1b**, $r = 3.40 \times 10^{-2}$ min^{-1}. Activator **1a** also did more work than **1b** performing a 5% reduction with a turnover number (TON) of 40 versus a 1.8% reduction with a TON of 14 after 600 min. Catalysts **1** and **2a** belong to different generations.[55] In **1**, the amido-*N* nitrogen atoms are attached to six sp^2 and two sp^3 carbon atoms. In **2,** all eight carbons attached to the four amido-*N* nitrogen atoms are sp^2 hybridized, thereby significantly reducing the ability of the macrocycle to donate electron density to the iron center. The introduction of a nitro group at each aromatic ring further reduces the basicity of the amido nitrogen atoms of **2a** to further augment the reactivity. At neutral pH, **2a** is known to both form Ac and oxidize substrates more rapidly than any other TAML catalyst to date.[56] However, **2a** is less effective than either **1a** or **1b** in the degradation of Met showing a rate of 1.58×10^{-2} min^{-1}, an overall reduction of 1% and a TON of 8 under similar conditions. We attribute this to the shorter lifetime of **2a** versus **1a** or **1b**. Of the three catalysts tested, **1a** is the most effective in the degradation of Met considering both the amount and the rate of the decomposition.

2.2.3 Effect of pH on the catalyzed oxidation process in buffered solutions

The trend in the rate of Met degradation with increasing pH differs substantially from that usually observed for TAML activators functioning in water. As described in Chapter 1, TAML catalysis follows a two-step stoichiometric mechanism.[57] The resting catalyst (Rc) is activated by H_2O_2 to form an active catalyst (Ac). Ac then oxidizes a substrate to give a product and regenerate Rc; both the first and second steps are comprised of multiple

elementary reactions. The first step, catalyst activation, is typically rate-determining (d[S]/dt ~ k_I[H_2O_2][Fe]). In the Met degradation system, a linear dependence of the rate (*r*) of **1a** catalyzed Met oxidation on [H_2O_2] (3–10 mM) was observed at pH 7 as would be expected for a system in which catalyst activation is rate determining (Table 2.7).[57] The value of the rate constant for TAML catalyst activation, k_I, follows a bell shaped trend with respect to increasing pH.[53,58] For **1a**, k_I reaches a maximum value around pH 10.5.[53] As a result when catalyst activation is rate determining, the rate of substrate oxidation (d[S]/dt) is expected to increase as the proton concentration decreases within the pH range of 6.5–9 if [H_2O_2] and [Fe] are held constant.[53] At pH 6.5 in D_2O, the **1a** catalyzed Met oxidation *r* is 5.77×10^{-2} min^{-1}, lower than that observed at pH 7 (Table 2.6). However, the pH 7.5 *r* is 4.19×10^{-2} min^{-1}, also less than the pH 7 *r* of 8.36×10^{-2} min^{-1} and no oxidation is observed at pH 9. The oxidation of Met at pH 6.5–7 follows the trend expected for a system in which catalyst activation is rate-determining. This seems to be unrealistic given the resilience of Met. Moreover, the behavior observed within the pH range of 7.5–9 is anomalous. We suspect this behavior has a complex origin which is being further examined. The maximum reaction rate within the pH range of 6.5–9 is achieved at ~ pH 7. A pH range of 7–10.5 is proposed for drinking water in order to achieve water quality objectives and corrosion control.[59]

Table 2.6 Summary of Met degradation under different conditions. $[H_2O_2] \approx 5 \times 10^{-3}$ M.

Cat	pH	[Cat] × 10^7 M	$[Met]_0$ × 10^4 M	$r \times 10^2$ / min^{-1} [a]	TON	Met. Decomp. / %	AA / % [b]	t_∞ / min.
1a	7.0	4.00 [c]	3.18	8.36	40	5	1.8	600
1b	7.0	4.33 [c]	3.45	3.40	14	1.8	0.3	600
2a	7.0	3.90 [c]	3.45	1.58	8	1.0	0.3	750
1a	7.0	4.00 [d]	3.18	NA	NA	31.0	12	3640
1b	7.0	4.33 [e]	3.45	NA	NA	3.5	1	1480
1a	NA	4.16 [d]	3.33	NA	NA	7.0	4	3650
1a	6.5	4.16 [c]	3.33	5.77	26	3.3	1	770
1a	7.5	4.16 [c]	2.97	4.19	22	3.1	1	760
1a	9.0	4.16 [c]	3.42	NA	NA	NA	0.4	770

[a]The rate *r* is calculated from the slope of the line of best fit to the first three measurements of substrate concentration divided by catalyst concentration ($r = d[S]/dt \times 1/[Fe]_0$); [b]The percentage of acetic acid (AA) formed is calculated as a relative percentage compared to starting Met absolute integral ($Ac\% = ({}^{Abs}Int_{1.92})/({}^{Abs}Int_{1.34})_0$), i.e. if all Met is converted to acetic acid, the percentage will be 100%; [c]An aliquot of catalyst and an aliquot of H_2O_2 were added to the reaction mixture; [d]An aliquot of catalyst was added to the reaction mixture every 12 hours, five aliquots of catalyst were added in total and an additional aliquot of H_2O_2 was added to the reaction mixture at 36 h; [e]An additional aliquot of catalyst was added at 12 h.

Table 2.7 Reaction rate at different $[H_2O_2]$.

Cat	pH	[Cat] × 10^7 M	$[Met]_0$ × 10^4 M	$[H_2O_2]$ × 10^3 /M	$r \times 10^2$ / min^{-1} [a]	TON	Met. Decomp. / %	CH_3COOH Formed / % [b]	t_∞ / min.
1a	7.0	3.94	3.03	0.31	NA	NA	NA	NA	NA
1a	7.0	3.98	2.95	3.6	5.5	33	4.5	1.6	1000
1a	7.0	3.91	3.00	10.5	13.27	61	8	3.7	1000
1a	7.0	4.00	3.18	5.3	8.36	40	5	1.8	600

[a]The rate *r* is calculated from the slope of the line of best fit to the first three measurements of substrate concentration divided by catalyst concentration ($r = d[S]/dt \times 1/[Fe]_0$); [b]The percentage of acetic acid is calculated as a relative percentage compared to the initial Met absolute integral ($Ac\% = ({}^{Abs}Int_{1.92})/({}^{Abs}Int_{1.34})_0$), i.e. if all Met is converted to acetic acid, the percentage will be 100%.

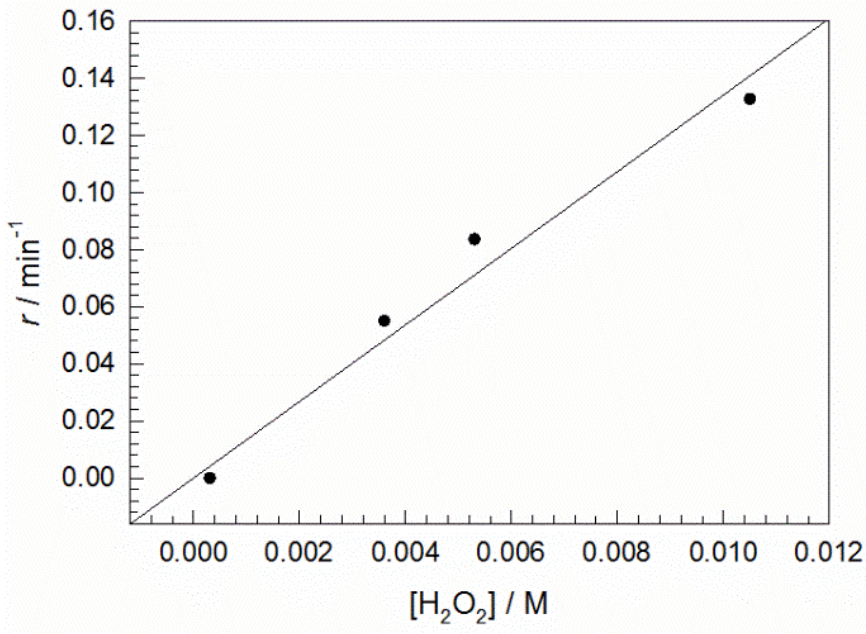

Figure 2.5 Rate *r* dependence on $[H_2O_2]$ in pH 7 D_2O (0.01 M phosphate). All conditions are as described in Table 2.7.

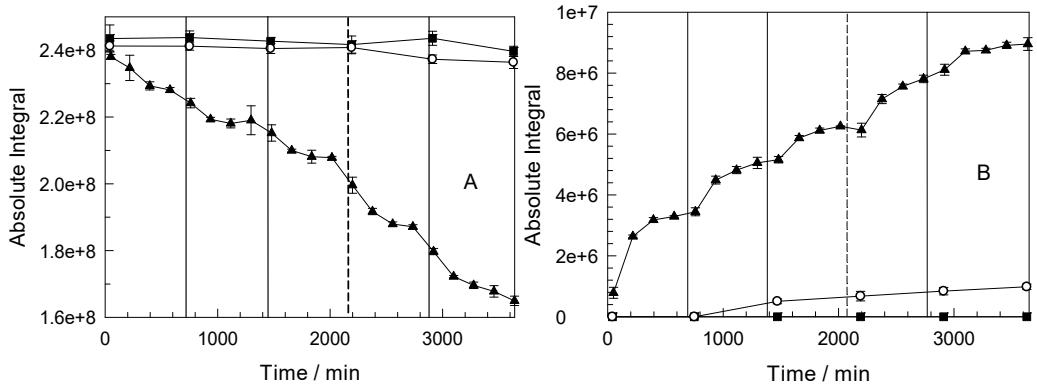

Figure 2.6 Met reduction and acetaldehyde formation in pH 7 buffered D_2O. Symbols distinguish **1a** reaction from controls. Black squares: Met; White circles: Met and H_2O_2; Black triangles: Met, H_2O_2, and **1a**. A: Reduction in the absolute integral of the signal corresponding to the Met CH_3 groups at 1.34 ppm with time (31% reduction at 3640 min). B: Increase in the absolute integral of the signal corresponding to acetaldehyde CH_3 groups at 2.25 ppm with time (3.7% production at 3640 min as a relative percentage of the initial absolute integral of the Met CH_3 groups). Conditions: pH 7 D_2O (0.01 M phosphate), [Met] = 3.18×10^{-4} M, $[H_2O_2] = 5.30 \times 10^{-3}$ M, [**1a**] = 4.00×10^{-7}

M. The vertical lines indicate the addition of an aliquot of **1a** every 12 h. The dashed vertical line indicates the addition of both an aliquot of **1a** and an aliquot of H_2O_2 at 36 h.

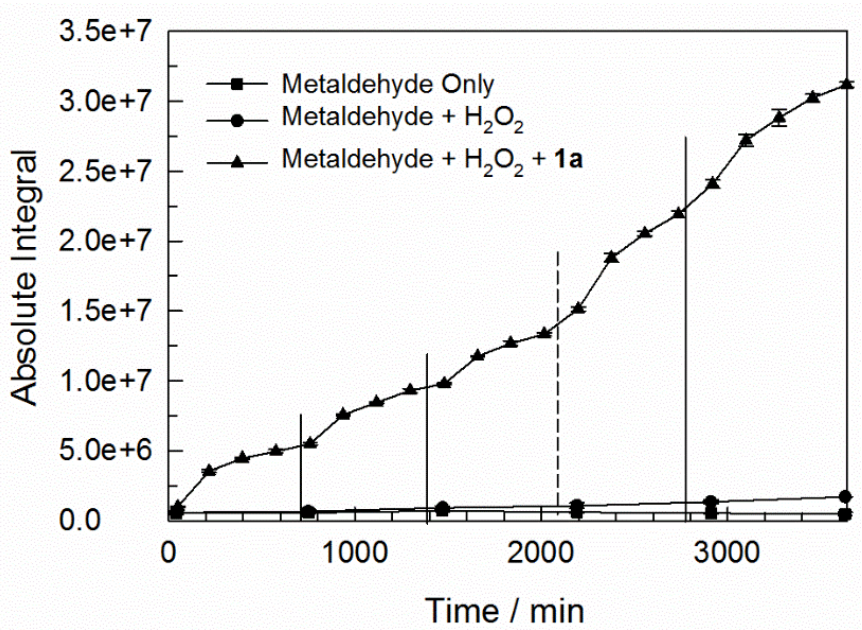

Figure 2.7 Increase in the absolute integral of the signal corresponding to acetic acid CH_3 groups at 1.92 ppm with time (12% production at 3640 min as a relative percentage of the initial absolute integral of the Met CH_3 groups). Conditions: pH 7 D_2O (0.01 M phosphate), [Met] = 3.18×10^{-4} M, [H_2O_2] = 5.30×10^{-3} M, [**1a**] = 4.00×10^{-7} M. The vertical lines indicate the addition of an aliquot of **1a** to the reaction mixture every 12 h. The dashed vertical line indicates the addition of both an aliquot of **1a** and an aliquot of H_2O_2 to the reaction mixture at 36 h.

2.2.4 Multiple treatments with 1/H_2O_2 in pH 7 buffered solutions

The efficacy of multiple aliquots of **1a** in a solution buffered at pH 7 was determined (Figure 2.8, Table 2.6). The reaction was initiated by the addition of one aliquot of H_2O_2 to a buffered solution of **1a** and Met. An additional aliquot of the **1a** stock solution was added every 12 h. In total five aliquots of catalyst were added and the reaction was monitored for 60 h. One additional aliquot of H_2O_2 was added at 36 h. Met consumption

and acetic acid production ceased prior to each catalyst addition. Both resumed upon each addition of **1a**. We have long interpreted this result as evidence that the catalyst is undergoing inactivation during the slow oxidation process.[60,61] The net effect of these treatments was a 31% reduction in the concentration of Met. More complete Met degradation could have been achieved through further additions of catalyst. However, we chose to stop at this level of reduction to focus instead on the developments that might remove all of the Met with less TAML activator aliquots and one such approach is detailed in Chapter 3.

Kinetic traces of the acetic acid production (Figure 2.7) reveal a similar trend to that shown for acetaldehyde in Figure 2.6B. The acetic acid and acetaldehyde produced accumulate over multiple treatments and reach a final ratio of ca. 3:1, accounting for about half of the decomposed Met. The performance of **1b** under identical conditions was assessed for comparison. One aliquot of H_2O_2 was added to a buffered solution of **1b** and Met to initiate the reaction. An additional aliquot of the **1b** stock solution was added at 12 h. In total two aliquots of catalyst were added and the reaction was monitored for 24 h. These treatments effected a 3.5% reduction in the concentration of Met with a final ratio of acetic acid to acetaldehyde of 1.3:1 (Figure 2.8). For comparison the first two treatments with **1a**/H_2O_2 accomplished a 9% reduction in 24 h. The greater Met decomposition at 24 h and more benign product mixture of **1a** indicate that it has superior performance properties in comparison to those of **1b**.

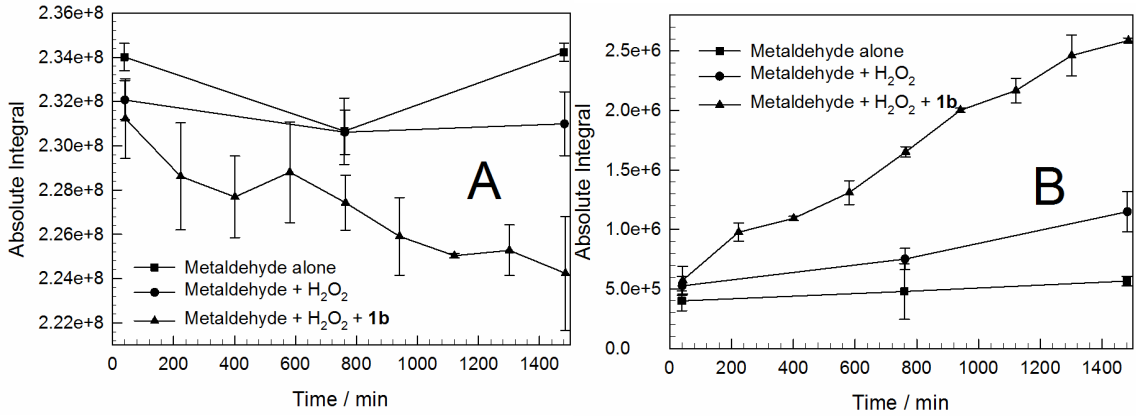

Figure 2.8 A: Reduction in the absolute integral of the signal corresponding to the Met CH_3 groups at 1.34 ppm with time (3.5% reduction at 1480 min). B: Increase in the absolute integral of the signal corresponding to acetic acid CH_3 groups at 1.92 ppm with time (1% production at 1480 min as a relative percentage of the initial absolute integral of the metaldehyde CH_3 groups). Conditions: pH 7 D_2O (0.01 M phosphate), [Met] = 3.45×10^{-4} M, [H_2O_2] = 5.48×10^{-3} M, [**1b**] = 4.33×10^{-7} M. An additional aliquot of **1b** was added to the reaction mixture at 12 h.

2.2.5 Treatment with multiple aliquots of 1a/H_2O_2 in an unbuffered solution

The degradation of Met by multiple aliquots of **1a**/H_2O_2 in unbuffered D_2O was also followed (Figure 2.9) as this approximates the ideal treatment conditions for large-scale water purification. The reaction was initiated by the addition of one aliquot of H_2O_2 to an unbuffered solution of **1a** and Met. An additional aliquot of the **1a** stock solution was added every 12 h. In total five aliquots of catalyst were added and the reaction was monitored for 60 h. One additional aliquot of H_2O_2 was added at 36 hours. These treatments reduced the concentration of Met by 7%. The acetaldehyde produced by each aliquot of **1a** is rapidly consumed by the next aliquot of **1a** (Figure 2.9B), unlike catalysis in buffered solutions where it accumulates (Figure 2.6B). The final ratio of acetic acid to acetaldehyde was 6:1, an even more benign product mixture than that produced under buffered conditions. The consumption of acetaldehyde and comparatively acetic acid rich product ratio were

interpreted as evidence of increased acetaldehyde oxidation over that which occurs in buffered solutions. Kinetic traces of acetic acid production (Figure 2.10) show a trend similar to that observed in the buffered case (Figure 2.7). As the reaction progressed through multiple additions of **1a**, the acetic acid C<u>H</u>$_3$ signal drifted downfield (Figure 2.11). This is indicative of a decreasing solution pH[48] consistent with the production and subsequent deprotonation of acetic acid. This was not observed in buffered solutions. The reduced Met decomposition is probably due, at least in part, to the lowering of the pH with the progression of the process in the absence of buffer. In a real world system where the concentration of Met would be much lower this effect should be minimal. Again, these results indicate the need for a more aggressive, longer-lived TAML activator en route to being able to deal with this exceptionally persistent contaminant in the real world.

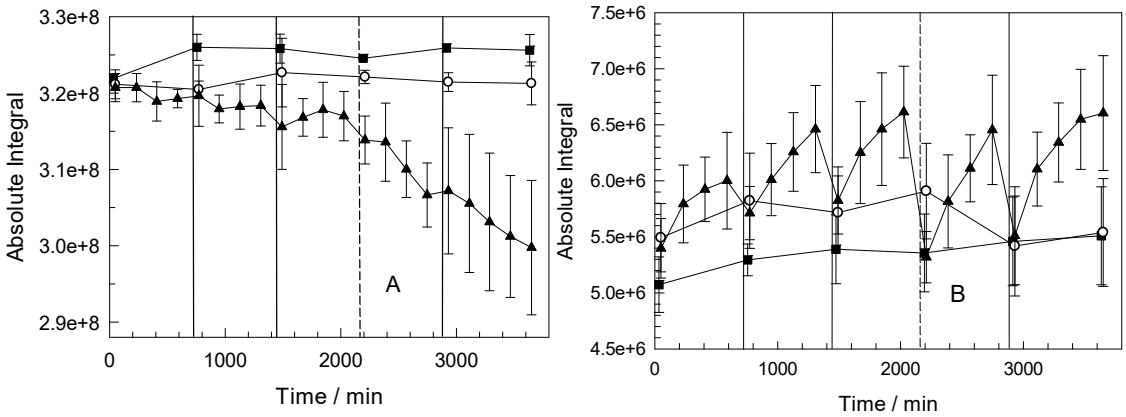

Figure 2.9 Met reduction and acetaldehyde formation in unbuffered D_2O. Symbols distinguish **1a** reaction from controls. Black squares: Met; White circles: Met and H_2O_2; Black triangles: Met, H_2O_2, and **1a**. A: Reduction in absolute integral of the Met CH_3 groups at 1.34 ppm with time (7% reduction at 3650 min). B: Acetaldehyde formed according to absolute integral at 2.25 ppm in the ^{1}H NMR spectra. Conditions: D_2O, [Met] = 3.33×10^{-4} M, [H_2O_2] = 5.53×10^{-3} M, [**1a**] = 4.16×10^{-7} M. The vertical lines indicate the addition of an aliquot of catalyst to the reaction mixture every

12 h. The dashed vertical line indicates the addition of one equivalent of H_2O_2 at 36 h after the start of the reaction.

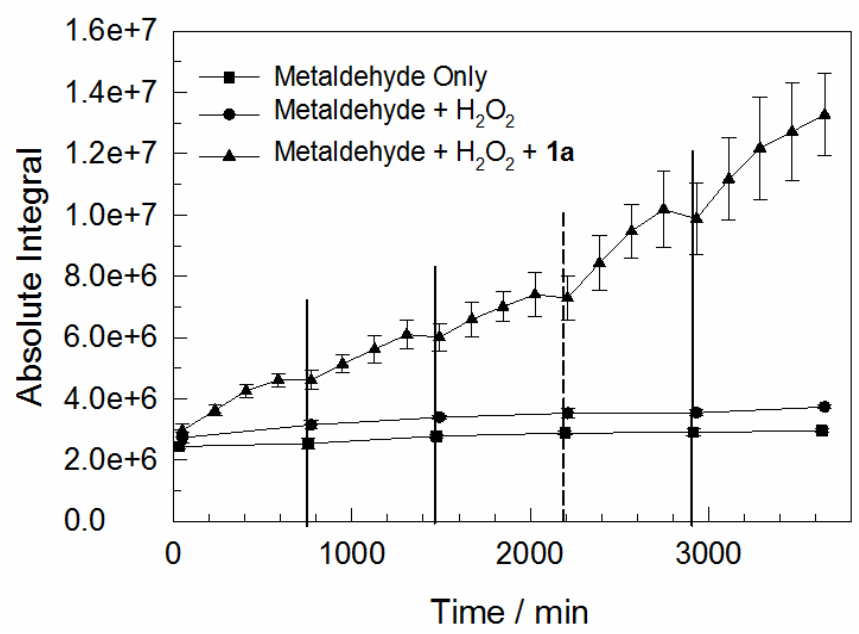

Figure 2.10 Increase in the absolute integral of the signal corresponding to acetic acid CH_3 groups initially at 1.92 ppm (δ changes with time) (4% production at 3650 min as a relative percentage of the initial absolute integral of the Met CH_3 groups). Conditions: D_2O, [Met] = 3.33×10^{-4} M, [H_2O_2] = 5.53×10^{-3} M, [**1a**] = 4.16×10^{-7} M. The vertical lines indicate additions of an aliquot of **1a** every 12 h. The dashed vertical line indicates the addition of one equivalent of H_2O_2 at 36 h after the start of the reaction.

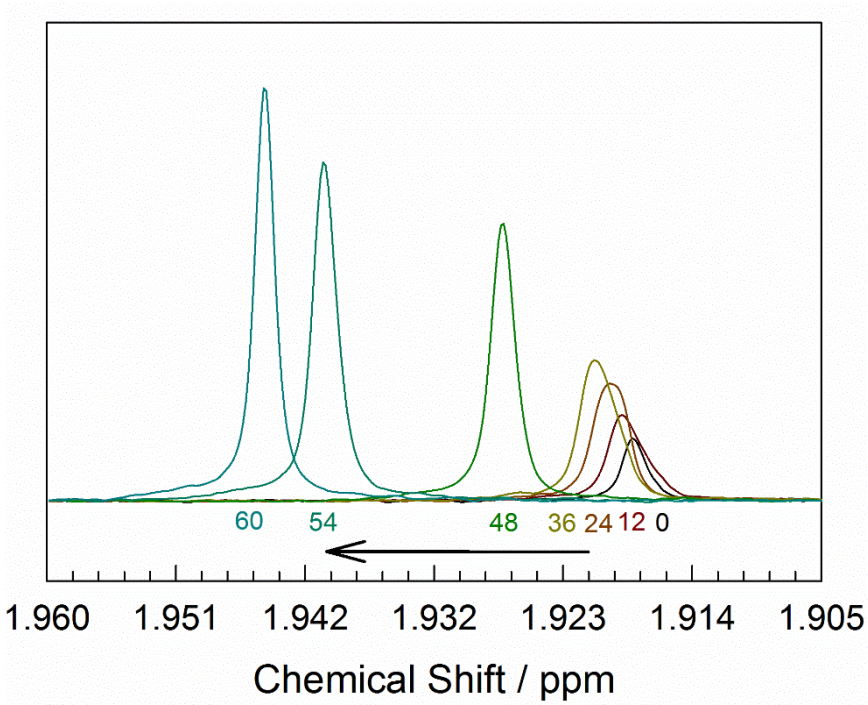

Figure 2.11 Downfield drift of the CH_3 peak of acetic acid in the ^1H NMR spectra as the reaction progressed (numbers below peaks show the reaction hours at each measurement). Conditions: D_2O, [Met] = 3.33×10^{-4} M, [H_2O_2] = 5.53×10^{-3} M, [**1a**] = 4.16×10^{-7} M. Every 12 hours an aliquot of **1a** was added. At 36 h an aliquot of H_2O_2 was added.

2.3. Conclusion

We have long known that TAML/H_2O_2 processes are very efficient in remediating water contaminants. In this work we have shown that this system is also effective in oxidizing the extremely persistent Met slowly. Qualitative comparisons can be made between TAML/H_2O_2 systems and other reported treatments that are specific for Met remediation. Since TAML/H_2O_2 does not rely upon adsorption, it is more likely to accommodate a range of substrates of varying structure than the Arvia process. Since TAML/H_2O_2 is an oxidative process, it is likely to be more general than the acid catalyzed decomposition employed by SAFMS. In addition, all of the tested TAML processes produced more acetic acid than

acetaldehyde while SAFMS produces acetaldehyde exclusively. We evaluate this work at its current state of development as very promising progress, but do not consider the system is ready yet as a real-world solution in the particular case of this especially persistent MP. Areas for further study include the generation of catalysts with both greater reactivity and longer lifetime with the aim of achieving faster and more complete decomposition giving acetic acid alone. We judge that the biggest single challenge for making TAML catalysis routine for Met degradation lies with the development of new catalysts that have longer lifetimes and higher aggression—and this is where our efforts are currently focused. Nevertheless, Chapter 3 investigates the impact of substituting NaClO for H_2O_2 and introduces oxidant choice as a new design tool to improve catalyst lifetime and therefore efficiency.

2.4 Experimental

2.4.1 Materials

All reagents, components of buffer solutions, and solvents were of at least ACS reagent grade and used as received. Met (Acros, 99%) was recrystallized in ethanol[62] and stored at 4 ºC. Met stock solutions (0.3 mM) were prepared by sonicating appropriate quantities of Met in buffered D_2O (99.9%, Cambridge Isotope Laboratories, Inc.) at room temperature for 3 h. Phosphate (0.01 M, pH 6.5–7.5) and carbonate (0.01 M, pH 9.0) buffers were prepared in D_2O and monitored with an Accumet™ AB15 pH meter at room temperature. The stated pH values of these D_2O solutions are uncorrected pH meter readings. TAML® activator **2a** was synthesized by published methods.[56] Compounds **1a** and **1b** were obtained from GreenOx Catalysts, Inc. **1b** was purified by column chromatography on C18-silica

gel with a water/methanol eluent (95/5, v/v) prior to use. Stock solutions of TAML activators (2×10^{-4} M) were prepared in D_2O (**1a** and **1b**) or H_2O (**2a**), and stored at 4 ºC. Hydrogen peroxide stock solutions were prepared by diluting 30% aqueous H_2O_2 with D_2O. The concentration of H_2O_2 stock solutions were monitored daily by measuring the UV-Vis absorbance at 230 nm ($\varepsilon = 72.4\ M^{-1}cm^{-1}$).[63]

2.4.2 Instrumental

UV-Vis measurements were performed on an Agilent 8453 UV-Vis spectrophotometer equipped with an 8-cell transporter and thermostatic temperature controller. Solution temperatures were maintained at 25 ºC in capped quartz cuvettes (1.0 cm). IR measurements were achieved via a Mattson ATI Affinity 60 AR FTIR spectrometer using KBr pellet. 1D ^{1}H spectra were recorded at 300 K on a Bruker Avance™ III 500 NMR spectrometer operating at 500.13 MHz. The water signal was suppressed using the presaturation experiment (zgpr) from the Bruker pulse programs library. Chemical shifts are reported in parts per million relative to TMSP (internal standard for water solutions). Each sample was scanned 128 times over 16.5 minutes. The Bruker TopSpin™ 3.0 software was used to process the NMR data. Absolute integrals for each proton peak were used for quantification. Each data point with error bars is the average of three measurements. No measurable broadening of signals due to the accumulation of catalyst was observed at the catalyst concentrations employed.

2.5 References

(1) Moreau, P.; Burgeot, T.; Renault, T. *Environ. Sci. Pollut. Res.* **2015**, *22*, 8003.

(2) Booze, T. F.; Oehme, F. W. *Fund. Appl. Toxicol.* **1986**, *6*, 440.

(3) Edwards, D. *Reregistration Eligibility Decision for Metaldehyde* US, 2006.

(4) European Food Safety Authority. *Conclusion on the peer review of the pesticide risk assessment of the active substance metaldehyde*, European Food Safety Authority, 2010.

(5) Cardoso, D. N.; Santos, M. J. G.; Soares, A. M. V. M.; Loureiro, S. *Chemosphere* **2015**, *132*, 1.

(6) Hollingsworth, R. G.; Armstrong, J. W.; Campbell, E. *Nature* **2002**, *417*, 915.

(7) Simms, L.; Wilson, M. *Pestic. Outlook* **2002**, *13*, 270.

(8) Metaldehyde Stewardship Group. http://www.getpelletwise.co.uk/; Vol. 2016.

(9) Busquets, R.; Kozynchenko, O. P.; Whitby, R. L. D.; Tennison, S. R.; Cundy, A. B. *Water Res.* **2014**, *61*, 46.

(10) Nabeerasool, M. A.; Campen, A. K.; Polya, D. A.; Brown, N. W.; van Dongen, B. E. *Water* **2015**, *7*, 3057.

(11) Autin, O. Ph.D. Thesis, Cranfield University, 2012.

(12) Doria, F. C.; Borges, A. C.; Kim, J. K.; Nathan, A.; Joo, J. C.; Campos, L. C. *Water Air Soil Poll.* **2013**, *224*.

(13) Pesticide Database Network.; Pesticide Action Network North America: 2016; Vol. 2016.

(14) Kay, P.; Grayson, R. *Water Environ. J.* **2014**, *28*, 410.

(15) Tao, B.; Fletcher, A. J. *J. Hazard. Mater.* **2013**, *244*, 240.

(16) Lazartigues, A.; Banas, D.; Feidt, C.; Brun-Bellut, J.; Thomas, M. *Environ. Sci. Pollut. R.* **2012**, *19*, 2802.

(17) Bullock, M. M.S. Thesis, Cranfield University, 2014.

(18) Mathiesen, K.; The Guardian: 2013; Vol. 2015.

(19) Drinking Water Inspectorate. *Drinking water--A report by the Chief Inspector of Drinking Water*, Drinking Water Inspectorate, 2008-2015.

(20) Tang, L. L.; DeNardo, M. A.; Gayathri, C.; Gil, R. R.; Kanda, R.; Collins, T. J. *Environ. Sci. Technol.* **2016**, *50*, 5261.

(21) Kay, P.; Grayson, R.; Mciwem *Water Environ. J.* **2014**, *28*, 410.

(22) Eggen, R. I.; Hollender, J.; Joss, A.; Scharer, M.; Stamm, C. *Environ. Sci. Technol.* **2014**, *48*, 7683.

(23) TrojanUV. *TrojanUV Solutions: Removal of Metaldehyde, a Pesticide Found in UK Drinking Water Sources*.

(24) Scheideler, J.; Bosmith, A. *Aqua Gas* **2014**, *94*, 52.

(25) Gessner, P. K.; Hasan, M. M. *J. Pharm. Sci.* **1987**, *76*, 319.

(26) Binnie, C.; Kimber, M. *Basic Water Treatment*; Fifth ed.; ICE Publishing: London, UK, 2013.

(27) Environment Agency *Position Statement: Environment Agency position on Metaldehyde*, 2011.

(28) Katsoyiannis, I. A.; Canonica, S.; von Gunten, U. *Water Res.* **2011**, *45*, 3811.

(29) Autin, O.; Hart, J.; Jarvis, P.; MacAdam, J.; Parsons, S. A.; Jefferson, B. *Water Res.* **2013**, *47*, 2041.

(30) G. F. IJpelaar; D. J. H. Harmsen; Heringa, M. *UV disinfection and UV/H_2O_2 oxidation: by-product formation and control*; Kiwa WR, 2007.

(31) James, C. P.; Germain, E.; Judd, S. *Sep. Purif. Technol.* **2014**, *127*, 77.

(32) Marshall, J. *Water UK briefing paper on metaldehyde*, 2013.

(33) B. Tao; Fletcher, A. J. *Sep. Purif. Technol.* **2014**, *124*, 195.

(34) U.S. Environmental Protection Agency *Health Assessment Document for Acetaldehyde*, Environmental Criteria and Assessment Office, Office of Health and Environmental Assessment, Office of Research and Development, 1987.

(35) U.S. Environmental Protection Agency http://www3.epa.gov/airtoxics/hlthef/acetalde.html, 2000.

(36) LeBel, G. L.; Benoit, F. M. In *Proceedings of the 28th Annual Water Quality Technology Conference* Salt Lake City, UT, 2000.

(37) Autin, O.; Hart, J.; Jarvis, P.; MacAdam, J.; Parsons, S. A.; Jefferson, B. *Appl. Catal. B-Environ.* **2013**, *138*, 268.

(38) Rolph, C. A.; Jefferson, B.; Villa, R. In *Progress in Slow Sand and Alternative Biofiltration Processes: Further Developments and Applications*; Nobutada Nakamoto, Nigel Graham, M. Robin Collins, Gimbel, R., Eds.; IWA Publishing: London, UK, 2014, p 195.

(39) Tao, B.; Fletcher, A. *Chem. Eng. J.* **2016**, *284*, 741.

(40) Hassel, O.; Mark, H. *Z. physik. Chem.* **1924**, *111*, 357.

(41) Pauling, L.; Carpenter, D. C. *J. Am. Chem. Soc.* **1936**, *58*, 1274.

(42) Craven, E. C.; Jowitt, H.; Ward, W. R. *J. Appl. Chem.* **1962**, *12*, 526.

(43) Wei, F. F.; Furihata, K.; Koda, M.; Hu, F. Y.; Miyakawa, T.; Tanokura, M. *J. Agric. Food. Chem.* **2012**, *60*, 1005.

(44) Bharti, S. K.; Roy, R. *Trac-Trend. Anal. Chem.* **2012**, *35*, 5.

(45) Wider, G.; Dreier, L. *J. Am. Chem. Soc.* **2006**, *128*, 2571.

(46) Environment Agency. *The determination of metaldehyde in waters using chromatography with mass spectrometric detection*, 2009.

(47) Bao, M. L.; Pantani, F.; Griffini, O.; Burrini, D.; Santianni, D.; Barbieri, K. *J. Chromatogr. A* **1998**, *809*, 75.

(48) Tynkkynen, T.; Tiainen, M.; Soininen, P.; Laatikainen, R. *Anal. Chim. Acta.* **2009**, *648*, 105.

(49) Dolder, L. K. *Veterinary Medicine* **2003**, *98*, 213.

(50) E. M. Arnett; W. E. Barkley; P. Beak; E. D. Becker; H. E. Bryndza; I. L. Chang; C. Creutz; R. L. Danheiser; E. M. Gordon; R. J. Lackmeyer; L. Magid; T. F. McBride; A. M. Norberg; E. W. Petrillo; S. H. Pine; Thompson, F. M. *Prudent Practices in the Laboratory: Handling and Disposal of Chemicals*; National Academy Press: Washington, D. C., USA, 1995.

(51) Sparks, S. E.; Quistad, G. B.; Cole, L. M.; Casida, J. E. *Pestic. Biochem. Physiol.* **1996**, *55*, 226.

(52) Autin, O.; Hart, J.; Jarvis, P.; MacAdam, J.; Parsons, S. A.; Jefferson, B. *Water Res.* **2012**, *46*, 5655.

(53) Popescu, D. L.; Chanda, A.; Stadler, M. J.; Mondal, S.; Tehranchi, J.; Ryabov, A. D.; Collins, T. J. *J. Am. Chem. Soc.* **2008**, *130*, 12260.

(54) Shen, L. Q.; Beach, E. S.; Xiang, Y.; Tshudy, D. J.; Khanina, N.; Horwitz, C. P.; Bier, M. E.; Collins, T. J. *Environ. Sci. Technol.* **2011**, *45*, 7882.

(55) Warner, G. R.; Mills, M. R.; Enslin, C.; Pattanayak, S.; Panda, C.; Panda, T. K.; Sen Gupta, S.; Ryabov, A. D.; Collins, T. J. *Chem. Eur. J.* **2015**, *21*, 6226.

(56) Ellis, W. C.; Tran, C. T.; Denardo, M. A.; Fischer, A.; Ryabov, A. D.; Collins, T. J. *J. Am. Chem. Soc.* **2009**, *131*, 18052.

(57) Chahbane, N.; Popescu, D. L.; Mitchell, D. A.; Chanda, A.; Lenoir, D.; Ryabov, A. D.; Schramm, K. W.; Collins, T. J. *Green Chem.* **2007**, *9*, 49.

(58) Ghosh, A.; Mitchell, D. A.; Chanda, A.; Ryabov, A. D.; Popescu, D. L.; Upham, E. C.; Collins, G. J.; Collins, T. J. *J. Am. Chem. Soc.* **2008**, *130*, 15116.

(59) Federal-Provincial-Terretorial Committee; Health Canada: 2015; Vol. 2015.

(60) Emelianenko, M.; Torrejon, D.; DeNardo, M. A.; Socolofsky, A. K.; Ryabov, A. D.; Collins, T. J. *J. Math. Chem.* **2014**, *52*, 1460.

(61) Chanda, A.; Ryabov, A. D.; Mondal, S.; Alexandrova, L.; Ghosh, A.; Hangun-Balkir, Y.; Horwitz, C. P.; Collins, T. J. *Chem. Eur. J.* **2006**, *12*, 9336.

(62) Fukuta, N. *Nature* **1963**, *199*, 475.

(63) George, P. *Biochem. J.* **1953**, *55*, 220.

Chapter 3

Is Chlorine Working with TAML?

—The impacts of substituting NaClO for H_2O_2 in the most effective TAML system for removing metaldehyde

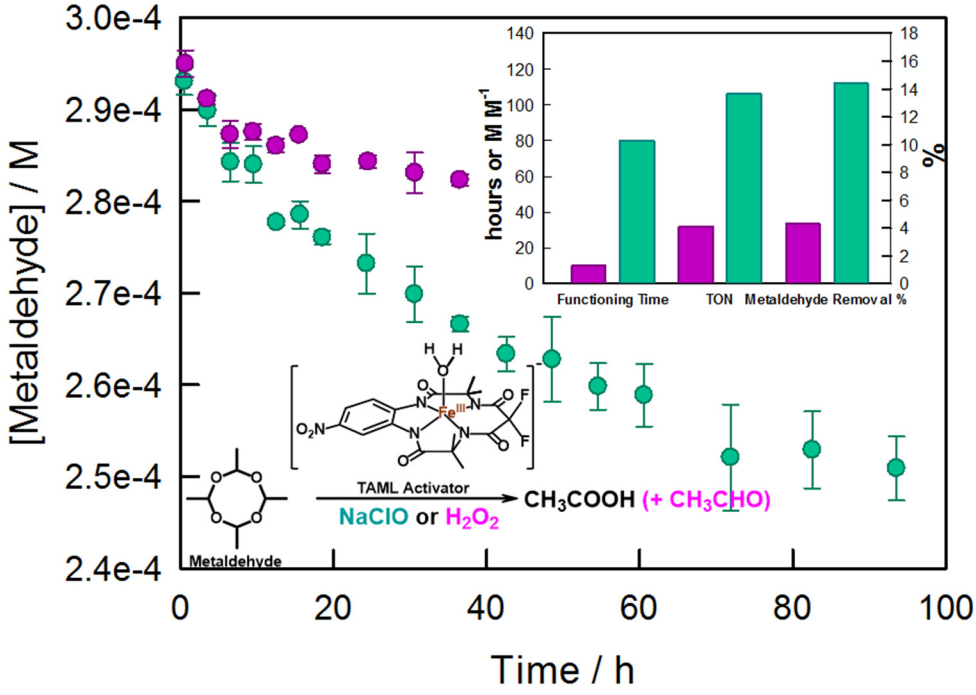

3.1 Introduction

While we are pursuing catalyst design as one method of increasing TAML degradation performance, we were curious as to what gains could be realized through the use of oxidants other than H_2O_2. Such systems could enable us to avoid H_2O_2-dependent catalyst inactivation processes altogether, thus enhancing the performance of current TAML catalysts as well as optimizing future activators. Hypochlorite is widely employed in US water disinfection processes[1] where it is generated in situ from chlorine gas at a low cost.[2] We have long known that TAML activators catalyze hypochlorite reactions.[3] NaClO activates TAML catalysts to give Fe^{V}=O complexes from -40 °C[4] to room temperature,[5] highlighting a similarity with TAML/H_2O_2 catalysis.[6] Therefore, we were curious as to what the effects of substituting NaClO for H_2O_2 in TAML systems would be. In water treatment, chlorine use often results in the formation of hazardous disinfection byproducts (DBPs) including the carcinogen chloroform.[7,8] When Br^- is present in water, bromate might also form as a DBP. Consequently, catalyst performance and DBP formation were examined in TAML/NaClO systems.

Metaldehyde (Met, Chart 3.1) is an exceptionally oxidation resistant pollutant. Its employment results in contamination of environmental waters at concentrations of regulatory concern. Due to its extreme persistence, remediation of Met contamination is challenging. This makes Met an ideal boundary substrate for testing the TAML/NaClO system since chlorine alone is ineffective in decomposing metaldehyde.[9] The previous chapter has shown that TAML/H_2O_2 system (Chart 3.1) is capable of slowly oxidizing metaldehyde to give a mixture of acetic acid and acetaldehyde. Here we examine the **1a** (Chart 3.1, 0.4–6.4 μM) catalyzed degradation of metaldehyde (0.33 mM) by NaClO

(0.008–0.02 M) at 25 °C and pH 7. Remarkably as will be shown, the shift from **1a**/H_2O_2 to **1a**/NaClO results in a threefold improvement in process technical performance. The process was monitored by ^{1}H NMR. No chloroform was detected by this method. However, preliminary gas chromatography mass spectrometry (GC-MS) studies of **1a**/NaClO oxidation of cinnamic acid revealed the formation of chloroform and other chlorinated compounds. In contrast with **1a**/H_2O_2 systems (see Chapter 6 for details), ion chromatography (IC) experiments detected bromate formation in the **1a**/NaClO system in the presence of bromide. On the other hand, chlorite, a toxic DBP formed in the chlorination of water,[10] is consumed by **1a**.

Chart 3.1 Structures of TAML catalysts and substrates used in this study.

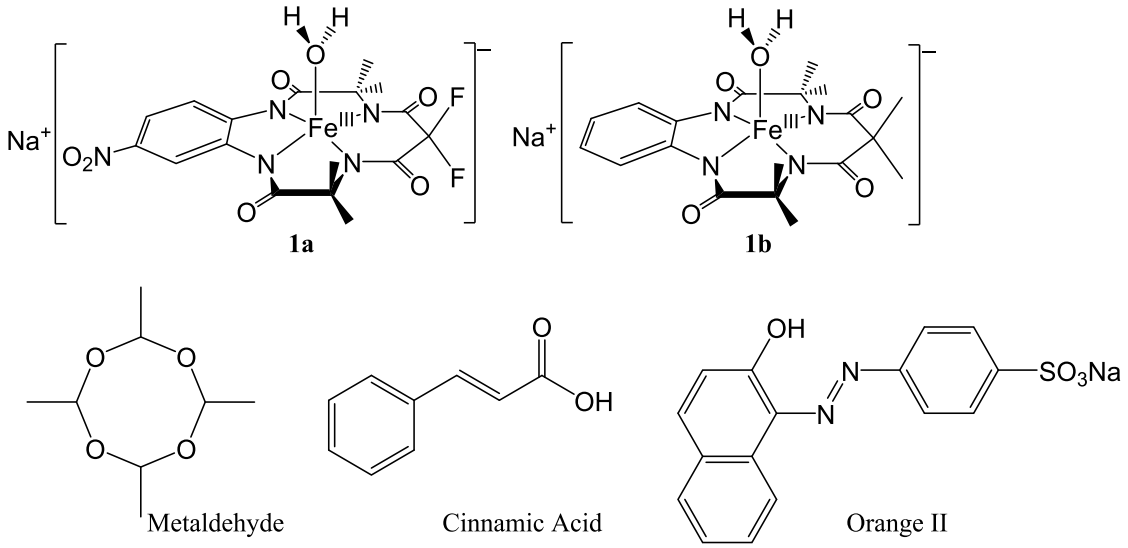

3.2 Results and discussion

3.2.1 Degradation of metaldehyde with TAML/NaClO system

3.2.1.1 The choice of oxidant is a process design tool for advancing TAML catalyst lifetimes. To assess the relative performances of **1a**/NaClO and **1a**/H_2O_2, measurements were performed under identical conditions. As shown in Figure 3.1A, the [Met] is unaffected by either NaClO or H_2O_2 alone. The NaClO kinetic trace shows that a single **1a** aliquot (3.98×10^{-7} M) effects a 14.4% reduction in the absolute integral of the 1.34 ppm Met C<u>H</u>$_3$ signal over the approximate duration of catalysis of 80 hours (Table 3.1). For comparison, in the corresponding experiment, a 4.3% reduction is observed for **1a**/H_2O_2 over the approximate duration of catalysis, which this time lasts only 10 hours. In both cases, the relationship between [Met] and time is initially linear allowing calculation of the initial oxidation rates (v = d[S]/dt) by fitting a linear form. While the initial rates of Met consumption are identical, a turnover number (TON) of 106 is observed in the NaClO system compared to the 32 in the H_2O_2 system, a three-fold improvement. These reaction features are also visible in the kinetic traces for acetic acid production (Figure 3.1B), with ca. 5 times more acetic acid being produced by **1a**/NaClO. Under these conditions **1a**/H_2O_2 generates an acetic acid:acetaldehyde product ratio of 3:1. The respective acetic acid and acetaldehyde rat LD_{50} values are 3310 and 661 mg kg^{-1} suggesting that this acetic acid enrichment is desirable.[11] The near exclusive production of acetic acid by **1a**/NaClO leads to an even more benign product mixture. Since chlorination of water containing organic matter generates hazardous disinfection byproducts (DBPs), including carcinogenic chloroform,[7,8] we have monitored for chloroform production—none was detected within the limits of the NMR technique.

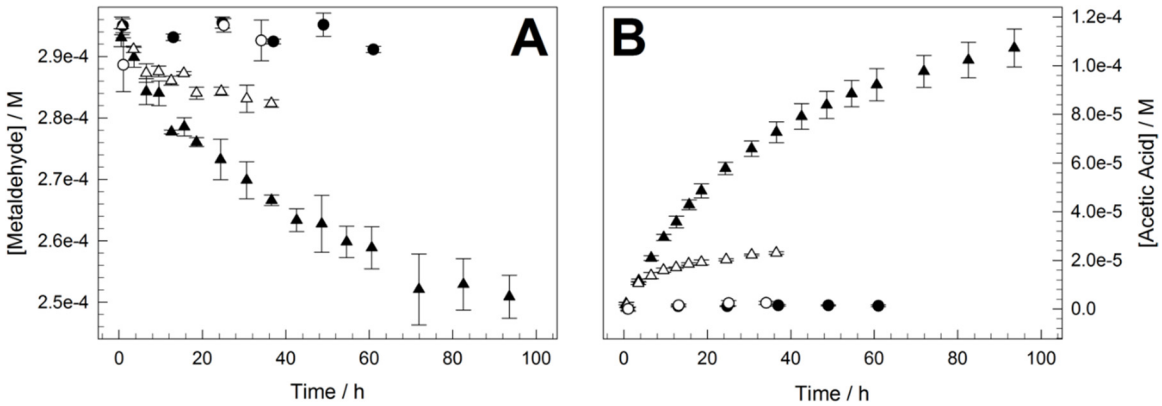

Figure 3.1 Oxidation of Met (2.95×10^{-4} M) by NaClO (3.8×10^{-3} M, 13 eq) or H_2O_2 (3.61×10^{-3} M, 12 eq) at pH 7. Kinetic traces of (**A**): metaldehyde consumption and (**B**): acetic acid formation. Circles: metaldehyde plus oxidant control experiments (● NaClO and ○ H_2O_2). Triangles: **1a** (3.98×10^{-7} M) catalyzed oxidations (▲ NaClO and △ H_2O_2). Conditions: pH 7 D_2O (0.01 M phosphate), reactions were allowed to proceed at room temperature. Concentrations were calculated from the absolute integrals of the metaldehyde and acetic acid $C\underline{H}_3$ signals at 1.34 and 1.92 ppm, respectively. The initial ^{1}H NMR integrals for the trace amounts of acetic acid that formed on sonication of metaldehyde were subtracted from those of the total acetic acid.

Table 3.1 Comparison of the **1a**/NaClO and **1a**/H_2O_2 systems in catalysis of metaldehyde degradation at pH 7. Conditions: [Met] = 2.95×10^{-4} M, [**1a**] = 3.98×10^{-7} M, [NaClO] = 3.8×10^{-3} M, [H_2O_2] = 3.6×10^{-3} M.

Oxidant	$v \times 10^8$ / M min^{-1}[a]	Removal / %	Major Products	TON	Functioning Time
NaClO	2.4 ± 0.4	14.4 ± 0.9	acetic acid	106 ± 6	80 h
H_2O_2	2.2 ± 0.3	4.3 ± 0.7	acetaldehyde and acetic acid	32 ± 5	10 h

[a]The rate (v) is calculated from the slope of the line of best fit to the first three [Met] measurements (v = d[Met]/dt).

The identical rate of Met oxidation observed for the two oxidants is informative. TAML catalysts function via the stoichiometric mechanism introduced in Chapter 1. The resting catalysts (Fe^{III}) undergo activation by an oxidant (k_I) to form active catalysts (Ac) which then oxidize a substrate (S) to give Fe^{III} and product(s) (k_{II}) or undergo inactivation (k_i)—

the reverse of catalyst activation, k_{-I}, is kinetically negligible. Equation 3.1 models the initial rate of substrate oxidation (Fe_{Tot} is the total concentration of catalyst).[35] For particularly difficult to oxidize substrates, catalyst activation outpaces substrate oxidation (k_I[Ox]>k_{II}[S]) and eq 3.1 simplifies to eq 3.2.

$$\frac{d[S]}{dt} = \frac{k_I k_{II}[Ox][S]}{k_{-I}+k_I[Ox]+k_{II}[S]} Fe_{Tot} \quad (3.1)$$

$$\frac{d[S]}{dt} = k_{II}[S]Fe_{Tot} \quad (3.2)$$

$$\ln\frac{S_0}{S_\infty} = \frac{k_{II}}{k_i}[Fe^{III}]_{tot} \quad (3.3)$$

For most substrates, k_I[Ox]<k_{II}[S] and catalyst activation is rate determining. However, Met oxidation is extremely slow. Of the tested TAML/H_2O_2 processes,[12] the **1a** system delivered the highest measurable rate and percent removal. The eq 3.3 (see Chapter 1 for details) estimated k_{II} value for **1a**/H_2O_2 is 120 ± 30 M^{-1} s^{-1}, ca. 340 times lower than the corresponding value for Orange II of 41,000 ± 1,000 M^{-1} s^{-1},[13] noting of course that the Orange II k_{II} and k_i were measured in H_2O while the Met data were recorded in D_2O.[13] The eq 3.3 estimated **1a**/H_2O_2 (D_2O) Met k_{II} is comparable to the known **1a**/H_2O_2 (H_2O) k_I of 350 ± 2 M^{-1} s^{-1}, which applies for the oxidation of nearly all substrates in water. Since k_I ~ k_{II} for the Met system, and [H_2O_2] > 10 × [Met], the oxidation of this very difficult substrate is rate-determining and eq 3.2 applies. This is further supported by the similarity of the observed rates of Met oxidation for both the **1a**/H_2O_2 and **1a**/NaClO systems which also provides strong evidence for rate determining substrate oxidation by a common Ac. Noting again that acetaldehyde is observed in the **1a**/H_2O_2 (D_2O) study, it follows that the known oxidation of acetaldehyde by NaClO[14] probably accounts for the virtual absence of acetaldehyde in the **1a**/NaClO product mixture. Since, as indicated by eq 3.3, ln(S_0/S_∞) is

fixed by $k_{II}Fe^{III}_{Tot}/k_i$, and both the NaClO and H_2O_2 processes share a common rate determining step with a common Ac, the NaClO performance advantage must derive from a decrease in k_i which is reflected in the greater reduction in [Met] and longer operating time. Considering that k_{II} and k_i have been found to track linearly for all TAML catalysts, this gain in operational stability with preservation of oxidative activity is remarkable.[13]

Inactivation of TAML catalysts has been found to follow both intramolecular suicidal[15-17] and intermolecular H_2O_2-dependent pathways[16,18] which are unimolecular in catalyst. To minimize the impacts of the latter in catalysis, a low [H_2O_2] is generally employed. In one case, a system in which H_2O_2 is generated enzymatically in situ has been devised.[19] By using NaClO we have eliminated the H_2O_2-dependent catalyst inactivation pathways altogether. The TON decreases by 70% on changing from NaClO to H_2O_2, indicating that in D_2O at least 70% of the k_i processes are attributable to H_2O_2 dependent catalyst inactivation. The eq 3.3 estimated NaClO k_i value of $(3.0 \pm 0.8) \times 10^{-4}$ s^{-1}, which is ca. 70 % less than the recently published **1a**/H_2O_2 k_i[13] of $(1.1 \pm 0.3) \times 10^{-3}$ s^{-1}, fits precisely with the conclusion that changing the oxidant increases the lifetime of the catalyst. The lifetime extension observed for the **1a**/NaClO catalysis further establishes the importance of understanding the nature of the H_2O_2 dependent inactivation pathway in TAML/H_2O_2 catalysis.

3.2.1.2 Effects of different catalyst concentrations. The identical rates of **1a**/H_2O_2 and **1a**/NaClO Met consumption are slow (Table 3.1). The effect of [**1a**] on the oxidation was examined with the aim of increasing both these rates and the percent of Met oxidized. Since the percent of Met oxidation by H_2O_2 with [**1a**] = 3.98×10^{-7} M was small, only higher [**1a**] experiments were performed in the H_2O_2 system (Figure 3.1). Surprisingly, the anticipated

increase in rate and percent Met consumption with increasing [**1a**] to 1.66 × 10^{-6} M was not observed. Instead, the kinetic trace is largely indistinguishable from that of the control experiment (Figure 3.2).

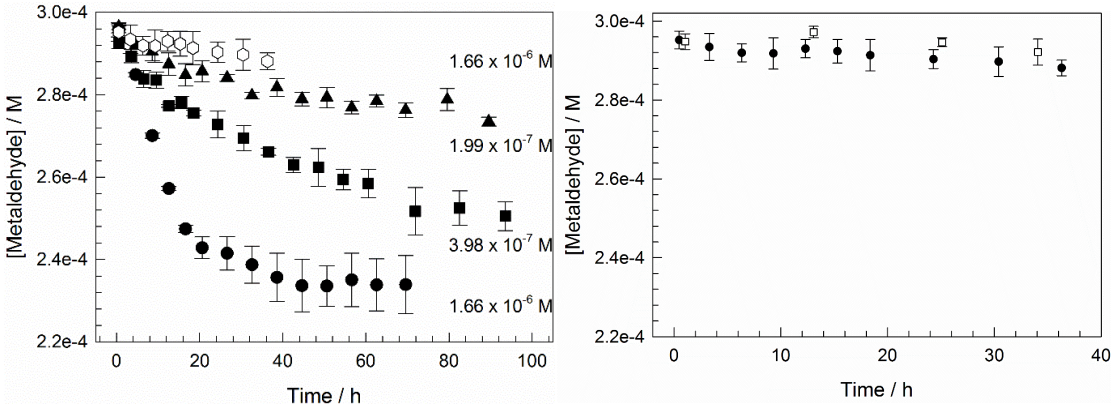

Figure 3.2 Left: kinetic traces of **1a** catalyzed metaldehyde oxidation. [**1a**] values are shown on the figure next to the corresponding kinetic traces. Hollow: [H_2O_2] = 3.61 × 10^{-3} M (12.2 equivalents); Black: [NaClO] = 3.8 × 10^{-3} M (12.8 equivalents). Other conditions: pH 7 D_2O (0.01 M phosphate), $[Met]_0$ = 2.95 × 10^{-4} M. Right: **1a** catalyzed metaldehyde degradation by H_2O_2 with the highest tested concentration of catalyst. Metaldehyde and H_2O_2 only (hollow square □); metaldehyde, H_2O_2, and **1a** (solid circle ●).

Kinetic traces of the oxidation of Met (2.95 × 10^{-4} M) by NaClO (3.8 × 10^{-3} M) were recorded for three different [**1a**] values: 1.99 × 10^{-7} M, 3.98 × 10^{-7} M, and 1.66 × 10^{-6} M (Figure 3.2). As shown in Table 3.2 and Figure 3.3, the initial rates of Met consumption increased linearly with [**1a**] but the TON did not remain constant. At [**1a**] of 1.99 × 10^{-7} M and 3.98 × 10^{-7} M, TONs of ~100 are observed. However, at [**1a**] of 1.66 × 10^{-6} M, the TON decreased by ~60%—the corresponding percentages of Met oxidation are 7.8, 14.4 and 21 %. In each case, approximately half of the theoretical amount of acetic acid, the only observable major product, is produced (kinetic traces of acetic acid generation are

shown in Figure 3.4). At the lower two [**1a**] values the NaClO catalysis is observed to function for about 90 h, but at the highest [**1a**] the catalysis lasts only for 30 h.

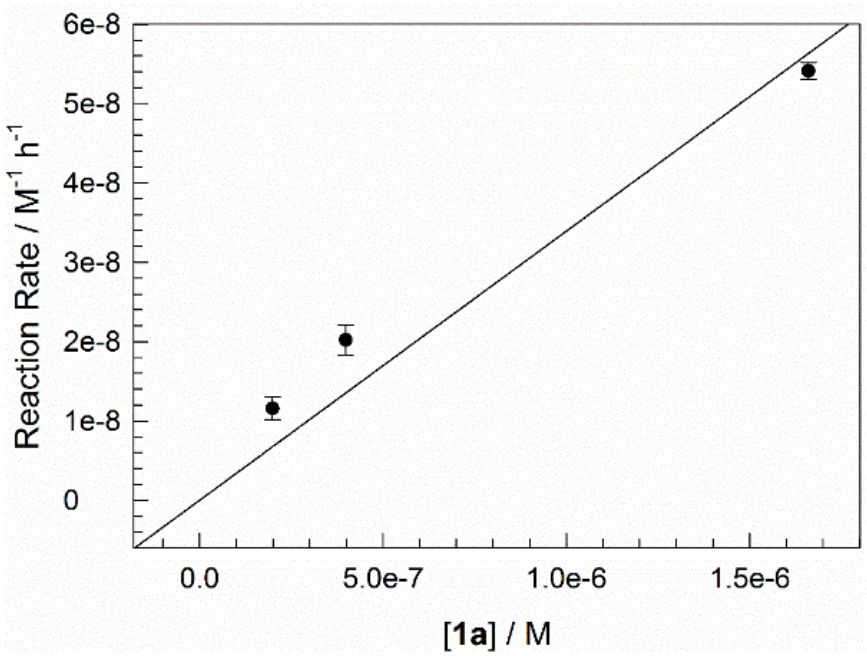

Figure 3.3 Initial rates of **1a** catalyzed metaldehyde oxidation by NaClO as a function of [**1a**]. Conditions: pH 7.1 D_2O (0.01 M phosphate), [Met] = 2.95×10^{-4} M, [NaClO] ≈ 3.8×10^{-3} M (12.8 equivalents), [**1a**] = 1.99×10^{-7} M, 3.98×10^{-7} M, 1.66×10^{-6} M, respectively.

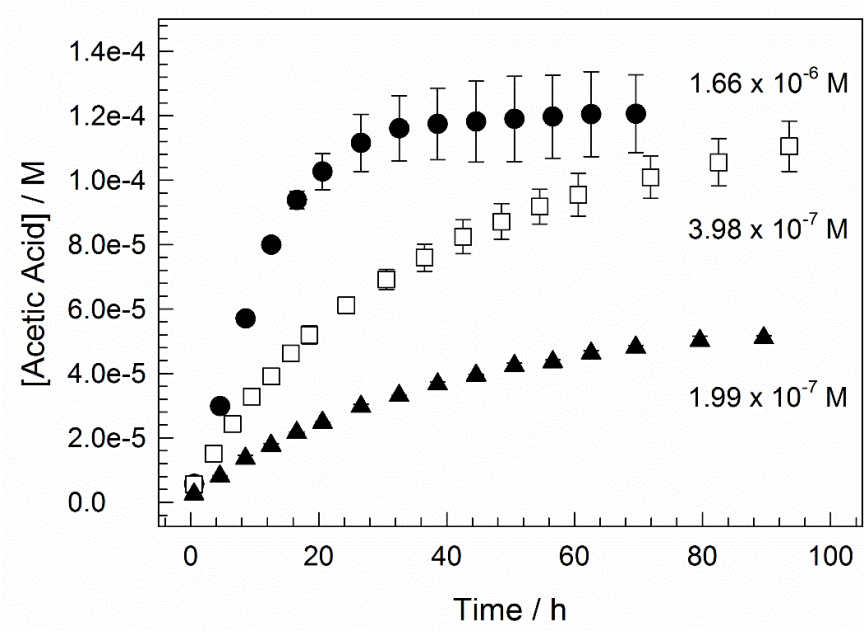

Figure 3.4 Kinetic traces of acetic acid formation during **1a** catalyzed metaldehyde oxidation by NaClO. Numbers indicate [**1a**]. The other conditions are as described in the caption of Figure 3.2.

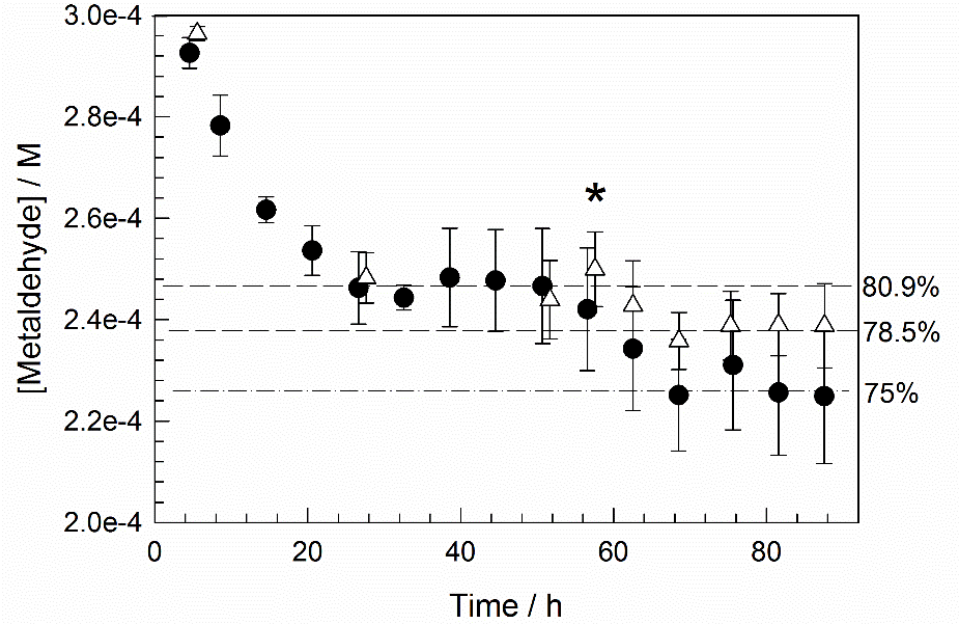

Figure 3.5 1a catalyzed metaldehyde oxidation by NaClO with the highest tested concentration of catalyst. Conditions: pH 7 D_2O (0.01 M phosphate). [Metaldehyde] = 2.99×10^{-4} M, [**1a**] = 1.66×10^{-6} M, [NaClO] = 3.51×10^{-4} M. The '*' indicates the addition of one aliquot of **1a** (hollow triangle △) or NaClO (solid circle ●).

Typically, TAML catalysis is conducted with excess oxidant and stops when all of the catalyst is inactivated. Catalysis resumes upon introduction of a fresh TAML aliquot.[12,13,16,20] In the experiment with [**1a**] = 1.66 × 10^{-6} M, Met consumption did not resume after introducing an additional aliquot of **1a** or of NaClO (3.51 × 10^{-4} M) at 50 h (Figure 3.5), giving evidence for both irreversible catalyst inactivation and complete oxidant consumption. This behavior is unusual and is being examined further.

Table 3.2 Summary of metaldehyde degradation at different [**1a**] values; [Met] = 2.95 × 10^{-4} M, [NaClO] ≈ 3.8 × 10^{-3} M.

[**1a**] × 10^{-7} M	v × 10^{8} / M min^{-1}[a]	TON	Met Removal / %	Acetic acid formed / %[b]	t_∞[c] / h
1.99	1.2 ± 0.2	116 ± 6	7.8 ± 0.4	4.1 ± 0.1	90
3.98	2.0 ± 0.2	106 ± 6	14.4 ± 0.9	9.0 ± 0.7	90
16.6	5.4 ± 0.1	37 ± 5	21 ± 3	10 ± 1	30

[a]The rate v was calculated from the slope of the line of best fit to the first five [Met] measurements (v = d[Met]/dt); [b]The percentage of acetic acid (AA) formation was calculated from the $C\underline{H}_3$ absolute integral relative to the initial metaldehyde signal (AA% = $({}^{Abs}Int_{1.92})/({}^{Abs}Int_{1.34})_0 \times 100$); [c]Reaction time.

In both the H_2O_2 and NaClO systems, catalyst lifetime and TON diminished significantly on increasing [**1a**] from 2–4 × 10^{-7} M to 1.66 × 10^{-6} M. This suggested that higher order processes in [**1a**] had become kinetically relevant. We have previously estimated contributions from inactivation pathways that are bimolecular in catalyst, labeled k_{2i} processes, to be negligible at catalyst concentrations <1 × 10^{-6} M, and these experimental results support the prior estimates.[13,16,17,20] The detection of these higher order processes here suggests that a k_{2i} pathway makes significant contributions to the rate of catalyst inactivation in both systems. However, increasing [**1a**] impacted the H_2O_2 and NaClO processes differently. In the NaClO system, increasing [**1a**] from 3.98 × 10^{-7} M to 1.66 ×

10^{-6} M gave a 6.6% increase in the percent of Met oxidized (Table 3.2). In the H_2O_2 system, this same [**1a**] increase reduced Met oxidation from 4.3% to effectively zero within experimental error (Figure 3.2). We have interpreted this loss of catalysis in the following way.

In the H_2O_2 case with [**1a**] = 1.66×10^{-6} M, given the estimated k_{II} of 120 ± 30 $M^{-1}s^{-1}$ and setting an approximation for the oxidation percentage of 2 % (Figure 3.2), eq 3.3 gives an estimated k_i value of ca. 1.0×10^{-2} s^{-1}. This is an order of magnitude greater than the k_i for **1a**/H_2O_2 measured at [**1a**] $\approx 10^{-8}$ M where inactivation is exclusively unimolecular in catalyst indicating that the peroxide dependent k_{2i} inactivation processes must greatly outpace those unimolecular in catalyst. Equation 3.3 is very sensitive to the estimated oxidation percentage. If values <2% are chosen instead, even higher k_i values result. The analogous NaClO process with [**1a**] = 1.66×10^{-6} M has a k_i of 8.5×10^{-4} s^{-1}; this is at least one order of magnitude less than the corresponding H_2O_2 value and is comparable to the k_i values found for unimolecular catalyst inactivation at low [**1a**]. Thus, one can deduce that at high [**1a**], the use of NaClO results in productive catalysis because the peroxide-dependent k_{2i} processes are absent. However, at high [**1a**] = 1.66×10^{-6} M the eq 3.3 estimated k_i in the NaClO system is ca. threefold greater than those of the lower [**1a**] experiments, indicating that other k_{2i} processes operate in the NaClO system. These results highlight the importance of determining the mechanism(s) of the k_{2i} process(es) and developing a mathematical expression that accounts for them and allows us to precisely determine k_{2i} as these developments would advance our understanding of k_{2i} and should aid in the design of superior catalysts for high [TAML] processes.

3.2.1.3 More complete metaldehyde removal with continuous additions of catalyst and oxidant. Because of the presence of k_{2i} processes, deep Met removal is most efficiently accomplished by using multiple catalyst doses that ensure that [**1a**] < ca. 1×10^{-6} M at all times. The optimized **1a** aliquot was 4×10^{-7} M. The data shown in Figure 3.6 represent two separate experiments demonstrating the efficacy of multiple [**1a**] = 4×10^{-7} M aliquots. Experiment 1 employed a $[Met]_0$ of 3.32×10^{-4} M. Since Met mineralization demands 20 equivalents of NaClO, a slight excess (7.61×10^{-3} M) was added. The first catalyst aliquot consumed Met for 72 h before the reaction ceased. Seven additional **1a** aliquots were added leading to a slow oxidation of 75.3% over 576 h.

After the addition of the fifth catalyst aliquot, the position of the $C\underline{H}_3COO^-$ ^1H NMR signal at 1.956 ppm indicated a solution pH of 5.2, 1.8 units less than the initial pH of 7 (Figure 3.7).[12,21] Therefore at 360 h, NaClO (4.79×10^{-3} M) was added to nearly return the $C\underline{H}_3COO^-$ signal to its initial value while providing additional oxidant. The initial metaldehyde concentration ($[Met]_0$), change in metaldehyde concentration (Δ[Met]), TON, and percent Met degradation for each catalyst aliquot are summarized in Table 3.3. The amount of metaldehyde removed by catalyst aliquots 1-8 declines with $[Met]_0$.

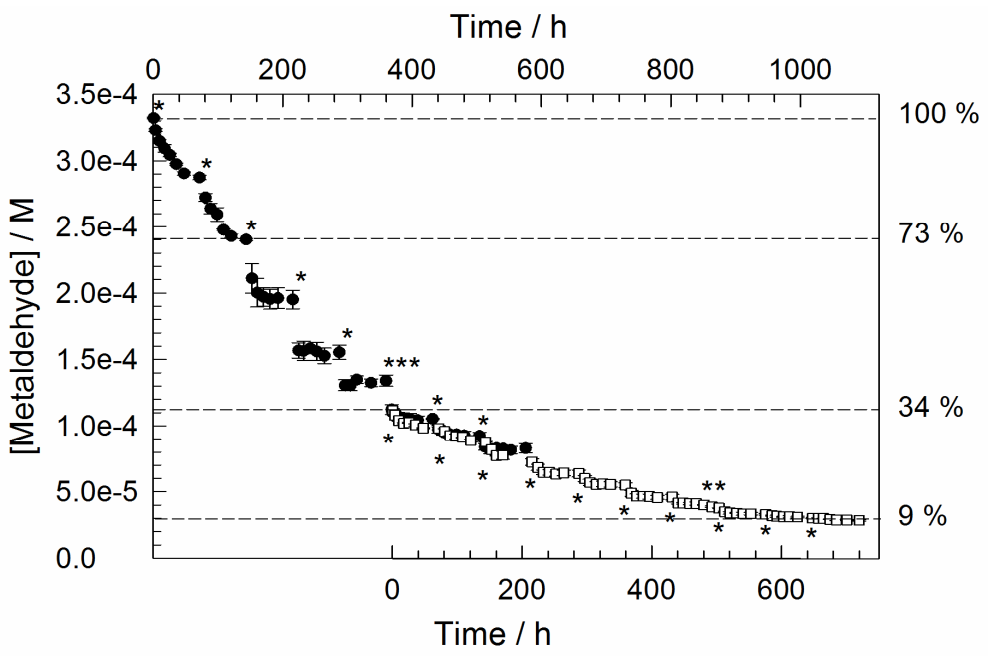

Figure 3.6 Kinetic traces of metaldehyde degradation by NaClO catalyzed by **1a** in pH 7.0 D_2O (0.01 M phosphate). Two experiments are shown. Experiment 1: solid circle (●) and top time axis, $[Met]_0 = 3.32 \times 10^{-4}$ M, [**1a**] = 4.0×10^{-7} M, [NaClO] = 7.61×10^{-3} M. Experiment 2: hollow square (□) and bottom time axis, $[Met]_0 = 1.12 \times 10^{-4}$ M, [**1a**] = 4.0×10^{-7} M, [NaClO] = 4.71×10^{-3} M. For both experiments: *indicates the addition of one 4.0×10^{-7} M catalyst aliquot, **indicates the addition of 3.44×10^{-3} M NaClO, ***indicates the addition of one 4.0×10^{-7} M aliquot catalyst along with 4.79×10^{-3} M NaClO.

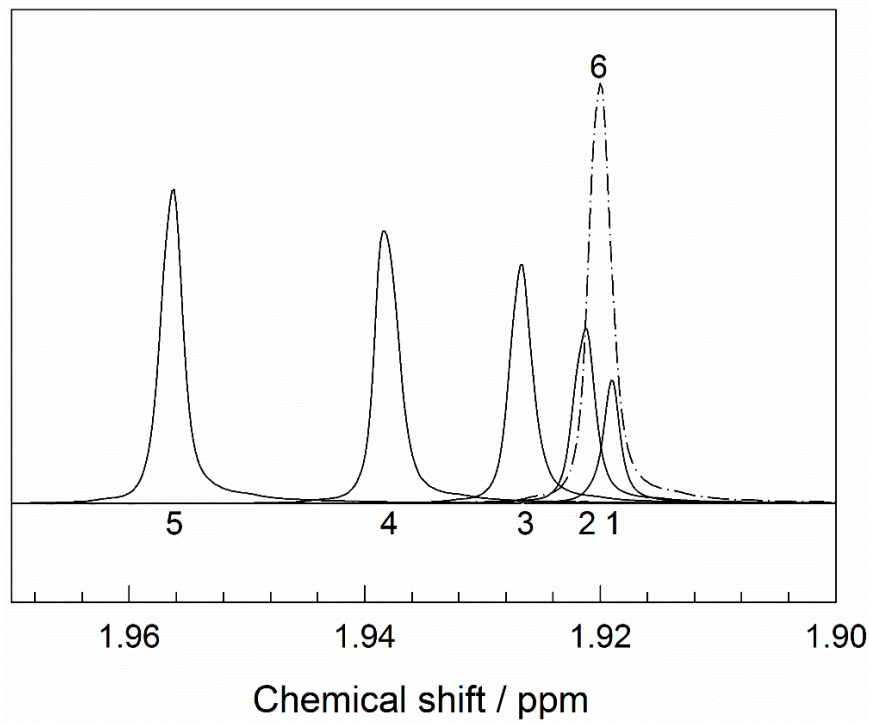

Figure 3.7 Drift in the $C\underline{H}_3COO^-$ chemical shift. The proton peaks are obtained from the last recorded spectra for oxidation by each catalyst aliquot. The numbers indicate the identity of the catalyst aliquot. The dashed peak indicates the addition of NaClO with catalyst aliquot 6 which nearly returns the $C\underline{H}_3COO^-$ peak to the original chemical shift. Other conditions are as described in the caption of Figure 3.6.

In Experiment 2, the oxidation of a fresh 1.12×10^{-4} M Met solution was studied (Figure 3.6 hollow squares) to examine if the ongoing deterioration in Met removal was a function of accumulating acetate or inactivated catalyst products. The Experiment 2 initial metaldehyde concentration ($[Met]_0$), change in metaldehyde concentration ($\Delta[Met]$), TON, and percent Met degradation for each catalyst aliquot are also summarized in Table 3.3. There is considerable agreement between the data sets. If the [Met] is followed along the black dotted curve of Experiment 1 through the adjacent white squares of Experiment 2, the result is representative of one continuous degradation process. Here, the [Met] of a 330 μM solution can be reduced an order of magnitude in ~47 days by treatment with 0.02 M

NaClO in the presence of 16 aliquots (4.0×10^{-7} M each, 6.4 μM total) of **1a**. Such a process would consume less than 60 equivalents of NaClO and proceed with an average TON of 66. This is significantly less than the Experiment 1 aliquot 1 TON of 112 ± 6. TONs steadily declined with $[Met]_0$ (Figure 3.8 and Table 3.3). This dependence holds for all aliquots of both Experiments 1 and 2 despite variations in solution pH and [NaClO]. This is evidence that the diminished catalyst performance cannot be attributed to processes involving acetate or catalyst inactivation products. Instead, eq. 3.3 well predicts this behavior—the $\Delta[Met]/[Met]_0$ proportionality observed represents a fixed 4×10^{-7} M catalyst aliquot removal percentage which indicates that k_{II} and k_i track each other closely across the studied pH range.

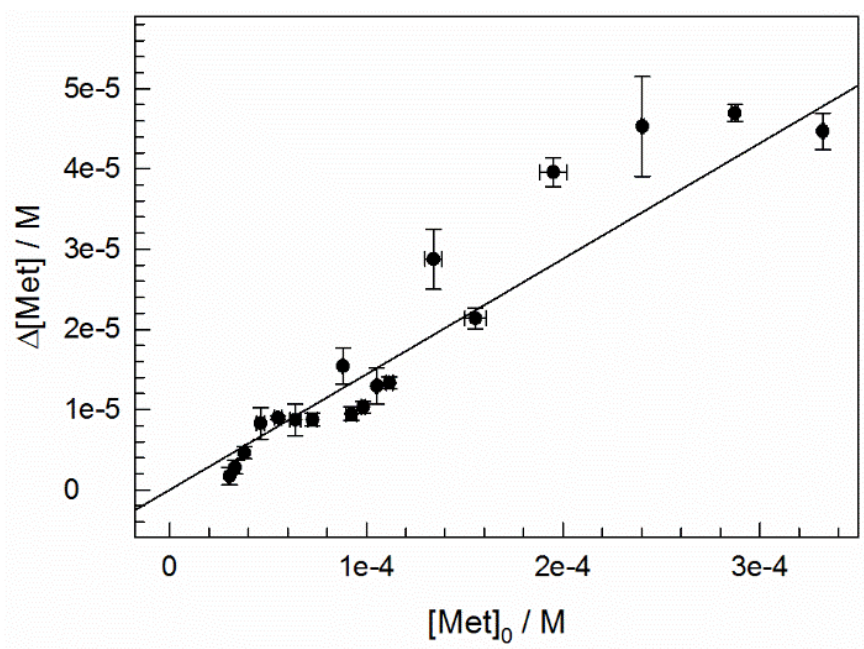

Figure 3.8 Correlation between Δ[Met] and $[Met]_0$. Each data point represents the Δ[Met] effected by each Experiment 1 and 2 catalyst aliquot. The line gives the eq 3.3 predicted Δ[Met] values with $k_i = 3.0 \times 10^{-4}$ s^{-1}, $k_{II} = 120$ $M^{-1}s^{-1}$, and [**1a**] = 4.0×10^{-7} M. The other conditions are as indicated in the Figure 3.6 caption and Table 3.3.

Table 3.3 Summary of Experiments 1 and 2 with conditions as described in Figure 3.6.

# Cat.	$[Met]_0$ /× 10^{-4} M	Δ[Met] /× 10^{-4} M	% degrad.	TON	$d[Met]_0/d[Ic]^e$
1[a]	3.320 ± 0.006	0.45 ± 0.02	13.5 ± 0.7	112 ± 6	130 ± 30
2[a]	2.87 ± 0.02	0.47 ± 0.01	16.3 ± 0.3	117 ± 3	110 ± 30
3[a]	2.404 ± 0.008	0.45 ± 0.06	19 ± 3	110 ± 20	90 ± 20
4[a]	1.95 ± 0.07	0.40 ± 0.02	20.3 ± 0.4	99 ± 5	80 ± 20
5[a]	1.55 ± 0.05	0.21 ± 0.01	13.7 ± 0.4	53 ± 3	60 ± 20
6[a]	1.34 ± 0.04[b]	0.29 ± 0.04	21 ± 2	72 ± 9	50 ± 10
7[a]	1.053 ± 0.005	0.13 ± 0.02	12 ± 2	32 ± 6	40 ± 10
8[a]	0.92 ± 0.03	0.094 ± 0.009	10 ± 1	24 ± 2	36 ± 9
1[c]	1.12 ± 0.02	0.13 ± 0.01	11.9 ± 0.4	33 ± 2	40 ± 10
2[c]	0.98 ± 0.01	0.10 ± 0.01	10.5 ± 0.6	26 ± 2	40 ± 10
3[c]	0.880 ± 0.003	0.15 ± 0.02	18 ± 3	39 ± 6	30 ± 10
4[c]	0.73 ± 0.02	0.087 ± 0.008	12 ± 1	22 ± 2	28 ± 7
5[c]	0.64 ± 0.03	0.09 ± 0.02	14 ± 3	22 ± 5	25 ± 7
6[c]	0.55 ± 0.02	0.090 ± 0.003	16.3 ± 0.9	22 ± 1	21 ± 6
7[c]	0.46 ± 0.02[d]	0.08 ± 0.02	18 ± 3	21 ± 5	18 ± 5
8[c]	0.379 ± 0.002	0.046 ± 0.08	12 ± 2	12 ± 2	15 ± 5
9[c]	0.332 ± 0.006	0.028 ± 0.09	8 ± 2	7 ± 2	13 ± 4
10[c]	0.304 ± 0.004	0.02 ± 0.01	6 ± 3	4 ± 3	12 ± 3

3.2.1.4 Summary. The rate of substrate consumption in **1a** catalyzed Met transformation is not sensitive to the identity of the oxidant employed, a strong indication of catalysis by the same reactive intermediate in both the NaClO and H_2O_2 systems. However, by lowering the rate of catalyst inactivation which we attribute to elimination of contributions from H_2O_2 dependent processes, this TAML/NaClO system delivers a three-fold k_{II}/k_i enhancement over the **1a**/H_2O_2 system. Importantly, no chloroform was detected by ^{1}H NMR. At [**1a**] > 1 × 10^{-6} M, inactivation pathways which are bimolecular in catalyst and outpace those unimolecular in catalyst rendering **1a**/H_2O_2 transformation of Met completely ineffective and establishing an upper bound for [TAML] in H_2O_2 systems. The

use of NaClO at these [**1a**] restores functioning catalysis though k_{2i} processes which outpace k_i processes still operate. Further investigations of the mechanisms of the here discovered k_{2i} processes and the differences between the H_2O_2 and NaClO systems are underway.

3.2.2 Preliminary studies on DBPs in the TAML/NaClO system

The formation of DBPs, a major drawback of chlorination as discussed in Chapter 1, must be investigated in any study of a water treatment system employing chlorine. In this section, the potential for TAML/NaClO to form three types of DBPs that can be found in water treatment systems employing chlorine is evaluated by GC-MS, IC, and UV-vis measurements. Preliminary results reveal that under some conditions TAML/NaClO also produces DBPs.

3.2.2.1 Formation of chlorinated organic compounds. As discussed in above, the available evidence indicates that both TAML/NaClO and TAML/H_2O_2 oxidation of metaldehyde proceed via a similar mechanistic pathway with a similar Ac. Chlorinated DBPs are not expected to form via this pathway. However, when substrates that can be oxidized by NaClO are present, it is likely that both NaClO and TAML catalyzed pathways operate. We wondered what the impact of the presence of TAML would be on the quantity of chlorinated DBPs formed in such NaClO systems. Chlorination of water containing cinnamic acid, a structurally simple constituent of natural organic matter (NOM), generates chlorinated DBPs[22] making the system ideal for assessing the impacts of TAML catalysts on the product distribution.

Analysis of the products of cinnamic acid oxidation by **1a**/NaClO by GC-MS showed the formation of a series of chlorine-containing compounds. With the aid of the GC-MS library, we were able to identify several of the major common chlorinated products which include chloroform, chlorobenzene, dichloromethane, and a mixture of monochloro-styrene isomers. An integration of these compound peaks indicates that the addition of TAML to the cinnamic acid reaction solution did not decrease the formation of chlorinated DBPs. While the presence of **1a** does alter the composition of the product mixture compared to that of chlorination alone, the **1a** catalyzed process generates a similar amount of chloroform and greater amount of chlorobenzene (Figure 3.9). Initially, NaClO treatment alone generates a significant greater amount of chlorostyrene isomers than does the **1a**/NaClO system (Figure 3.10). However, the compound(s) disappeared in the NaClO system, presumably due to deeper but slower oxidations. The accumulation of these compounds in the **1a**/NaClO system was not observed. This may be due to more rapid oxidation of these compounds by the Ac of **1a**. After seven days, the amount of chlorostyrene(s) detected in both the catalyzed and uncatalyzed processes is identical. These results suggest that the presence of catalyst **1a** accelerates the oxidation processes observed in the NaClO system but does form chlorinated-DBPs if precursors are in the water. Depending on residence and treatment times, the lower initial concentrations of chlorostyrene observed in the **1a** system may enable a significant improvement in water treatment resulting in the distribution of water having lower amounts of DBPs.

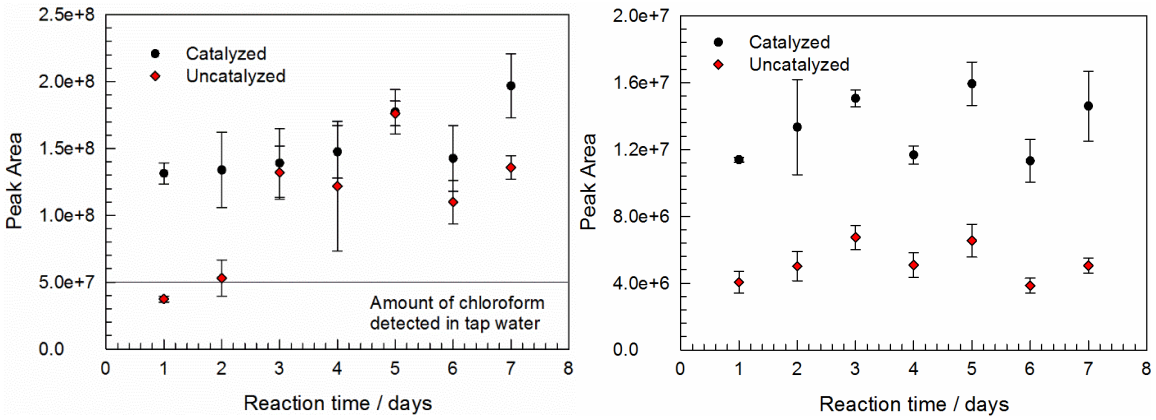

Figure 3.9 Comparison of chloroform (left) and chlorobenzene (right) formation between the catalyzed and uncatalyzed chlorination processes. Conditions: 6 mL reaction mixture in a 10 mL vial, pH 7.0 (0.01 M phosphate), [Cinnamic Acid] = 5.0×10^{-5} M, [**1a**] = 3.0×10^{-7} M, [NaClO] = 2.43×10^{-3} M (50 equiv.). The reaction was quenched with excess Na_2SO_3 after certain periods of time. Samples were injected into the GC-MS using headspace solid phase microextraction (SPME).

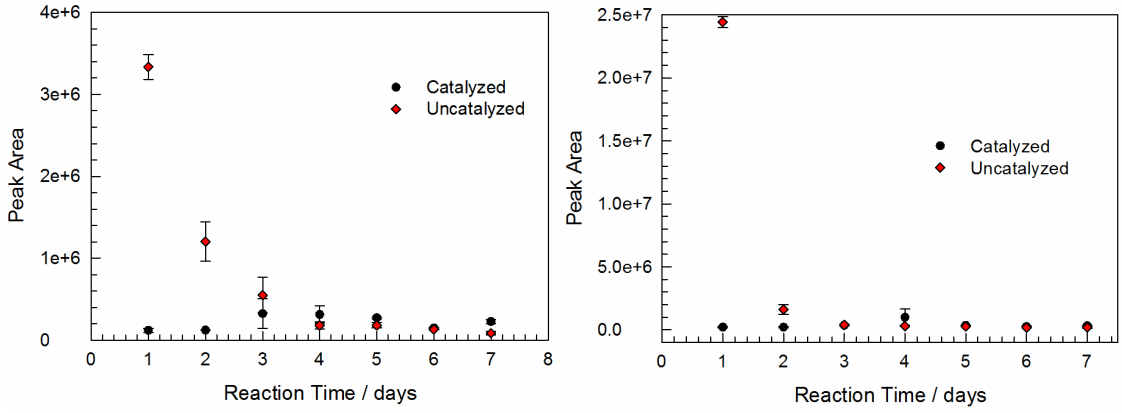

Figure 3.10 Comparison of the two chloro-styrene isomers (left and right) formation between catalyzed and uncatalyzed chlorination processes. Conditions are as described in Figure 3.9.

3.2.2.2 Formation of bromate. Though the presence of iron compounds does not increase bromate formation during the chlorination of bromide containing waters,[23] this has not been demonstrated for TAML catalysts which, as discussed above, form high valent reactive intermediates on NaClO treatment. NaClO treatment of a solution containing bromide and

of an identical solution containing **1b** did not produce detectable concentrations of bromate (Figure 3.11). However, treatment of an identical solution containing **1a** resulted in formation of bromate at a concentration of ~230 µg/L. Though the bromate formation mechanism catalyzed by **1a** is unknown, this preliminary result indicates that **1a**/NaClO is not a suitable treatment method for waters containing high bromide concentrations.[24] Chlorite (ClO_2^-, ~55 µg), a DBP, was formed in the solutions that did not contain a TAML catalyst. However, no chlorite was detected in those containing either **1a** or **1b**. Consequently, additional experiments were conducted to determine whether resting TAML catalysts are activated by chlorite and, in the process, remove this toxic DBP from water.

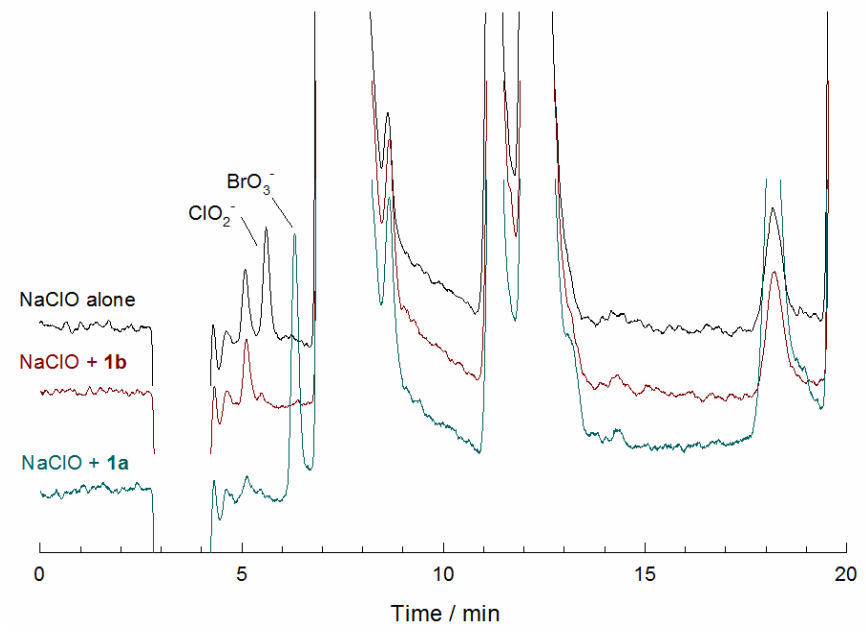

Figure 3.11 Ion chromatographs of reaction solutions containing Br^- and NaClO in the absence of or presence of either **1a** or **1b**. Conditions: [NaClO] = 5.5×10^{-4} M (41 mg/L), [Br^-] = 1.4×10^{-2} M (1.12 mg/L), [**1a**] = 4.75×10^{-7} M (247 µg/L), [**1b**] = 4.73×10^{-7} M (221 µg/L). The reaction mixtures were allowed to stand overnight (20 h), then [Na_2SO_3] = 1.5×10^{-3} M was added to remove NaClO and the mixture was analyzed by ion chromatography.

*3.2.2.3 Chlorite consumption by **1a**.* To determine whether chlorite can activate TAML catalysts to perform oxidation chemistry, solutions containing chlorite or chlorate and the azo dye Orange II in the presence or absence of ***1a*** were monitored by UV-Vis spectroscopy. Orange II is a relatively easily oxidized dye commonly employed in TAML mechanistic studies.[13,25] Orange II is not oxidized by chlorite or chlorate alone or the **1a**/chlorate system however it is slowly consumed by **1a**/chlorite (Figure 3.12). Orange II oxidation by **1a**/NaClO was also monitored for reference. The results indicate that chlorite is capable of activating TAML catalyst **1a** to perform oxidation chemistry.

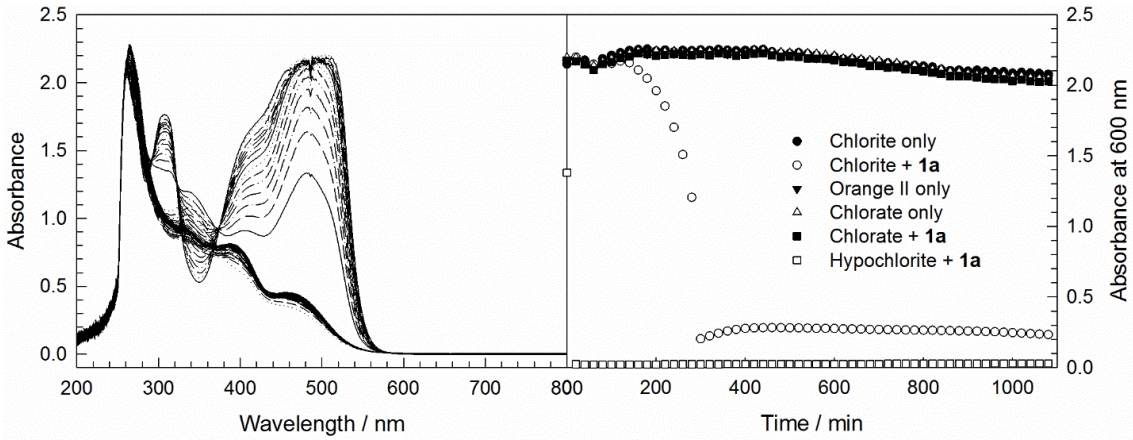

Figure 3.12 Orange II oxidation by chlorite or chlorate or hypochlorite in the presence or absence of catalyst **1a** in unbuffered water monitored via UV-vis. Conditions: H_2O, $[ClO_2^-] = 1.44 \times 10^{-3}$ M, $[ClO_3^-] = 1.16 \times 10^{-3}$ M, [**1a**] = 4.89×10^{-7} M, [Orange II] = 2.0×10^{-4} M. Left: spectra change of Orange II oxidized by chlorite catalyzed by **1a**; Right: kinetic traces of Orange II oxidation under different conditions as described in the figure.

3.3 Conclusion

The enhanced catalyst lifetime observed on substitution of NaClO for H_2O_2 in **1a** catalyzed Met degradation which allows more substrate degradation and a higher efficiency of

catalyst performance indicates that gains can be made in TAML catalysis through oxidant substitution. However, caution must be exercised in the use of NaClO to achieve these gains in water treatment applications as micropollutant oxidation by TAML/NaClO can yield DBPs. Further studies will be required to see if whether or not TAML/NaClO improves DBP safety overall compared to the uncatalyzed process. Special care should be taken in the application of TAML/NaClO to treatment of waters containing very high concentrations of Br^- or NOM as bromate and chlorinated DBPs may also form.

3.4 Experimental

3.4.1 Materials

All reagents, components of buffer solutions, and solvents were at least ACS reagent grade and were used as received. Metaldehyde (Acros, 99%) was recrystallized in ethanol and stored in the fridge.[26] Metaldehyde stock solutions (0.3 mM) were generated by sonicating a measured amount of metaldehyde in buffered D_2O (99.9%, Cambridge Isotope Laboratories, Inc.) at room temperature for 3 h. Buffers with designated pHs (6.2-7.0) were prepared with 0.01 M phosphate and monitored by an accumet™ AB15 pH meter at room temperature. DCl in D_2O was added to adjust the reaction mixture pH to 7.0 after NaClO addition. The pH values reported for the buffered D_2O solutions are the uncorrected pH meter readings. TAML activators **1a** and **1b** were obtained from GreenOx Catalysts, Inc. and **1b** was further purified by elution through a C18-silica gel column with a water/methanol (v/v 95/5) mixture as the eluent. Stock solutions of TAML activators (2×10^{-4} M) were prepared in D_2O, and stored in fridge. The concentrations of H_2O_2 and NaClO

were quantified by measuring the UV-vis absorbance at 230 nm (ε = 72.4 $M^{-1}cm^{-1}$)[27] and 293 nm (ε = 350 $M^{-1}cm^{-1}$),[28] respectively.

3.4.2 Instrumental

UV-Vis measurements were performed on an Agilent 8453 UV-Vis spectrophotometer equipped with an 8-cell transporter and thermostatic temperature controller. Solution temperatures were maintained at 25 ºC in capped quartz cuvettes (1.0 cm).

1D ^{1}H spectra were recorded at 300 K on a Bruker Avance™ III 500 NMR spectrometer operating at 500.13 MHz. The water signal was suppressed using the presaturation experiment (zgpr) from the Bruker pulse programs library. Chemical shifts are reported in parts per million relative to TMSP (internal standard for water solutions). Each sample was scanned 128 times over 16.5 minutes. The Bruker TopSpin™ 3.0 software was used to process the NMR data. The absolute integral of each proton peak was used for quantification. Each data point is the average of three measurements and the error bars shown are the standard deviation.

GC-MS analyses were performed on a Thermo scientific TRACE GC (column: Restek, Rxi®-XLB, 0.25 mm ID) with DSQ MS equipped with a LEAP Combi PAL® autosampler. Headspace solid phase microextraction (SPME) method (Table 3.4) was applied as the sampling method. The optimized SPME method parameters are shown in Table 3.4. A Supelco® Carboxen/PDMS fiber (75 µm) was used for SPME. Samples were injected via the splitless injection mode. The GC oven temperature program is as shown in Table 3.5.

Table 3.4 SPME parameters for headspace extraction of chlorinated DBPs for GC-MS analysis.

Pre-incubation Time / s	10
Incubation Temperature / ºC	35
Extraction Time / min	2
Desorption Time / min	5

Table 3.5 Temperature ramping program for GC-MS analysis of chlorinated compounds.

	Rate / ºC min^{-1}	Temperature / ºC	Hold Time / min
Initial	–	35	1
Ramp 1	10	220	1
Ramp 2	25	300	3

Ion chromatography: A dionex DX500 chromatograph consisting of an LC25 chromatography oven, a GP 50 gradient pump, an ED 40 electrochemical detector, an AS 40 automated sampler and an ERS® 500 self-regenerating suppressor was used for IC studies. The analytical column used was a Dionex IonPac AS9-HC (4mm × 250mm) and the guard column used was a Dionex IonPac AG9-HC (4mm × 50mm). The data were analyzed using Chromeleon chromatography software (version 6.70). Analysis was performed according to EPA method 300.1: 9 mM isocratic Na_2CO_3 in deionized water (18.1 mΩ-cm) was the eluent and the flow rate was set at 1 mL min^{-1}, SRS current was set at 100 mA, the oven temperature was 35 °C and injection volume was 200 µL. The detection limit for bromate is Ca. 7 µg/L in deionized water. A series of ion standards were analyzed via IC using EPA method 300.1[29] and their elution time are listed in the table below.

Table 3.6 Elution time of different ions analyzed by EPA method 300.1.

Ion	F^-	ClO_2^-	BrO_3^-	Cl^-	NO_2^-
Name	Fluoride	Chlorite	Bromate	Chloride	Nitrite
Elution time / min	4.4	5.7	6.5	7.3	9.2
Ion	Br^-	ClO_3^-	NO_3^-	PO_4^{3-}	SO_4^{2-}
Name	Bromide	Chlorate	Nitrate	Phosphate	Sulfate
Elution time / min	11.2	12.8	14.0	17.4	22.2

3.4.3 Reaction processes for detection

GC-MS: The reactions were carried out directly in 10 mL screw-capped GC-MS sample vials with a reaction mixture volume of 6 mL. Cinnamic Acid (5.0×10^{-5} M), **1a** (3.0×10^{-7} M) and NaClO (2.43×10^{-3} M, 50 equiv) were added to a pH 7.0 (0.01 M phosphate) buffer. The vials were then sealed with parafilm and allowed to stand for the indicated periods of time. The reactions were then quenched with excess Na_2SO_3 before injection into the GC-MS sampled by SPME.

IC: Both NaClO (5.5×10^{-4} M, 41 mg/L) and catalyst (either **1a** or **1b**, 4.75×10^{-7} M, 247 μg/L or 4.73×10^{-7} M, 221 μg/L) were added to a bromide solution (1.12 mg/L) and allowed to sit overnight (20 h). Na_2SO_3 (1.5×10^{-3} M) was then added at the specified time interval to quench the reaction by eliminating NaClO for IC analysis.

3.5 References

(1) U.S. Environmental Protection Agency *The History of Drinking Water Treatment*, 2000.

(2) Deborde, M.; von Gunten, U. *Water Res.* **2008**, *42*, 13.

(3) Collins, T. J.; Gordon-Wylie, S. W. US Patent 5,847,120, 1998.

(4) Mills, M. R.; Burton, A. E.; Mori, D. I.; Ryabov, A. D.; Collins, T. J. *J. Coord. Chem.* **2015**, *68*, 3046.

(5) Ghosh, M.; Singh, K. K.; Panda, C.; Weitz, A.; Hendrich, M. P.; Collins, T. J.; Dhar, B. B.; Sen Gupta, S. *J. Am. Chem. Soc.* **2014**, *136*, 9524.

(6) Kundu, S.; Annavajhala, M.; Kurnikov, I. V.; Ryabov, A. D.; Collins, T. J. *Chem. Eur. J.* **2012**, *18*, 10244.

(7) Sedlak, D. L.; von Gunten, U. *Science* **2011**, *331*, 42.

(8) Yang, X.; Shang, C. *Environ. Sci. Technol.* **2004**, *38*, 4995.

(9) Marshall, J. *Water UK briefing paper on metaldehyde*, 2013.

(10) Hrudey, S. E. *Water Res.* **2009**, *43*, 2057.

(11) Edward M. Arnett; W. Emmett Barkley; Peter Beak; Edwin D. Becker; Henry E. Bryndza; Imogene L. Chang; Carol Creutz; Rick L. Danheiser; Eric M. Gordon; Robert J. Lackmeyer; Lee Magid; Thomas F. McBride; Ann M. Norberg; Edward W. Petrillo; Stanley H. Pine; Fay M. Thompson; Tamae Maeda Wong; Kasandra Gowen; Sarah W. Plimpton; Butera., J. F. *Prudent Practices in the Laboratory: Handling and Disposal of Chemicals*; National Academy Press: Washington, D.C., 1995.

(12) Tang, L. L.; DeNardo, M. A.; Gayathri, C.; Gil, R. R.; Kanda, R.; Collins, T. J. *Environ. Sci. Technol.* **2016**, *50*, 5261.

(13) DeNardo, M. A.; Mills, M. R.; Ryabov, A. D.; Collins, T. J. *J. Am. Chem. Soc.* **2016**, *138*, 2933.

(14) Abe, K.; Hagiwara, J.; Machida, W. *J. Japan Soc. Air Pollut.* **1980**, *15*, 21.

(15) Bartos, M. J.; Gordon-Wylie, S. W.; Fox, B. G.; Wright, L. J.; Weintraub, S. T.; Kauffmann, K. E.; Munck, E.; Kostka, K. L.; Uffelman, E. S.; Rickard, C. E. F.; Noon, K. R.; Collins, T. J. *Coordin. Chem. Rev.* **1998**, *174*, 361.

(16) Chanda, A.; Ryabov, A. D.; Mondal, S.; Alexandrova, L.; Ghosh, A.; Hangun-Balkir, Y.; Horwitz, C. P.; Collins, T. J. *Chem. Eur. J.* **2006**, *12*, 9336.

(17) Horwitz, C. P.; Fooksman, D. R.; Vuocolo, L. D.; Gordon-Wylie, S. W.; Cox, N. J.; Collins, T. J. *J. Am. Chem. Soc.* **1998**, *120*, 4867.

(18) Sen Gupta, S.; Stadler, M.; Noser, C. A.; Ghosh, A.; Steinhoff, B.; Lenoir, D.; Horwitz, C. P.; Schramm, K. W.; Collins, T. J. *Science* **2002**, *296*, 326.

(19) Miller, J. A.; Alexander, L.; Mori, D. I.; Ryabov, A. D.; Collins, T. J. *New J. Chem.* **2013**, *37*, 3488.

(20) Emelianenko, M.; Torrejon, D.; DeNardo, M. A.; Socolofsky, A. K.; Ryabov, A. D.; Collins, T. J. *J. Math. Chem.* **2014**, *52*, 1460.

(21) Tynkkynen, T.; Tiainen, M.; Soininen, P.; Laatikainen, R. *Anal. Chim. Acta.* **2009**, *648*, 105.

(22) Sinikova, N. A.; Shaydullina, G. M.; Lebedev, A. T. *J. Anal. Chem.* **2014**, *69*, 1300.

(23) Liu, C.; von Gunten, U.; Croue, J. P. *Water Res.* **2013**, *47*, 5307.

(24) Popescu, D. L.; Chanda, A.; Stadler, M. J.; Mondal, S.; Tehranchi, J.; Ryabov, A. D.; Collins, T. J. *J. Am. Chem. Soc.* **2008**, *130*, 12260.

(25) Chahbane, N.; Popescu, D.-L.; Mitchell, D. A.; Chanda, A.; Lenoir, D.; Ryabov, A. D.; Schramm, K.-W.; Collins, T. J. *Green Chem.* **2007**, *9*, 49.

(26) Fukuta, N. *Nature* **1963**, *199*, 475.

(27) George, P. *Biochem. J.* **1953**, *55*, 220.

(28) Kelm, M.; Pashalidis, I.; Kim, J. I. *Appl. Radiat. Isotopes* **1999**, *51*, 637.

(29) D.Pfaff, J.; Hautman, D. P.; Munch, D. J. *Method 300.1 Determination of Inorganic Anions in Drinking Water by Ion Chromatography*, 1999.

Chapter 4

How Is TAML Catalysis Affected by Conditions?

—The Effects of Organic Co-solvents, D_2O, Anions, and Temperature on Functioning TAML Catalysis

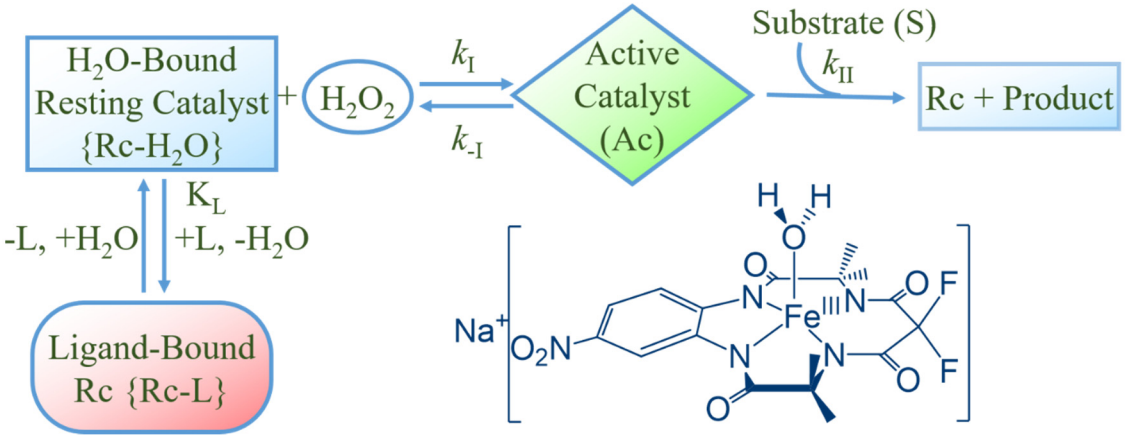

4.1 Introduction

As reviewed and discussed in previous chapters, TAML/H_2O_2 catalysis in water typically follows a two-step stoichiometric mechanism.[1] The resting catalysts (Rc) are reversibly activated by H_2O_2 to form active catalysts (Ac, eq. 4.1, k_{-I} is usually negligible) which either oxidize substrates to return Rc (eq. 4.2) or undergo inactivation to form inactive catalysts (Ic, eq. 4.3). For most TAML processes, the catalyst behavior is well-modeled by this sequence of events (see Chapter 1 for details). However, the TAML processes to which this model has largely been applied operate within a relatively narrow range of conditions where H_2O is the solvent and solutes other than the oxidant do not strongly interact with the Rc and are only present in low concentrations. We were curious about the impacts on TAML processes of switching the reaction solvent to D_2O as required for the use of the ^1H NMR reaction monitoring technique presented in Chapters 2 and 3. We also wondered if the presence of organic solvents would affect the TAML catalytic cycles. Such changes in solvent might have consequences for processes typically observed in aqueous TAML catalysis. One process of particular interest was the exchange of a solvent molecule occupying an axial site on the iron atom for a molecule of oxidant, which one can reasonably consider as critical for catalyst activation. Studies of these behaviors may shed light on the mechanism of activation of the Rc by H_2O_2, the step which is often rate determining in TAML catalysis. Since multiple studies of Orange II (OrII) oxidation by TAML/H_2O_2 catalysis are available which have shown this system to obey the mechanism shown in eqs 4.1–4.3 particularly well, a large database of values for the rate constants k_I, k_{II}, and k_i in OrII oxidation has recently been made available,[1,2] and OrII consumption is easily monitored by UV-Vis spectroscopy, OrII was chosen as the substrate for these

studies of the effects of altering the solvent composition on functioning TAML catalysis as indicated by changes in the rate constants k_I and k_{II} .

Resting Catalyst (Rc) + H_2O_2 ⇄ Active Catalysts (Ac) k_I, k_{-I} (4.1)

Ac + Substrate (S) → RC + Product k_{II} (4.2)

Ac → Inactive Catalyst (IC) k_i (4.3)

4.1.1 An introduction to the rate constants calculation

Application of the steady state assumption to [Ac] and mass balance equation to the total concentration of catalyst, Fe_{Tot}, for the sequence of events shown in eqs 4.1 and 4.2 gives eq 4.4, a mathematical form for the dependence of the rate of substrate oxidation, -d[S]/dt on [H_2O_2], [S], k_{-I}, k_I, and k_{II}. Since this analysis does not incorporate the catalyst inactivation process shown in eq 4.3, eq 4.4 only applies to the initial rate of substrate consumption. Since the k_{-I} term is usually insignificant, eq 4.4 can be simplified to give eq 4.5.

$$-\frac{d[S]}{dt} = \frac{k_I k_{II}[H_2O_2][S]}{k_{-I}+k_I[H_2O_2]+k_{II}[S]} Fe_{Tot} \quad (4.4)$$

$$-\frac{d[S]}{dt} = \frac{k_I k_{II}[H_2O_2][S]}{k_I[H_2O_2]+k_{II}[S]} Fe_{Tot} \quad (4.5)$$

Equation 4.5 is employed in experimental measurements of the rate constants k_I and k_{II}. Depending on the values of k_I and k_{II}, as well as the [H_2O_2] and [S] at which measurements are made, the trends in -d[S]/dt with varying [S] and [H_2O_2] can take one of three forms. Each form constitutes a region. The region(s) in which a set of measurements lie depends on the relationship between k_I[H_2O_2] and k_{II}[S] and determines whether k_I, k_{II}, or both can be determined from the data obtained. The three regions are as follows:

(i) When $k_I[H_2O_2] >> k_{II}[S]$, eq 4.5 can be simplified to give eq 4.6

$$-\frac{d[S]}{dt} = k_{II}[S]Fe_{Tot} \tag{4.6}$$

In this region, -d[S]/dt is independent of $[H_2O_2]$ and is linearly dependent on [S], Fe_{Tot}, and k_{II}. The rate constant k_{II} can therefore be obtained from the slope of the line of best fit to the dependence of -d[S]/dt on [S], provided all measurements are made at the same Fe_{Tot}. Here, substrate oxidations by Ac are rate-determining. Therefore, this is referred to as the 'k_{II} region'. Since catalyst activation by H_2O_2 is usually the slowest step of the TAML catalytic cycle as for most synthetic catalysts,[3] only the behavior of TAML processes employing a high $[H_2O_2]$ and slowly reacting substrates (low k_{II}) are found here.

(ii) When $k_I[H_2O_2] << k_{II}[S]$, eq 4.5 can be simplified to give eq 4.7

$$-\frac{d[S]}{dt} = k_I[H_2O_2]Fe_{Tot} \tag{4.7}$$

Here, catalyst activation is rate determining. Consequently, this is referred to as the 'k_I region'. In the k_I region, the initial rate of substrate oxidation exhibits first order dependences on $[H_2O_2]$ and Fe_{Tot}. In this region, k_I can be obtained from the slope of the line of best fit to the dependence of -d[S]/dt on $[H_2O_2]$, provided all measurements are made at the same Fe_{Tot}. In order to ensure that measurements of a process will be made in the k_I region, $[H_2O_2]$ is kept low and a high [S] is maintained.

(iii) When $k_I[H_2O_2] \sim k_{II}[S]$, eq 4.5 cannot be simplified. Instead, eq 4.8, the inverse of eq 4.5 is used to determine both k_I and k_{II}.

$$-\frac{dt}{d[S]} = \frac{1}{k_{II}[S]Fe_{Tot}} + \frac{1}{k_I[H_2O_2]Fe_{Tot}} \tag{4.8}$$

Since both the catalyst activation and substrate oxidation processes contribute to the observed rate of substrate oxidation here, this region is referred to as the 'mixed region'. Both k_I and k_{II} can be obtained from the slope and intercept of the line of best fit to the dependence of –dt/d[S] on either $[S]^{-1}$ or $[H_2O_2]^{-1}$ as indicated by eq 4.8.

4.2 Results and discussion

The above discussed methods were used to obtain the rate constants k_I and k_{II} for aqueous **1a**/H_2O_2 catalysis in the presence of varying concentrations of organic solvents, in D_2O rather than H_2O, and at different reaction temperatures. A significant decrease in reaction rate has been observed in the presence of large percentage of methanol or acetone, while acetonitrile has significantly less impact on retarding the reaction rate. A kinetic isotope effect (KIE) of ~1.7 was calculated for the catalyst activation process, k_I, of both **1a** and **1b**, indicating an involvement of proton in the Ac formation from H_2O_2 and Rc interaction. The enthalpy of **1a** activation was calculated.

Chart 4.1 Structures of catalysts (**1a** and **1b**) and model compound (Orange II) used in this study.

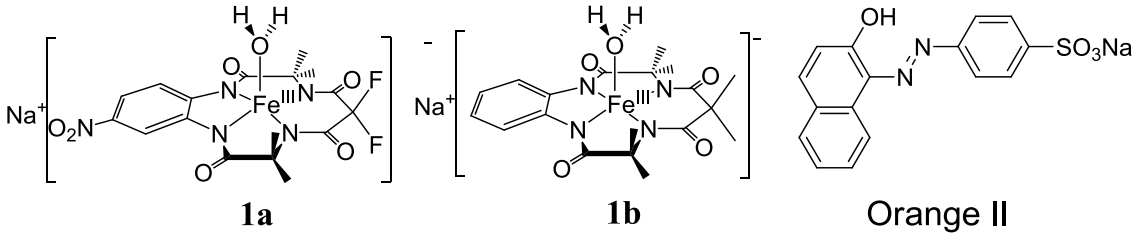

4.2.1 Inhibition of catalyst activation by organic co-solvents

Methanol, acetonitrile, and acetone are three organic solvents commonly encountered in TAML chemistry. TAML catalyst stock solutions are routinely prepared in methanol.[2] Cryogenic studies of the formation of high valent TAML complexes on addition of oxidant and their reactivity[4,5] employ acetonitrile as the solvent. Room temperature studies of the oxidation of substrates having low solubility in water employ acetonitrile as a co-solvent. Acetone is often used to clean quartz cuvettes before and after UV-vis measurements. Most TAML studies only employ low concentrations of these solvents as needed and their impacts on the catalyzed reactions are not well understood. Here, we examined how different concentrations of these organic solvents affect catalyst activation in OrII oxidation by **1a**/H_2O_2.

The presence of high concentrations of organic solvents noticeably retarded the overall reaction rate. To determine whether these were affecting the catalyst activation process, the relationship between the eq 4.7 or 4.8 was used to calculate the rate constants k_I while varying the [co-solvent]. These studies revealed an inverse proportionality between k_I and [organic solvent] which holds for all three co-solvents studied (Figures 4.1–4.3). Since in these studies the eq. 4.7 and 4.8 calculated k_I varies with [co-solvent], the so obtained k_I values are referred to as $k_{I_{Obs}}$ in this section.

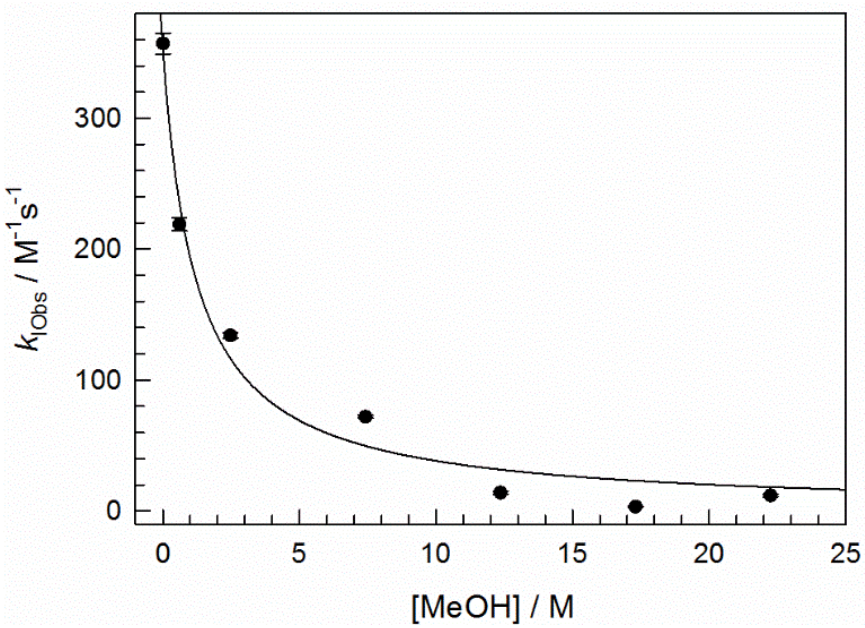

Figure 4.1 Measured rate constants $k_{I_{Obs}}$ for OrII oxidation catalyzed by **1a** at varied methanol concentrations. Conditions: pH 7 (0.01 M phosphate), 25 °C, [**1a**] = 2 × 10^{-8} M, [OrII] = 3.56 × 10^{-5} M. Methanol percentages ranging from 2.4–90%. Solid line is the regression result using eq. 4.10 (see below for explanation). Experimental details can be found in Table 4.5.

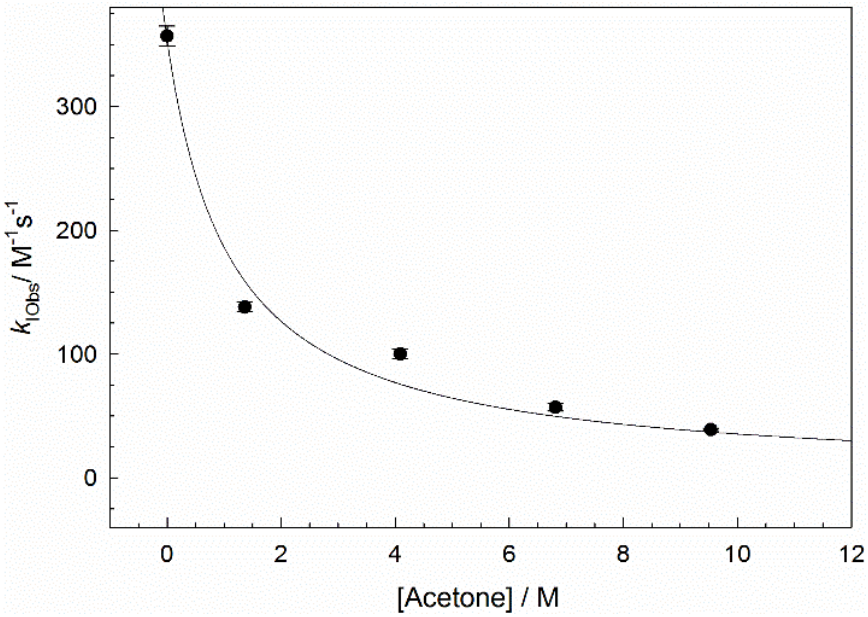

Figure 4.2 Measured rate constants $k_{I_{Obs}}$ for OrII oxidation catalyzed by **1a** at varied acetone concentrations. Conditions: pH 7 (0.01 M phosphate), 25 °C, [**1a**] = 2 × 10^{-8} M, [OrII] = 3.56 ×

10^{-5} M. Acetone percentages ranging from 10–90%. Solid line is the regression result using eq. 4.10. Experimental details can be found in Table 4.5.

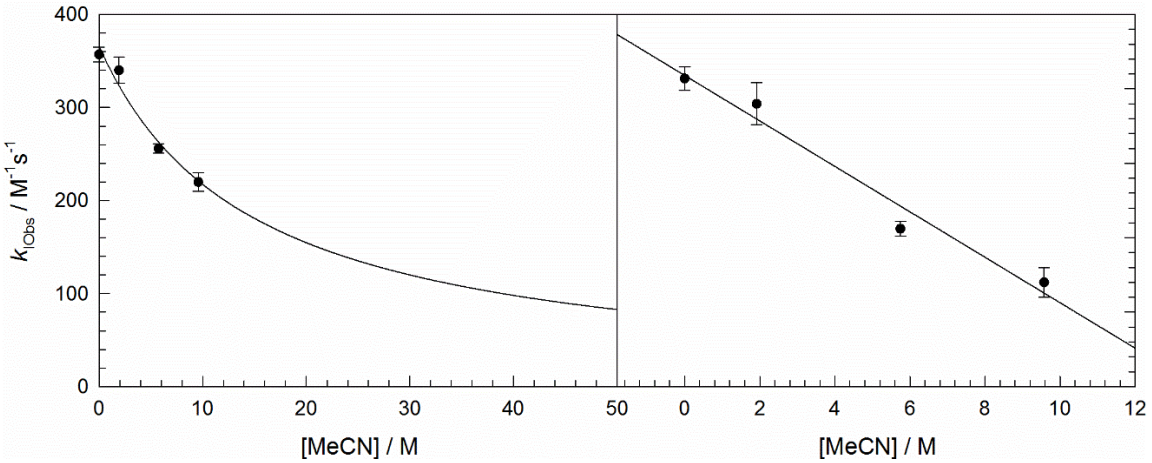

Figure 4.3 Measured rate constants k_{IObs} for OrII oxidation catalyzed by **1a** at varied acetonitrile concentrations. Conditions: pH 7 (0.01 M phosphate), 25 °C, [**1a**] = 2 × 10^{-8} M, [OrII] = 3.56 × 10^{-5} M. Solid line on the left is a regression result with the data points using eq. 4.10. Solid line on the right is the regression result with the data points applying linear function. Acetonitrile percentages ranging from 10–50%. Experimental details can be found in Table 4.5.

We wondered whether this affect could derive from reversible inhibition of the catalyst activation via equilibrium binding (K_L) of the solvent (L) to the Rc giving an adduct ({Rc-L}) which does not undergo activation by H_2O_2 (Scheme 4.1).

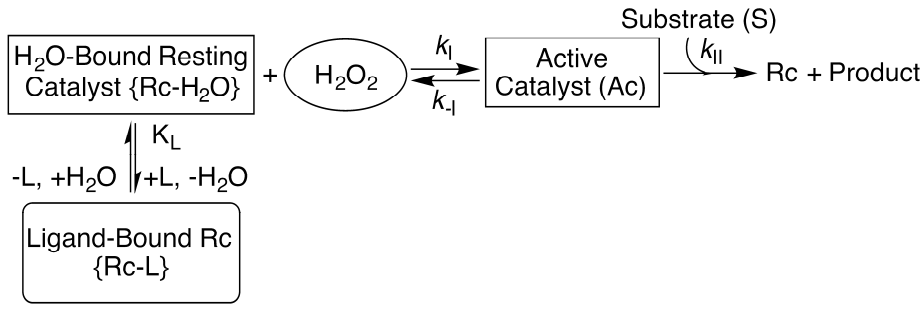

Scheme 4.1 Proposed mechanism for competitive prohibition of organic solvent in TAML catalysis. Only the free catalyst can be activated.

At the present time, we favor the following rationalization of the observed kinetics. Consideration of the sequence of events shown in Scheme 4.1 gives a new rate expression from which rate constants can be calculated by applying steady state assumption to [Ac] and the mass balance equation for Fe_{Tot}, eq 4.9. Comparison of eq 4.7 with eq 4.9 gives eq 4.10, a simple expression for $k_{I_{Obs}}$ as a function of k_I. Fitting eq 4.10 to the data in Figure 4.1–4.3 gives the values listed in Table 4.1. However, the $k_{I_{Obs}}$ measured with acetonitrile can also be fit as a linear function (Figure 4.3). As can be seen from the R^2 values in Table 4.1, the dependence of $k_{I_{Obs}}$ on [co-solvent] is well modeled by eq 4.10. The solid lines shown in Figure 4.1–4.3 were generated using eq 4.10 and the reported $k_{I_{Obs}}$ and k_I values giving visual confirmation of this goodness of fit.

$$-\frac{d[S]}{dt} = \frac{\frac{k_I}{1+K_L[L]}k_{II}[H_2O_2][S]}{\frac{k_I}{1+K_L[L]}[H_2O_2]+k_{II}[S]}Fe_{Tot} \tag{4.9}$$

$$k_{I_{Obs}} = \frac{k_I}{(1+K_L[L])} \tag{4.10}$$

Table 4.1 Calculated binding constants for organic solvents.

L	K_L / M^{-1}	k_I / $M^{-1}s^{-1}$	r^2
None	NA	350 ± 2	NA
$(CH_3)_2CO$	0.9 ± 0.2	354 ± 19	0.98
CH_3OH	0.8 ± 0.2	350 ± 20	0.98
CH_3CN	0.067± 0.009	370 ± 10	0.97

Reactions between the **1a**/H_2O_2 and each organic co-solvent were monitored by ^{1}H NMR to determine whether the organic solvents could be oxidized during functioning TAML catalysis of OrII oxidation. The acetonitrile spectra show no difference before and after the addition of catalyst. Spectra of the methanol and acetone reactions do show singlet peaks indicating small amounts of product formation. The identity of these products could not be assigned. Since the rate constants are determined from data recorded during the first 15 minutes of each reaction, the readily oxidized dye OrII was present in the reactions from which the rate constants were determined, and substantial oxidation of the organic co-solvents did not occur within 3 hours in the absence of OrII, contributions to the rate constants from the oxidation of the organic co-solvents were considered to be negligible.

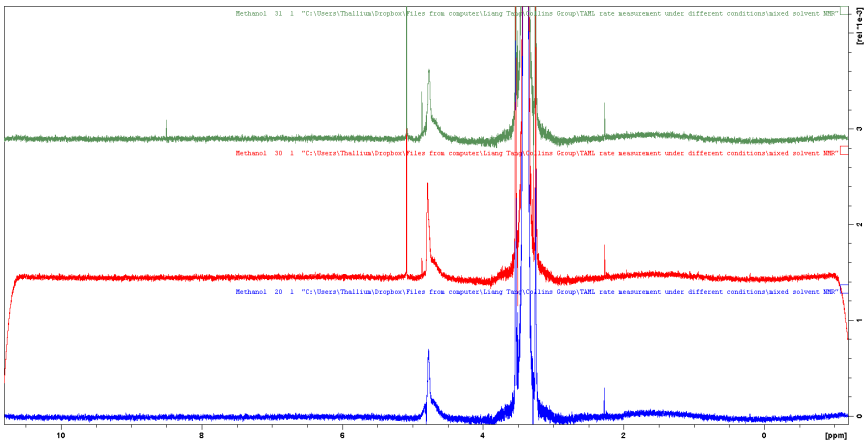

Figure 4.4 NMR spectra of a reaction solution containing methanol and **1a**/H_2O_2. Conditions: pH 7 D_2O (0.01 M phosphate), [**1a**] = 3.3×10^{-8} M, [H_2O_2] = 2.3×10^{-2} M, 10 μL MeOH in 600 μL reaction mixture. Blue: spectra recorded before H_2O_2 addition; red: spectra recorded 3 h after H_2O_2 addition; green: spectra recorded 20 h after H_2O_2 addition.

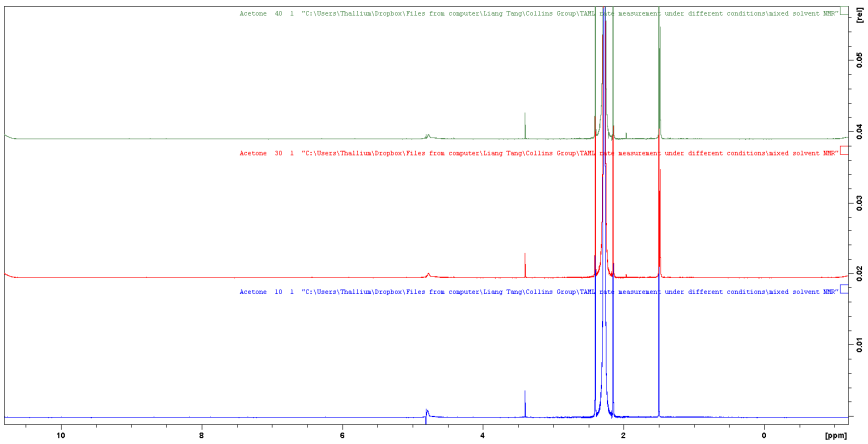

Figure 4.5 NMR spectra of a reaction solution containing acetone and **1a**/H_2O_2. Conditions: pH 7 D_2O (0.01 M phosphate), [**1a**] = 3.3×10^{-8} M, [H_2O_2] = 2.3×10^{-2} M, 10 μL acetone in 600 μL reaction mixture. Blue: spectra recorded before H_2O_2 addition; red: spectra recorded 3 h after H_2O_2 addition; green: spectra recorded 20 h after H_2O_2 addition.

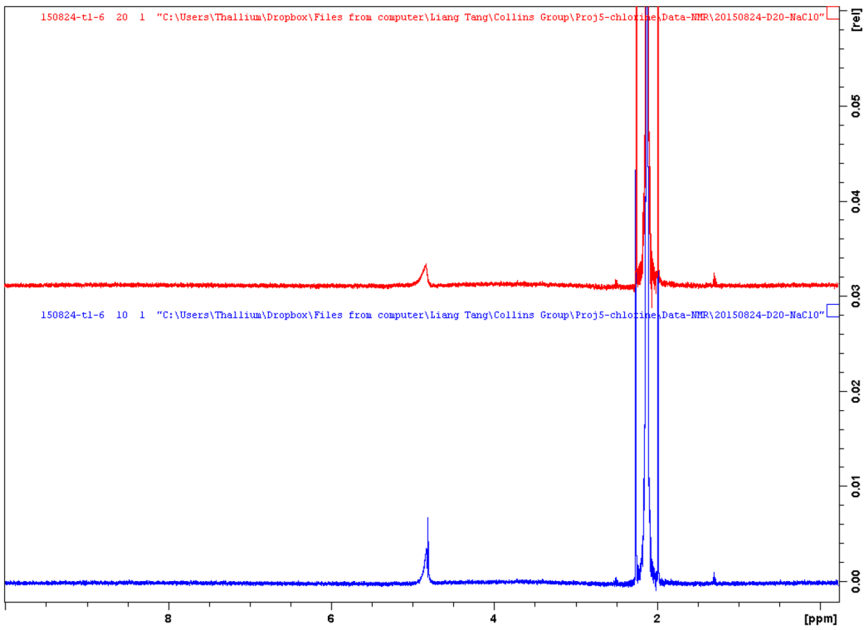

Figure 4.6 NMR spectra of a reaction solution containing acetonitrile and **1a**/H_2O_2. Conditions: pH 7 D_2O (0.01 M phosphate), [**1a**] = 3.3×10^{-8} M, [H_2O_2] = 2.3×10^{-2} M, 10 μL acetonitrile in 600 μL reaction mixture. Blue: spectra recorded before H_2O_2 addition; red: spectra recorded 2 h after H_2O_2 addition.

Several interesting conclusions can be drawn from the data. *First, the inhibition of k_I by co-solvents is consistent with weak binding of the solvent lone pairs to the iron atom of the TAML Rc which does not adversely impact catalysis in most TAML applications.* The iron atoms of TAML activators are known to function as Lewis acids. The sp hybridized lone pair of the acetonitrile nitrogen atom is a weaker donor than the sp^3 lone pair of the methanol oxygen atom. Thus the stronger binding of methanol than acetonitrile indicated by the higher K_L of the former is consistent with both co-solvents binding to the iron center as Lewis bases provided that backbonding to acetonitrile does not occur. The acetone and methanol K_L values are identical. At first we were intrigued by this. Though the acetone data appear to be anomalous, it too can be rationalized as binding of a Lewis acid to Fe. If

the acetone binding occurs through donation of electron density from an sp^2 oxygen lone pair to the iron center, this interaction would be expected to increase the electrophilicity of the carbonyl carbon of the bound acetone. Since there are large amounts of H_2O present, this compound would likely form the hydrate. The larger than expected K_L would then arise from binding of at least one of more donating the sp^3 oxygen atoms of the hydrate. The identical acetone and methanol K_L values indicate that only one of the hydrate O atoms is bound at any one time. All of the K_L values are ≤ 1.1 indicating that the solvents do not strongly bind to the resting catalyst and that this inhibition will not be observed for OH containing substrates and products of most TAML processes.

Second, the transition state of the rate determining step of catalyst activation is not sensitive to the polarity of the bulk solvent and water molecules from the bulk solvent are not involved in the rate determining step. Both the concentrations of solvents added and the polarity of these solvents vary widely. These drastically alter both the concentration of water in and polarity of the solvent mixture. However, the k_I values determined in the presence of co-solvent are either identical to or nearly identical to that measured in the absence of co-solvent. It follows that the rate determining step is insensitive to concentration of water or the polarity of the solvent mixture over the measured ranges.

Third, one TAML bound H_2O plays a role in the activation process. All of the solvents studied exchange reversibly with H_2O. H_2O_2 is not significantly larger than H_2O. It is reasonable to conclude that {Rc-L} exchanges L for H_2O_2. However, the sequence of events shown in Scheme 4.1, which gives eq 4.9 that accurately models the observed catalyst activation process, does not incorporate a pathway for the activation of {Rc-L}by H_2O_2. Therefore, this pathway of activation must not contribute significantly to the rate of

formation of Ac. Consequently, one axial water molecule must play a role in the activation of the Rc.

4.2.2 Effect of anions other than phosphates on functioning TAML catalysis of OrII oxidation

Since the presence of organic co-solvents was observed to decrease k_I and attributed to binding to the Lewis acidic metal center, the effect of solvated anions on k_I and k_{II} was investigated. A series of anions that are commonly encountered in waters were chosen for study. The k_{II} values for the oxidation of OrII determined in the presence of the studied anions were identical to that measured in their absence (Table 4.2). The k_I and k_{II} values observed at $[F^-]$ of 5×10^{-4} M are identical to those measured in the absence of F^-. However, the presence of much higher concentrations of Cl^- and CH_3COO^- did cause decreases in k_I. More data is required to perform an analysis such as that presented in the section 4.2.1 of this chapter which may permit the assignment of the nature of the observed interferences with catalyst activation. If this interference is found to have a concentration dependence indicative of an equilibrium binding to Rc similar to that of the organic solvents, TAML processes will not be effected by F^- at concentrations below the regulatory limit (4 mg/L or 2.1×10^{-4} M, USEPA[6]).

Table 4.2 Experimental results for Or II degradation in the presence of anions other than phosphates.

Salt Added	[Anion] / M	Regime	k_I / $M^{-1}s^{-1}$	$10^{-4} \times k_{II}$ / $M^{-1}s^{-1}$
None	NA	k_I	303 ± 7	NA
None	NA	Mixed	357 ± 8	(7.9 ± 0.7)
NaF	5×10^{-4}	k_I	355 ± 6	NA
NaF	5×10^{-4}	Mixed	347 ± 7	(6.9 ± 0.7)
NaCl	7×10^{-3}	k_I	289 ± 4	NA
NaCl	7×10^{-3}	Mixed	285 ± 6	(9 ± 1)
CH_3COOK	0.604	k_I	122 ± 5	NA
CH_3COOK	0.604	Mixed	88 ± 3	(8 ± 3)

4.2.3 Effect of deuterated water

It has been postulated that a proton transfer is involved in the rate-determining step in catalyst activation. To gain a more detailed understanding of the catalyst activation process, the KIE of k_I was determined. The KIE of the k_I process was determined to be ca. 1.7 for both **1a** and **1b** (Table 4.3). This weak primary KIE indicates that the H-X bond is cleaved in the rate-limiting step.[7] Tunneling is not involved in the process. Given that an exchange of H_2O_2 for H_2O occurs at iron, the TAML Ac are considered to be Fe^V=O complexes, and an O−H bond is broken in the process, it is likely that the O−H bond of H_2O_2 is cleaved during catalyst activation.

Table 4.3 Calculated isotope effect for catalysts **1a** and **1b** at pH 7.

Cat	pH	[Cat] × 10^8 / M	[OrII] × 10^5 / M	[H_2O_2] ×10^4/ M	Regime	X_2O	k_I / $M^{-1}s^{-1}$	KIE
1b	7	9.89	3.56	0.765−7.64	k_I	H	26.2 ± 0.6	NA
1b	7[a]	9.78	3.53	0.797−7.97	k_I	D	15.9 ± 0.2	1.65
1a	7	1.96	4.45	1.38−20.7	k_I	H	303±7	NA
1a	7[1]	1.96	2.51	1.68−17.3	k_I	D	183±8	1.66

[a]pH as measured by pH meter in D_2O

4.2.4 Effect of temperature

To further assess the composition of the rate determining step of catalyst activation, the temperature dependence of k_I was determined. The Arrhenius equation models the temperature dependence of reaction rate constants. Deduction from Arrhenius equation gives the Eyring equation (eq. 4.11) that describes the relationship between observed rate constants and enthalpy and entropy of activation of a reaction. By plotting ln (k/T) against T^{-1}, both enthalpy and entropy can be calculated. Note that entropy is only useful when the measured rate constant is that of a single step reaction.[7]

$$\ln\frac{k}{T} = \frac{-\Delta H^{\ddagger}}{R}\cdot\frac{1}{T} + \ln\frac{k_B}{h} + \frac{\Delta S^{\ddagger}}{R} \tag{4.11}$$

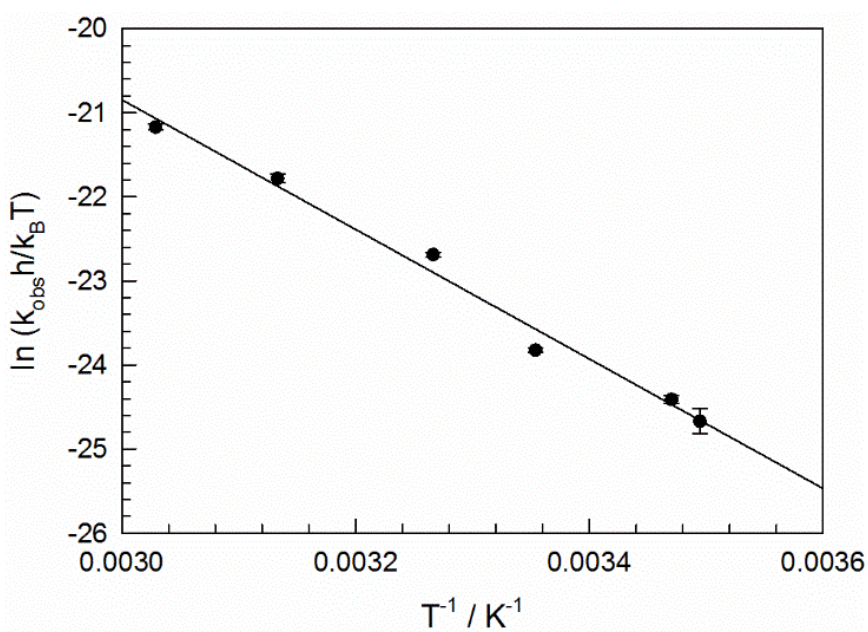

Figure 4.7 k_I dependence on temperature. Conditions: pH 7 (0.01 M phosphate), [**1a**] = 2×10^{-8} M, [Orange II] = 3.56×10^{-5} M. The solid line is a linear regression result of the data points.

Table 4.4 Rate constants used for Eyring equation plotting.

T / °C	Regime	k_I / $M^{-1}s^{-1}$	R^2	k_I average
13	k_I	131 ± 4	0.96	120 ± 20
	Mixed	100 ± 30	0.90	
15	k_I	91 ± 3	0.96	150 ± 10
	Mixed	210 ± 10	0.96	
25	k_I	303 ± 7	0.98	330 ± 10
	Mixed	357 ± 8	0.99	
33	k_I	860 ± 20	0.98	900 ± 30
	Mixed	930 ± 30	0.98	
46	k_I	2220 ± 50	0.99	2300 ± 100
	Mixed	2400 ± 200	0.94	
57	k_I	4800 ± 100	0.97	4400 + 200
	Mixed	4000 ± 200	0.97	

The enthalpy of activation calculated from Figure 4.4 equals 15.3 ± 0.7 kcal mol^{-1} (r^2 = 0.99). For one reaction, if the enthalpy of activation ($\Delta H^{\ddagger}$) calculated from k_{obs} is less than 5 kcal mol^{-1}, the reaction is considered possibly diffusion controlled, a $\Delta H^{\ddagger}$ larger than 20 kcal mol^{-1} indicates a likely bond cleavage in the transition state.[7] Intermediate values, such as that observed in our experiment, indicates that either bond formation dominates in the transition state, or bond cleavage is compensated by new bond formation.[7] Unfortunately, since we have been unable to separate contributions from the equilibrium binding of H_2O_2 to the iron center of Rc from the measured values of the rate constant k_I, the origins of the entropy of activation calculated from these data (5 ± 3 cal mol^{-1} K^{-1}) are very difficult to assign at this time.

4.2.5 Proposed mechanism

According to above observations, three important clues are obtained for the rate-determining step during TAML catalyst activation by H_2O_2: (*i*) one axial H_2O molecule which departs as H_2O_2 approaches the iron center plays a role in the catalyst activation process; (*ii*) an O−H bond from H_2O_2 is cleaved; (*iii*) Both bond formation and bond cleavage occur in the rate determining step of catalyst activation and bond formation dominates. A mechanism that satisfies all three of these requirements is proposed in Scheme 4.2. It is proposed that the transition state for the rate determining step of catalyst activation involves a five-membered ring in which the O−H and O−O bonds of an axially ligated H_2O_2 molecule are broken with concerted O−H bond formation to the departing H_2O and Fe−O pi bond formation.

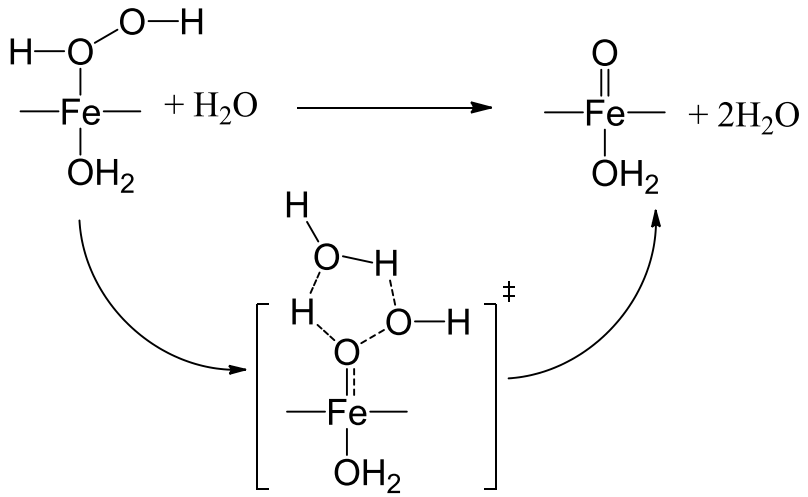

Scheme 4.2 Proposed mechanism for reaction intermediate formation during catalyst activation.

4.3 Conclusion

This preliminary study focuses on the mechanistic study of TAML catalysts (**1a** and **1b**) activation process at pH 7 using OrII as a model compound. It was found that the presence of organic solvents significantly retarded the reaction rate. These rate decreases have been attributed to inhibition of catalyst activation caused by the reversible binding of organic solvent molecules to the iron center. The organic solvent bound resting catalyst complex does not undergo activation suggesting that the axial water molecule for which H_2O_2 is exchanged plays a role in the formation of the active catalyst. Anions also decrease the rate of catalyst activation and this effect may derive from a reversible binding to the iron atom of the resting catalyst similar to that observed for organic solvents. The KIE of the rate determining step of catalyst activation indicates that an O−H bond is broken in this process. Temperature and kinetic isotope effect studies provide better understanding of the catalyst activation processes by indicating that the transition state for the catalyst activation process involves both bond breaking and bond making. In sum, these findings support the theory that the catalyst activation process involves an equilibrium exchange of an axial H_2O of the resting catalyst for H_2O_2 and breaking of the O−H and O−O bonds of H_2O_2 which occurs with formation of an O−H bond to the departing water and an Fe−O pi bond. The important practical message from these results is that common solvent and ion effects on the reaction kinetics are relatively slight and likely to be unimportant in the major regime of applied interest, water purification, when weakly binding Lewis bases such as these solvents are present in trace quantities.

4.4 Experimental

4.4.1 Materials

All reagents, components of buffer solutions, and solvents were at least ACS reagent grade (Aldrich, Fisher) and were used as received. TAML activators **1a** and **1b** were obtained from GreenOx Catalysts, Inc. Stock solutions of **1a** and **1b** (2×10^{-5} M) were prepared in water and stored at 4 °C. Orange II (Sigma-Aldrich) was recrystallized from H_2O:EtOH (1:3). Orange II stock solutions were prepared in pH 7, 0.01 M phosphate buffer and stored at room temperature.

4.4.2 Methods

UV-vis measurements were performed at 25 °C unless otherwise noted in plastic cuvettes (1.0 cm) using a photodiode array Agilent 8453 UV-vis spectrometer equipped with an automatic thermostatted 8-cell positioner. 1D ^{1}H spectra were recorded at 300 K on a Bruker Avance^{TM} III 500 NMR spectrometer operating at 500.13 MHz with presaturation method to suppress the water signal.

Table 4.5 Experimental details and rate constants obtained for the analyses performed in this chapter.

Cat.	[Cat] / × 10^{-8} M	[Or II] / × 10^{-5} M	pH	Temp. / °C	solvent[a]	Regime	[H_2O_2] / × 10^{-4} M	k_{1Obs}	r^2	$k_{II Obs}$	ε_{500}	r^2
1a	1.96	4.45	**7**	25	100% buffer	k_1	1.38-20.7	303 ± 7	0.981	NA	[a]	NA
						mixed	13.8-282	357 ± 8	0.995	(7.9±0.7)E4		
1a	1.96	4.45	**6**	25	100% buffer	k_1	6.91-56.4	28 ± 2	0.755	NA	[a]	NA
						mixed	27.6-282	36 ± 1	0.989	(1.46±0.18)E4		
1a	1.96	4.45	**8**	25	100% buffer	k_1	1.38-27.6	1106 ± 26	0.970	NA	[a]	NA
						mixed	13.8E-282	1383 ± 69	0.962	(2.17±0.3)E5		
1a	1.96	3.56	7	**13**	100% buffer	k_1	2.17-10.9	131±4	0.959	NA	18600±200	0.991
						mixed	21.7-192	104±26	0.899	(2.97±0.74)E4		
1a	1.96	3.57	7	**15**	100% buffer	k_1	0.71-14.1	91±3	0.959	NA	19240±240	0.989
						mixed	13.7-186	213±11	0.964	9836±2916		
1a	1.96	3.56	7	**33**	100% buffer	k_1	0.75-7.49	860±20	0.985	NA	19100±300	0.98
						mixed	11.2-199	930±30	0.981	(1.26±0.09)E5		
1a	1.96	3.57	7	**46**	100% buffer	k_1	0.71-10.7	2218±46	0.986	NA	19130±210	0.993
						mixed	14.2-188	2350 ± 165	0.940	(1.74±0.13)E5		
1a	1.96	3.56	7	**57**	100% buffer	k_1	74.9-3.75	4760 ± 120	0.969	NA	17700±300	0.982
						mixed	7.49-59.6	4050 ± 160	0.971	(4.8±0.6)E5		
1a	1.96	3.56	7	25	10% **acetone** + 90% buffer	k_1	0.73-7.28	226±4	0.987	NA	18800 ±200	0.991
						mixed	21.9-193	138±4	0.986	(6.2±0.8)E4		
1a	1.96	3.57	7	25	30% **acetone** + 70% buffer	k_1	0.72-14.3	87±3	0.928	NA	19430±178	0.994
						mixed	14.3-193	100±4	0.979	(1.590±0.003)E4		
1a	1.96	3.56	7	25		k_1	2.19-11.0	49±2	0.925	NA	18000 ±150	0.994

					50% **acetone** + 50% buffer	mixed	14.6-118	57±3	0.959	4900 ± 300		
1a	1.96	3.57	7	25	70% **acetone** + 30% buffer)	k_1	2.14-10.7	24 ± 1	0.862	NA	16710±140	0.995
						mixed	2.14-189	39 ± 1	0.970	1473 ± 121		
1a	1.96	3.56	7	25	90% **acetone** + 10% buffer	No reaction	200					
1a	1.96	3.56	7	25	2.4% **MeOH** + 97.6% buffer	k_1	0.72-7.22	303±9	0.979	NA	19500 ±300	0.984
						mixed	21.7-195	219±5	0.994	(1.0±0.1)E5		
1a	1.96	3.56	7	25	10% **MeOH** + 90% buffer	k_1	0.73-10.9	132±3	0.973	NA	18000 ±400	0.963
						mixed	10.9-192	134±2	0.996	(4.2±0.4)E4		
1a	1.96	3.57	7	25	30% **MeOH** + 70% buffer	k_1	0.80-12.0	63 ± 2	0.952	NA	20420 ± 250	0.995
						mixed	7.97-130E	72 ± 1	0.998	(1.246±0.052)E4		
1a	1.96	3.56	7	25	50% **MeOH** + 50% buffer	k_1	2.17-10.9	20±1	0.844	NA	18100 ±400	0.954
						mixed	21.7-191	14±1	0.975	3800 ± 400		
1a	1.96	3.57	7	25	70% **MeOH** + 30% buffer	mixed	12.0-217	3.4 ± 0.2	0.977	780 ± 142	19950 ± 194	0.994
1a	1.96	3.56	7	25	90% **MeOH** + 10% buffer	mixed	33.6-395	12±1	0.932	1300 ± 400	16620 ±60	0.998
1a	1.96	3.56	7	25	0.6040M **CH_3COOK** in buffer	k_1	2.14-11.0	122±5	0.881	NA	17300 ± 400	0.955
						mixed	22.0-189	88±3	0.982	(8±3)E4		
1a	1.96	3.56	7	25	2.47M **CH_3COOK** in buffer	No reaction observed due to solubility issue of orange II in the solution						

1a	1.96	3.57	7	25	30% **DMSO** + 70% buffer	No reaction	30					
1a	1.96	3.56	7	25	10% **MeCN** + 90% buffer	k_1	0.71-10.7	285±5	0.975	NA	18500 ±300	0.975
						mixed	10.7-185	340±14	0.972	(3.6±0.3)E4		
1a	1.96	3.57	7	25	30% **MeCN** + 70% buffer	k_1	0.72-7.22	253 ± 8	0.968	NA	18100 ± 400	0.995
						mixed	10.8-197	256 ± 5	0.994	(2.9±0.1)E4		
1a	1.96	3.56	7	25	50% **MeCN** + 50% buffer	k_1	0.72-7.22	194±9	0.903	NA	17400 ±300	0.974
						mixed	10.8-114	220±10	0.980	(1.7±0.1)E4		
1a	1.96	2.51	7[b]	25	**D_2O** buffer	k_1	1.68-17.3	183 ± 8	0.849	NA	17010 ± 312	0.989
						mixed	12.6-173	274 ± 12	0.976	(3.1±0.2)E4		
1a	1.96	4.45	**7**	25	100% buffer with 500 μM [**NaF**]	k_1	0.72-7.21	355 ± 6	0.992	NA	18900 ± 300	0.977
						mixed	10.8-192	347 ± 7	0.990	(6.9±0.7)E4		
1a	1.96	4.45	**7**	25	100% buffer with 7mM [**NaCl**]	k_1	0.74-11.1	289 ± 4	0.990	NA	19000 ± 300	0.985
						mixed	14.8-196	285 ± 6	0.990	(9±1)E4		
1b	2.16	3.56	7	25	100% buffer	k_1	0.71-10.6	26.3 ± 0.5	0.982	NA	19000 was used	
						mixed	14.2-114	46 ± 3	0.955	1670±60		
1b	9.89	3.56	7	25	100% buffer	k_1	0.77-7.64	26.2 ± 0.6	0.974	NA	20500 ± 200	0.985
						mixed	1.14-2.29	46 ± 4	0.934	1600±200		
1b	9.89	3.56	7[b]	25	D_2O buffer	k_1	0.80-7.97	15.9 ± 0.2	0.998	NA	18100 ± 200	0.986
						mixed	11.9-22.9	28 ± 2	0.943	1160±90		

[a] 19000 was used; [b] buffer refers to 0.01 M phosphate buffer; [b] pH meter reading is 7.

4.5 References

(1) Chahbane, N.; Popescu, D. L.; Mitchell, D. A.; Chanda, A.; Lenoir, D.; Ryabov, A. D.; Schramm, K. W.; Collins, T. J. *Green Chem.* **2007**, *9*, 49.

(2) DeNardo, M. A.; Mills, M. R.; Ryabov, A. D.; Collins, T. J. *J. Am. Chem. Soc.* **2016**.

(3) Chanda, A.; Ryabov, A. D.; Mondal, S.; Alexandrova, L.; Ghosh, A.; Hangun-Balkir, Y.; Horwitz, C. P.; Collins, T. J. *Chem. Eur. J.* **2006**, *12*, 9336.

(4) Mills, M. R.; Burton, A. E.; Mori, D. I.; Ryabov, A. D.; Collins, T. J. *J. Coord. Chem.* **2015**, *68*, 3046.

(5) Kundu, S.; Thompson, J. V.; Ryabov, A. D.; Collin, T. J. *J. Am. Chem. Soc.* **2011**, *133*, 18546.

(6) USEPA https://www.epa.gov/your-drinking-water/table-regulated-drinking-water-contaminants, 2016; Vol. 2016.

(7) Ryabov, A. D. *Six Concise Lectures on Mechanisms of Chemical Reactions in Solution* Carnegie Mellon University, 2011.

Chapter 5

Is it possible to replace H_2O_2 by even cheaper dioxygen for TAML-catalyzed oxidation?

—A Peroxidase to Oxygenase/Oxidase Switch of the TAML Catalyst in Reverse Micelles

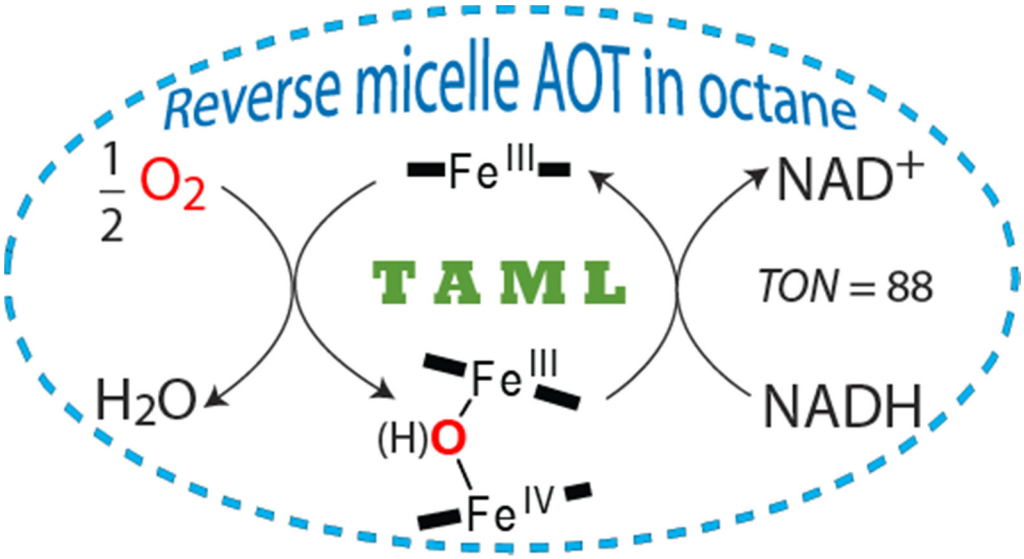

5.1 Introduction

As has been discussed in the previous chapters, superior activity of TAML activators (Chart 5.1) has been demonstrated for H_2O_2 or organic peroxides catalysis in water.[1-5] It would be beneficial to switch the primary oxidant to the omni-present dioxygen. An effort to steer TAML chemistry from peroxide towards oxygen has been made in this study.

5.1.1 Advantage of dioxygen as a primary oxidant

While H_2O_2 is a desirable green oxidant, its concentrated solutions are potentially hazardous[6] and it comes at a real production and delivery cost. In contrast, dioxygen is freely available and is the principal biochemical oxidizing agent. Therefore, our foremost strategic goal for TAML activator-based catalysis has been to master the use of O_2 as the primary oxidant.[7-9] TAML activators in the ferric state are readily oxidized by O_2 in weakly-coordinating organic solvents such as CH_2Cl_2 to produce Fe^{IV} species.[10] While iron(IV) TAML activators have been shown to oxidize some substrates in organic solvents, comparably efficient catalysis to the aqueous systems has yet to be observed.[10-12] TAML catalysis in water is characteristically conducted aerobically. Yet unless an oxidant such as hydrogen peroxide is added, no catalysis is observed—with the current suite of catalysts, bulk water appears thus far to be incompatible with facile oxygen activation. Two conditions appear to be favorable for oxygen activation. First, the TAML medium should be rich in O_2: under ambient conditions, this situation is best accommodated in organic solvents. Second, water should surround TAML activators for maintaining high catalytic activity. Recent studies have shown that some, but not too much water is important for TAML oxidations in organic solvents.[13-17] The amount of water should not be large because H_2O molecules compete with O_2 for coordination sites on Fe^{III}. Hydrogen bonding and/or

polarity effects may also play some role. In bulk water iron(III) TAML activators are six-coordinate species with two axial water ligands,[18] which is consistent with the observed inactivity of oxygen activation where 55 M H_2O effectively blocks O_2 binding to Fe^{III}.

Chart 5.1 Compounds involved in this study including the catalysts **1a** and **1b**, the homovalent μ-oxo-bridged iron(IV) dimer **2a** and heterovalent μ-oxo(hydroxo)-bridged iron(IV/III) dimer **3a** discussed in this work, and the substrates β-nicotinamide adenine dinucleotide reduced dipotassium/disodium salt (NADH), Pinacyanol chloride (PNC) and hydroquinone (HQ).

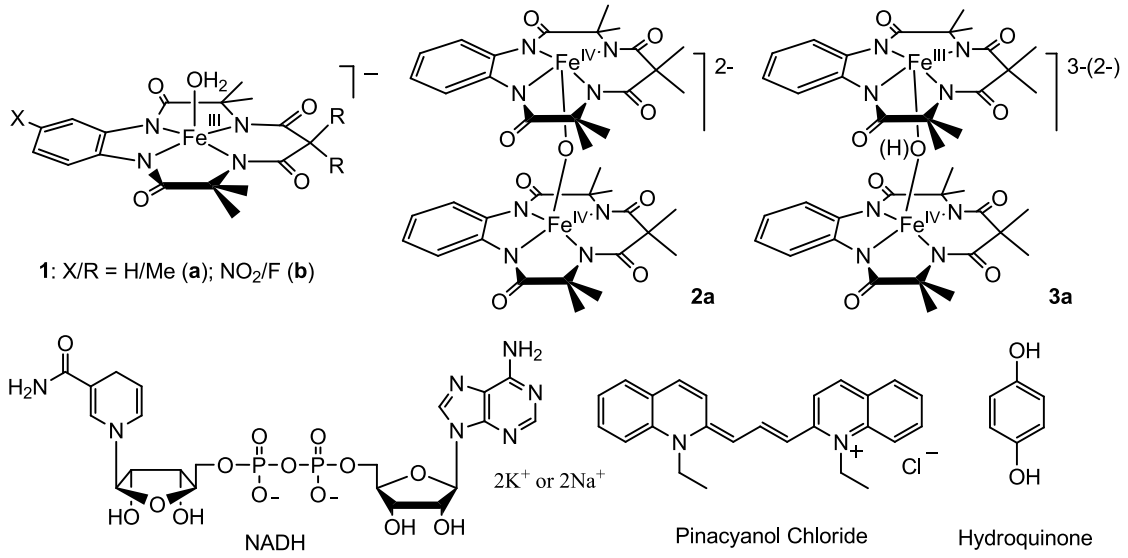

5.1.2 Reverse micelles

The two above conditions are in principle attainable using a system of reverse micelles.[19-21] A system of reverse micelles is comprised of aqueous microparticles in organic media such as *n*-octane (Figure 5.1). The micellar wall is composed of surfactant molecules—the sodium salt of bis(2-ethylhexyl)sulfosuccinate (Aerosol OT or AOT) is commonly used.[22] The hydrophobic tails are directed at the bulk organic medium, whereas the hydrophilic heads comprise the encapsulating surface of the microreactor inner water cavity.[21] Reverse

micelles of AOT have been thoroughly investigated[22] and, importantly, have often been used as media for catalysis by peroxidase enzymes,[21,23] the biocatalysts closest to TAMLs.[2] TAML activators have excellent solubility properties for guaranteeing sequestration in reverse micellar microreactors; the *n*-octanol/water partition coefficient for **1a** (Chart 5.1) is 0.036.[24,25] The size of the microreactor and the water content within is determined by the degree of hydration, *i.e.* the water-to-surfactant molar ratio in the bulk system: w_0 = $[H_2O]/[AOT]$.[21] The solubility of O_2 in *n*-octane is an order of magnitude higher than that in water[26] and therefore TAML-containing reverse micelles will be surrounded by an O_2-rich medium favorable for the oxidation of Fe^{III}. At the same time Fe^{III} will be in contact with water, the amount of which is regulated by the degree of hydration w_0.

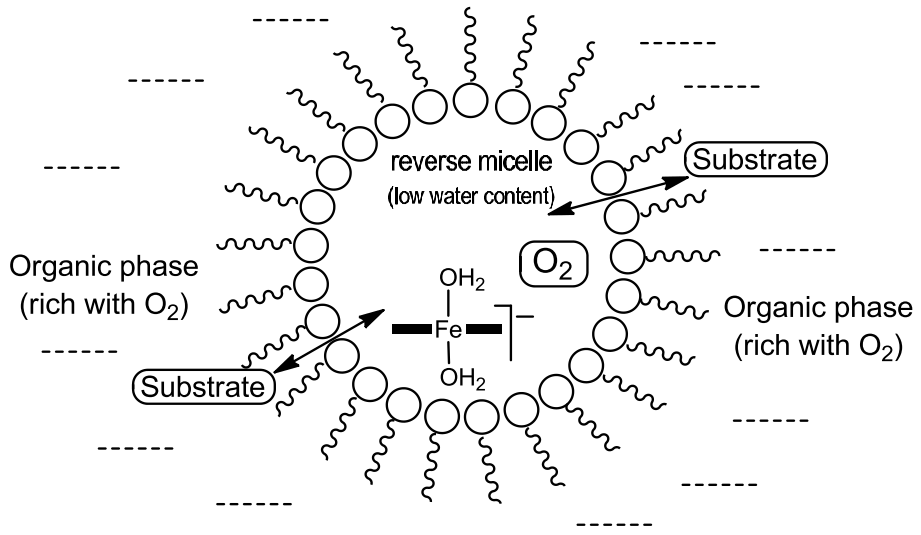

Figure 5.1 Schematic drawing of the reverse micelle incorporating TAML activators.

In this work it has been possible to show that oxidative catalysis is possible for reactive electron donors using **1** in reverse micelles of AOT in *n*-octane *in the absence* of an added

oxidant such as H_2O_2 but in the presence of ambient O_2. In particular, my studies demonstrated the following. (*i*) Dioxygen oxidizes **1a** in the reverse micellar medium to multiple iron(IV)-containing species. (*ii*) These species coexist with the starting iron(III) TAML. (*iii*) The iron(IV) species are the homovalent dimer $Fe^{IV}Fe^{IV}$ **2a** and the less-oxidized heterovalent dimer $Fe^{III}Fe^{IV}$ **3a**.[27] (*iv*) Compound **3a** in reverse micellar medium has been detected by EPR. (*v*) TAML activators in this reverse micellar medium catalyze the oxidation by O_2 of reactive electron donors such as the dye Pinacyanol chloride (PNC), NADH and hydroquinone (Chart 5.1). (*vi*) The oxidation of NADH is a photocatalytic process, the rate of which is directly proportional to the flash frequency. (*vii*) The catalytic activity of TAML activators is a function of both the degree of hydration w_0 and the pH. (*viii*) The dyes Orange II and Safranin O, which are more resistant to oxidation than PNC, are not oxidized by O_2 in this system. (*ix*) A second order dependence on **1a** concentration is found for both NADH and PNC oxidation processes, indicating that the heterovalent dimer **3a** is a reactive intermediate in the catalytic reaction cycle.

5.2 Results and discussion

5.2.1 Oxidation and speciation of TAML activators in the reverse micelles

5.2.1.1 A preliminary comment on speciation of iron in reverse micelles. Chart 5.2 shows species that one might anticipate to coexist in reverse micelles. $Fe^{III}OH_2$ is the starting **1a**. EPR silent diamagnetic d^4 species $Fe^{IV}Fe^{IV}$ and integer spin $Fe^{IV}O$ (S = 1) are made from **1a** and *t*-BuOOH in water;[28] they dominate at pH below and above 10, respectively. $Fe^{V}O$ is characteristically produced from **1a** and *m*-chloroperoxybenzoic acid or hypochlorite at –40 °C in MeCN.[29,30] The Fe^{III} superoxo complex $Fe^{III}O_2$ was made from **1a** and KO_2 at

–5 °C in MeCN.[31] $Fe^{III}Fe^{IV}$ was generated in a 50% glycerol aqueous solution with 1 eq. H_2O_2.[32] By analyzing data from UV-vis and EPR spectra, it has been possible to build a convincing case for the iron speciation of the reverse micellar media.

Chart 5.2 Iron species that could coexist in the reverse micelles. Species in parenthesis were obtained in MeCN.

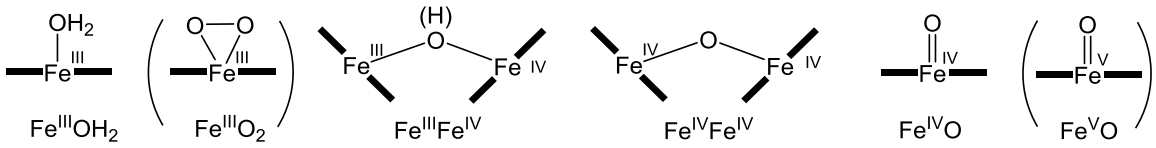

5.*2.1.2 Studies of **1a** in the reverse micelles by UV-vis spectroscopy.* In non-protic organic solvents, the TAML activator **1a** is known to be oxidized by O_2 to the $Fe^{IV}Fe^{IV}$ dimer **2a**.[10] The oxidation does not occur in pure water. As discussed above, the overall water content in the system of AOT reverse micelles is much lower than in bulk water, which should increase the O_2 exposure of **1a** and favor its oxidation. The first evidence for such oxidation was obtained by recording the UV-vis spectra of **1a** at variable pH (8–12) and degree of hydration w_0 (3–25). Complex **1a** does not absorb light above 600 nm. Thus, the observed buildup of broad bands in the range of 600–1100 nm in the AOT reverse micelles (Figure 5.2) was a reliable signal that iron(III) oxidation occurs in the presence of O_2.[10,28] The spectra obtained at w_0 3, 7 and 25 (pH 8) vary in the 600−1100 nm range indicating that more than one species was formed and that the selectivity depends on w_0. The inset to Figure 5.2 shows that at pH 8, the species generated at w_0 3 were more stable than those at w_0 25.

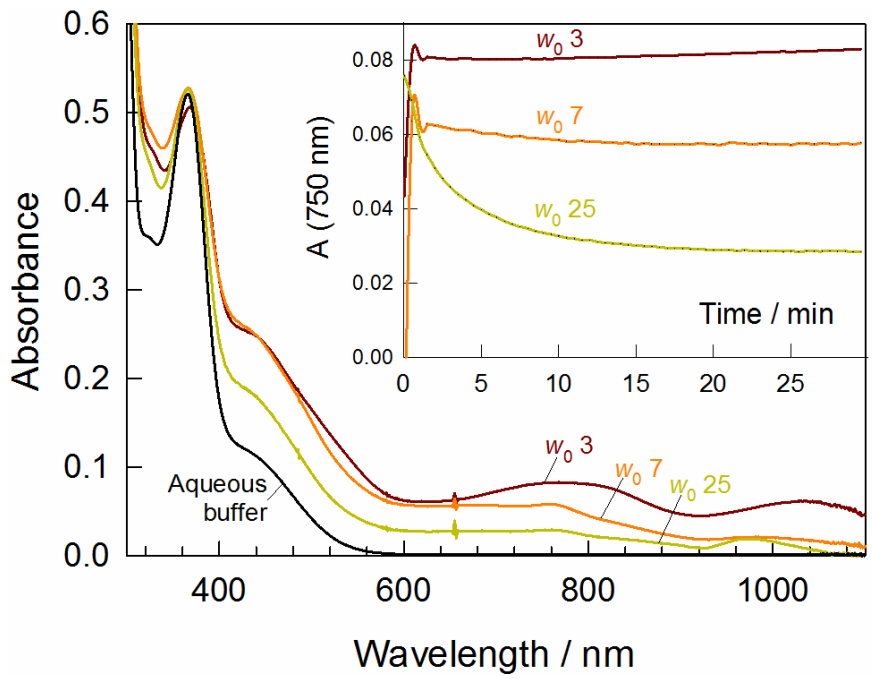

Figure 5.2 Spectra of **1a** in the AOT reverse micelles in *n*-octane recorded 20 min after mixing all components. The spectrum of **1a** in the aqueous buffer (bottom) is shown for comparison. Conditions: [**1a**] = 1.36×10^{-4} M, pH 8, w_0 = 3, 7 and 25; 25 °C. Inset shows changes of absorbance at 750 nm with time for the three different values of w_0.

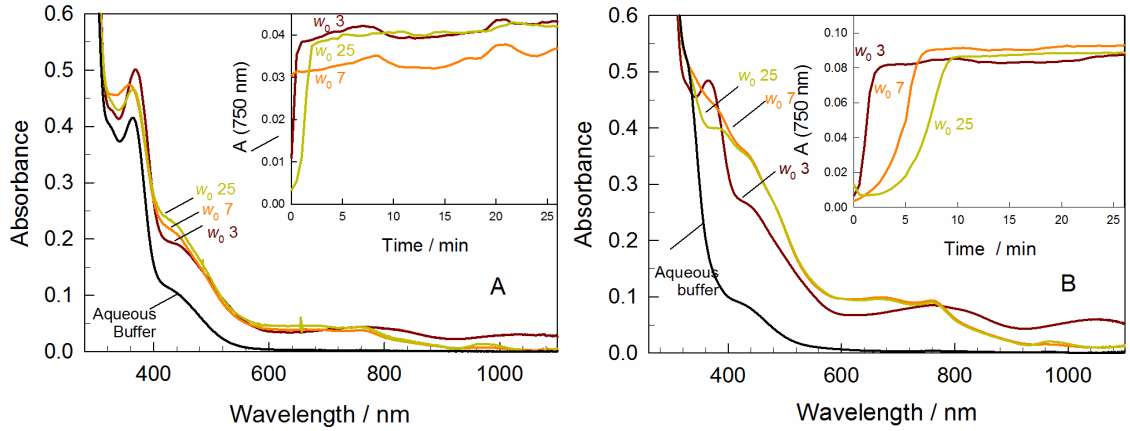

Figure 5.3 Spectra of **1a** in the AOT reverse micelles in *n*-octane recorded 20 min after mixing all components. The spectrum of **1a** in the aqueous buffer (bottom) is shown for comparison. Conditions: [**1a**] = 1.36×10^{-4} M, pH 10 (**A**) and 12 (**B**), w_0 = 3, 7 and 25; 25 °C. Inset shows changes of absorbance at 750 nm with time at different w_0.

Spectra similar to those in Figure 5.2 were generated at pH 10 and 12 (Figure 5.3). Oxidized iron species were produced in the AOT reverse micelles under all conditions studied, but form slower at higher pH and higher w_0. Figures 5.2 and 5.3 allow for the complexes to be labelled as likely or unlikely components of the reverse micellar media as explained next. The characteristic 360 nm band of **1a** was present under all studied conditions in the reverse micellar media. The species $Fe^{IV}Fe^{IV}$ and $Fe^{IV}O$ have been characterized previously[28] as products of the reaction between **1a** and *t*-BuOOH in water[28]—dominating at pH below and above 10, respectively. Both are diamagnetic EPR silent d^4 species, and their involvement in the speciation of the reverse micellar media is discussed in detail in section 5.2.1.4. The UV-vis data provided evidence for the presence of $Fe^{IV}Fe^{IV}$ in the broad bands that can be observed at 800 and 1050 nm. The $Fe^{V}O$ complex was originally produced from **1a** and *m*-chloroperoxybenzoic acid at –40 °C in MeCN.[29] Prior experience suggests that $Fe^{V}O$ is unlikely to be stable under the conditions used herein.[13] The $Fe^{V}O$ complex in MeCN exhibits the characteristic UV-vis peak at 630 nm—there is no identifiable equivalent in Figures 5.2 and 5.3. Similarly, $Fe^{III}O_2$ made by Nam *et al*. from **1a** and KO_2 at –5 °C in MeCN was not present.[31] The UV-vis spectra were ambiguous regarding the presence of mononuclear $Fe^{IV}O$. The heterovalence dimer **3a** has the broad bands at 440 and 760 nm,[32] the formation of which in the reverse micelle system is made clear from Figures 5.2 and 5.3 and the following EPR experiment.

*5.2.1.3 EPR spectroscopy of **1a** in the reverse micelles.* The EPR spectra of **1a** ($Fe^{III}OH_2$) in water,[18] **3a** ($Fe^{III}Fe^{IV}$) in 50% glycerol[27] and $Fe^{V}O$ in MeCN[29] have been characterized previously. The remaining species of Chart 5.2 are EPR silent. As stated above, the generation of $Fe^{III}O_2$ and $Fe^{V}O$ from **1a** and O_2 is improbable. The EPR spectrum of **1a** in

the reverse micelles (pH 8−12, Figure 5.4) displayed a signal from the $Fe^{III}OH_2$ $S = 3/2$ species (g = 4.0, 2.0)[18] and the $Fe^{III}Fe^{IV}$ $S = ½$ species with g = 1.99, 2.11, 2.14.

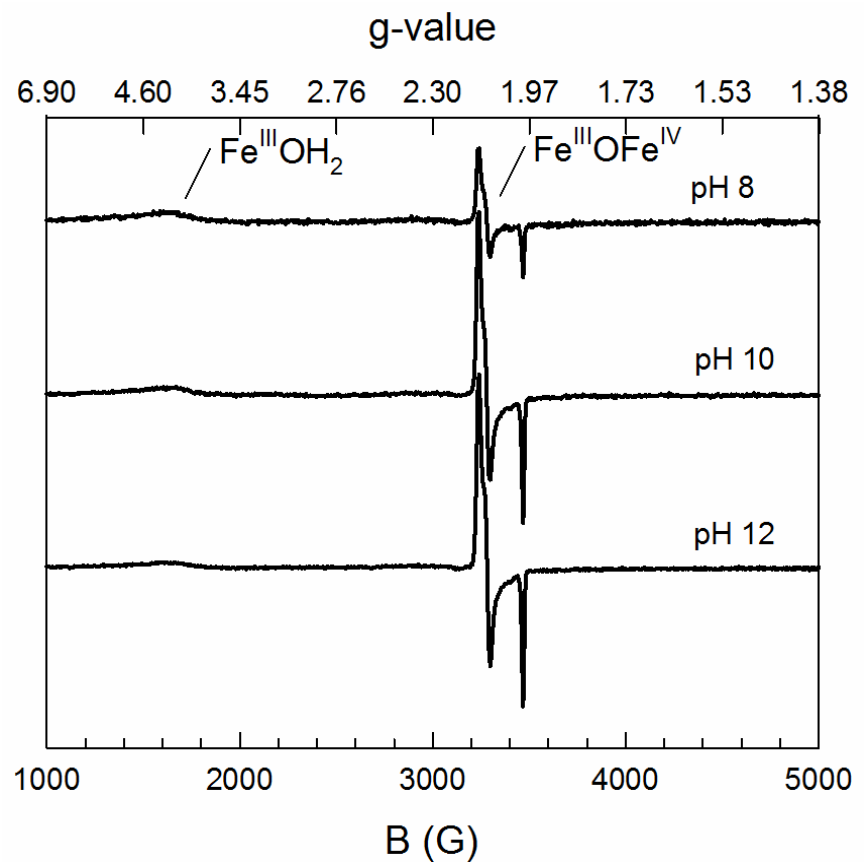

Figure 5.4 EPR spectra of **1a** in reverse micelles, w_0 10 at different pHs. Total iron 1.53×10^{-4} M. Measured concentrations of $Fe^{III}Fe^{IV}$ as dimer are 1×10^{-5} M, 2.5×10^{-5} M, and 2.8×10^{-5} M at pH 8, 10 and 12, respectively.

5.2.1.4 Speciation of iron in reverse micelles. The EPR study confirmed the existence of the $Fe^{III}Fe^{IV}$ (**3a**) species formed from **1a** and O_2 in the reverse micelles. The plausible coexisting species are thus $Fe^{III}OH_2$, $Fe^{III}Fe^{IV}$, $Fe^{IV}Fe^{IV}$ and $Fe^{IV}O$ (Chart 5.2). In water, $Fe^{IV}Fe^{IV}$ and $Fe^{IV}O$ exist in a pH controlled equilibrium.[28] The former dominates at pH < 10, the latter at pH > 12. It is important to note that the effective pH in the AOT reverse

micelles may differ from the pH of the aqueous buffer introduced (and indicated throughout). The acidity can be higher near the interface for negatively charged surfactants.[33] The effective pH is usually by 1–3 units lower in the AOT reverse micelles than in the bulk water depending on w_0,[34,35] though the difference may be smaller than 1 unit when w_0 is high.[22] Therefore, $Fe^{IV}O$ is unlikely a dominating species and may not form at all. The absence of the peak around 435 nm in Figures 5.2 and 5.3, which is typical of $Fe^{IV}O$ (ε_{435} = 2500 M^{-1} cm^{-1}),[28] gives additional evidence. Thus, the remaining species to be considered are $Fe^{III}OH_2$, $Fe^{III}Fe^{IV}$ and $Fe^{IV}Fe^{IV}$. The last has a sharper band at 481 nm, a broader band at 856 nm, whereas the band at 365 nm is weaker as compared to that of $Fe^{III}OH_2$. The less oxidized $Fe^{III}Fe^{IV}$ dimer has two bands at 440 and 760 nm.[27] These bands allowed semi-quantitative interpretation from the spectral data in the range of 760–930 nm where $Fe^{III}OH_2$ does not absorb. The estimations were obtained using eqs 5.1 and 5.2 that connect absorbances at 760 and 930 nm to concentrations of the iron dimers using the known values of ε_{760} and ε_{930} (2500 and 425 M^{-1} cm^{-1} for $Fe^{III}Fe^{IV}$[32] vs. 4820 and 3056 M^{-1} cm^{-1} for $Fe^{IV}Fe^{IV}$, respectively). The extinction coefficients were assumed to be approximately independent of w_0 and pH.

$$A_{760} = 2500[Fe^{III}Fe^{IV}] + 4820[Fe^{IV}Fe^{IV}] \quad (5.1)$$

$$A_{930} = 425[Fe^{III}Fe^{IV}] + 3056[Fe^{IV}Fe^{IV}] \quad (5.2)$$

The amount of $Fe^{III}OH_2$ shown in Figure 5.5 was obtained by subtracting 2×[$Fe^{III}Fe^{IV}$] and 2×[$Fe^{IV}Fe^{IV}$] from the total iron in the system. $Fe^{III}OH_2$ dominates under almost all conditions tested, i.e. there is incomplete oxidation of Fe^{III} by O_2 in the reverse micelles under the conditions studied. More heterovalent dimer $Fe^{III}Fe^{IV}$, the major Fe^{IV}-containing

material, is formed at higher pH and moderate w_0, consistent with the fact that basic conditions stabilize $Fe^{III}Fe^{IV}$ in aqueous glycerol.[32] The homovalent dimer is present at low w_0 and pH 8 since aprotic organic medium and this pH are both favorable for $Fe^{IV}Fe^{IV}$.[10,28] The Fe^{IV} percentage drops at higher w_0 because "wet" micelles are closer to bulk water where **1a** is not oxidized by O_2.[10]

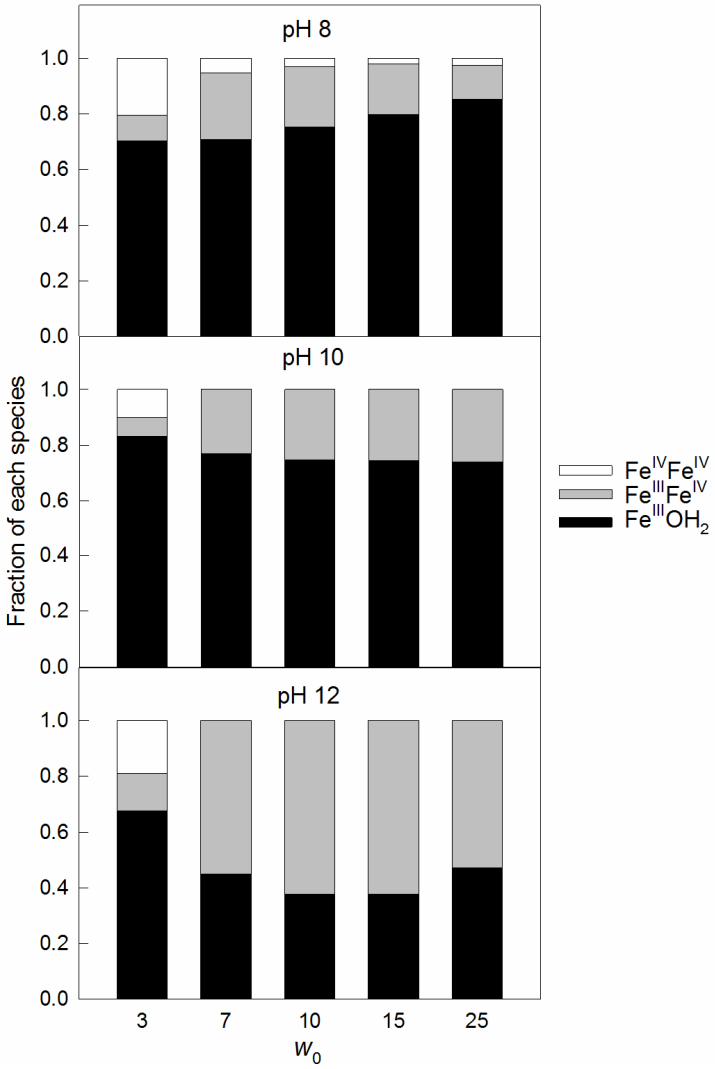

Figure 5.5 Estimated fractions of $Fe^{III}OH_2$, $Fe^{III}Fe^{IV}$, and $Fe^{IV}Fe^{IV}$ (all derived from **1a**) in the AOT reverse micelles at different pH and w_0. For other conditions, see caption to Figure 5.2 and Figure 5.3.

The data in Figure 5.5 should be considered as qualitative because water inside reverse micelles is dissimilar to bulk water in terms of polarity, acidity and microscopic viscosity.[19,35] As a result, the environment of **1a** varies with the degree hydration w_0 of the reverse micelles and the ε values in reverse micelles and pure water may differ. Nevertheless, estimates in Figure 5.5 for the UV-vis data agree with the EPR results in Figure 5.4 because the spin quantitation gives the yields of $Fe^{III}Fe^{IV}$ of 13, 33 and 37% at pH 8, 10 and 12, respectively, at w_0 10 and total iron of 1.5×10^{-4} M. Thus, **1a** is oxidized in the O_2-rich system into Fe^{IV} species in the absence of peroxides. The catalytic activation of O_2 by **1a** in these reverse micelles will now be described.

5.2.2 Oxidation of substrates by dioxygen catalyzed by TAML activators

5.2.2.1 Catalytic oxidation of NADH in reverse micelles. The NADH/NAD^+ couple is the essence of numerous biological processes[36-38] including those catalyzed by NAD^+-dependent dehydrogenases, viz. enzymes that are widely used in organic synthesis.[37,39] These enzymatic processes are of limited use due to the cost of NAD^+.[40] Reliable systems for NAD^+ regeneration are needed to advance the utility for the NADH/NAD^+ couple in synthetic processes as the current methods are still not adequately effective.[41] TAMLs are known to catalyze the oxidation of NADH by enzymatically produced H_2O_2 under mild conditions.[42] Therefore NADH was the first substrate I chose to examine for study of TAML/O_2 catalytic oxidation the reverse micelles.

Smooth conversion of NADH into NAD^+ was monitored by UV-vis spectroscopy at 340 nm (maximum for NADH; NAD^+ does not absorb) at w_0 in the range of 3 to 25 and pH 8, 10 and 12. At pH 10 the isosbestic point holds at 286 nm (Figure 5.6A). Control experiments in the reverse micelles in the absence of **1a** showed negligible oxidation of

NADH within the same time period (Figure 5.7A). The conversion of NADH into NAD^+ rather than into smaller fragments was proven by HPLC[43] by comparing the elution times of the product and authentic NAD^+. At pH 10 and w_0 10, no NADH was observed after 9 h by UV-vis spectroscopy when the spectra were recorded every 30 s (see below for explanations). The 83% yield of NAD^+ was calculated from the HPLC data. This corresponds to the turnover number (TON) of 88 and turnover frequency (TOF) of 0.003 s^{-1} at [**1a**] = 2.46×10^{-6} M and [NADH] = 2.6×10^{-4} M. The control experiment in the absence of **1a** showed 67% NADH and 27% NAD^+ by HPLC after 9 h. Catalyst **1a** converts NADH into the 'enzymatically active' NAD^+. Alcohol dehydrogenase (ADH) and ethanol rapidly reduce NAD^+ formed to NADH.[41] 95% NADH reappears almost instantly, much faster than the NADH oxidation (Inset to Figure 5.6B). These results lead to the conclusion that the oxidation proceeds according to eq 5.3.

$$\mathrm{NADH} + \tfrac{1}{2}\mathrm{O_2} + \mathrm{H^+} \xrightarrow{\mathrm{TAML}} \mathrm{NAD^+} + \mathrm{H_2O} \tag{5.3}$$

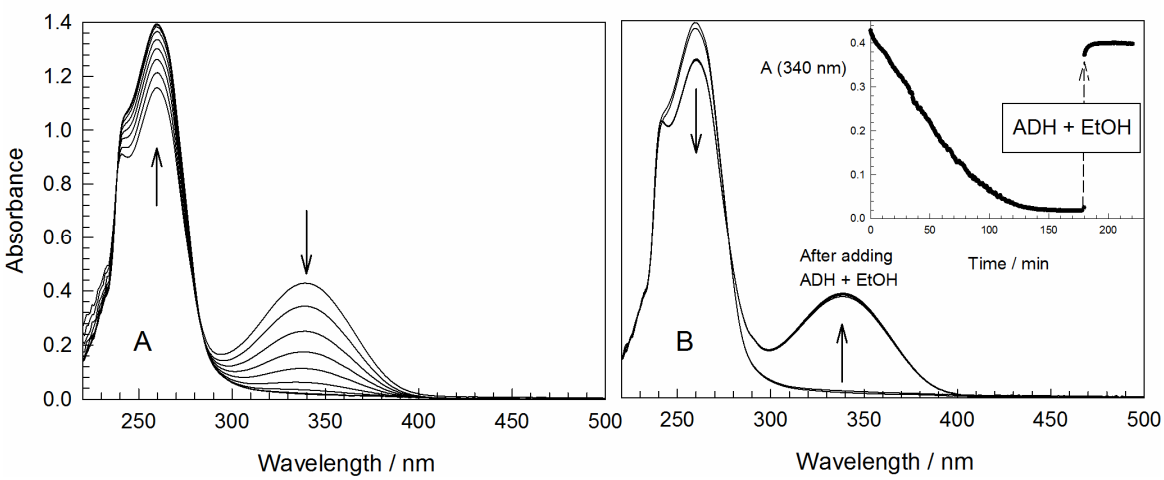

Figure 5.6 (A) Spectral changes that accompany **1a**-catalyzed oxidation of NADH into NAD^+ by O_2 and (B) regeneration of NADH by ADH/EtOH. Time interval between spectra shown in A is 20 min (scans were made every 30 s). ADH (from *Saccharomyce cerevisiae*, 0.7 mg, 210 units in 50

μL water) and 10 μL EtOH were added to the reaction mixture after 3 h followed by vigorous shaking. Inset in B illustrates the time scale of TAML-catalyzed oxidation and the enzyme-catalyzed regeneration of NADH. Conditions: 0.1 M AOT, pH 10 (0.01 M carbonate), $w_0 = 7$; [**1a**] = 2.46×10^{-6} M, [NADH] = 9.9×10^{-5} M.

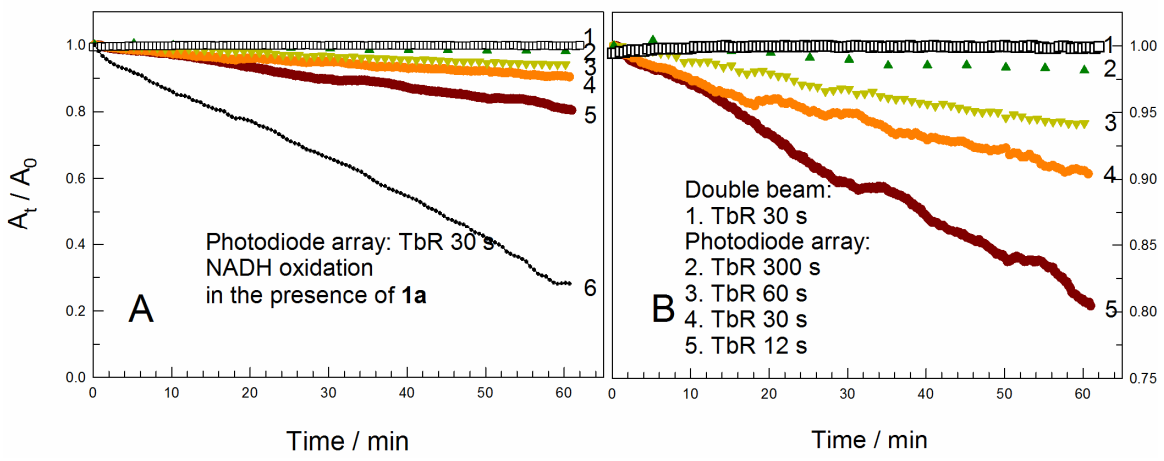

Figure 5.7 A. Kinetic curves for NADH oxidation in both the absence and presence of **1a** registered with both double beam (Curve 1) and photodiode array instruments (Curves 2-6) applying different pulse frequencies for the photodiode array instrument. An NADH degradation curve (6) in the presence of **1a** was shown for comparison in Figure 5.7A. B. Y axis zoom for the five runs of A in which **1a** was absent (Curves 1-5). TbR is the time between recording successive spectra. Other conditions: pH 10, $w_0 = 10$, [NADH] = 5.14×10^{-5} M.

Whenever the catalytic reduction of O_2 is being studied, it is important to be sure that adventitious oxidizing agents are not intruding into the reaction chemistry.[44] A major concern is the presence of peroxidic impurities in the components of the reaction media. To rule out the possible involvement of peroxides, **1b**, which is more reactive in oxidations by H_2O_2 in pure water than **1a**,[2] was used as the catalyst in the reverse micellar oxidation of NADH. Fluorinated TAMLs such as **1b** react with O_2 in aprotic solvents much more slowly than their methylated counterparts.[10] The data in Figure 5.8 show that **1b** is 5-times

less reactive than **1a** in the reverse micelles at pH 10 and w_0 3. This establishes that adventitious peroxides are unlikely major participants. Furthermore, colorimetric testing for peroxide with KI and peroxide test strips produced no color changes.[45] These results support the case that **1a** does indeed launch an oxygenase-like process (eq 5.3) in the reverse micelles and that H_2O_2 is not involved.

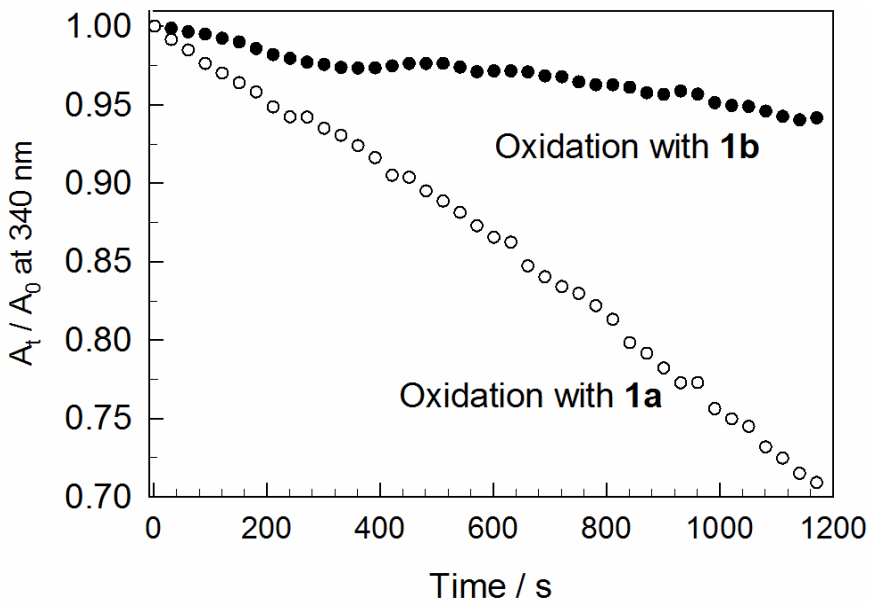

Figure 5.8 Changes of absorbance of NADH at 340 nm during **1a-** and **1b-**catalyzed oxidation of NADH by O_2 at pH 10 and w_0 3. Conditions: **1a**-catlayzed NADH oxidation: [NADH] = 5.16×10^{-5} M, [**1a**] = 2.47×10^{-6} M; **1b**-catlayzed NADH oxidation: [NADH] = 5.16×10^{-5} M, [**1b**] = 2.45×10^{-6} M.

Next, the ability of the iron(IV) complex **2a**[10] to oxidize NADH ([Fe^{IV}]:[NADH] = 1:1.05) was tested in reverse micelles in degassed media under argon to preclude or at least minimize autoxidation. The NADH absorbance around 340 nm decreased on addition of **2a** indicative of the oxidation of NADH (Figure 5.9). NAD^+ was produced in 62 and 52% yields with the respect to the total iron according to UV-vis and HPLC data, respectively

(Table 5.1). When ferric **1a** was employed in place of **2a** under otherwise identical conditions, the yield of NAD^+ fell to 14% (HPLC). That any oxidation was observed at all suggested that O_2 was not excluded completely by the degassing procedure. These facts support the hypothesis that NADH can be oxidized by **2a** and allow us to conclude that catalyst-based oxidations are competent to produce the observed chemistry in these reaction systems where one has always be on the lookout for adventitious free radical autoxidation.

Table 5.1 Results of HPLC study of reactions of NADH (2.1×10^{-4} M) with iron(III) (**1a**) and iron(IV) (**2a**) species (both 2.0×10^{-4} M with respect to a monomeric form) in the reverse micelles at w_0 7 and pH 12.

Iron Species	Amount with respected to added NADH / %		Yield of NAD^+ with respect to total iron / %	Conditions
	NAD^+	NADH		
None	0	100	0	Solution A
2a	25	70	52	Reaction time 20 min
2a	85	0	180	After exposure to air for 15 min following the reaction
1a	7	82	14	Reaction time 20 min
1a	63	1	132	After exposure to air for 15 min following the reaction

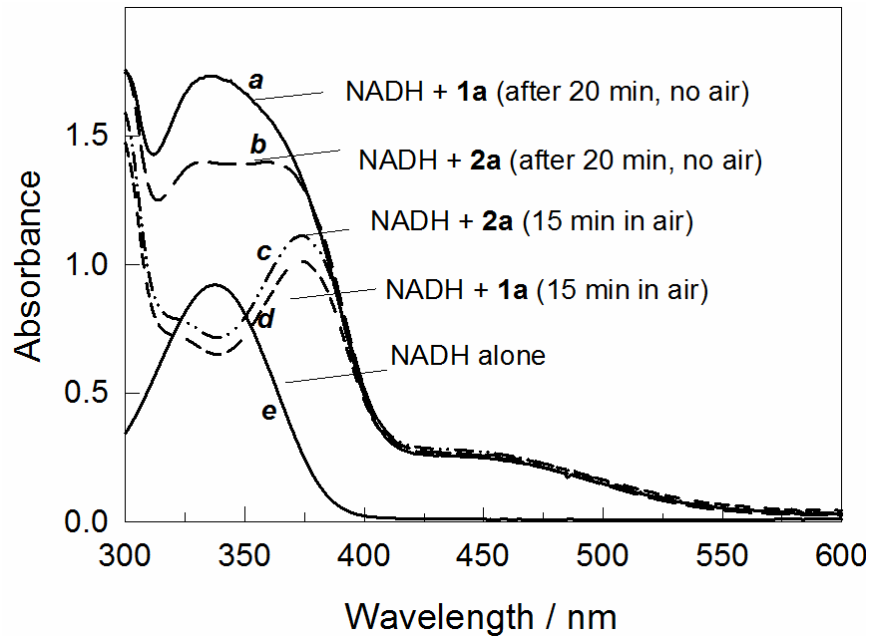

Figure 5.9 UV-vis spectra of NADH in the presence of **1a** or **2a** (1.5 mL methanol was added to 1.5 mL reaction mixture to quench the reaction). Conditions: pH 12, w_0 = 7, [NADH] = 2.1×10^{-4} M, [total iron] = 2.0×10^{-4} M. (**a**, **b**: spectra of NADH reacted with **1a** or **2a** in the absence of O_2; **c**, **d**: spectra of NADH reacted with **1a** or **2a** after exposure to air for 15 min; **e**: spectrum of NADH alone).

5.2.2.2 Comparison of initial rates of NADH oxidation. NADH is slowly oxidized in reverse micelles in the absence of **1a** as shown in Figure 5.7. TAML **1a** accelerates the oxidation to such extent that the spontaneous process can be neglected in many cases. Nevertheless, the initial rates shown in 3D Figure 5.10 were corrected for the uncatalyzed reaction in the absence of **1a**. The degree of hydration w_0 is a key factor that regulates the reactivity. Reaction 5.3 is strikingly faster in lower w_0 micelles. One explanation is that water impedes the binding of O_2 to the Fe^{III} center, thus slowing the catalytic rate. However, the actual concentrations of iron species and/or NADH within a microreactor will be changing with w_0. The catalyst will certainly partition preferentially into water than the

organic solvent, so concentration effects cannot be neglected and perhaps provide the dominant explanation.[46] Reaction 5.3 is much less sensitive to pH than to w_0.

5.2.2.3 Effect of light on the catalyzed NADH oxidation in reverse micelles. TAML-catalyzed reaction 5.3 is accelerated by light. The effect was established by changing the scanning frequency when the NADH oxidation was monitored by a photodiode array UV-vis spectrometer. The process was noticeably faster when spectra were registered more frequently, i.e. when the flash frequency (F_f = inverse time between recording (TbR) of successive spectra) was higher (Figure 5.11). The slowest rate was registered when reaction 5.3 was followed using a double beam UV-vis spectrometer but it increased *linearly* with increasing flash frequency when the photodiode array instrument was used (Inset to Figure 5.11). The straight line has an insignificant positive intercept which may reflect a dark process. A double beam spectrometer emits much less light to the sample than a photodiode array instrument which utilizes the undispersed light beam in the 190−1100 nm spectral region. Reactions susceptible to "diode array acceleration" are known and have recently been reviewed.[47] The majority of these processes involve O_2. The mechanisms do not involve species in long-lived excited states and are usually complex requiring individual systematic studies.

The light accelerates the uncatalyzed oxidation of NADH in the reverse micelles in the absence of **1a** (Figure 5.7). Thus, the irradiation affects NADH. Experiments with Pinacyanol chloride (Figure 5.12) suggest that irradiation does not impact **1a** directly. The bleaching rate of PNC was found to be practically insensitive to the flash frequency of the photodiode array spectrometer (Figure 5.12); a minor effect is ascribed to the reported photo-degradation of aggregated PNC in water,[48] which is also observed in the absence of

1a (Inset to Figure 5.12). The kinetics of absorbance growth at 750 nm has been studied to probe the formation of $Fe^{III}Fe^{IV}$ and/or $Fe^{IV}Fe^{IV}$ from **1a** and O_2 in the reverse micelles as a function of the flash frequency at w_0 15 and pH 12. Under such conditions the rates are lower and the measurements are more accurate. No light effect was registered (see Figure 5.13) indicating that NADH is the photosensitive component of reaction 5.3.

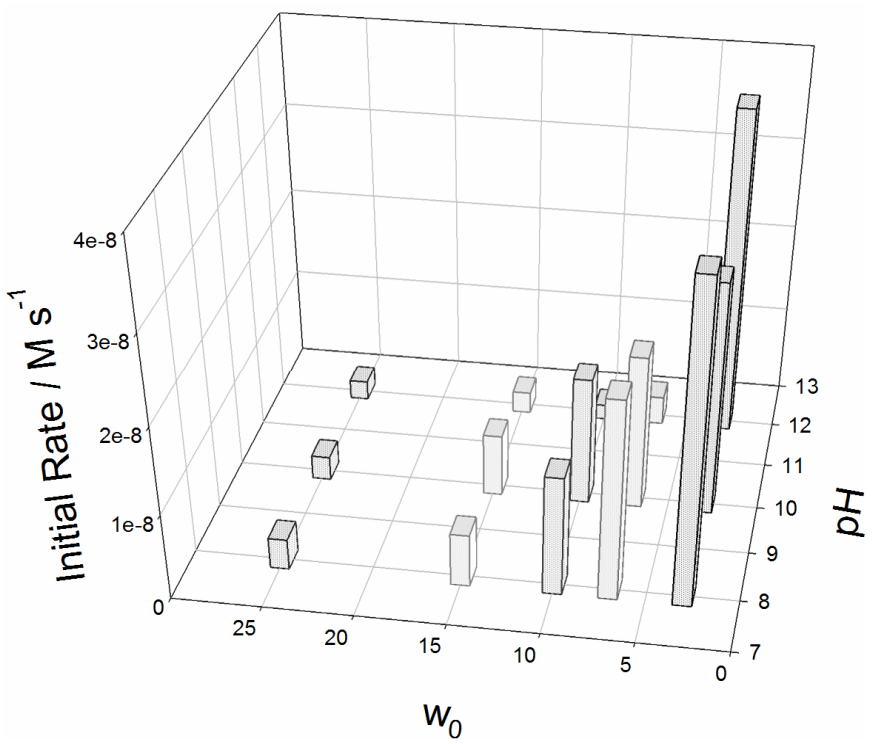

Figure 5.10 Initial rates of NADH oxidation catalyzed by **1a** in reverse micelles. Conditions: [**1a**] = 2.5×10^{-6} M, [NADH] = 5.12×10^{-5} M, the flash frequency is 30 s. See text for explanations.

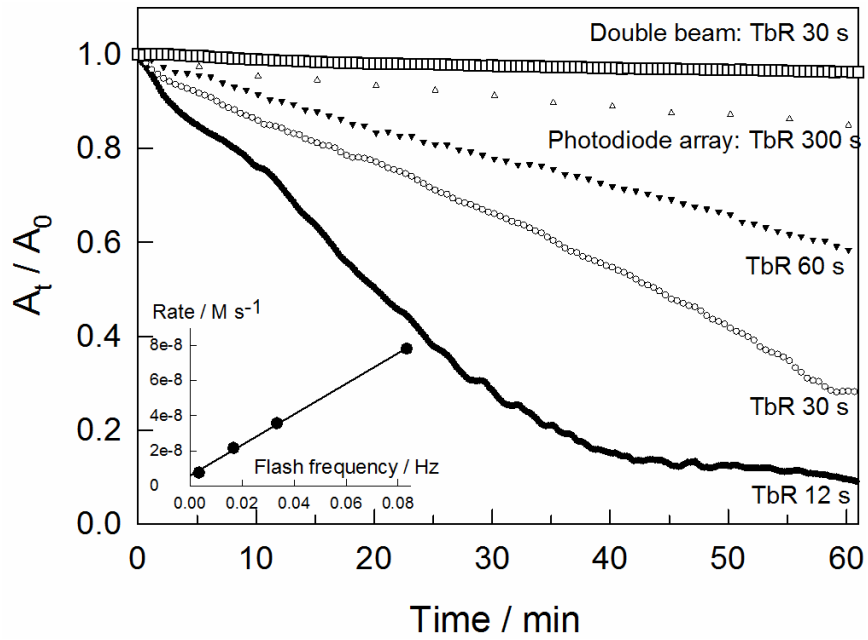

Figure 5.11 Kinetics of NADH oxidation registered by different UV-vis spectrometers applying different pulse frequencies. Top curve was obtained using a double beam instrument and lower curves were produced using a photodiode array instrument. TbR is the time between recordings of successive spectra. Other conditions: pH 10, w_0 = 10, [NADH] = 5.14×10^{-5} M, [**1a**] = 2.39×10^{-6} M.

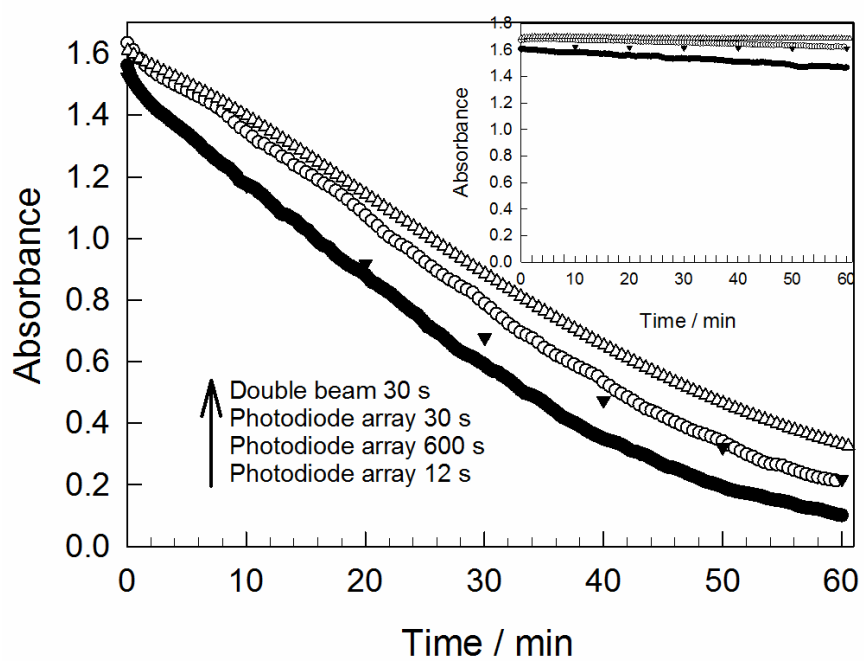

Figure 5.12 Catalyzed Pinacyanol chloride (PNC) oxidation by **1a** applying different pulse frequencies using photodiode array and double beam spectrometer. Conditions: pH 10, w_0 = 10, [PNC] = 2.71×10^{-5} M, [**1a**] = 1.52×10^{-6} M. Inset: PNC oxidation in the absence of **1a**. Time between recordings of successive spectra is 12, 30 and 600 s.

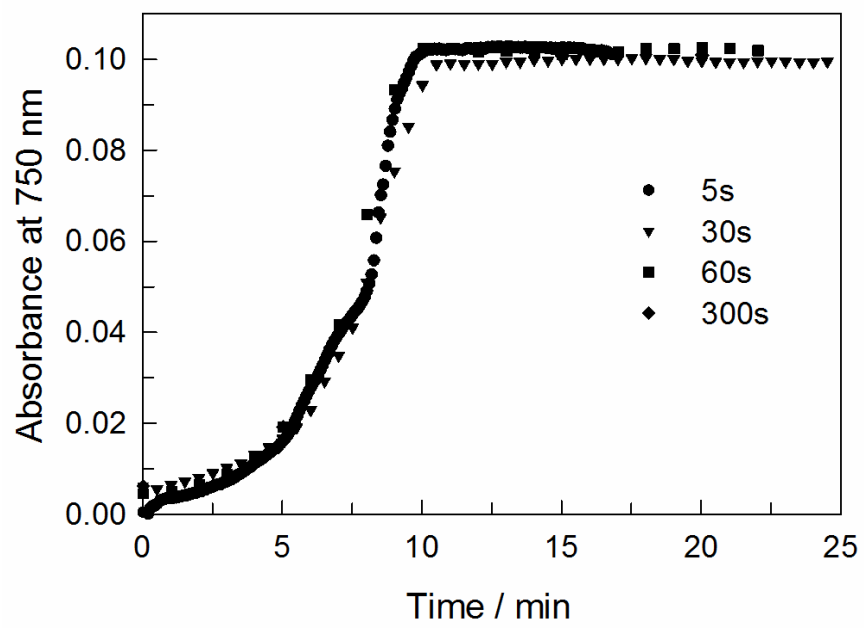

Figure 5.13 Absorbance change of **1a** at 750 nm applying different TbR (time between recordings of successive spectra) in the reverse micelles. Conditions: pH 12, w_0 = 15, [**1a**] = 1.36×10^{-4} M. Spectra were recorded every 5 s, 30 s, 60 s and 300 s using photodiode array UV-vis.

5.2.2.4 Oxidation of Pinacyanol Chloride and Hydroquinone. In 1998, PNC was used to unveil the catalytic activity of **1a**/H_2O_2.[49] As noted above, PNC decomposes slowly in the reverse micelles without **1a** (Figure 5.12)—the process is faster in water at pH 10 due to the aggregation of PNC to form a dark solid.[50] The oxidation of PNC by O_2 in the reverse micelles is strongly catalyzed by **1a** at pH 10 (Figures 5.12 and 5.14). The bleaching of PNC was investigated in some detail at w_0 3, 10 and 25 and pH 8, 10 and 12 (Table 5.2). It is rather slow at pH 8, as is typical of the lower activity of **1a**/H_2O_2 in water at neutral/acidic pHs.[51] At pH 10, the fastest bleaching was observed at w_0 10, but it slowed down in the dry micelles at w_0 3 (Figure 5.15). The oxidation of Fe^{III} to Fe^{IV} and the oxidative bleaching of PNC by Fe^{IV} are affected oppositely by w_0. Lower w_0 values favor the former process but disfavor the latter. Under the optimal conditions (w_0/pH = 10/12) in the presence of just 1%

1a, TON and TOF equal 90 and 1.6×10^{-3} s^{-1}, respectively. The **1a**-catalyzed oxidation of PNC by O_2 in the reverse micelles is less deep than by H_2O_2 in water. Figure 5.14 shows that a decrease of the main 600 nm peak is accompanied by a build-up of a smaller peak at 350 nm, which was not observed in the aqueous solution.[52]

Table 5.2 Comparison of the efficacy of catalysis by **1a** in oxidation of Pinacyanol chloride (PNC) (4.5×10^{-5} M) by O_2 in reverse micelles under different conditions at 25 °C.

w_0	$10^7\times$[**1a**]/M	Time/h	PNC bleached as measured at 600 nm / %		
			pH 8	pH 10	pH 12
			With/without **1a**		
	5	48	44/11	43/11	67/8
3	12.5	16	51/5	46/5	64/4
	50	3	24/0.2	8/0.3	22/0.1
	5	16	62/5	84/9	100/5
10	12.5	3	37/1	66/1	95/1
	50	3	96/1	97/1	97/1
	5	48	42/10	82*/24	100*/6
25	12.5	16	13/3	40/4	99*/2
	50	3	22/2	43/1	39/1

* A gradual change of color was observed in the cuvette and a darker color was at the bottom (no precipitate observed) which is supposed to be attributed to the instability of the reverse micelle system.

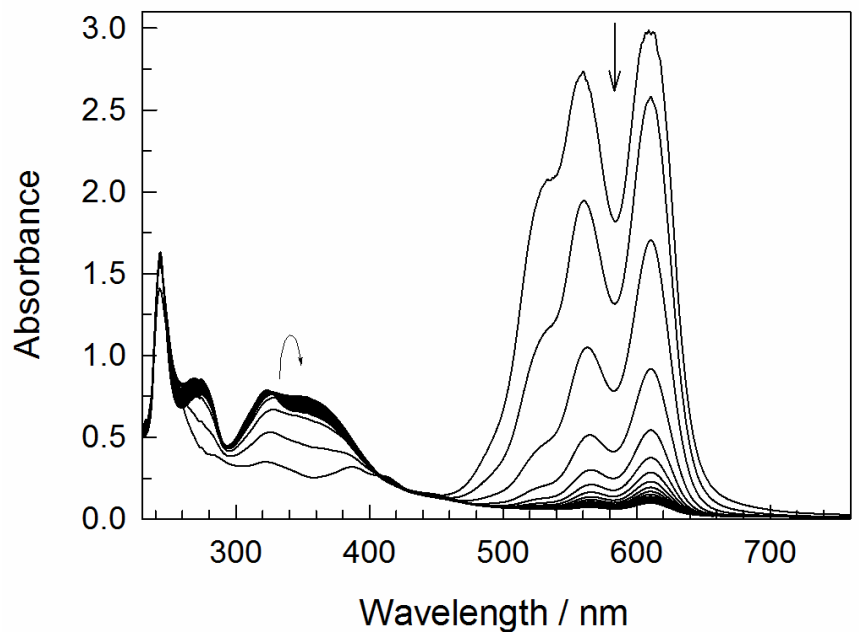

Figure 5.14 Spectral changes that accompany **1a**-catalyzed oxidation of PNC by O_2 in the reverse micelles. Conditions: pH 10, w_0 = 10, [PNC] = 4.5×10^{-5} M, [**1a**] = 5×10^{-6} M, spectra shown with 10 min intervals.

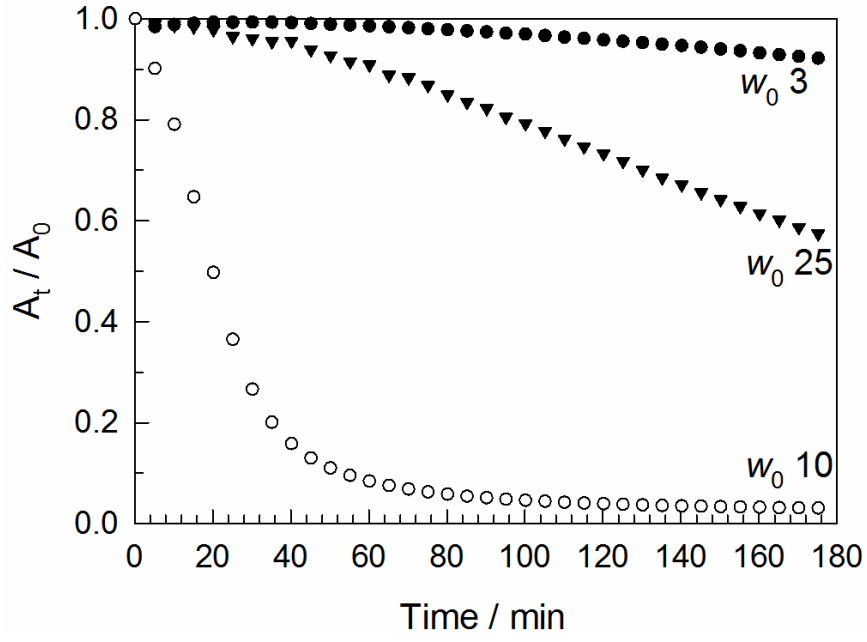

Figure 5.15 Changes of percentage of PNC during **1a**-catalyzed bleaching of PNC by O_2 at pH 10 and variable w_0 (3, 10 and 25) calculated from PNC absorbance at 600 nm. Conditions: [PNC] = 4.5×10^{-5} M, [**1a**] = 5.0×10^{-6} M.

The rapid oxidation of hydroquinone (HQ, λ_{max} 289 nm) to 1,4-benzoquinone (λ_{max} 247 nm)[53] is convenient to study by UV-vis spectroscopy.[53] The process is very fast under basic conditions and is followed by a second oxidation step.[54] The spontaneous oxidation of HQ was found to be slow in the reverse micelles prepared using a tiny amount of water (w_0 ~1.6, see Section 5.4) and studied immediately after preparation. The oxidation of HQ is faster in the presence of **1a** under all conditions tested. Notably, the HQ oxidation was faster in wet micelles with higher w_0 (Figure 5.16), in contrast with the oxidation of NADH, which was found to be more rapid in micelles with low w_0, or PNC, which occurred most rapidly at intermediate w_0. This is probably because the effective pH inside the water pools decreases with w_0 to favor HQ stability. A secondary oxidation process is also visible for HQ at higher pH (pH 10 and 12, Figure 5.17).

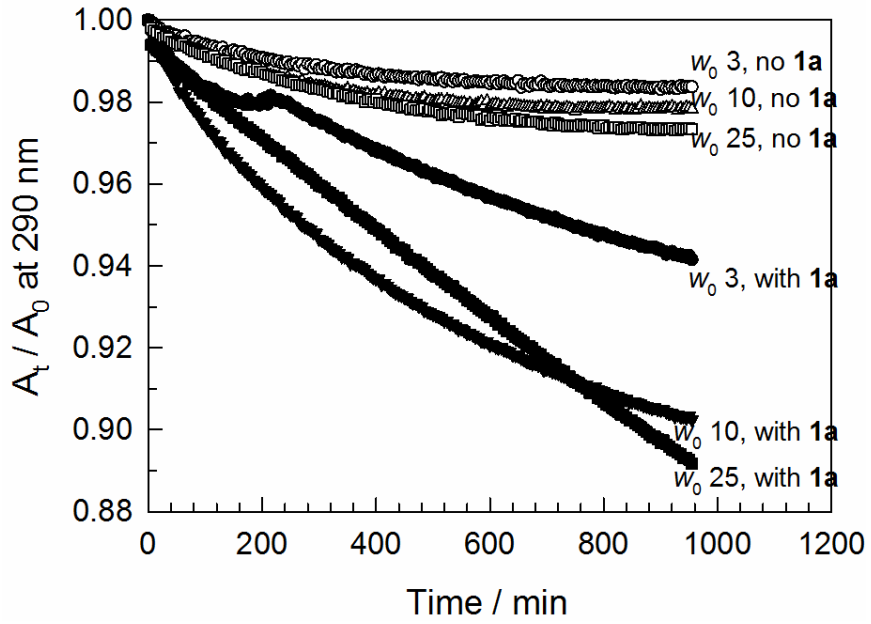

Figure 5.16 Hydroquinone oxidation under different conditions. Conditions: pH 8, w_0 = 3, 10, 25, [HQ] = 6.0×10^{-4} M, [**1a**] = 2.5×10^{-6} M.

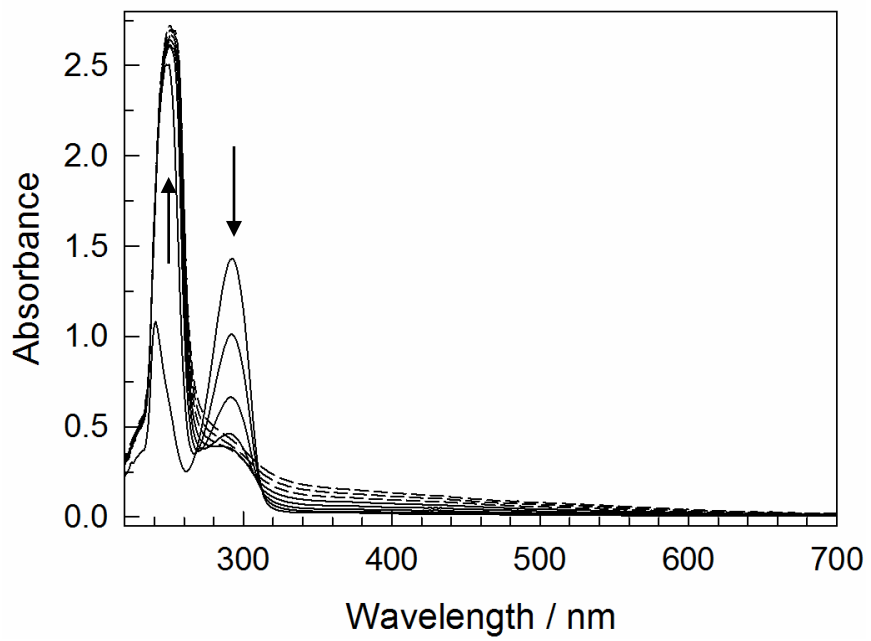

Figure 5.17 Spectral changes that accompany **1a**-catalyzed oxidation of hydroquinone by O_2. Conditions: pH 10, w_0 10, [HQ] = 6.0×10^{-4} M, [**1a**] = 2.5×10^{-6} M, spectra were recorded every 100 min. Solid and dash lines show the primary and secondary oxidative processes, respectively.

Chart 5.3 Structures of Orange II and Safranin O dyes.

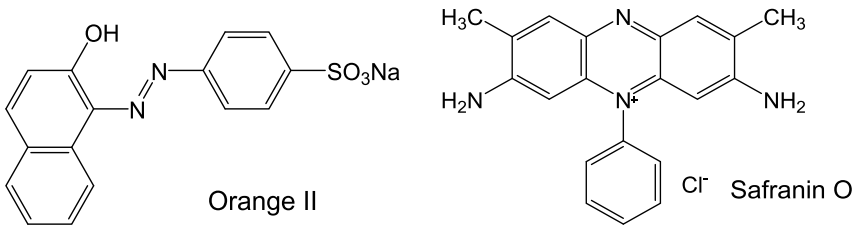

5.2.2.5 Limitations of reverse micelles as media for TAML-catalyzed oxidation by O_2. TAML activators catalyze the bleaching of Orange II[1] and Safranin O[55] (Chart 5.3) dyes by H_2O_2 in water. These two dyes are more difficult to decolorize than PNC.[52] Orange II has become widely used for assaying the catalytic activity of synthetic oxidation catalysts.[1,5,25,56-59] Neither Orange II nor Safranin O were decolorized in the presence of **1a**

in the AOT reverse micelles even in the presence of equimolar amounts of **1a** and Orange II or Safranin O in the reaction media.

5.2.2.6 Reactivity Comparisons of TAML Species. The oxygenase activity of TAML activators in the reverse micelles established in this work is moderate—**1a**/O_2 does not bleach what are facile targets in water, like Orange II, but does catalyze the mild oxidation of reactive electron donors such as NADH—enzymatically active NAD^+ is produced with TON of 88. The TOF of 0.003 s^{-1} is, however, lower than those recently reported for O_2 oxidations involving iron(III) complex of *meso*-tetrakis(4-sulfonatophenyl)porphyrin (0.11 in the aqueous phosphate buffer of pH 7)[60] and **1a** in the presence of glucose oxidase/*D*-glucose (ca. 0.03 at pH 7.5).[42] The lower reactivity of TAML activators in these processes is adequately understood at a molecular level because there is a clear parallel between the reactivity and the iron oxidation state as shown in Chart 5.2 where the iron oxidation state in characterized TAML species increases from left to right (from 3+ to 5+)—$Fe^{V}O$ expresses a ca. 10^4 fold rate advantage over $Fe^{IV}Fe^{IV}$ in organic media.[13,14] Monomers $Fe^{IV}O$ are known to be more reactive than dimers $Fe^{IV}Fe^{IV}$ in aqueous solutions.[61] Thus, the dominating speciation of iron here as the least oxidized and oxidizing $Fe^{III}Fe^{IV}$ explains the observed reactivity picture.

However, the identification of oxidized iron complexes does not substantiate that these are the reactive intermediates in a catalytic cycle—a proposed reactive intermediate should always be supported by appropriate kinetic evidence. Therefore, in the following section the results of kinetic investigations of **1a**-catalyzed oxidations of PNC and NADH by O_2 in reverse micelles of AOT in *n*-octane are presented, choosing degree of hydration w_0 = 10 and pHs 8 and 10. The data presented below reveal the existence of a second-order

pathway in [**1a**] for both PNC and NADH oxidations, which (*i*) supports the hypothesis that dimer **3a** (Chart 5.1) could be a dominant reactive species under specified conditions[32] and (*ii*) is compatible with the fact that only reactive reducing agents are subject to oxidation—from the accumulated evidence on the relative reactivities of Fe^{V} and Fe^{IV} TAML species,[13] it is clear that **3a** is only mildly oxidizing.

5.2.3 Study into the oxidation mechanism in the reverse micelle system[62]

5.2.3.1 Kinetics of PNC Oxidation. Previously, the kinetics of PNC bleaching by H_2O_2 catalyzed by **1a** has been investigated in aqueous media—the process results in a deep fragmentation of the PNC molecule.[52] Therefore, it seemed logical to also examine this dye in kinetic studies in the reverse micelles as a possibly useful model compound. Typical results of the kinetic study are presented in Figure 5.18. At pH 8, the initial rate is virtually independent of the [PNC] in the range of $(0.45–4.45)\times10^{-5}$ M. In contrast, the initial rate is strongly dependent on [**1a**] in the range of $(0.50–5.56)\times10^{-6}$ M, with the reaction order in the catalyst being equal to two. The second order pathway in [**1a**] is a new feature in catalysis by TAML activators. When TAMLs function in water utilizing H_2O_2 or organic peroxides as primary oxidants, first order kinetics in [TAML] is commonly observed,[12,51] though a reaction order of one half has also been confirmed.[63]

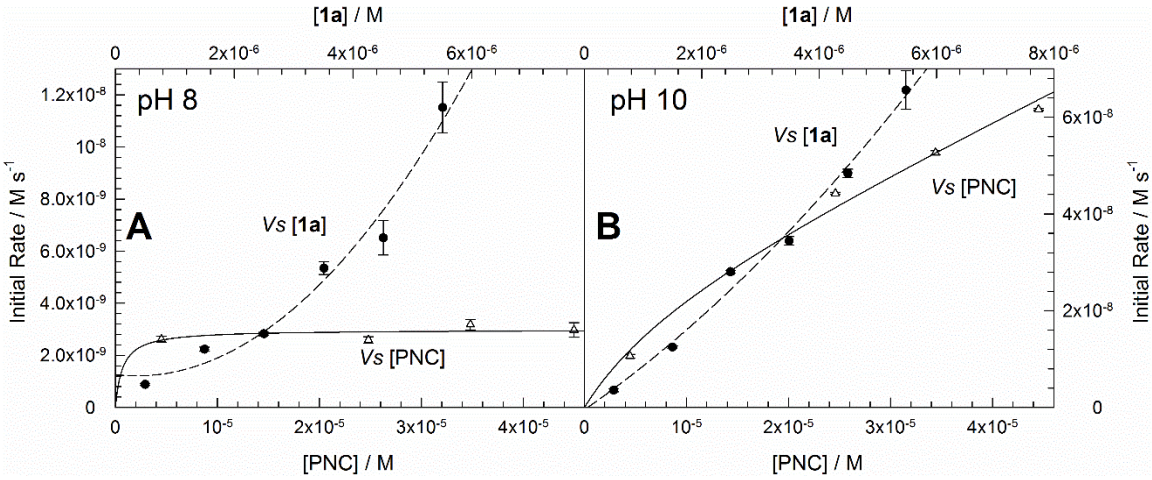

Figure 5.18 Initial rates of **1a**-catalyzed PNC oxidation by O_2 as functions of the concentrations of PNC (Δ) and **1a** (●) in reverse micelles of AOT in *n*-octane at pH 8 (A) and 10 (B), w_0 10. A: pH 8, [**1a**] = 2.50×10^{-6} M at variable PNC; [PNC] = 1.45×10^{-5} M at variable **1a**. B: pH 10, [**1a**] = 2.49×10^{-6} M at variable PNC; [PNC] = 1.43×10^{-5} M at variable **1a**. Time between recordings of successive spectra is 30 s. TAML dashed lines are calculated using k_A and k_B from Table 5.3. NADH solid lines are calculated using the following values of eq 5.7 (α/s^{-1}, $\beta/M\ s^{-1}$, and γ/M) equal, respectively, (~0; 3×10^{-9}; and 7×10^{-7}) at pH 8 and (1×10^{-3}; 2×10^{-8}; and 1×10^{-5}) at pH 10.

At pH 10, the rate is noticeably dependent on [PNC] in the same concentration range, while the reaction order in [**1a**] is higher than one, but less than two, suggesting a mixed reaction order in the catalyst, i.e. the coexistence of first- and second-order pathways in [**1a**]. Therefore, the kinetic data were fitted to eq 5.4.

$$\text{Initial Rate} = v_0 + k_A[\mathbf{1a}] + k_B[\mathbf{1a}]^2 \tag{5.4}$$

The minor term v_0, which is particularly noticeable at pH 8, corresponds to the non-catalyzed pathway of PNC disappearance as a result of direct autoxidation/aggregation of PNC,[64] the existence of which was confirmed in this study in control experiments in the absence of **1a**.[32] Interestingly, the k_A term is practically negligible at pH 8 where pure second order kinetics in [**1a**] is observed (Figure 5.18A). The kinetic data in Figure 5.18B

were fitted to eq 5.4 and the best-fit values of k_A and k_B are summarized in Table 5.3. The data collected at pH 8 were also fitted to eq 5.4 assuming $k_A \sim 0$. The results are also summarized in Table 5.3.

Table 5.3 Kinetic parameters of eq 5.4 for **1a**-catalyzed oxidation of PNC and NADH by O_2 in AOT reverse micelles in *n*-octane at w_0 10 and 25 °C.

Substrate	pH	v_0 / M s^{-1}	k_A / s^{-1}	k_B / M^{-1} s^{-1}	r^2
PNC	8	(1.3±0.6)×10^{-9}	~0	(0.37±0.07)×10^{3}	0.9610
	10 [a)]	(0±2)×10^{-9}	(8±2)×10^{-3}	(0.6±0.3)×10^{3}	0.9868
NADH	8	(3 ± 3) × 10^{-9}	(6±2)×10^{-3}	(1.0±0.4)×10^{3}	0.9722
	10	(1.3±0.8)×10^{-9}	~0	(2.11±0.05)×10^{3}	0.9885

5.2.3.2 Kinetics of NADH oxidation. In the above, it has been shown that the oxidation of NADH by O_2 in reverse micelles occurs with the presumptive stoichiometry of eq 5.3.[32] In contrast with the bleaching of PNC, oxidation of NADH depends highly on the light flux. Correspondingly, all kinetic data were collected recording spectra every 30 s at pH 8 and 10 keeping the degree of hydration fixed. The results of kinetic investigation of NADH oxidation are demonstrated in Figure 5.19. Careful inspection of the data reveals mechanistically important similarities with the data collected for PNC, although these occur at different pHs for the two substrates. The [NADH] and [**1a**] were varied in the ranges of (0.22–2.25)×10^{-4} and (0.50–5.53)×10^{-6} M, respectively. Note that for PNC a second order in [**1a**] and zero order in [substrate] were found at pH 8 (Figure 5.18A). In the case of NADH such a behavior is observed at pH 10 (Figure 5.19B). A mixed order in [**1a**] (eq 5.4) and a stronger dependence on [substrate] are observed at pH 10 for PNC (Figure 5.18B) and at pH 8 for NADH (Figure 5.19A). Most importantly, it should be noted

that, for both substrates, a finding of second order in [**1a**] is accompanied by zero order in [substrate], and a finding of mixed order in [**1a**] correlates with a measurable [substrate] dependency.

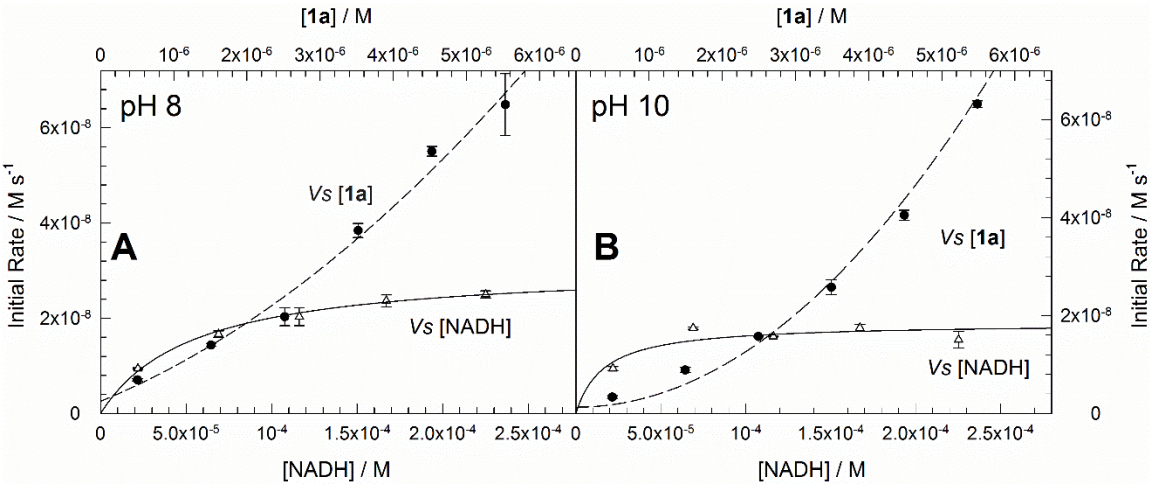

Figure 5.19 Initial rates of **1a**-catalyzed oxidation of NADH by O_2 as functions of concentrations of NADH (Δ) and **1a** (●) in reverse micelles of AOT in *n*-octane at pH 8 (A) and 10 (B), w_0 = 10. A: pH 8, [**1a**] = 2.52×10^{-6} M at variable NADH; [NADH] = 1.16×10^{-4} M at variable **1a**. B: pH 10, [**1a**] = 2.49×10^{-6} M at variable NADH; [NADH] = 1.16×10^{-4} M at variable **1a**. Time between recordings of successive spectra is 30 s. TAML dashed lines are calculated using k_A and k_B from Table 5.3. NADH solid lines are calculated using the following values of eq 5.7 (α/s^{-1}, $\beta/M\ s^{-1}$, and γ/M) equal, respectively, (2×10^{-5}; 2×10^{-8}; and 4×10^{-5}) at pH 8 and (~0; 2×10^{-8}; and 2×10^{-5}) at pH 10.

The effect of O_2 concentration on the initial rate of NADH oxidation was studied and the rate was found to have very low sensitivity to O_2 (Figure 5.20). NADH was chosen for the O_2 dependency study because it is more straightforward to work with dissolving easily upon shaking the reaction media—PNC with its tendency to aggregate requires sonication. Therefore, the reaction mechanism should account for this fact as well.

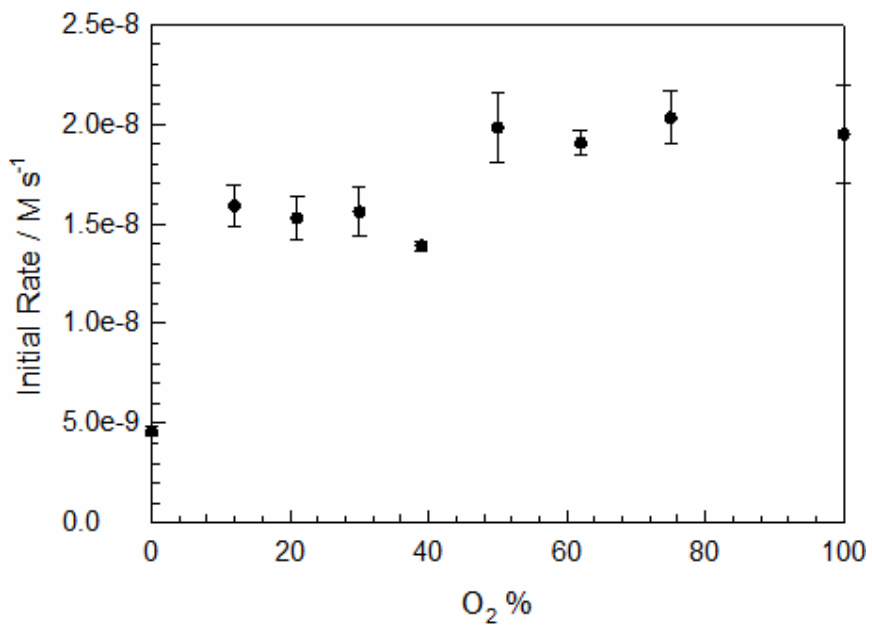

Figure 5.20 Rate dependence on O_2 concentration. Conditions: pH 10, $w_0 = 7$, [NADH] = 5.09×10^{-5} M, [**1a**] = 2.49×10^{-6} M. The gas mixture was purged for 15 min before addition of catalyst to initiate the reaction. Gas mixture was purged through the cuvette during the reaction.

5.2.3.3 Mechanism of PNC and NADH oxidation. Any proposed mechanism for the processes studied must be consistent with the following findings: (*i*) When the rate is second order in [**1a**], it is also zero order in [S] for both PNC and NADH. (*ii*) When the rate is mixed order in [**1a**], it is also non-zero order in [S] for both PNC and NADH. (*iii*) The reaction rate has very low sensitivity to the [O_2]. These three conditions are satisfied by the stoichiometric mechanism presented in Scheme 5.1, under the assumptions that (*a*) in the NADH case, S is its photoactivated form NADH*; (*b*) the reversible oxidation of the Fe^{III}-TAML occurs fast; (*c*) the concentration of the intermediate $[Fe^{III}Fe^{IV}]^{3-}$ is negligible compared to those of $[Fe^{III}OH_2]^-$ and $[Fe^{IV}O]^{2-}$, i.e. the mass balance equation appears as $Fe_t \approx [Fe^{III}OH_2]^- + [Fe^{IV}O]^{2-}$, where Fe_t is the total concentration of iron. At the μM catalyst concentrations employed for the study, none of the catalyst species are observable.

$$4\,[Fe^{III}OH_2]^- + O_2 + 4\,OH^- \rightleftharpoons 4\,[Fe^{IV}O]^{2-} + 2\,H_2O \qquad K_1$$

$$[Fe^{IV}O]^{2--} + [Fe^{III}OH_2]^- \rightleftharpoons [Fe^{III}Fe^{IV}]^{3-} \qquad k_2, k_{-2}$$

$$[Fe^{IV}O]^{2-} + S \rightarrow [Fe^{III}OH_2]^- + \text{Primary product(s) (PP)} \qquad k_3$$

$$[Fe^{III}Fe^{IV}]^{3-} + S \rightarrow 2\,[Fe^{III}OH_2]^- + PP \qquad k_4$$

$$PP + [Fe^{IV}O]^{2-} / [Fe^{III}Fe^{IV}]^{3-} \rightarrow\rightarrow \text{Final product/s} + [Fe^{III}OH_2]^- \qquad \textit{fast}$$

Scheme 5.1 Stoichiometric mechanism of **1a**-catalyzed oxidation of PNC and NADH (S) by O_2 in reverse micelles. For simplicity, complex **3a** is denoted as $[Fe^{III}Fe^{IV}]^{3-}$.

In Scheme 5.1, the first step is a rapidly established equilibrium obviously comprised of a series of elementary reactions. With the assumptions noted above and applying the steady-state approximation with respect to $[Fe^{III}Fe^{IV}]^{3-}$, one arrives at the two-term eq 5.5 for the catalyzed oxidations which includes first- and second-order terms in [**1a**].

$$-\frac{d[S]}{dt} = \frac{K_1^{0.25}k_3[O_2]^{0.25}[OH^-][S]}{1+K_1^{0.25}[O_2]^{0.25}[OH^-]}[\mathbf{1a}] + \frac{K_1^{0.25}k_2k_4[O_2]^{0.25}[OH^-][S]}{(1+K_1^{0.25}[O_2]^{0.25}[OH^-])^2(k_{-2}+k_4[S])}[\mathbf{1a}]^2 \qquad (5.5)$$

Consistent with the experimental observations, eq 5.5 predicts a very low dependence of the rate on the concentration of O_2. Equation 5.5 could be re-written in more compact forms as eq 5.6 by substituting $a = K_1^{0.25}[O_2]^{0.25}[OH^-]$ and $b = (1 + K_1^{0.25}[O_2]^{0.25}[OH^-])$ or eq 5.7, the latter to emphasize the rate dependence on the concentration of S.

$$-\frac{d[S]}{dt} = \frac{ak_3[S]}{b}[\mathbf{1a}] + \frac{ak_2k_4[S]}{b^2(k_{-2}+k_4[S])}[\mathbf{1a}]^2 \qquad (5.6)$$

$$-\frac{d[S]}{dt} = \alpha[S] + \frac{\beta[S]}{\gamma+[S]} \qquad (5.7)$$

Equation 5.6 accounts for the second order dependence in [**1a**] and the zero order dependence in [S] provided $k_{-2} << k_4[S]$ when the first order pathway in [**1a**] is negligible because, under such conditions, eq 5.6 collapses to eq 5.8.

$$-\frac{d[S]}{dt} = \frac{ak_2}{b^2}[\mathbf{1a}]^2 \quad (5.8)$$

Equation 5.8 holds for PNC and NADH at pH 8 and 10, respectively. When the reaction order in [**1a**] is mixed, the rate should display a dependence on [S] because according to eq 5.6, the first-order pathway in [**1a**] requires the first order dependence in [S]. This case is particularly evident in Figure 5.18B.

There is evidence that Fe^{III} reacts rapidly with O_2. In previous section it was shown that Fe^{III} reacts fast with O_2 in reverse micelles (Figures 5.2 and 5.3). The formation of all iron(IV) species at pH 8 and 10 (w_0 10) occurs in dozen of seconds, whereas less than 0.2% of NADH is oxidized under comparable conditions (Figure 5.21). It has been also demonstrated that after the rapid oxidation of iron in the absence of substrate, the iron(III) species still remain dominant in the reaction media. Note that the investigation into Fe^{IV}-containing species with various spectroscopies was carried out at very high catalyst concentrations (~1.5×10^{-4} M), which greatly favors the formation of dimers compared to the catalytic condition when the catalyst is at a much lower concentration (~2.5×10^{-6} M). This is consistent with an equilibrium as in K_1 in which $Fe_t \approx [Fe^{III}OH_2]^-$. This, however, does not alter the mechanistic conclusions because if $Fe_t \approx [Fe^{III}OH_2]$, because eq 5.6 still holds with $b \approx 1$.

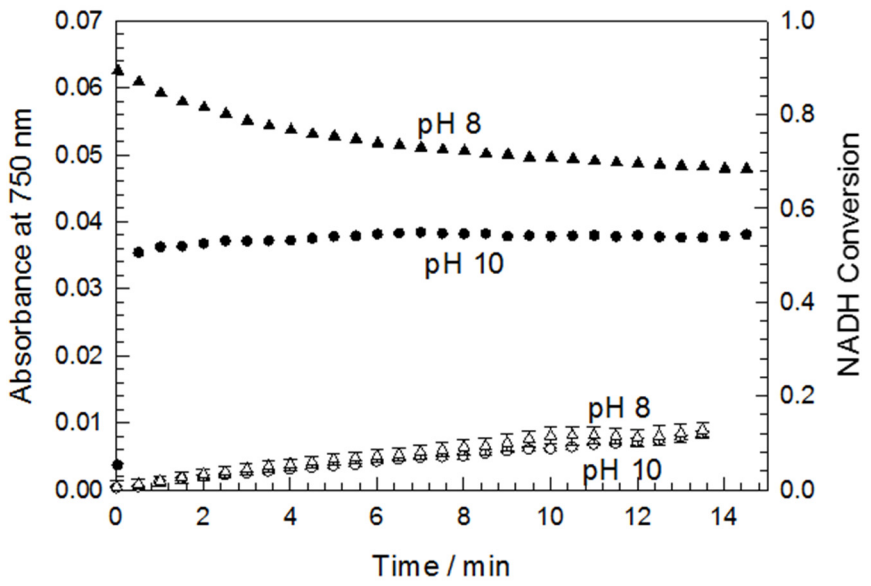

Figure 5.21 Comparison of time-scales for the formation of iron(IV) species (▲ and ●) and oxidation of NADH (Δ and ○) in reverse micelles at w_0 10. Conditions: formation of iron(IV) species: 0.1 M activated charcoal purified AOT[32] in *n*-octane, [**1a**] = 1.36×10^{-4} M. At pH 8, the reaction is too fast to obtain a zero-point datum. NADH oxidation: 0.1 M AOT, [**1a**] = 2.5×10^{-6} M, [NADH] = 1.16×10^{-4} M.

The swopping of the behavior observed by comparison of Figure 5.18 and Figure 5.19 is unusual, i.e. the k_B pathway dominates at different pH for PNC and NADH. In other words, there are no matching contributions of k_A and k_B pathways to overall rates. PNC and NADH differ structurally; different are charges, acid-base properties, etc. The dependencies of rates of **1a**-catalyzed oxidations of PNC and NADH by H_2O_2 on their concentrations in water is distinctly different.[65,66] Therefore, k_A and k_B pathways (eq 5.4) may contribute diversely to overall rates for these substrates at different pH. Both terms of eq 5.6 are complex. Parameters K_1, k_2, k_{-2}, k_3 and k_4 contribute to the rate. Both terms depend in a different way on S concentration. It is thus quite possible that pH changes of all kinetic parameters may substantially alter the contributions of the k_A and k_B terms to the overall

rate. It is more important that the second order in **1a**, which is accompanied by the zero order in S, was found for both PNC and NADH proving the participation of the dimeric species.

It is interesting to consider the partial contributions, $P(k_A)$ and $P(k_B)$, of the first- and second-order pathways in the oxidations of PNC and NADH as a function of [**1a**] when the mixed order in [**1a**] is in operation, i.e. at pH 10 and 8 for PNC and NADH, respectively. It is convenient to define $P(k_A)$ and $P(k_B)$ relying on eq 5.4 as follows:

$$P(k_A) = \frac{k_A[\mathbf{1a}]}{k_A[\mathbf{1a}] + k_B[\mathbf{1a}]^2} \tag{5.9}$$

and

$$P(k_B) = \frac{k_B[\mathbf{1a}]^2}{k_A[\mathbf{1a}] + k_B[\mathbf{1a}]^2} \tag{5.10}$$

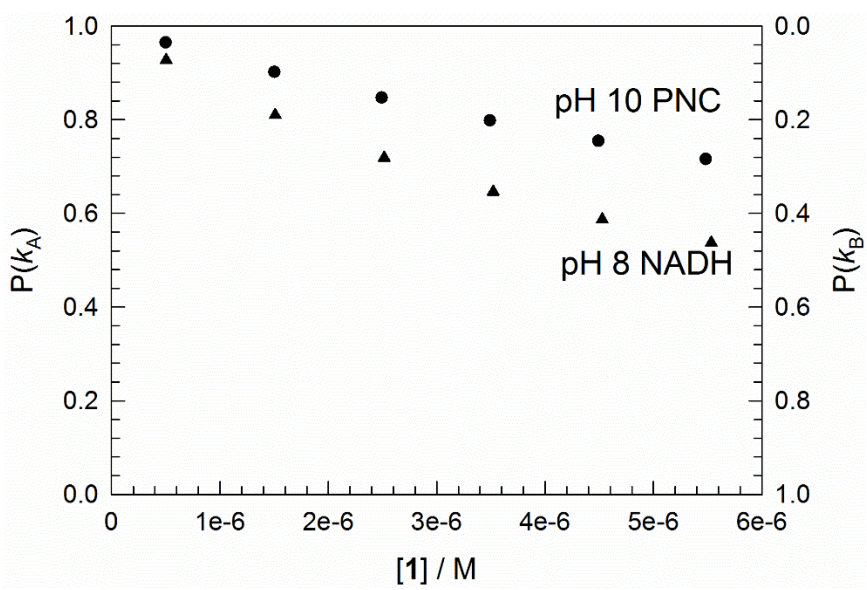

Figure 5.22 Calculated values of $P(k_A)$ and $P(k_B)$ as a function of concentration of **1a** at pH 8 ([NADH] = 1.16×10^{-4} M) and 10 ([PNC] = 1.43×10^{-5} M) at w_0 = 10 (see text for details).

Calculated values of $P(k_A)$ and $P(k_B)$ as a function of [**1a**] are demonstrated in Figure 5.22. As could be anticipated, contributions from the second-order pathways, $P(k_B)$, increase with increased total concentration of **1a**, reaching nearly 50% in the NADH oxidation at pH 8 and ca. 30% in the degradation of PNC at pH 10. Note that $P(k_B)$ becomes absolutely dominant for both PNC and NADH on reverting the pHs to 8 and 10, respectively.

To summarize, this kinetic study has provided solid evidence for the participation of dimeric oxidized iron species in the oxidation by dioxygen of reactive electron donors exemplified by the Pinacyanol chloride dye and the NADH cofactor in reverse micelles of AOT in *n*-octane. Deep kinetic analysis leads to the conclusion that the reactive intermediate is the mixed-valent $[Fe^{III}Fe^{IV}]^{3-}$ dimer **3a**, the contribution of which to the overall reactivity depends upon the nature of the substrate and the pH. Under certain conditions, dimer **3a** is the only reactive species with clean second order kinetics in the catalyst. Dimer **3a** ($[Fe^{III}Fe^{IV}]^{3-}$) contains less oxidized iron compared to monomeric[28] $[Fe^{IV}O]^{2-}$ or dimeric[10] $[Fe^{IV}Fe^{IV}]^{2-}$ and particularly compared to the monomeric iron(V) species $[Fe^{V}O]^{-}$.[29] This explains why just reactive reducing agents such as NADH and PNC undergo catalytic oxidations by O_2 in the reverse micelles.

5.3 Conclusion

By catalyzing the oxidation of NADH to NAD^+ by O_2 in AOT reverse micelles with a TON of 88, peroxidase-mimicking TAML activators have been shown to be capable of oxidase-mimicry under appropriately engineered conditions. The oxygen oxidations are less aggressive than hydrogen peroxide oxidations. Nevertheless oxygen is special, making the findings important and suggesting that more research should be carried out to explore

whether or not TAML activators can function effectively using affordable molecular oxygen in a wide range of oxidation processes.

The lower reactivity of **1a** in these reverse micelles may have advantages. Typically, TAML activators in basic water catalyze multi-step, deep oxidation of organic substrates by H_2O_2[12] fragmenting and nearly mineralizing persistent pollutants including polychlorophenols,[67] organophosphorus pesticides[68] and many others.[12] Here, the mild process for NADH, even with light induction, is reminiscent of cellular processes where the NAD^+ is available for catalytic cycling. Thus, the activity achieved may be of use for transformations of fragile molecules by O_2 that avoids destructive deep oxidation.

5.4 Experimental

5.4.1 Materials

All reagents, components of buffer solutions, and solvents were at least ACS reagent grade (Aldrich, Fisher, Acros, Fluka) and were used as received. TAML activators **1a**,**b** were obtained from GreenOx Catalysts, Inc. *n*-Octane was used as received (99 %+, extra pure, Acros) or additionally distilled (99 %+, extra dry, Acros). Stock solutions of **1a** (0.001 and 0.027 M) and **1b** (0.001 M) were prepared in the 0.01 M buffered aqueous solutions using phosphate for pH 8 and 12 but carbonate for pH 10; all were stored in a fridge. Hydroquinone (1 mg, Acros, 99.5%) recrystallized from acetone was dissolved in a mixture of 0.1 M AOT in *n*-octane (15.3 mL) and 48 μL 0.01 M phosphate (pH 8 or 12) or carbonate (pH 10) buffer. This allowed to prepare the 6×10^{-4} M solution of HQ in the dry reverse micelles. The solutions with larger w_0 were made by adding aqueous buffer to the stock solution. Stock solutions of H_2O_2 were prepared from 30% H_2O_2 and the concentration was

determined by measuring the absorption at 230 nm (ε = 72.4 M^{-1} cm^{-1}).[69] AOT (Aerosol OT, BioXtra 99%+, Aldrich) was either used as received or additionally purified by activated charcoal and dried in a vacuum oven for 40 h as recommended elsewhere.[70] Solutions of AOT in *n*-octane (0.1 M) were shown to be peroxide-free using the peroxide test strips (0.5–25 ppm, EM Quant).[45] The AOT solutions were also treated with aqueous KI[45] and no color change due to I_2 was observed. Negative peroxide tests were obtained for AOT before and after the purification. Reverse micelles of various w_0 were prepared by adding a corresponding amount of the aqueous buffer of known pH to 0.1 M AOT in *n*-octane. For example, the sample with w_0 7 and pH 8 was prepared by adding the buffer (25 µL, pH 8) to 1975 µL 0.1 M AOT followed by vigorous shaking. Concentrations of all components reported throughout refer to the entire volume of the solution including *n*-octane, AOT and buffer components.

NADH and NAD^+ were purchased from Sigma-Aldrich or MP Biomedicals and used as received. Their stock solutions were prepared daily using HPLC grade water. The extinction coefficients (ε) of NADH in reverse micelles were measured after adding 0.1 M AOT in *n*-octane to 2 mg NADH dissolved in 60 µL pure water in a 5 mL volumetric flask. The ε_{340} values of 4760, 4980, 5070, 5130, and 5200 (all ± 20) M^{-1} cm^{-1} at w_0 3, 7, 10, 15, and 25, respectively, were used in kinetic measurements. Pinacyanol chloride (Aldrich) was used without further purification. Orange II (Sigma-Aldrich) was recrystallized from 1:3 H_2O:EtOH. Safranin O (Acros) was used as received. Alcohol dehydrogenase from *Saccharomyce cerevisiae* was a Sigma-Aldrich preparation.

5.4.2 Methods

UV-vis measurements were performed at 25 °C in capped quartz cuvettes (1.0 cm) using either a photodiode array Agilent 8453 UV-vis spectrometer equipped with an automatic thermostatted 8-cell positioner or a double beam Shimadzu UV 1800 instrument having the thermostatted 6-cell positioner. HPLC measurements were carried out[43] using a Shimadzu Prominence 2D HPLC instrument equipped with LC-20AB binary pump (method 1) or LC-20AD quaternary pump (method 2), SIL-20A autosampler and SPD-M20A photodiode array detector (see below).

EPR Measurements. Solutions of **1a** (0.15 mM) in the reverse micelles were transferred into EPR tubes and frozen by liquid nitrogen. X-band (9.66 GHz) EPR spectra were recorded on either a Bruker ESP 300 equipped with an Oxford ESR-910 liquid helium cryostat. All experimental data were collected under nonsaturating microwave conditions. The quantification of signals was relative to a CuEDTA spin standard. The microwave frequency and the magnetic field were calibrated with a frequency counter and an NMR gaussmeter, respectively. The temperature was calibrated with resistors (CGR-1-1000) from LakeShore. A modulation frequency of 100 kHz and modulation amplitude of 1 mT was used for all spectra. Data analysis, spin quantification, and simulations of the EPR were performed with the software SpinCount written by Prof. MPH.

NADH and NAD^+ analysis by HPLC. The 250×4.6 mm Agilent Microsorb-MV 100 C18 column was used for NADH and NAD^+ analysis.

Method 1. Two eluents were employed which is a simplified method of method 2. Eluent A was a 0.05 M potassium phosphate buffer, pH 6.0; eluent B was a mixture v/v of 60% A and 40% MeOH. The temperature was maintained at 40 °C across the column. The

gradients used as described elsewhere[43] are shown in Table 5.4. The flow rate was constant 1.0 mL/min.

Table 5.4 HPLC Method 1 eluent gradient for the analysis of NADH and NAD^+.

Time (min)*	% Eluent A**	% Eluent B***
0.0	100	0
4.0	100	0
5.0	98.5	1.5
10.0	96.5	3.5
15.0	96.5	3.5
15.1	75	25
30.0	75	25
32.0	100	0
35.0	100	0

*The flow rate was constant 1.0 mL/min.
**Eluent A is 0.05 M phosphate buffer, pH 6.0.
***Eluent B is 60:40 v/v A: MeOH.

Method 2. The HPLC utilized four eluents. Eluent A was a 0.05 M potassium phosphate buffer, pH 6.0; eluent B was a mixture v/v of 60% A and 40% MeOH; eluent C was 100% MeOH; eluent D was HPLC grade water. The temperature was maintained at 40 ℃ across the column. The gradient used is shown in Table 5.5. The flow rate was constant 1.0 mL/min.

The extraction of products from the reverse micelles was initiated by addition of 2 mL water to 2 mL reaction mixtures. After vigorous shaking, the emulsion was centrifuged at 8000 rpm for 10 min using an Eppendorf minispin centrifuge. The aqueous bottom phase was removed by a glass pipet and analyzed.

Table 5.5 HPLC Method 2 eluent gradient for the analysis of NADH and NAD^+.

Time (min)*	% Eluent A**	% Eluent B***	% Eluent C****	% Water
0.0	100	0	0	0
9.0	100	0	0	0
10.0	98.5	1.5	0	0
15.0	96.5	3.5	0	0
20.0	96.5	3.5	0	0
20.1	75	25	0	0
28.0	75	25	0	0
29.0	0	0	100	0
40.0	0	0	100	0
45.0	0	0	0	100
50.0	100	0	0	0
55.0	100	0	0	0

*The flow rate was constant 1.0 mL/min.
**Eluent A is 0.05 M phosphate buffer, pH 6.0.
***Eluent B is 60:40 v/v A: MeOH.
****Eluent C is 100% MeOH.

The extinction coefficients of NADH (340 nm) and PNC (560 nm) used for rate calculations in the mechanistic study were measured under different conditions and are summarized in Table 5.6. All measurements were carried out in ambient air, i.e. at atmospheric concentration of dioxygen.

Table 5.6 Extinction coefficients ε (M^{-1} cm^{-1}) of NADH at 340 nm and PNC at 560 nm used for reaction rate calculations presented in Figure 5.18 and Figure 5.19.

pH	NADH	PNC
8	$(5.68 \pm 0.03)\times10^3$	$(5.78\pm0.06)\times10^4$
10	$(5.70\pm0.05)\times10^3$	$(3.46\pm0.07)\times10^4$

NADH oxidation was used for probing the effect of O_2 on the initial rate of NADH oxidation at w_0 = 7. The experiments were performed using *n*-octane solutions saturated with ambient air, where the gas composition was changed by purging with mixtures of different ratios of Ar and O_2. The gas mixture was purged for 15 min before addition of **1a** via syringe. The purging continued during the reaction. The reaction mixture was stirred by a magnetic bar.

5.4.3 Procedures

For the reaction of **2a** with NADH in the absence of oxygen, the "freeze-pump-thaw" method was applied. A mixture of unpurified AOT in *n*-octane (19.75 mL, 0.1 M), NADH in water (100 μL, 0.04 M) and pH 12 buffer (150 μL, w_0 7) in a 50 mL Schlenk flask was degassed three times (solution A). Solution A (1.5 mL) was added to a capped quartz cuvette containing 1.5 mL methanol and shaken fiercely. Two transparent layers formed after standing and the UV-vis spectrum of the lower layer (methanol) was measured. The methanol layer was further used for HPLC measurement (1 mL water was added to 1 mL methanol solution to prepare the HPLC sample). Compound **2a** (6.37 mg, 4×10^{-6} mol) in a 5 mL two-necked round bottom flask was degassed and degassed acetonitrile (500 μL) was added. The solution of **2a** (231 μL) was added to solution A and stirred for 20 min. The color of the mixture turned from light brown to light yellow and 1.5 mL was added to methanol (1.5 mL) for UV-vis measurements. Methanol was used because **2a** turns back to **1a** within 1 min in this solvent.[10] For the experiment with **1a**, similar procedure was used. Unpurified AOT in *n*-octane (9.875 mL 0.1 M), NADH in water (50 μL 0.04 M), pH 12 buffer (25 μL) and acetonitrile (125 μL) in a 25 mL Schlenk flask were degassed three

times (solution B). Compound **1a** (9.3 mg, 2×10^{-5} mol) dissolved in pH 12 buffer (500 μL) was degassed. Compound **1a** (50 μL) was then added to solution B (w_0 7).

5.5 References

(1) Chahbane, N.; Popescu, D.-L.; Mitchell, D. A.; Chanda, A.; Lenoir, D.; Ryabov, A. D.; Schramm, K.-W.; Collins, T. J. *Green Chem.* **2007**, *9*, 49.

(2) Ghosh, A.; Mitchell, D. A.; Chanda, A.; Ryabov, A. D.; Popescu, D. L.; Upham, E.; Collins, G. J.; Collins, T. J. *J. Am. Chem. Soc.* **2008**, *130*, 15116.

(3) Popescu, D.-L.; Chanda, A.; Stadler, M. J.; Mondal, S.; Tehranchi, J.; Ryabov, A. D.; Collins, T. J. *J. Am. Chem. Soc.* **2008**, *130*, 12260.

(4) Ellis, W. C.; Tran, C. T.; Denardo, M. A.; Fischer, A.; Ryabov, A. D.; Collins, T. J. *J. Am. Chem. Soc.* **2009**, *131*, 18052.

(5) Ellis, W. C.; Tran, C. T.; Roy, R.; Rusten, M.; Fischer, A.; Ryabov, A. D.; Blumberg, B.; Collins, T. J. *J. Am. Chem. Soc.* **2010**, *132*, 9774.

(6) Jones, C. W. *Applications of hydrogen peroxide and derivatives*; The Royal Society of Chemistry: Cambridge, 1999.

(7) Stahl, S. S.; Lippard, S. J.; Wiley-VCH Verlag GmbH: 1999, p 303.

(8) Bakač, A. *Inorg. Chem.* **2010**, *49*, 3584.

(9) Campbell, A. N.; Stahl, S. S. *Acc. Chem. Res.* **2012**, *45*, 851.

(10) Ghosh, A.; Tiago de Oliveria, F.; Toshihiro Yano, T.; Nishioka, T.; Beach, E. S.; Kinoshita, I.; Münck, E.; Ryabov, A. D.; Horwits, C. P.; Collins, T. J. *J. Am. Chem. Soc.* **2005**, *127*, 2505.

(11) Collins, T. J.; Khetan, S. K.; Ryabov, A. D. In *Handbook of Green Chemistry*; Anastas, P. T., Crabtree, R. H., Eds.; WILEY-VCH Verlag GmbH & KgaA: Weinheim, 2009, p 39.

(12) Ryabov, A. D. *Adv. Inorg. Chem.* **2013**, *65*, 118.

(13) Kundu, S.; Van Kirk Thompson, J.; Ryabov, A. D.; Collins, T. J. *J. Am. Chem. Soc.* **2011**, *133*, 18546.

(14) Kundu, S.; Van Kirk Thompson, J.; Shen, L. Q.; Mills, M. R.; Bominaar, E. L.; Ryabov, A. D.; Collins, T. J. *Chem. Eur. J.* **2015**, *21*, 1803.

(15) Ghosh, M.; Singh, K. K.; Panda, C.; Weitz, A.; Hendrich, M. P.; Collins, T. J.; Dhar, B. B.; Sen Gupta, S. *J. Am. Chem. Soc.* **2014**, *136*, 9524.

(16) Panda, C.; Debgupta, J.; Diaz Diaz, D.; Singh, K. K.; Sen Gupta, S.; Dhar, B. B. *J. Am. Chem. Soc.* **2014**, *136*, 12273.

(17) Kwon, E.; Cho, K.-B.; Hong, S.; Nam, W. *Chem. Commun.* **2014**, *50*, 5572.

(18) Ghosh, A.; Ryabov, A. D.; Mayer, S. M.; Horner, D. C.; Prasuhn, D. E., Jr.; Sen Gupta, S.; Vuocolo, L.; Culver, C.; Hendrich, M. P.; Rickard, C. E. F.; Norman, R. E.; Horwitz, C. P.; Collins, T. J. *J. Am. Chem. Soc.* **2003**, *125*, 12378.

(19) Fendler, J. H. *Acc. Chem. Res.* **1976**, *9*, 153.

(20) Pileni, M. P. *J. Phys. Chem.* **1993**, *97*, 6961.

(21) *Enzymes in reverse micelles (microemulsions): theory and practice*; Levashov, A. V.; Klyachko, N. L., Eds.; Marcel Dekker Inc., 2003.

(22) De, T. K.; Maitra, A. *Adv. Colloid Interface Sci.* **1995**, *59*, 95.

(23) Biasutti, M. A.; Abuin, E. B.; Silber, J. J.; Correa, N. M.; Lissi, E. A. *Adv. Colloid Interface Sci.* **2008**, *136*, 1.

(24) Stadler, M. J. PhD Thesis, Carnegie Mellon University, 2007.

(25) Banerjee, D.; Apollo, F. M.; Ryabov, A. D.; Collins, T. J. *Chem. Eur. J.* **2009**, *15*, 10199.

(26) Battino, R.; Johnson, S. A.; Clever, H. L.; Thomsen, E. S.; Cramer, A. L.; Long, P. L.; Derrick, M. E. *Solubility Data Ser.* **1981**, *7*, 214.

(27) Gunderson, W. A. PhD Thesis, Carnegie Mellon University, 2009.

(28) Chanda, A.; Shan, X.; Chakrabarti, M.; Ellis, W.; Popescu, D.; Tiago de Oliveria, F.; Wang, D.; Que, L., Jr.; Collins, T. J.; Münck, E.; Bominaar, E. L. *Inorg. Chem.* **2008**, *47*, 3669.

(29) Tiago de Oliveira, F.; Chanda, A.; Banerjee, D.; Shan, X.; Mondal, S.; Que, L., Jr.; Bominaar, E. L.; Münck, E.; Collins, T. J. *Science* **2007**, *315*, 835.

(30) Mills, M. R.; Burton, A. E.; Mori, D. I.; Ryabov, A. D.; Collins, T. J. *J. Coord. Chem.* **2015**, *68*, 3046.

(31) Hong, S.; Sutherlin, K. D.; Park, J.; Kwon, E.; Siegler, M. A.; Solomon, E. I.; Nam, W. *Nat. Commun.* **2014**, *5*.

(32) Tang, L. L.; Gunderson, W. A.; Weitz, A. C.; Hendrich, M. P.; Ryabov, A. D.; Collins, T. J. *J. Am. Chem. Soc.* **2015**, *137*, 9704.

(33) Abuin, E. B.; Biasutti, M. A.; Silber, J. J.; Correa, N. M.; Lissi, E. A. *Adv. Colloid Interface Sci.* **2008**, *136*, 1.

(34) Grandi, C.; Smith, R. E.; Luisi, P. L. *J. Biol. Chem.* **1981**, *256*, 837.

(35) Shield, J. W.; Ferguson, H. D.; Bommarius, A. S.; Hatton, T. A. *Ind. Eng. Chem. Fund.* **1986**, *25*, 603.

(36) Pollak, N.; Dolle, C.; Ziegler, M. *Biochem. J.* **2007**, *402*, 205.

(37) Gamenara, D.; Seoane, G.; Saenz-Méndez, P.; Domínguez de María, P. *Redox Biocatalysis: Fundamentals and Applications*; Wiley: Hoboken, New Jersy, 2013.

(38) Uppada, V.; Bhaduri, S.; Noronha, S. B. *Curr. Sci.* **2014**, *106*, 946.

(39) Weckbecker, A.; Groger, H.; Hummel, W. *Biosystems Engineering I: Creating Superior Biocatalysts* **2010**, *120*, 195.

(40) Wichmann, R.; Vasic-Racki, D. *Biosystems Engineering I: Creating Superior Biocatalysts* **2005**, *92*, 225.

(41) Golub, E.; Freeman, R.; Willner, I. *Angew. Chem. Int. Ed.* **2011**, *50*, 11710.

(42) Miller, J. A.; Alexander, L.; Mori, D. I.; Ryabov, A. D.; Collins, T. J. *New J. Chem.* **2013**.

(43) Markham, K. A.; Kohen, A. *Curr. Anal. Chem.* **2006**, *2*, 379.

(44) Scheeline, A.; Olson, D. L.; Williksen, E. P.; Horras, G. A.; Klein, M. L.; Larter, R. *Chem. Rev.* **1997**, *97*, 739.

(45) Carroll, W. F. J.; Foster, B. L.; Barkley, W. E.; Cook, S. H.; Fivizzani, K. P.; Izzo, R.; Jacobson, K. A.; Maupins, K.; Moloy, K.; Ogle, R. B.; Palassis, J.; Phifer, R. W.; Reinhardt, P. A.; Thompson, L. T.; Winfield, L. *Prudent Practices in the Laboratory*; The National Academies Press: Washington, D. C., United States, 2011.

(46) Berezin, I. V.; Martinek, K.; Yatsimirskii, A. K. *Usp. Khim.* **1973**, *42*, 1729.

(47) Fabian, I.; Lente, G. *Pure Appl. Chem.* **2010**, *82*, 1957.

(48) Byers, G. W.; Gross, S.; Henrichs, P. M. *Photochem. Photobiol.* **1976**, *23*, 37.

(49) Horwitz, C. P.; Fooksman, D. R.; Vuocolo, L. D.; Gordon-Wylie, S. W.; Cox, N. J.; Collins, T. J. *J. Am. Chem. Soc.* **1998**, *120*, 4867.

(50) Khouri, S. J.; Buss, V. *J. Solution Chem.* **2010**, *39*, 121.

(51) Ryabov, A. D.; Collins, T. J. *Adv. Inorg. Chem.* **2009**, *61*, 471.

(52) Mitchell, D. A.; Ryabov, A. D.; Kundu, S.; Chanda, A.; Collins, T. J. *J. Coord. Chem.* **2010**, *63*, 2605.

(53) Li, Y. B.; Trush, M. A. *Arch. Biochem. Biophys.* **1993**, *300*, 346.

(54) James, T. H.; Snell, J. M.; Weissberger, A. *J. Am. Chem. Soc.* **1938**, *60*, 2084.

(55) Chanda, A.; Ryabov, A. D.; Mondal, S.; Alexandrova, L.; Ghosh, A.; Hangun-Balkir, Y.; Horwitz, C. P.; Collins, T. J. *Chem. Eur. J.* **2006**, *12*, 9336.

(56) Theodoridis, A.; Maigut, J.; Puchta, R.; Kudrik, E. V.; Van Eldik, R. *Inorg. Chem.* **2008**, *47*, 2994.

(57) Ember, E.; Rothbart, S.; Puchta, R.; van Eldik, R. *New J. Chem.* **2009**, *33*, 34.

(58) Rothbart, S.; Ember, E. E.; van Eldik, R. *New J. Chem.* **2012**, *36*, 732.

(59) DeNardo, M. A.; Mills, M. R.; Ryabov, A. D.; Collins, T. J. *J. Am. Chem. Soc.* **2016**, *138*, 2933.

(60) Maid, H.; Boehm, P.; Huber, S. M.; Bauer, W.; Hummel, W.; Jux, N.; Groeger, H. *Angew. Chem., Int. Ed.* **2011**, *50*, 2397.

(61) Banerjee, D. PhD Thesis, Carnegie Mellon University, 2008.

(62) Tang, L. L.; Ryabov, A. D.; Collins, T. J. *ACS Catal.* **2016**, *6*, 3713.

(63) Banerjee, D.; Ryabov, A. D.; Collins, T. J. *J. Coord. Chem.* **2015**, *68*, 3032.

(64) Manna, K.; Panda, A. K. *Spectrochim. Acta Mol. Biomol. Spectrosc.* **2009**, *74*, 1268.

(65) Miller, J. A.; Alexander, L.; Mori, D. I.; Ryabov, A. D.; Collins, T. J. *New J. Chem.* **2013**, *37*, 3488.

(66) Mitchell, D. A.; Ryabov, A. D.; Kundu, S.; Chanda, A.; Collins, T. J. *J. Coord. Chem.* **2010**, *63*, 2605.

(67) Sen Gupta, S.; Stadler, M.; Noser, C. A.; Ghosh, A.; Steinhoff, B.; Lenoir, D.; Horwitz, C. P.; Schramm, K.-W.; Collins, T. J. *Science* **2002**, *296*, 326.

(68) Chanda, A.; Khetan, S. K.; Banerjee, D.; Ghosh, A.; Collins, T. J. *J. Am. Chem. Soc.* **2006**, *128*, 12058.

(69) George, P. *Biochem. J.* **1953**, *54*, 267.

(70) Menger, F. M.; Yamada, K. *J. Am. Chem. Soc.* **1979**, *101*, 6731.

Chapter 6

Appendices and Future Prospective

6.1 Assessment of bromate formation on TAML/H_2O_2 treatment of aqueous bromide solutions

The formation of carcinogenic bromate from bromide in ozone water treatment is one of the most significant health and environmental safety disadvantages of ozone processes. Consequently, it is important to understand if TAML processes are free from or also suffer from this negative. In this preliminary study, mixtures of bromide with TAML/H_2O_2 were analyzed by ion chromatography (IC) to examine if bromate will form during TAML/H_2O_2 treatment of aqueous solutions containing bromide. Here, DI water was used to minimize the interference from the chloride ion IC peak. TAML catalysts **1a** and **1b** (Chart 6.1) with H_2O_2 were both tested and a control experiment in the presence of H_2O_2 alone was performed. Both H_2O_2 and the catalyst were added to the bromide solution, and the reaction solution was incubated for 20 h. The solution was then subjected to analysis by IC. The chromatograph of the **1a**/H_2O_2 reaction mixture showed a barely detectable peak at ~6.5 min (the region where bromate elutes) with a peak area approaching the detection limit. Chromatographs of the **1b**/H_2O_2 and H_2O_2 control reaction solutions show a prominent peak at 5.1 min which overlaps the bromate peak region rendering bromate detection by IC impossible. This huge peak is attributed to H_2O_2. Consequently, an additional aliquot of **1a** was added. After incubation for 24 h, this additional aliquot removed the residual H_2O_2 eliminating the interfering peak. The IC spectra of the reaction solutions subjected to this two-step treatment were similar to that of the single **1a** treatment, showing a peak that was too small to quantify with confidence. In all cases, the amount of bromate that might have been formed is very small (<10 μg/L). The concentrations of bromide remaining in the solutions after the reaction were quantified (before additional **1a** for the **1b** and control

experiments) and the calculated bromide concentrations are listed in Table 6.1. However, the changes in bromide concentration are too small to be interpreted with confidence. Therefore, future work should focus on the use of a more accurate method/instrument (for example, method 326.0 with post-column reaction[1]) than that used herein to quantify the amount of bromate formed by TAML catalysis in the absence of readily oxidizable substrates. However, as was discussed in Chapter 1, the mechanism of bromate formation by both molecular ozone and •OH proceeds via formation of HOBr/OBr^- or Br•.[2,3] Since H_2O_2 effectively returns HOBr/OBr^- to bromide and no radical is involved in TAML catalysis in the absence of readily oxidized substrates,[4,5] TAML/H_2O_2 treatment is not expected to generate large quantities of bromate.

A pH 7/8 solution (0.01 M phosphate) was also tested using the above method. Unfortunately, the detection limit for bromate was higher in the presence of 0.01 M phosphate and the IC method used was not capable of detecting bromate at concentrations < 10 μg/L.

Chart 6.1 Structures of TAML catalysts used in this study (**1a** and **1b**).

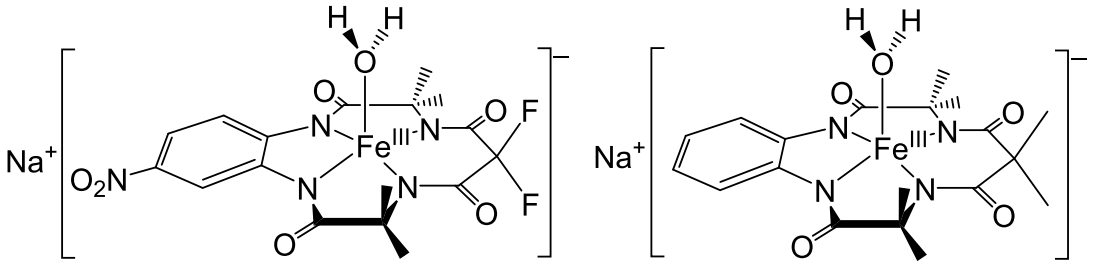

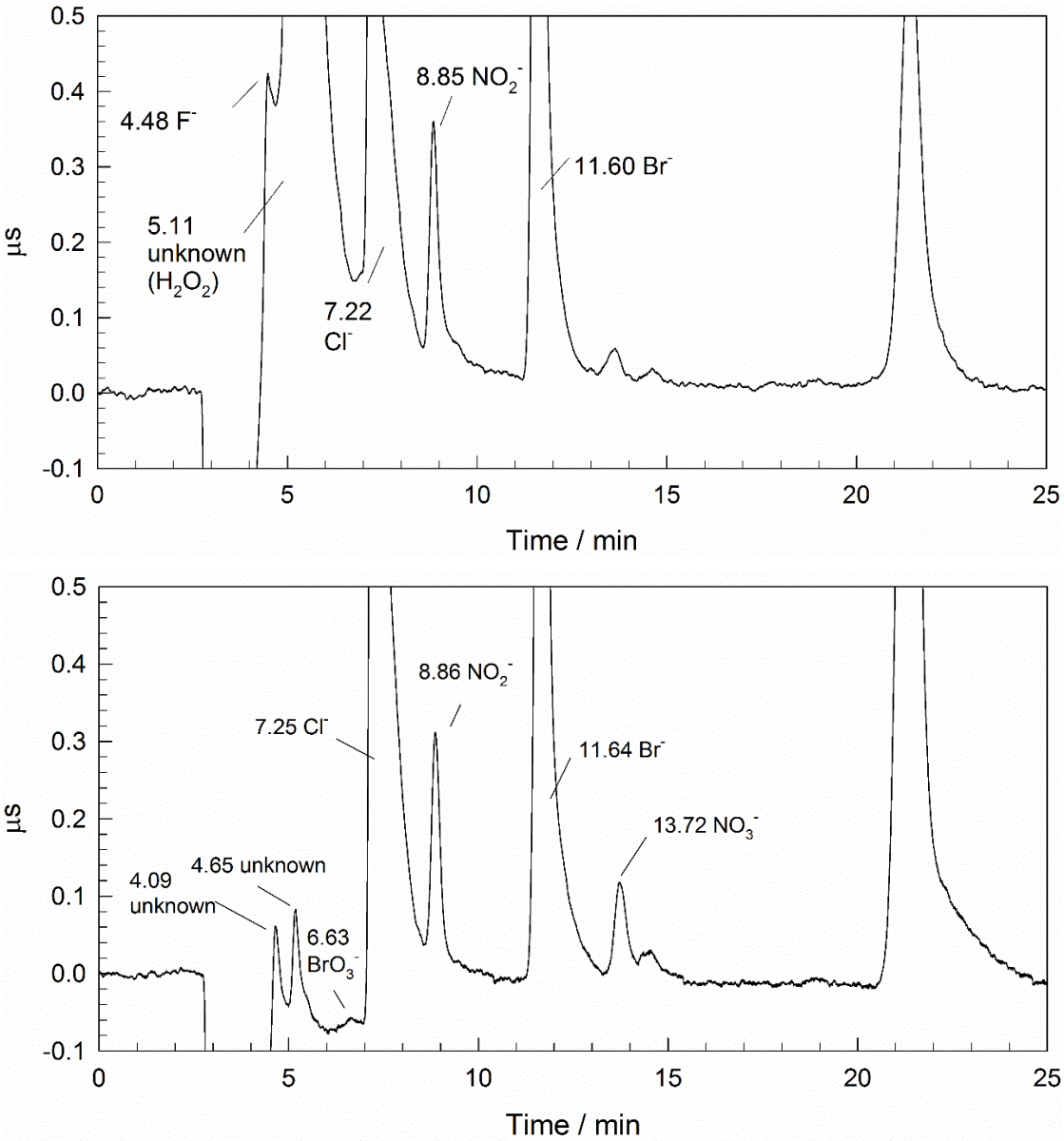

Figure 6.1 IC analysis of reaction between bromide and hydrogen peroxide. Upper: bromide reacted with hydrogen peroxide. Lower: catalyst **1a** was added to the reaction mixture (after 1 day) and allowed to stay overnight to remove the peroxide peak. Conditions: $[H_2O_2] = 4.06 \times 10^{-3}$ M (138 mg/L), $[Br^-] = 1.115$ mg/L, the mixture were allowed to stand overnight (> 20 h). **1a** was added after the analysis to remove hydrogen peroxide peak, [**1a**] = 4.73×10^{-7} M (246 µg/L). Numbers indicate elution time.

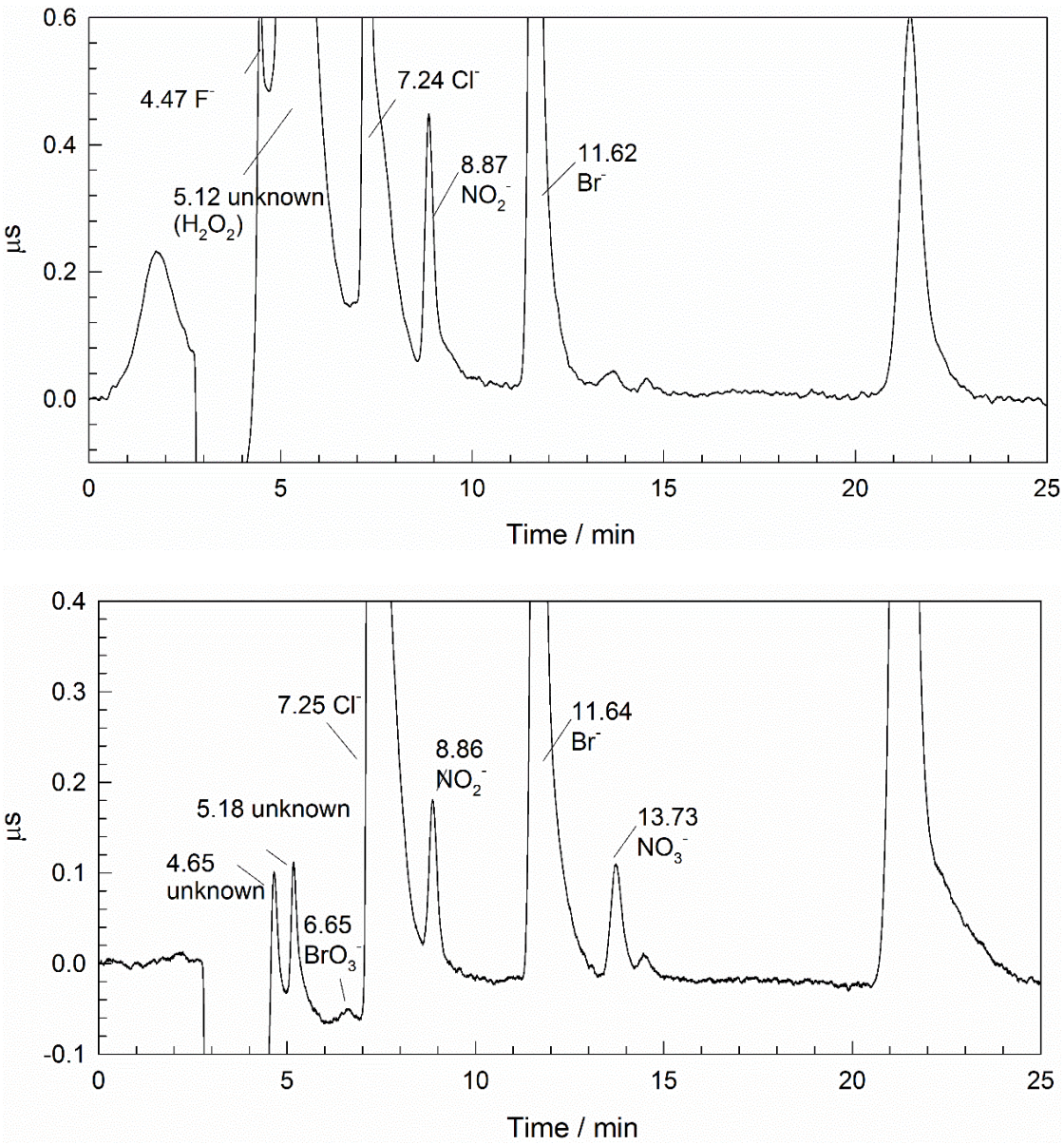

Figure 6.2 IC analysis of reaction between bromide and hydrogen peroxide catalyzed by **1b**. Upper: bromide reacted with hydrogen peroxide at the presence of **1b**. Lower: catalyst **1a** was added to the reaction mixture (after 1 day) and allowed to stay overnight to remove the peroxide peak. Conditions: $[H_2O_2] = 4.06 \times 10^{-3}$ M (138 mg/L), $[Br^-] = 1.115$ mg/L, [**1b**] $= 4.80 \times 10^{-7}$ M (224 μg/L). The mixture were allowed to stand overnight (> 20 h). **1a** was added after the analysis to remove hydrogen peroxide peak, [**1a**] $= 4.73 \times 10^{-7}$ M (246 μg/L). Numbers indicate elution time.

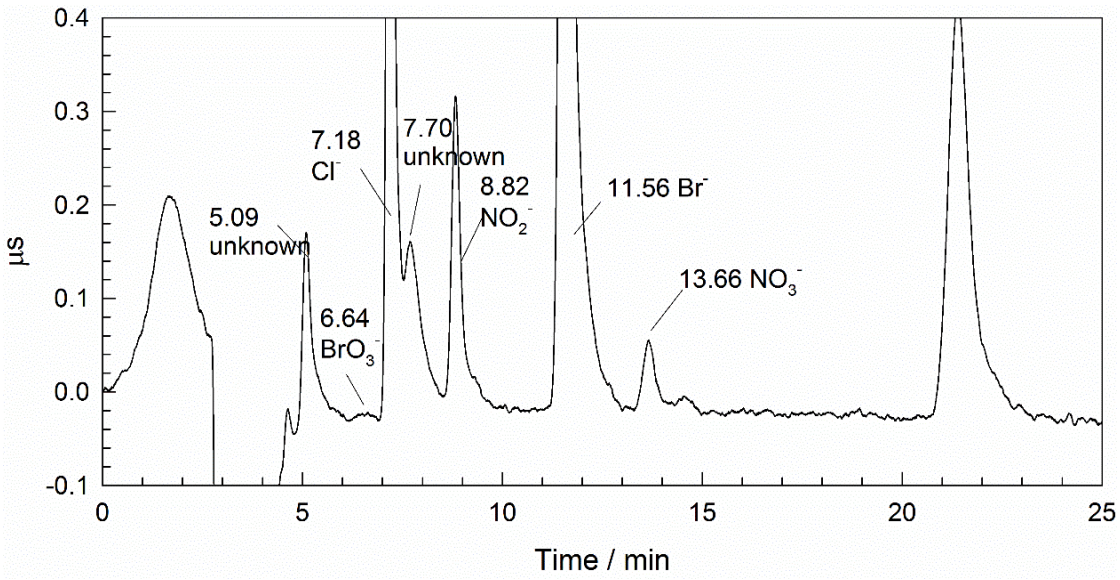

Figure 6.3 IC analysis of reaction between bromide and hydrogen peroxide catalyzed by **1a**. Conditions: $[H_2O_2] = 4.06 \times 10^{-3}$ M (138 mg/L), $[Br^-] = 1.115$ mg/L, [**1a**] $= 4.73 \times 10^{-7}$ M (246 µg/L). The mixture were allowed to stand overnight (> 20 h) and injected for IC analysis.

Table 6.1 Concentrations of bromide (mg/L) detected in solution after treatment with TAML/H_2O_2. Conditions are as described in Figures 6.1–6.3.

Description	Sample 1	Sample 2	Sample 3	Average	Starting
H_2O_2 alone	1.106	1.108	1.098	1.104	1.115
H_2O_2 + **1a**	1.119	1.114	1.129	1.121	1.115
H_2O_2 + **1b**	1.106	1.110	1.104	1.107	1.115

6.2 UV-vis examination of the catalyst species formed on treatment of 1a with H_2O_2 and NaClO at high catalyst concentrations.

In this preliminary work, the formation of dimers of TAML catalysts on treatment with H_2O_2 and NaClO was examined at [TAML] > 1×10^{-6} M. In previous work, a complex determined by EPR and Mössbauer spectroscopies to be a $Fe^{III}O(H)Fe^{IV}$ dimer (**2b**, Chart 6.2), was observed to form upon addition of 1 equivalent (eq) of H_2O_2 to solutions of **1b**

(0.5–2.0 × 10^{-3} M) at pH 11.8 (0.01 M, phosphate) with 50% glycerol.[6] The $Fe^{III}O(H)Fe^{IV}$ dimer is a very weak oxidant, only undergoing reduction by easily oxidized electron donors such as NADH, Pinacyanol chloride, and hydroquinone.[7]

Chart 6.2 Structures of TAML derived **2** and **3**.

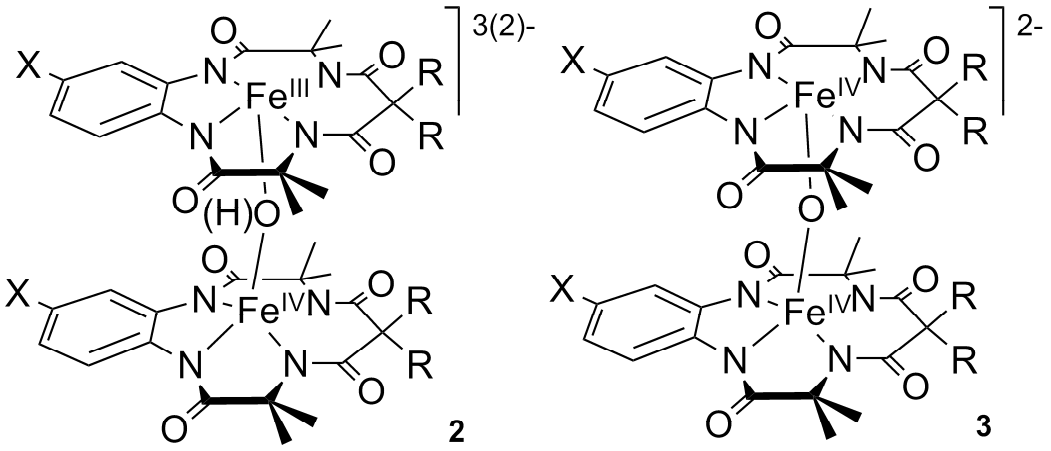

Addition of 1 eq of NaClO to a 1 × 10^{-4} M **1a** solution at 25 °C in pH 7 buffer (0.01 M, phosphate) gives **3a**, based on its known spectroscopic properties (Figure 6.4).[5,8-10] On standing, the **3a** solution decays to give **2a**, based on the similarity of its UV-vis spectrum to that of characterized **2b**.[6] Addition of a second aliquot of NaClO returns **3a**, and this cycle can be repeated multiple times. With each cycle, the total absorbances of **2a** and **3a** decrease, indicating gradual degradation of the catalyst species in these solutions. In contrast, addition of 1 eq of H_2O_2 to an identical **1a** solution results in rapid formation of **2a** (Figure 6.5). The **2a** spectrum is more stable with H_2O_2 and remains so throughout introduction of subsequent H_2O_2 aliquots over 100 min. The UV-vis behavior of both processes suggests that an invisible reducing agent is consuming oxidized catalyst species

returning the system always to **2a**. It is well known that TAML catalysts can oxidize water to oxygen.[11,12]

Taken together, these results suggest a different behavior of **1a** catalyst at high concentrations between **1a**/NaClO and H_2O_2 oxidation systems. We have long postulated the room temperature treatment of Fe^{III} with either oxidant in H_2O to give a formally Fe^{V} intermediate.[13] Low temperature NaClO and mCPBA studies in CH_3CN have found this to be an Fe^{V}=O. At -40 °C in CH_3CN, Fe^{V}=O and Fe^{III} rapidly comproportionate to give Fe^{IV}-O-Fe^{IV} dimers (**3**).[9,10] The experiment performed in this study suggests that on standing, **3a** undergoes conversion to the very poor oxidant **2a**. H_2O_2 treatment does not oxidize **2a**, however NaClO treatment returns **3a** rendering it available for catalysis. While further studies are necessary, these results implicate **2a** formation as a likely k_{2i} process in H_2O_2 systems not observed in NaClO systems due to a rescuing of **2a** by the more potent oxidant. Though this process is not significant for NaClO treatment, other inactivation processes that are bimolecular in iron (k_{2i}) leading to a loss of coordinated iron do function in NaClO systems that employ high [**1a**].

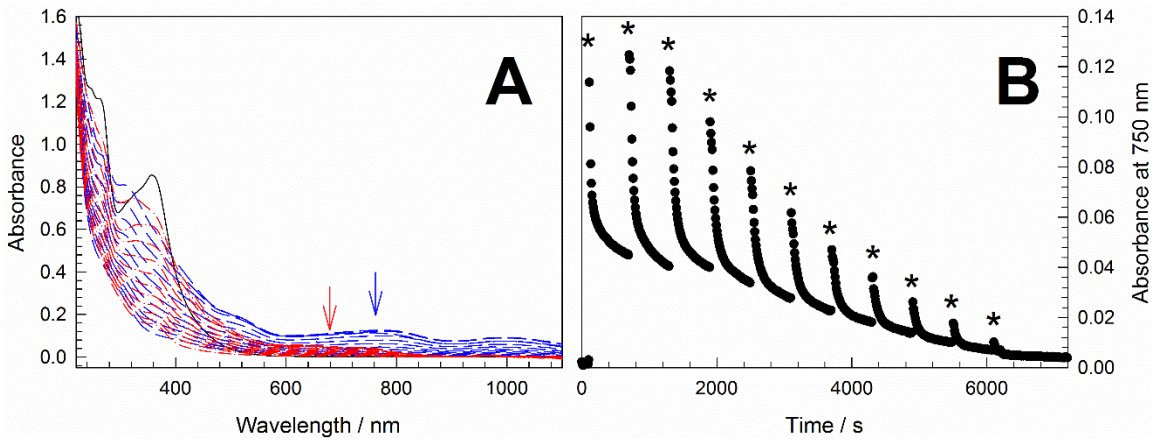

Figure 6.4 Oxidation of **1a** by multiple 1 equivalent aliquots of NaClO. Conditions: pH 7, 0.01 M phosphate buffer, [**1a**] = 1.015 × 10^{-4} M, [NaClO] = 1.035 × 10^{-4} M for each aliquot. Left: UV-vis spectra of **3a** and **2a** formation. Black line: **1a** spectrum; Blue lines: spectra recorded immediately after each NaClO aliquot addition; Red lines: spectra recorded 10 min after each NaClO aliquot addition. Arrows indicate the progression of each set of spectra upon successive NaClO aliquot additions. Right: Absorbance change at 750 nm; Each '*' indicates the addition of 1 NaClO aliquot.

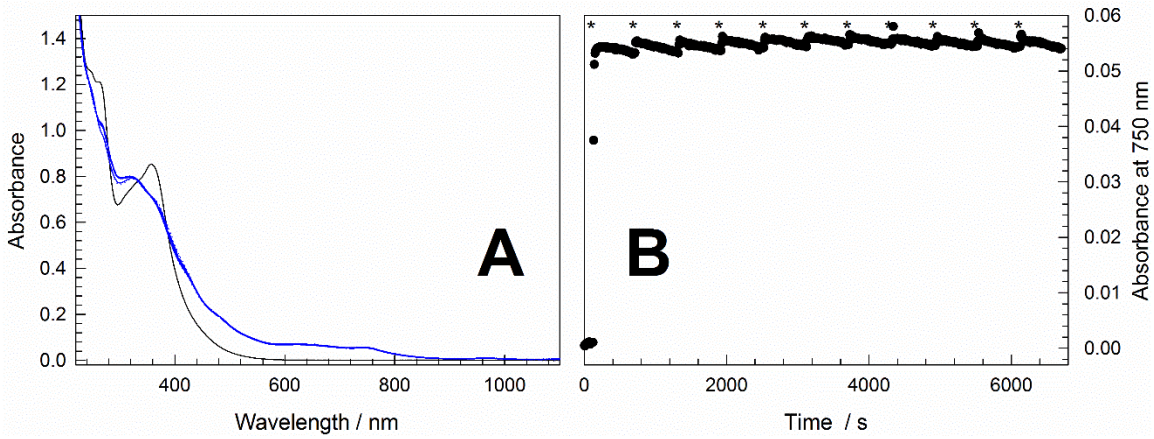

Figure 6.5 1a oxidation upon addition of multiple 1 equivalent H_2O_2 aliquots monitored by UV-vis. Conditions: pH 7 (0.01 M, phosphate), [**1a**] = 1.015 × 10^{-4} M, [H_2O_2] = 1.08 × 10^{-4} M for each aliquot. Left: UV-vis spectra of **2a** formation. Black line: **1a** spectrum; Blue lines: **2a** spectra recorded after the addition of 1st, 2nd, and 11th H_2O_2 aliquots. Right: absorbance change at 750 nm; Each '*' indicates the addition of 1 H_2O_2 aliquot.

6.3 Future Prospective

The more thoroughly we have investigated TAML catalysis, the more we have realized so much remains unknown. Many interesting questions remain to be solved. The experimental results I have obtained during my graduate studies suggest several areas which are ripe for further study.

One such area is TAML catalysis of substrate oxidations by environmentally friendly oxidants other than NaClO or H_2O_2 such as ozone (O_3). The results presented herein demonstrate the advances that can be made through the use of NaClO as an alternative to H_2O_2, namely avoidance of H_2O_2 dependent catalyst inactivation processes resulting in greatly enhanced catalyst lifetime. However, treatment with chlorine often results in the formation of chlorinated disinfection byproducts. I wonder if a similar lifetime gain could be achieved through the use of O_3 which does not suffer from this drawback. Such processes would have to be monitored for bromate formation. A detailed study comparing TAML catalyzed substrate oxidation processes by these different oxidants would also be informative.

The metaldehyde degradation studies presented herein indicate that catalyst inactivation processes that are bimolecular in catalyst (k_{2i} processes) become kinetically relevant at catalyst concentrations greater than 1×10^{-6} M. Further, the k_{2i} processes which operate in the H_2O_2 and NaClO oxidation systems differ. The studies of TAML processes at even higher catalyst concentrations monitored by UV-vis spectroscopy introduced in this chapter also show differences in the performances of the TAML catalyst in the presence of these two oxidants. Unfortunately, no systematic study of these k_{2i} processes has been performed yet. Determination of the mechanism(s) of these k_{2i} processes could lead to

mathematical relationships that allow optimization of processes which demand catalyst concentrations greater than 1×10^{-6} M or even modifications of the catalyst ligand structure to give activators which operate with k_{2i} values lower than those of the suite of catalysts currently available. As for the k_{2i} processes, we have yet to definitively assign the mechanisms of catalyst activation (k_I). Since catalyst activation is often rate determining in TAML systems, these studies could guide the design of catalysts that are more rapidly activated resulting in higher overall rates of substrate oxidation.

As discussed in Chapter 1, TAML/H_2O_2 has been considered as a promising water treatment process for the removal of numerous micropollutants. Before real-world application of TAML catalysis in water treatment, the potentially hazardous formation of byproducts during TAML treatment of waters containing natural organic matter should be thoroughly investigated in a manner similar to the studies of bromate formation presented herein.

6.4 Experimental

6.4.1 Materials

All reagents, components of buffer solutions, and solvents were at least ACS reagent grade and were used as received. pH 7.0 and 8.0 buffers were prepared with 0.01 M phosphate buffer. TAML catalysts **1a** and **1b** were obtained from GreenOx Catalysts, Inc., and **1b** was additionally purified by passing through a C18-silica gel column using a water/methanol (v/v 95/5) mixture as eluent. Stock solutions of TAML activators (2×10^{-4} M) were prepared in pure water and stored in fridge. The concentration of H_2O_2 and NaClO

was quantified by measuring the UV-vis absorbance at 230 nm (ε = 72.4 $M^{-1}cm^{-1}$)[14] and 293 nm (ε = 350 $M^{-1}cm^{-1}$)[15] respectively.

6.4.2 Instrumental

UV-Vis measurements were performed on an Agilent 8453 UV-Vis spectrophotometer equipped with an 8-cell transporter and thermostatic temperature controller. Solution temperatures were maintained at 25 °C in capped quartz cuvettes (1.0 cm).

Ion chromatography: A dionex DX500 chromatography consisting of an LC25 chromatography oven, a GP 50 gradient pump, an ED 40 electrochemical detector, an AS 40 automated sampler and an ERS® 500 self-regenerating suppressor was used for IC studies. The analytical column used was a Dionex IonPac AS9-HC (4mm × 250mm) and the guard column used was a Dionex IonPac AG9-HC (4mm × 50mm). The data were analyzed using Chromeleon chromatography software (version 6.70). Analysis was performed according to EPA method 300.1: 9 mM isocratic Na_2CO_3 in deionized water (18.1 mΩ-cm) was the eluent and the flow rate was set at 1 mL min^{-1}, SRS current was set at 100 mA, the oven temperature was 35 °C and injection volume was 200 µL.[16] The detection limit for bromate is around 7 µg/L in deionized water.

6.5 References

(1) Wagner, H. P.; Pepich, B. V.; Hautman, D. P.; Munch, D. J.; Halhi, E.; von Gunten, U. *Method 326.0 Determination of Inorganic Oxyhalide Disinfection By-Products in Drinking Water Using Ion Chromatography Incorporating the Addition of a Suppressor Acidified Postcolumn Reagent for Trace Bromate Analysis*, 2002.

(2) von Gunten, U.; Hoigne, J. *Environ. Sci. Technol.* **1994**, *28*, 1234.

(3) von Gunten, U.; Oliveras, Y. *Environ. Sci. Technol.* **1998**, *32*, 63.

(4) Collins, T. J.; Ryabov, A. D.; EPA: 2004-2007.

(5) Ghosh, A.; de Oliveira, F. T.; Yano, T.; Nishioka, T.; Beach, E. S.; Kinoshita, I.; Munck, E.; Ryabov, A. D.; Horwitz, C. P.; Collins, T. J. *J. Am. Chem. Soc.* **2005**, *127*, 2505.

(6) Tang, L. L.; Gunderson, W. A.; Weitz, A. C.; Hendrich, M. P.; Ryabov, A. D.; Collins, T. J. *J. Am. Chem. Soc.* **2015**, *137*, 9704.

(7) Tang, L. L.; Ryabov, A. D.; Collins, T. J. *ACS Catal.* **2016**, *6*, 3713.

(8) Chanda, A.; Shan, X. P.; Chakrabarti, M.; Ellis, W. C.; Popescu, D. L.; de Oliveira, F. T.; Wang, D.; Que, L.; Collins, T. J.; Munck, E.; Bominaar, E. L. *Inorg. Chem.* **2008**, *47*, 3669.

(9) Kundu, S.; Thompson, J. V.; Ryabov, A. D.; Collin, T. J. *J. Am. Chem. Soc.* **2011**, *133*, 18546.

(10) Ren, Q. Z.; Guo, Y. S.; Mills, M. R.; Ryabov, A. D.; Collins, T. J. *Eur. J. Inorg. Chem.* **2015**, 1445.

(11) Panda, C.; Debgupta, J.; Diaz, D. D.; Singh, K. K.; Gupta, S. S.; Dhar, B. B. *J. Am. Chem. Soc.* **2014**, *136*, 12273.

(12) Ellis, W. C.; McDaniel, N. D.; Bernhard, S.; Collins, T. J. *J. Am. Chem. Soc.* **2010**, *132*, 10990.

(13) Kundu, S.; Annavajhala, M.; Kurnikov, I. V.; Ryabov, A. D.; Collins, T. J. *Chem. Eur. J.* **2012**, *18*, 10244.

(14) George, P. *Biochem. J.* **1953**, *55*, 220.

(15) Kelm, M.; Pashalidis, I.; Kim, J. I. *Appl. Radiat. Isotopes* **1999**, *51*, 637.

(16) D.Pfaff, J.; Hautman, D. P.; Munch, D. J. *Method 300.1 Determination of Inorganic Anions in Drinking Water by Ion Chromatography*, 1999.